

NAVAL POSTGRADUATE SCHOOL

Monterey, California



DISSERTATION

**MODELING AND ANALYSIS OF CELLULAR CDMA
FORWARD CHANNEL**

by

Jan Elizabeth Tighe

March 2001

Thesis Advisor:

Tri T. Ha

Approved for public release; distribution is unlimited

20010627 101

REPORT DOCUMENTATION PAGE		Form Approved OMB No. 0704-0188	
Public reporting burden for this collection of information is estimated to average 1 hour per response, including the time for reviewing instruction, searching existing data sources, gathering and maintaining the data needed, and completing and reviewing the collection of information. Send comments regarding this burden estimate or any other aspect of this collection of information, including suggestions for reducing this burden, to Washington headquarters Services, Directorate for Information Operations and Reports, 1215 Jefferson Davis Highway, Suite 1204, Arlington, VA 22202-4302, and to the Office of Management and Budget, Paperwork Reduction Project (0704-0188) Washington DC 20503.			
1. AGENCY USE ONLY (Leave blank)	2. REPORT DATE March 2001	3. REPORT TYPE AND DATES COVERED Doctoral Dissertation	
4. TITLE AND SUBTITLE: Title (Mix case letters) Modeling and Analysis of Cellular CDMA Forward Channel		5. FUNDING NUMBERS	
6. AUTHOR(S) Tighe, Jan E., CDR USN		8. PERFORMING ORGANIZATION REPORT NUMBER	
7. PERFORMING ORGANIZATION NAME(S) AND ADDRESS(ES) Naval Postgraduate School Monterey, CA 93943-5000		10. SPONSORING / MONITORING AGENCY REPORT NUMBER	
9. SPONSORING / MONITORING AGENCY NAME(S) AND ADDRESS(ES) N/A		11. SUPPLEMENTARY NOTES The views expressed in this thesis are those of the author and do not reflect the official policy or position of the Department of Defense or the U.S. Government.	
12a. DISTRIBUTION / AVAILABILITY STATEMENT Approved for public release; distribution is unlimited		12b. DISTRIBUTION CODE	
13. ABSTRACT (maximum 200 words) <p>In this thesis, we develop the forward channel model for a DS-CDMA cellular system operating in a slow-flat Rayleigh fading and lognormal shadowing environment, which incorporates the extended Hata model to predict median path loss. Forward error correction is integrated into the model by applying convolution encoding with soft-decision decoding. The worst-case probability of bit error for a mobile user at the edge of the center cell of a seven-cell cluster is developed using Gaussian approximation. In estimating the probability of bit error, we develop a statistical model, which approximates the sum of d multiplicative chi-square(two degrees of freedom)-lognormal random variables as a multiplicative chi-square(with $2d$ degrees of freedom)-lognormal random variable. Using this approximation, we examine the performance of the cellular system under a range of shadowing conditions, for various user capacities and with antenna sectoring as they compare with Monte Carlo simulated results. Next, we modify our worst-case performance analysis to accommodate users that are distributed in the cell according to a specified distribution and compare results with the worst-case performance. Finally, we introduce fast power control into the forward channel and explore system performance with power control under a range of operating conditions as it compares with the fixed-power performance.</p>			
14. SUBJECT TERMS CDMA, Wireless, Performance Analysis, Rayleigh Fading, Lognormal Shadowing, Walsh Functions, Hata Model, Convolutional Codes, User Distribution, Power Control, Sum Distribution, Gaussian Approximation, Forward Channel Model, Antenna Sectoring			15. NUMBER OF PAGES
			16. PRICE CODE
17. SECURITY CLASSIFICATION OF REPORT Unclassified	18. SECURITY CLASSIFICATION OF THIS PAGE Unclassified	19. SECURITY CLASSIFICATION OF ABSTRACT Unclassified	20. LIMITATION OF ABSTRACT UL

THIS PAGE INTENTIONALLY LEFT BLANK

Approved for public release; distribution is unlimited

MODELING AND ANALYSIS OF CELLULAR CDMA FORWARD CHANNEL

Jan E. Tighe
Commander, United States Navy
B.S., United States Naval Academy, 1984

Submitted in partial fulfillment of the requirements for the degrees of

MASTER OF SCIENCE IN APPLIED MATHEMATICS

and

DOCTOR OF PHILOSOPHY IN ELECTRICAL ENGINEERING

from the

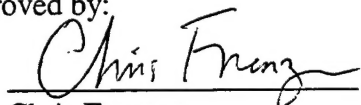
NAVAL POSTGRADUATE SCHOOL

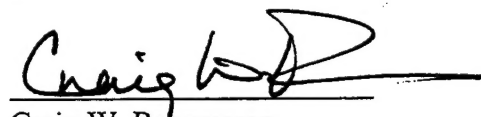
March 2001

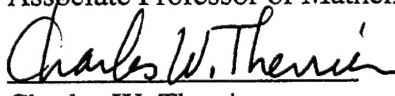
Author:

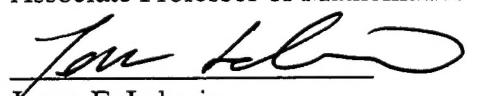

Jan E. Tighe

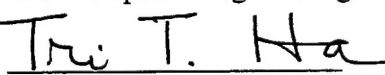
Approved by:


Chris Frenzen
Associate Professor of Mathematics

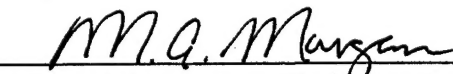

Craig W. Rasmussen
Associate Professor of Mathematics


Charles W. Therrien
Professor of Electrical
and Computer Engineering

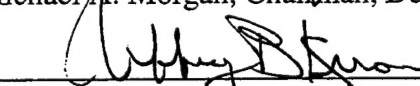

Jovan E. Lebaric
Visiting Associate Professor of
Electrical and Computer Engineering


Tri T. Ha
Professor of Electrical and Computer Engineering
Dissertation Supervisor

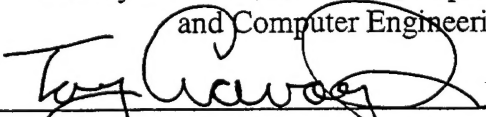
Approved by:


Michael A. Morgan, Chairman, Department of Mathematics

Approved by:


Jeffrey B. Knorr, Chairman, Department of Electrical
and Computer Engineering

Approved by:


Tony Ciavarelli, Associate Provost for Instruction

THIS PAGE INTENTIONALLY LEFT BLANK

ABSTRACT

In this thesis, we develop the forward channel model for a DS-CDMA cellular system operating in a slow-flat Rayleigh fading and lognormal shadowing environment, which incorporates the extended Hata model to predict median path loss. Forward error correction is integrated into the model by applying convolution encoding with soft-decision decoding. The worst-case probability of bit error for a mobile user at the edge of the center cell of a seven-cell cluster is developed using Gaussian approximation. In estimating the probability of bit error, we develop a statistical model, which approximates the sum of d multiplicative chi-square(two degrees of freedom)-lognormal random variables as a multiplicative chi-square(with $2d$ degrees of freedom)-lognormal random variable. Using this approximation, we examine the performance of the cellular system under a range of shadowing conditions, for various user capacities and with antenna sectoring as they compare with Monte Carlo simulated results. Next, we modify our worst-case performance analysis to accommodate users that are distributed in the cell according to a specified distribution and compare results with the worst-case performance. Finally, we introduce fast power control into the forward channel and explore system performance with power control under a range of operating conditions as it compares with the fixed-power performance.

THIS PAGE INTENTIONALLY LEFT BLANK

TABLE OF CONTENTS

I.	INTRODUCTION.....	1
A.	BACKGROUND.....	1
B.	OBJECTIVE.....	2
C.	RELATED WORK	3
D.	THESIS OUTLINE	4
II.	WALSH FUNCTIONS	7
A.	THE SET OF WALSH FUNCTIONS AS AN ALGEBRAIC GROUP	9
1.	Walsh Functions Defined.....	9
2.	Walsh Sequences Defined	13
3.	Generating Walsh Functions from Rademacher Functions....	14
4.	The Closure Property of Walsh Functions	21
B.	WALSH ORTHOGONALITY EXTENDED	23
1.	Walsh Subgroups of Order Four	25
2.	A Reduced Set of Walsh Functions.....	27
3.	Maximizing the Reduced Set \tilde{W}_N	31
4.	Generating a Maximum Set \tilde{W}_N	38
C.	AUTOCORRELATION OF WALSH FUNCTIONS	43
1.	Autocorrelation of Walsh Functions	43
2.	Average Autocorrelation of a Set of Walsh Functions W_N	46
2.	Average Autocorrelation of a Set of Walsh Functions W_N	47
D.	SUMMARY.....	52
III.	FORWARD CHANNEL MODEL.....	53
A.	BUILDING THE DS-CDMA FORWARD SIGNAL.....	54
1.	Direct Sequence Spread Spectrum CDMA	56
2.	The Transmitted Signal $S(t)$	63
B.	PROPAGATION IN THE MOBILE RADIO CHANNEL	64
1.	Large-Scale Path Loss.....	65
2.	Hata Model.....	68
3.	Lognormal Shadowing.....	71
4.	Small-Scale Fading Due to Multipath	75
C.	RAYLEIGH-LOGNORMAL CHANNEL MODEL.....	78
1.	The Forward Signal $s_o(t)$	78
2.	Co-Channel Interference $\varsigma(t)$	81
3.	The Received Signal $r(t)$	82
D.	SUMMARY.....	83

APPENDIX III-A	LOGNORMAL RANDOM VARIABLE	85
1.	Lognormal Random Variable Derived from a Gaussian Random Variable	85
2.	Transformation $Y = a/X$ of the Lognormal Random Variable	87
IV.	DS-CDMA PERFORMANCE ANALYSIS	91
A.	PERFORMANCE OF THE BASIC SYSTEM.....	93
1.	The Demodulated Signal $y_2(t)$	94
2.	The Decision Statistic Y	99
3.	Signal-to-Noise Plus Interference Ratio	103
4.	Probability of Bit Error \tilde{P}_e	106
B.	CONVOLUTIONAL ENCODING OF DS-CDMA	111
1.	Viterbi Branch and Path Metrics	111
2.	First-Event Error Probability	115
C.	APPROXIMATING THE SUM OF MULTIPLICATIVE CHI-SQUARE2- LOGNORMAL RANDOM VARIABLES	119
1.	Defining the Model \tilde{Z}_d	125
2.	Testing the Model \tilde{Z}_d	130
D.	BIT ERROR ANALYSIS OF DS-CDMA WITH FEC.....	136
E.	SUMMARY.....	140
APPENDIX IV-A	VARIANCE OF THE COCHANNEL INTERFERENCE	142
APPENDIX IV-B	DEVELOPING THE UNCODED PROBABILITY OF BIT ERROR	146
1.	Removing Dependency on the Chi-square R.V.	146
2.	Removing Dependency on the Lognormal R.V.	149
APPENDIX IV-C	MODELED AND SIMULATED PROBABILITY OF BIT ERROR FOR THE RAYLEIGH-LOGNORMAL CHANNEL USING 120° ANTENNA SECTORING	151
V.	INCORPORATING USER DISTRIBUTION AND POWER CONTROL INTO THE FORWARD CHANNEL MODEL.....	159
A.	USER DENSITY IN THE CELL.....	163
B.	RANDOMIZING TRANSMIT POWER ON THE FORWARD TRAFFIC CHANNELS.....	167
C.	SUMMARY.....	176
APPENDIX V-A	GEOMETRY OF PATH LOSS DISTANCES	178
1.	The Development of \mathcal{D}_1	179
2.	The Development of \mathcal{D}_2	180
3.	The Development of \mathcal{D}_3	181
4.	The Development of \mathcal{D}_4	183
5.	The Development of \mathcal{D}_5	184

6.	The Development of \mathcal{D}_6	185
APPENDIX V-B PROBABILITY OF BIT ERROR FOR THE		
RAYLEIGH-LOGNORMAL CHANNEL USING FORWARD		
	CHANNEL POWER CONTROL.....	187
VI.	CONCLUSIONS AND FUTURE WORK	195
A.	CONCLUSIONS.....	195
B.	FUTURE WORK	198
LIST OF REFERENCES		199
BIBLIOGRAPHY		203
INITIAL DISTRIBUTION LIST		207

THIS PAGE INTENTIONALLY LEFT BLANK

LIST OF FIGURES

Figure 2.1	Direct Sequence Spread Spectrum With Walsh Orthogonal Cover.	7
Figure 2.2	Direct Sequence Spread Spectrum Without Orthogonal Cover.	8
Figure 2.3	Set of Walsh Functions of Order Four.	10
Figure 2.4	Rademacher Functions for $k=3$	16
Figure 2.5	Building $w_6(t)$ as a Product of Rademacher Functions.	19
Figure 2.6	Set of Walsh Functions of Order Eight.	45
Figure 2.7	Set of Autocorrelation Functions for W_8	46
Figure 2.8	Average Autocorrelation Function, $\mathcal{A}_8(u)$ for the Set W_8	47
Figure 2.9	Average Autocorrelation Function, $\mathcal{A}_N(u)$ for the Set W_N	49
Figure 2.10	Revised Average Autocorrelation Function, $\widetilde{\mathcal{A}}_8(u)$ for the Set W_8	50
Figure 2.11	Autocorrelation Function of a PN Signal.	51
Figure 2.12	Revised Average Autocorrelation Function, $\widetilde{\mathcal{A}}_N(u)$ for a Set W_N	51
Figure 3.1	CDMA Forward and Reverse Channels.	53
Figure 3.2	Seven Cell Cluster.	55
Figure 3.3	Spectrum Spreading by a factor of N	57
Figure 3.4	Direct Sequence Spreading of Two Data Bits Using $w_3(t)$	58
Figure 3.5	Spectrum Spreading of Two Data Bits Using Sequences.	58
Figure 3.6	Spectrum Spreading of Two Data Bits Using $w_1(t)$	60
Figure 3.7	DS-CDMA Spreading and Despreading.	60
Figure 3.8	Product of Non-Synchronous Walsh Functions.	63
Figure 3.9	Spreading and Modulating the Information Signal.	63
Figure 3.10	Comparison of Hata Loss and Average Loss.	70
Figure 3.11	Multipath Propagation.	75
Figure 3.12	Baseband Rayleigh-Lognormal Channel Model.	79
Figure 4.1	Mobile User One in the Seven Cell Cluster.	91
Figure 4.2	Geometry of the Cell Hexagon.	92
Figure 4.3	Processing the Received Signal, $r(t)$	94
Figure 4.4	Performance of a DS-CDMA System in a Rayleigh Fading Channel. ...	123
Figure 4.5	Histogram of \mathcal{Z}_{10} and the PDF for $\widetilde{\mathcal{Z}}_{10}$ for $\sigma_{dB} = 7$	130
Figure 4.6	Histogram of \mathcal{Z}_{11} and the PDF for $\widetilde{\mathcal{Z}}_{11}$ for $\sigma_{dB} = 7$	131
Figure 4.7	Histogram of \mathcal{Z}_{12} and the PDF for $\widetilde{\mathcal{Z}}_{12}$ for $\sigma_{dB} = 7$	131
Figure 4.8	Histogram of \mathcal{Z}_{13} and the PDF for $\widetilde{\mathcal{Z}}_{13}$ for $\sigma_{dB} = 7$	131
Figure 4.9	Histogram of \mathcal{Z}_{14} and the PDF for $\widetilde{\mathcal{Z}}_{14}$ for $\sigma_{dB} = 7$	132
Figure 4.10	First Event Error Probability $\mathcal{P}_2(10)$ for $\sigma_{dB} = 7$ with 10 users per cell.	133

Figure 4.11	First Event Error Probability $\mathcal{P}_2(11)$ for $\sigma_{dB} = 7$ with 10 users per cell.	133
Figure 4.12	First Event Error Probability $\mathcal{P}_2(12)$ for $\sigma_{dB} = 7$ with 10 users per cell.	133
Figure 4.13	First Event Error Probability $\mathcal{P}_2(13)$ for $\sigma_{dB} = 7$ with 10 users per cell.	134
Figure 4.14	First Event Error Probability $\mathcal{P}_2(14)$ for $\sigma_{dB} = 7$ with 10 users per cell.	134
Figure 4.15	Probability of Bit Error for DS-CDMA with Rayleigh Fading and Lognormal Shadowing ($\sigma_{dB} = 7$) using a Rate $\frac{1}{2}$ Convolution Encoder with $v = 8$	135
Figure 4.16	Probability of Bit Error for DS-CDMA with FEC in Various Channel Conditions with 10 users per cell ($R_{cc} = 1/2$ and $v = 8$)	137
Figure 4.17	Probability of Bit Error for DS-CDMA with FEC in Various Channel Conditions with the Average SNR = 15 dB ($R_{cc} = 1/2$ and $v = 8$)	138
Figure 4.18	Probability of Bit Error for DS-CDMA using Sectoring for $\sigma_{dB} = 7$ with an SNR per Bit of 15 dB ($R_{cc} = 1/2$ and $v = 8$)	139
Figure 4.19	Transformation of the limits of integration, $(t, \lambda) \rightarrow (u, v)$	144
Figure 4.20	Probability of Bit Error for DS-CDMA with Rayleigh Fading and Lognormal Shadowing ($\sigma_{dB} = 2$) using 120° Sectoring ($R_{cc} = 1/2$ and $v=8$)	151
Figure 4.21	Probability of Bit Error for DS-CDMA with Rayleigh Fading and Lognormal Shadowing ($\sigma_{dB} = 3$) using 120° Sectoring ($R_{cc} = 1/2$ and $v=8$)	152
Figure 4.22	Probability of Bit Error for DS-CDMA with Rayleigh Fading and Lognormal Shadowing ($\sigma_{dB} = 4$) using 120° Sectoring ($R_{cc} = 1/2$ and $v=8$)	153
Figure 4.23	Probability of Bit Error for DS-CDMA with Rayleigh Fading and Lognormal Shadowing ($\sigma_{dB} = 5$) using 120° Sectoring ($R_{cc} = 1/2$ and $v=8$)	154
Figure 4.24	Probability of Bit Error for DS-CDMA with Rayleigh Fading and Lognormal Shadowing ($\sigma_{dB} = 6$) using 120° Sectoring ($R_{cc} = 1/2$ and $v=8$)	155

Figure 4.25	Probability of Bit Error for DS-CDMA with Rayleigh Fading and Lognormal Shadowing ($\sigma_{dB} = 7$) using 120° Sectoring ($R_{cc} = 1/2$ and $v=8$)	156
Figure 4.26	Probability of Bit Error for DS-CDMA with Rayleigh Fading and Lognormal Shadowing ($\sigma_{dB} = 8$) using 120° Sectoring ($R_{cc} = 1/2$ and $v=8$)	157
Figure 4.27	Probability of Bit Error for DS-CDMA with Rayleigh Fading and Lognormal Shadowing ($\sigma_{dB} = 9$) using 120° Sectoring ($R_{cc} = 1/2$ and $v=8$)	158
Figure 5.1	Circular Seven-Cell Cluster	160
Figure 5.2	Comparison of Probability of Bit Error for DS-CDMA in a Rayleigh-Lognormal ($\sigma_{dB} = 7$) Channel using 120° Sectoring ($R_{cc} = 1/2$ and $v=8$)	162
Figure 5.3	Probability of Bit Error for DS-CDMA with Rayleigh Fading and Lognormal Shadowing ($\sigma_{dB} = 7$) using a Linear User Distribution with 120° Sectoring and FEC ($R_{cc} = 1/2$ and $v=8$)	166
Figure 5.4	Probability of Bit Error for DS-CDMA with Rayleigh Fading and Lognormal Shadowing ($\sigma_{dB} = 7$) using Forward Power Control and Linear User Distribution with 120° Sectoring and FEC ($R_{cc} = 1/2$ and $v=8$)	172
Figure 5.5	Probability of Bit Error for DS-CDMA with Rayleigh Fading and Lognormal Shadowing ($\sigma_{dB} = 7$) vs. Users per Cell using Linear User Distribution with 120° Sectoring and FEC ($R_{cc} = 1/2$ and $v=8$)	174
Figure 5.6	Probability of Bit Error for DS-CDMA with Rayleigh Fading and Lognormal Shadowing ($\sigma_{dB} = 7$) vs. Users per Cell using Linear User Distribution with 60° Sectoring and FEC ($R_{cc} = 1/2$ and $v=8$)	175
Figure 5.7	Key Triangle of Relationships	178
Figure 5.8	Geometry for \mathcal{D}_1	179
Figure 5.9	Geometry for \mathcal{D}_2	180
Figure 5.10	Geometry for \mathcal{D}_3	181
Figure 5.11	Geometry for \mathcal{D}_4	183
Figure 5.12	Geometry for \mathcal{D}_5	184
Figure 5.13	Geometry for \mathcal{D}_6	185
Figure 5.14	Probability of Bit Error for DS-CDMA with Rayleigh Fading and Lognormal Shadowing ($\sigma_{dB} = 2$) using Power Control and 120° Sectoring ($R_{cc} = 1/2$ and $v=8$)	187

Figure 5.15	Probability of Bit Error for DS-CDMA with Rayleigh Fading and Lognormal Shadowing ($\sigma_{dB} = 3$) using Power Control and 120° Sectoring ($R_{cc} = 1/2$ and $v=8$)	188
Figure 5.16	Probability of Bit Error for DS-CDMA with Rayleigh Fading and Lognormal Shadowing ($\sigma_{dB} = 4$) using Power Control and 120° Sectoring ($R_{cc} = 1/2$ and $v=8$)	189
Figure 5.17	Probability of Bit Error for DS-CDMA with Rayleigh Fading and Lognormal Shadowing ($\sigma_{dB} = 5$) using Power Control and 120° Sectoring ($R_{cc} = 1/2$ and $v=8$)	190
Figure 5.18	Probability of Bit Error for DS-CDMA with Rayleigh Fading and Lognormal Shadowing ($\sigma_{dB} = 6$) using Power Control and 120° Sectoring ($R_{cc} = 1/2$ and $v=8$)	191
Figure 5.19	Probability of Bit Error for DS-CDMA with Rayleigh Fading and Lognormal Shadowing ($\sigma_{dB} = 7$) using Power Control and 60° Sectoring ($R_{cc} = 1/2$ and $v=8$)	192
Figure 5.20	Probability of Bit Error for DS-CDMA with Rayleigh Fading and Lognormal Shadowing ($\sigma_{dB} = 8$) using Power Control and 60° Sectoring ($R_{cc} = 1/2$ and $v=8$)	193
Figure 5.21	Probability of Bit Error for DS-CDMA with Rayleigh Fading and Lognormal Shadowing ($\sigma_{dB} = 9$) using Power Control and 60° Sectoring ($R_{cc} = 1/2$ and $v=8$)	194

LIST OF TABLES

Table 2.1	Gray Code Index Conversion for $k = 3$	17
Table 2.2	Association of Gray Code Index with Rademacher Function for $k = 3$...	18
Table 2.3	Walsh Functions from Rademacher Functions.	20
Table 2.4	Building the subgroup $\{w_0, w_1, w_6, w_7\}$	27
Table 2.5	The Set of Subgroups of Order Four for W_{16}	36
Table 2.6	Building a Valid Reduced Set \tilde{W}_{16}^*	40
Table 2.7	The Set of Subgroups of Order Four for W_{16}	42
Table 3.1	Spreading of One Information Bit using w_1 and c	61
Table 3.2	Despreading of One Information Bit using w_1 and c	61
Table 3.3	Application of w_2 to intracell traffic covered with w_1	62
Table 3.4	Path Loss Exponents in Various Environments from [19]	67
Table 4.1	Values of g_1 and g_2 for $\tilde{\mathcal{Z}}_d$	128

THIS PAGE INTENTIONALLY LEFT BLANK

EXECUTIVE SUMMARY

In the near future, the field of wireless mobile cellular communications will enter the domain of high-speed Internet access with the deployment of the third-generation cellular system (3G). While the second-generation systems currently in use are digital and support data-type traffic at low data rates, they were built to carry principally voice-type traffic. The third-generation system is *designed* to support data-type traffic at much higher data rates than the second-generation systems. Specifically, manufacturers are promising download rates on the order of 2.4 Mbps: roughly twice as fast as wired broadband. For fast-traveling users, the expected data rate is reduced to 144 kbps: better than a modem over a conventional phone line. The *actual* performance of third-generation systems, however, is yet to be determined. Accordingly, this body of work is aimed at building models and tools for predicting and enhancing the performance of cellular systems such as 3G.

The third-generation cellular system will employ a multiple access technique known as Direct Sequence Code Division Multiple Access (DS-CDMA). Multiple user access is a key feature in cellular system operations since it provides for the efficient use of assigned bandwidth to accommodate many users simultaneously. DS-CDMA systems assign mobile users orthogonal Walsh codes and spread the frequency spectrum of the user traffic using the designated Walsh code. All user traffic is spread across the same frequency band and transmitted simultaneously in a composite forward signal from the base station. Mobile users extract their traffic from the composite signal using their assigned code. In this thesis, we explore the algebraic group properties of a set of Walsh

codes, or Walsh functions. We introduce the idea of extending the orthogonality property of Walsh functions to ensure orthogonality between any set of three Walsh functions. Finally, we examine the autocorrelation functions for a set of Walsh functions and we develop an expression for the average autocorrelation for a set of Walsh functions.

This thesis specifically addresses the forward channel of a DS-CDMA cellular system. The forward channel carries traffic from the base station to a wireless mobile user in the cell. The performance of the forward channel is critical in third-generation systems since it will be used to download data from the Internet. Modeling the forward channel is complicated by the fact that the receiver is **mobile**. In general, the signal transmitted by the base station to the mobile user will lose a portion of its power based on the distance it must travel and the terrain over which it travels. Accordingly, we predict the average power received by a mobile user at a specific distance using large-scale propagation models. However, mobile users at the same distance could have terrain in their immediate vicinity that is vastly different and dynamically changing due to their mobility. This phenomenon, known as shadowing, results in *actual* path loss being different for users that are at the same distance from the base station. We reflect this variability in path loss using a lognormal random variable in our channel model. In addition to the large-scale propagation effects, a mobile user typically receives multiple copies of the forward signal that have been reflected off obstacles along various paths. The relative motion between the mobile and the base station induces a doppler shift on each of the multipath components. Furthermore, the obstacles that reflect the multipath components may be moving, which also causes a time-varying doppler shift of the received signal. The combined effects of multipath propagation and the doppler shifts

result in rapid fluctuations in the strength of the received signal, which is called small-scale fading. We represent the effects of small-scale fading in our channel model as a Rayleigh random variable. Accordingly, we combine the effects of large-scale lognormal shadowing and small-scale Rayleigh fading on the forward signal into a single unified channel model, which we use to analyze the performance of the system under various operating conditions.

In DS-CDMA cellular systems, the total signal that a mobile user will receive includes the forward signal from his base station and from the base stations of the six adjacent cells. In our analysis, we initially examine the worst-case scenario by placing the receiving mobile user at the edge of the hexagonal cell in the center of a seven-cell cluster. By doing so, our mobile user receives the forward signal from his base station at roughly the same power-level as that of the forward signal from the two nearest adjacent cells. The forward signals from the six adjacent cells constitute intercell interference. The mobile user's receiver must overcome the propagation effects, the intercell interference, and additive noise, in order to properly decode the intended traffic. To improve the chances of accurately decoding the signal, we incorporate Forward Error Correction (FEC) into our model in the form of convolutional encoding with soft-decision decoding. Furthermore, we include sectoring in our analysis, which reduces intercell interference by splitting the cell into sectors and utilizing highly directional antennas. Finally, we develop the probability of bit error, a measure of system performance, for the forward channel of a DS-CDMA cellular system operating in a Rayleigh fading and lognormal shadowing environment that employs FEC and sectoring.

We examine the performance of the forward channel under a range of operating conditions.

In order to obtain a less pessimistic view of performance of the forward channel, we modify the model by distributing the mobile users within the cell according to a probability distribution, rather than fixing the mobile at the worst-case position. We compare the distributed user results with that of the worst-case scenario.

In the analysis described above, we assume that the power in the forward signal is fixed for every channel and for all base stations. We modify our analysis to allow for fast power control on the forward channel in order to enhance performance of the system. Fast power control ensures that the power received by all mobile users is at a target power level, which is the same for all users. Based on feedback from the mobile users, the base station adjusts the power in each user channel to that which is necessary to achieve the target level. We develop the probability of bit error for the DS-CDMA system with fast power control operating in a Rayleigh-lognormal channel with FEC and sectoring. We compare the performance results of the system with power control to those of the fixed power system.

The forward channel model described above incorporates many of the system features that are expected to be included in the third-generation cellular systems, such as FEC, sectoring and fast power control. More importantly, it accounts for the combined propagation effects of Rayleigh fading and lognormal shadowing, which will dominate the operating environments of the third-generation cellular systems. Accordingly, we

expect that this research will aid system designers in the deployment of and future upgrades to the 3-G cellular system.

THIS PAGE INTENTIONALLY LEFT BLANK

ACKNOWLEDGMENTS

I wish to express my sincerest appreciation to my advisor, Professor Tri Ha. His exemplary mentorship has made this work possible. I especially want to thank him for allowing me to find my own path through the research. My respect and admiration for him extends beyond the realm of academics and research to encompass his high personal honor and integrity, which has left an indelible mark on my core.

I want to thank my Doctoral Committee members Professors Charles Therrien, Craig Rasmussen, Chris Frenzen, and Jovan Lebaric for their contributions, support and inspiration during my program.

I want to acknowledge the sacrifice made by the Naval Security Group in allowing me to pursue this program, which prevented me from serving the fleet and the community during this time. The support I received from NSG was critical to my success and most appreciated. I hope in the years to come the investment will prove worthy for the community and the Navy.

I wish to thank my family for their loving support during this stressful time. This work would not have been possible without the unflagging support and love of my husband David. My children Matt and Natalie endured my stress and absence without complaint for which I am indebted to them. Finally, I want to thank my parents Dr. Beverly James and Dr. James Chinn for always believing in me and, more importantly, making me believe that I could accomplish that which I set my mind to. The 'road less traveled' *has* made all the difference.

THIS PAGE INTENTIONALLY LEFT BLANK

I. INTRODUCTION

A. BACKGROUND

At the dawn of the twenty-first century, wired internet users have come to expect instantaneous access to e-mail, voice-mail, news, weather, music and video teleconferencing in the form of text, web pages, streaming audio and video. Wireless manufacturers are working diligently to bring a subset of these wired Internet features to mobile wireless users through the cellular telephone systems. For the moment, second-generation cellular systems predominate around the world and employ various types of multiple access techniques. While the second-generation systems are digital and can accommodate data services, they were principally designed for voice-type traffic. Accordingly, second-generation systems typically offer a meager 10 kbps in data transfer capability [1]. This data transfer rate frustrates mobile web users since it is significantly slower than a modem with a conventional phone line: the slow-lane on the wired information highway. Accordingly, wireless manufacturers are working on ways to improve the data-transfer capability of the second-generation systems. The transition of second-generation cellular systems to accommodate faster data rates is a stopgap measure pending the worldwide deployment of the third-generation cellular system (3G.)

The third-generation system is *designed* to support circuit and packet data at higher data rates than the second-generation systems by employing Wideband Code Division Multiple Access (W-CDMA) technology [2]. Manufacturers are promising download rates on the order of 2.4 Mbps. For highly mobile (vehicular) users, however,

the expected data rate is reduced to 144 kbps [3]. The *actual* performance of third-generation systems remains to be seen. The deployment of third-generation cellular systems in Japan is underway. In Europe third-generation cellular systems are expected to be on-line in 2002, and in the United States (possibly) by 2003. These deployment dates are targets for metropolitan centers, while worldwide deployment would come much later (2010), if ever.

B. OBJECTIVE

As system designers gear up for the deployment of the third-generation systems, they will require design tools and models that reflect the mobile radio channel environments that they will encounter. Furthermore, as we search for ways to improve 3G system performance, tools that model the environment precisely will become increasingly more important. This thesis provides such tools for Direct Sequence CDMA (DS-CDMA) cellular systems operating in fading and shadowing environments that are associated with mobile wireless communications. Specifically, we develop a tight upper bound on the probability of bit error for the forward channel of a CDMA cellular system in a slow flat Rayleigh fading environment, which is also affected by lognormal shadowing. In the performance analysis, we account for forward error correction in the form of convolutional encoding with soft decision decoding. Furthermore, we incorporate other performance enhancing techniques such as antenna sectoring and power control of the forward channel.

C. RELATED WORK

Most of the related work in DS-CDMA cellular performance has been focused on the reverse channel as in [4] through [6]. In some instances the results of the reverse channel analysis can be extended to the forward channel. While these investigations consider both shadowing and fading effects, they do not incorporate forward error correction in the analysis. In publications where forward error correction with soft decision decoding has been considered as in [7] through [10], the combined effects of shadowing and fading are not included in the analysis.

The performance of the forward DS-CDMA channel with power control in a Rayleigh fading channel was investigated in [11] without considering the effects of shadowing or forward error correction. Furthermore, [12] considers the effects of lognormal shadowing and Rayleigh fading separately and includes forward error correction in the form of Golay codes with hard decision decoding. In [13], Nakagami fading channels were considered using a weak Golay Code with hard decision decoding and the effects of shadowing were not included.

In summary, previous performance analyses of the DS-CDMA cellular system typically have considered only a subset of the channel effects when incorporating the benefits of forward error correction with soft decision decoding. Alternatively, the analyses have considered the combined effects of fading and shadowing, but have not incorporated forward error correction.

D. THESIS OUTLINE

In Chapter II, we examine the properties and generation of a set of Walsh functions, which are at the heart of DS-CDMA techniques. We prove the closure property for a set of Walsh functions. We introduce the idea of extending the orthogonality property for a reduced set Walsh functions so that product of any *three* Walsh functions from the reduced set is identically zero when integrated over the bit period. We conclude the chapter by developing a set of autocorrelation functions for the set of Walsh functions of order N , and by describing the average autocorrelation function for the entire set.

In Chapter III, we develop the forward channel model for the DS-CDMA cellular system using a seven-cell cluster. Our channel model takes into account both large-scale and small-scale propagation effects. We use the extended Hata model to predict path loss and incorporate Rayleigh fading and lognormal shadowing into the channel model. We develop the composite signal received by a mobile user in the center cell that includes the signal intended for the mobile, signals intended for other mobile users in the center cell (intracell interference), co-channel interference from the adjacent six cells, and additive noise. Finally, we place our mobile user at the corner of the hexagonal cell, in order to develop the performance for the worst-case.

In Chapter IV, we develop a Signal-to-Noise plus Interference Ratio (SNIR) and the bit-error probability for the DS-CDMA system in a Rayleigh-lognormal channel by using Gaussian approximation. We incorporate Forward Error Correction (FEC) in the

form of convolutional encoding with soft-decision decoding into our Rayleigh-lognormal forward channel model and develop a revised upper bound on the probability of bit error. In calculating the probability of bit error for the system with FEC analytically, we require the probability distribution function for a sum of d multiplicative chi-square(two degrees of freedom)-lognormal random variables. To simplify the performance analysis, we approximate this sum of d multiplicative random variables as a multiplicative chi-square(with $2d$ degrees of freedom)-lognormal random variable. We compare our modeled performance results with results that are simulated using Monte Carlo methods. We conclude the chapter by incorporating antenna sectoring into our model. Lastly, we analyze the performance of our Rayleigh-lognormal forward channel model under a wide range of shadowing conditions and for various numbers of users per cell.

In Chapter V, we modify the performance analysis of the previous chapter to incorporate user distribution within the cell. That is, rather than assuming our mobile user is located at the worst-case position in the corner of the cell, we assume that the position is random according to a specified distribution. We revise the upper bound on the probability of bit error for distributed users in order to gain a more realistic view of typical performance for the Rayleigh-lognormal forward channel model with FEC. We conclude the chapter by introducing forward channel power control as a means of enhancing the overall performance of the system. We analyze the performance of the system with power control under a wide range of shadowing conditions and for various numbers of users per cell.

In Chapter VI, we summarize our conclusions and provide areas of further research.

THIS PAGE INTENTIONALLY LEFT BLANK

II. WALSH FUNCTIONS

Walsh functions are at the heart of DS-CDMA cellular communications technology. They provide orthogonal cover on the forward traffic channel within each cell to overcome intracell interference. Each mobile user in the cell has a unique Walsh function assigned which encodes his traffic coming from the base station to the mobile handset. By applying his unique Walsh function to the traffic coming from the base station, the mobile user despreads and, in effect, decodes only the traffic that is intended for him. When his unique code is applied to the remaining intracell traffic in the channel, the orthogonality between his code and other user codes zeros out their interference. A simplified representation of this process is depicted in Figure 2.1.

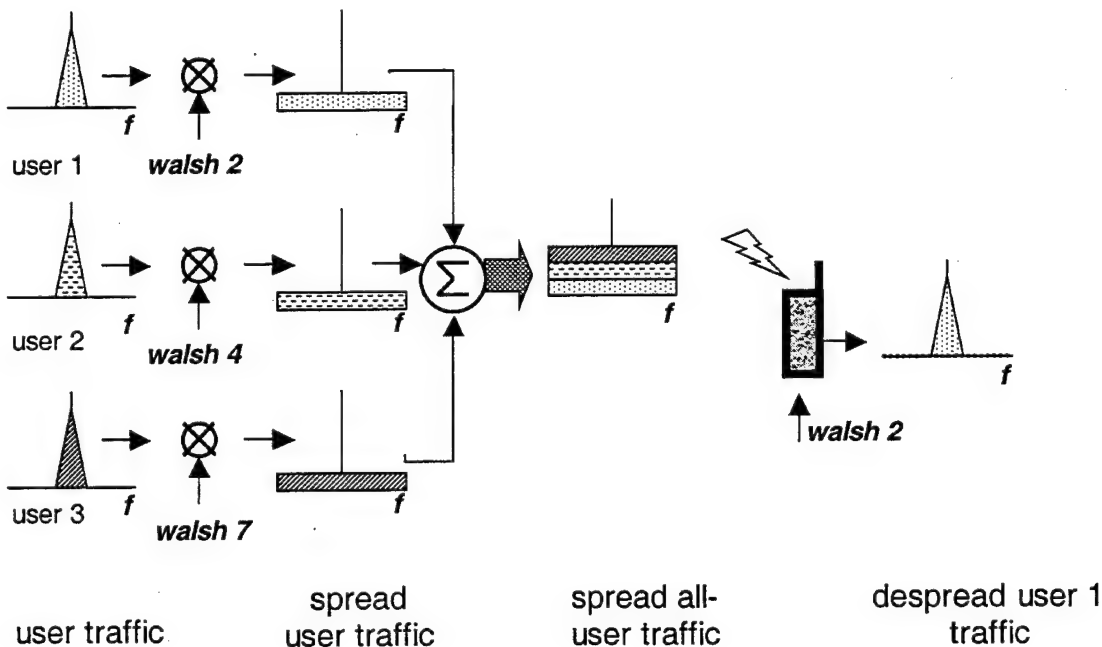


Figure 2.1 Direct Sequence Spread Spectrum With Walsh Orthogonal Cover.

If non-orthogonal functions, such as pseudorandom noise sequences, were used to spread the signal, the intracell traffic intended for other users would remain spread across the channel's frequency band. This intracell interference would contribute to the noise (and now interference) floor as depicted in Figure 2.2 instead of being eliminated. In Chapter 3, we develop the cellular model and look in depth at the construction of the forward channel using Walsh functions combined with pseudorandom noise sequences.

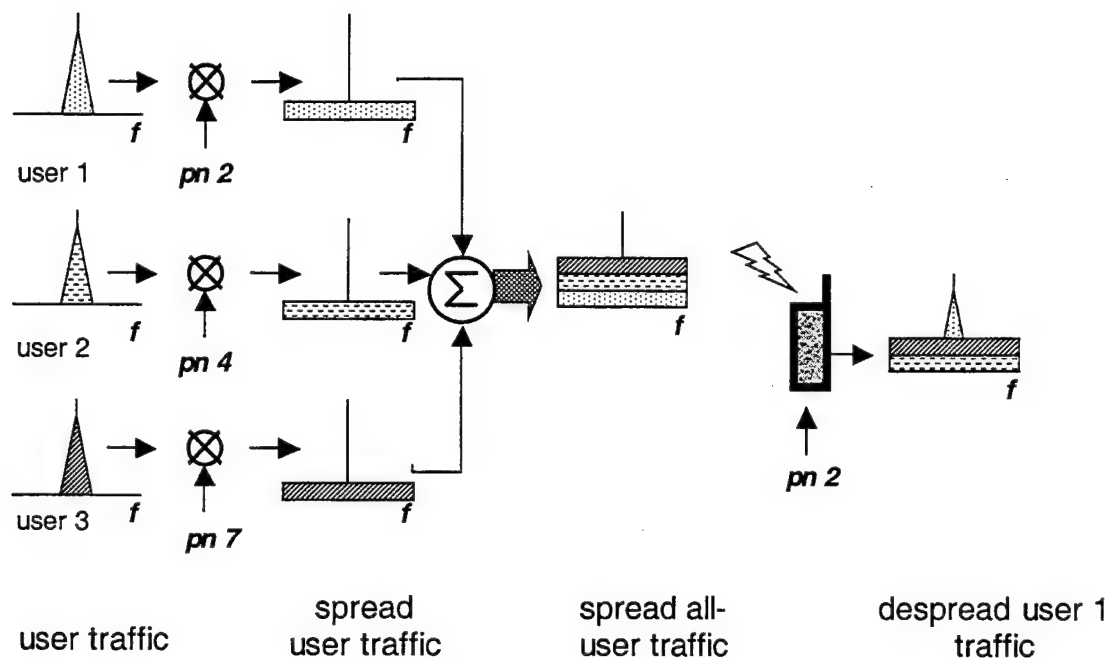


Figure 2.2 Direct Sequence Spread Spectrum Without Orthogonal Cover.

Walsh functions have many desirable properties, which we will examine in this chapter. We will look at ways that Walsh functions can be generated, how the set of Walsh functions form an algebraic group under multiplication, their autocorrelation functions, and an extension to the orthogonality property which may prove useful to the communications engineer.

A. THE SET OF WALSH FUNCTIONS AS AN ALGEBRAIC GROUP

Walsh functions were first conceived by J. L. Walsh [14] as a closed set of normalized orthogonal functions over the interval (0,1). Since that time, much work has been done to determine ways to generate these powerful functions. Today, there are at least four methods of efficiently generating a set of Walsh functions, and each method comes with its own enumeration or indexing scheme, as follows:

- ❖ Using the Walsh binary index and symmetry to instantly generate any member function, called Instant Walsh functions.
- ❖ Using a product of Rademacher functions, which we describe in this section.
- ❖ Using Hadamard matrices.
- ❖ Using generator matrices.

The above methods are well described in [15], and we will only outline those that are necessary to make our points. Using these innovations to construct and describe the set of Walsh functions more concisely, we have gained better insight into the algebraic group properties of the Walsh functions.

1. Walsh Functions Defined

We define the set of orthogonal Walsh functions of order N as $W_N = \{w_j(t); t \in (0, T), j = 0, 1, \dots, N-1\}$, consisting of $N = 2^t$ elements that are functions of time and that have the following properties as in [15];

- ❖ $w_j(t)$ takes on the values $\{+1, -1\}$ except at a finite number of points of discontinuity; where it is defined to be zero.
- ❖ $w_j(0) = 1$ for all j .
- ❖ $w_j(t)$ has precisely j sign changes in the interval $(0, T)$.
- ❖ $\int_0^T w_j(t) w_k(t) dt = \begin{cases} 0, & \text{if } j \neq k \\ T, & \text{if } j = k \end{cases}$
- ❖ Each function $w_j(t)$ is either odd or even with respect to the midpoint of the interval $(T/2)$.

Figure 2.3 depicts the four member functions of Walsh-4, $W_4 = \{w_0(t), w_1(t), w_2(t), w_3(t)\}$. In this case, the interval $(0, T)$ is broken into $N=4$ sections, with each section being $T_c = T/N = T/4$ time units long. We use Walsh binary

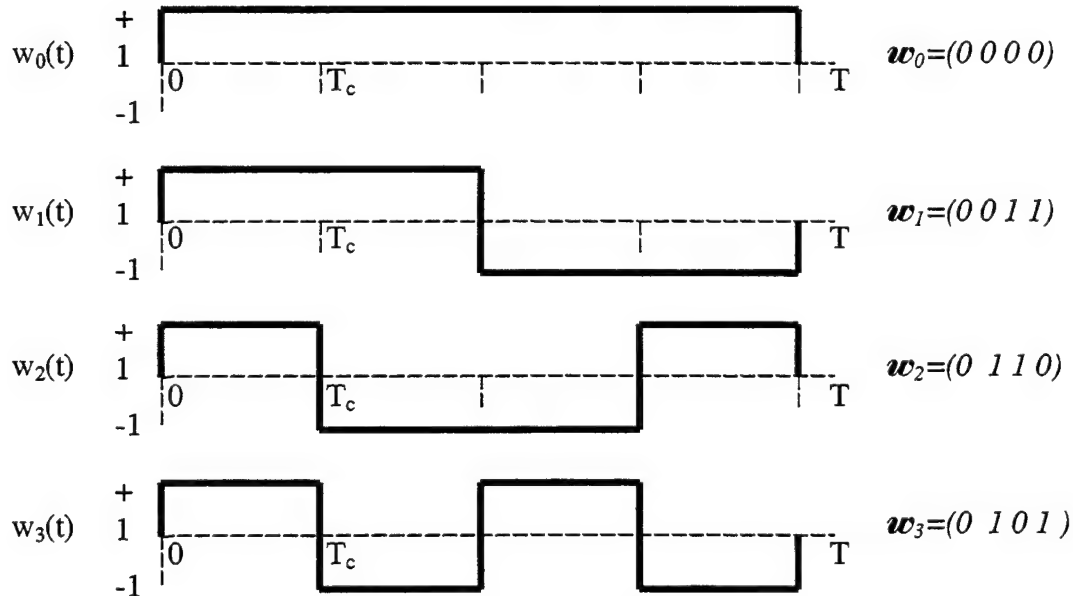


Figure 2.3 Set of Walsh Functions of Order Four.

indexing, which implies that the functions are ordered and numbered according to the number of sign changes (or visually zero crossings) on the interval. Other indexing schemes are related to the way in which the Walsh functions are generated.

The set of Walsh functions of order N forms an algebraic group under multiplication [15]; we will prove this fact later in this section. We define a group $\langle G, * \rangle$, as in [16], to consist of a set of elements G , together with an operation $*$ that is defined on G and that satisfies the following:

- ❖ Closure property. For all $a, b \in G$, $a * b \in G$.
- ❖ Associative property. For all $a, b, c \in G$, $(a * b) * c = a * (b * c)$.
- ❖ Identity property. There exists an element $e \in G$ such that

$$e * x = x * e = x \text{ for all } x \in G.$$
- ❖ Inverse property. For each $a \in G$, there exists an element $a' \in G$ that satisfies $a * a' = a' * a = e$.

In the case of Walsh functions we have a set of N elements, or member functions, together with the algebraic operation of multiplication (\bullet) forming a abelian (commutative) group $\langle W_N, \bullet \rangle$. The last three group properties are easy to see for Walsh functions of any order and for $t \in (0, T)$ as follows:

- ❖ The associative property is satisfied, since we are dealing with simple multiplication of time functions.
- ❖ The identity element is clearly $w_0(t) = 1$, for Walsh functions of any order.

- ❖ Each Walsh function serves as its own multiplicative inverse, since $w_j(t) \cdot w_j(t) = 1$ for all j .
- ❖ The order of the group is $N = 2^k$. Furthermore, the order of any non-identity element of the group is two, which implies that any element of the group can generate a subgroup of (at most) order two.

The closure property of Walsh functions remains to be proven. We will continue to lay the groundwork toward that end, and present the proof in Section 2.A.4. In fact, we will go a step further to show that the product of any two Walsh functions is not only a member of the set, but that it is a member that can be predicted by its binary index without ever looking at the waveforms. We will show that the product of any two Walsh functions, $w_i(t) \cdot w_j(t)$, is a Walsh function $w_k(t)$ that can be predicted by converting the Walsh indices i, j, k to their corresponding Walsh binary indices Q_i, Q_j, Q_k , and adding them modulo 2, i.e.,

$$Q_k = Q_i \oplus Q_j, \quad (2.1)$$

where \oplus denotes addition modulo 2.

The Walsh binary indices are k -tuples where $k = \log_2 N$. For example, using the set of Walsh functions W_4 shown in Figure 2.3, it is clear that $w_1(t) \cdot w_2(t) = w_3(t)$. We could have predicted this result without looking at the waveforms by applying (2.1) to the binary Walsh indices as follows: $Q_1 = (01)$; $Q_2 = (10)$; $Q_1 \oplus Q_2 = (11) = Q_3$, which implies that $w_1(t) \cdot w_2(t) = w_3(t)$. This is a powerful property, which we will use in the following sections before we have actually proven it.

2. Walsh Sequences Defined

Walsh functions may also be viewed and treated as binary sequences called Walsh sequences. The set of Walsh sequences of order N is denoted by $\mathbf{W}_N = \{\mathbf{w}_j; j = 0, 1, \dots, N-1\} = \{\mathbf{w}_0, \mathbf{w}_1, \dots, \mathbf{w}_{N-1}\}$. Each element $w_j(t) \in W_N$ has a corresponding binary Walsh sequence $\mathbf{w}_j \in \mathbf{W}_N$ represented as an N -tuple that is a member of the set of Walsh sequences. Since each of the N sections of any Walsh function is constant and continuous, each section can be represented separately by a binary number in the Walsh sequence. Typically, each section of the Walsh function that has the value $+1$ is represented by a binary zero in the Walsh sequence. The sections of the Walsh function that are -1 are represented by a binary 1 in the Walsh sequence. Figure 2.3 shows the Walsh sequences that correspond to the Walsh functions of order four.

Each Walsh function is mapped as described above to its corresponding Walsh sequence, such that $w_j(t) \rightarrow \mathbf{w}_j$, or $\mathbf{w}_j = (w_j(t))\mathbf{M}$. This notation means that the map or function \mathbf{M} acting on $w_j(t)$ produces the corresponding Walsh sequence \mathbf{w}_j . Accordingly, the mapping, $\mathbf{M} : W_N \rightarrow \mathbf{W}_N$ takes the entire set of Walsh functions to their corresponding Walsh sequences in a one-to-one and onto fashion.

The set of Walsh sequences of order N forms a group under modulo 2 addition; we denote this group by $\langle \mathbf{W}_N, \oplus \rangle$. Once again, the last three group properties are obvious, while the closure property is still elusive. Just as the product of two Walsh functions can be predicted using (2.1) with the Walsh binary index, we can predict the

modulo 2 addition of two Walsh sequences, using the same binary index and (2.1). This attribute guarantees that the operation is preserved under the mapping as follows:

$$(w_i(t) \cdot w_j(t)) \bullet \mathbf{M} = (w_i(t)) \bullet \mathbf{M} \oplus (w_j(t)) \bullet \mathbf{M}. \quad (2.2)$$

To prove that the function is preserved as defined in (2.2), we use (2.1), as follows:

$$\begin{aligned} (w_i(t) \cdot w_j(t)) \bullet \mathbf{M} &= (w_k(t)) \bullet \mathbf{M} \\ &= \mathbf{w}_k \\ &= \mathbf{w}_i \oplus \mathbf{w}_j \\ &= (w_j(t)) \bullet \mathbf{M} \oplus (w_i(t)) \bullet \mathbf{M}. \end{aligned}$$

Accordingly, we see that our mapping, $\bullet \mathbf{M}$, is one-to-one and onto and preserves the operation. Therefore, the group $\langle W_N, \bullet \rangle$ of Walsh functions under multiplication is isomorphic to the group $\langle \mathbf{W}_N, \oplus \rangle$ of Walsh sequences under modulo two addition as defined in [16]. We will use Walsh sequences to represent the Walsh functions for clarity in some instances, without any loss of generality.

3. Generating Walsh Functions from Rademacher Functions

One of the ways that Walsh functions can be generated is as a product of Rademacher functions. For any set W_N of Walsh functions of order $N = 2^k$, there is a corresponding set of Rademacher functions of order $1 + \log_2 N = 1 + k$, whose unique products completely form the set W_N of Walsh functions. We will define a set $\mathcal{R}_k = \{\mathcal{R}_n(t); t \in (0, T), n = 0, 1, \dots, k\}$ of orthogonal Rademacher functions of order $1+k$, as adapted from [16] and [17], where

$$\begin{aligned}
\mathcal{R}_0(t) &\equiv 1, \\
\mathcal{R}_1(t) &= \begin{cases} 1 & t \in [0, T/2) \\ -1 & t \in [T/2, T) \end{cases}, \\
\mathcal{R}_n(t) &= \mathcal{R}_1(2^{n-1}t) \quad n = 2, 3, \dots, k.
\end{aligned}$$

Each Rademacher function $\mathcal{R}_n(t)$, where $n \geq 1$, is made up of a single-cycle sine-like square wave with a period of $T/2^{n-1}$ that is repeated 2^{n-1} times over the interval $(0, T)$. From the preceding definition, we see that

$$\mathcal{R}_{n+m}(t) = \mathcal{R}_n(2^m t), \quad (2.3)$$

since

$$\begin{aligned}
\mathcal{R}_{n+m}(t) &= \mathcal{R}_1(2^{n+m-1}t) \\
&= \mathcal{R}_1(2^{n-1}(2^m t)).
\end{aligned}$$

and if we let $\tau = 2^m t$, then

$$\begin{aligned}
\mathcal{R}_{n+m}(t) &= \mathcal{R}_1(2^{n-1}\tau) \\
&= \mathcal{R}_n(\tau) \\
&= \mathcal{R}_n(2^m t).
\end{aligned}$$

Every set \mathcal{R}_k of Rademacher functions under multiplication has an identity element, $\mathcal{R}_0(t)$. Each element serves as its own multiplicative inverse, although a set of Rademacher functions does not form an algebraic group under multiplication, since it is not closed. Specifically, the product of any two Rademacher functions is not likely to be contained in the set \mathcal{R}_k . Furthermore, the product of any number of non-identity

Rademacher functions will not be an element of \mathcal{R}_k , unless they are all the same Rademacher function.

Figure 2.4 shows the set \mathcal{R}_3 of Rademacher functions, which are used to construct Walsh functions of order eight. In order to build the Walsh functions, we first

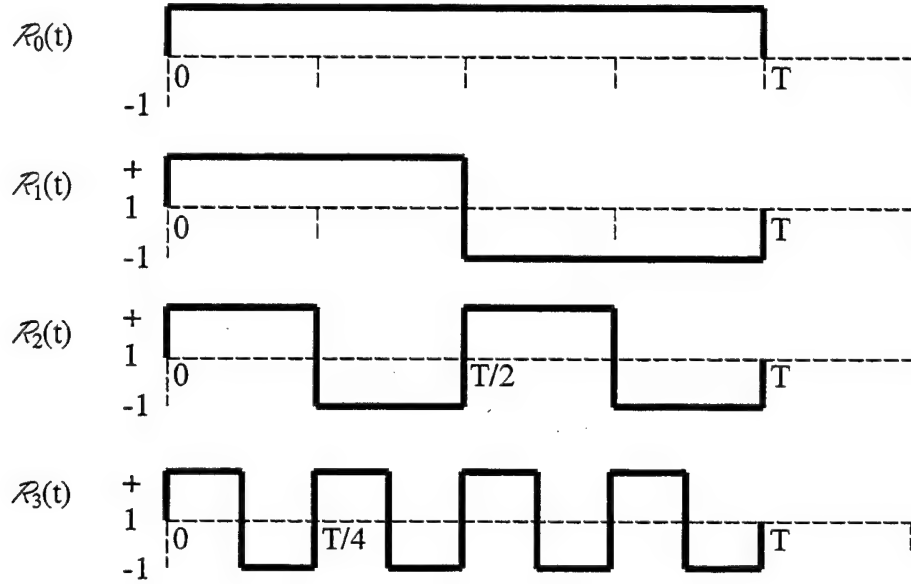


Figure 2.4 Rademacher Functions for $k=3$.

convert the Walsh binary index, Q_i , to a Gray code index [15], denoted G_i . Both types of indices are k -tuples, where $k = \log_2 N$, and are expanded as $Q_i = (q_{i1}, q_{i2}, \dots, q_{ik})$; $G_i = (g_{i1}, g_{i2}, \dots, g_{ik})$. The conversion from Q_i to G_i is accomplished using the following:

$$\begin{aligned} g_{i1} &= q_{i1}, \\ g_{ij} &= q_{ij-1} \oplus q_{ij}. \end{aligned} \tag{2.4}$$

For example, if we wanted to find the Gray Code index for $w_6(t) \in W_8$, we look at the Walsh binary index, $Q_6 = (q_{6,1}q_{6,2}q_{6,3}) = (110)$. Converting bit-by-bit, we find that

$$\begin{aligned} g_{6,1} &= q_{6,1} = 1, \\ g_{6,2} &= q_{6,1} \oplus q_{6,2} = 1 \oplus 1 = 0, \\ g_{6,3} &= q_{6,2} \oplus q_{6,3} = 1 \oplus 0 = 1. \end{aligned}$$

Accordingly, $G_6 = (101)$. Table 2.1 gives the conversions from Q_i to G_i for all $w_j(t) \in W_8$, where $k = 3$.

$Q_i = q_{i,1} \ q_{i,2} \ q_{i,3}$	$G_i = g_{i,1} \ g_{i,2} \ g_{i,3}$
$Q_0 = 0 \ 0 \ 1$	$G_0 = 0 \ 0 \ 0$
$Q_1 = 0 \ 0 \ 1$	$G_1 = 0 \ 0 \ 1$
$Q_2 = 0 \ 1 \ 0$	$G_2 = 0 \ 1 \ 1$
$Q_3 = 0 \ 1 \ 1$	$G_3 = 0 \ 1 \ 0$
$Q_4 = 1 \ 0 \ 0$	$G_4 = 1 \ 1 \ 0$
$Q_5 = 1 \ 0 \ 1$	$G_5 = 1 \ 1 \ 1$
$Q_6 = 1 \ 1 \ 0$	$G_6 = 1 \ 0 \ 1$
$Q_7 = 1 \ 1 \ 1$	$G_7 = 1 \ 0 \ 0$

Table 2.1 Gray Code Index Conversion for $k = 3$.

Using the Gray code index, we can now construct a set Walsh functions of any order $N = 2^k$, using a set of Rademacher functions of order $k+1$, by applying the following:

$$w_i(t) = \begin{cases} \prod_{\substack{j=1 \\ g_{i,j} \neq 0}}^k \mathcal{R}_{k+1-j}(t), & i \neq 0, \\ \mathcal{R}_0(t), & i = 0. \end{cases} \quad (2.5)$$

In forming the product in (2.5) for the $i \neq 0$ case, we only select the Rademacher functions that correspond to the non-zero elements of the Gray code index. The construction process defined in (2.5) is accomplished by associating each element of the Gray code index with a non-identity element of \mathcal{R}_k as follows, $g_{i,j} \rightarrow \mathcal{R}_{k+1-j}(t)$. If you consider the Gray code index G_i to be in ascending order according to $j = 1, 2, \dots, k$, then the associated Rademacher functions are paired in descending order as $k-1, \dots, 2, 1, 0$. Table 2.2 shows the association for the case of $k = 3$.

$G_i = g_{i,1} \ g_{i,2} \ g_{i,3}$	$g_{i,1}$	$g_{i,2}$	$g_{i,3}$
$\mathcal{R}_{k+1-j} \in \mathcal{R}_3$	$\mathcal{R}_3(t)$	$\mathcal{R}_2(t)$	$\mathcal{R}_1(t)$

Table 2.2 Association of Gray Code Index with Rademacher Function for $k = 3$.

Using the previous example of $w_6(t) \in W_8$, we know that $G_6 = (101)$. Accordingly,

$$\begin{aligned} w_6(t) &= \mathcal{R}_3(t) \cdot \mathcal{R}_1(t) \\ &= \mathcal{R}_1 \cdot \mathcal{R}_3. \end{aligned}$$

Figure 2.5 shows the two Rademacher waveforms and the resulting Walsh function waveform. It is clear that the product of the Rademacher functions, $\mathcal{R}_1 \mathcal{R}_3$, when multiplied section by section, is the resulting waveform labeled as $w_6(t)$. We see that this waveform also has six zero crossings, which defines $w_6(t)$.

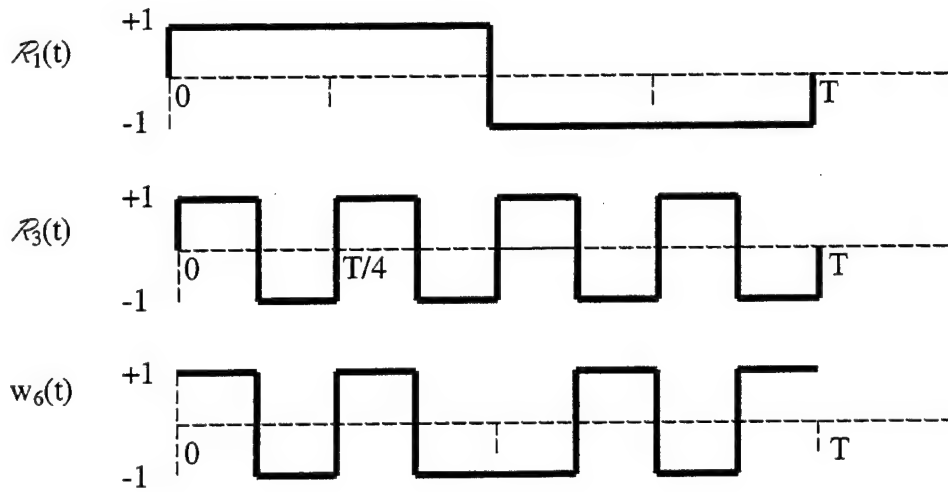


Figure 2.5 Building $w_6(t)$ as a Product of Rademacher Functions.

We have described how to go about generating Walsh functions from a set of Rademacher functions, but a more powerful fact is that **any** finite product of integer powers of Rademacher functions results in a Walsh function [17]. We can select any combination (with replacement) of Rademacher functions from the set \mathcal{R}_k , and their product will still be a Walsh function from the set W_N of order $N = 2^k$. This is clear when you consider that even powers of Rademacher functions are unity, and odd powers of Rademacher functions are the equal to the original function:

$$(\mathcal{R}_n)^i = \begin{cases} \mathcal{R}_n, & \text{for } i \text{ odd} \\ \mathcal{R}_0 = 1, & \text{for } i \text{ even} \end{cases}, \quad (2.6)$$

since for $i = 2k + 1$ (odd for $k = 0, 1, 2, \dots$),

$$(\mathcal{R}_n)^i = (\mathcal{R}_n)^{2k+1} = \mathcal{R}_n \cdot (\mathcal{R}_n)^{2k} = \mathcal{R}_n \cdot (\mathcal{R}_n^2)^k,$$

but

$$(\mathcal{R}_n(t))^2 = (\mathcal{R}_1(2^{n-1}t))^2 = (\mathcal{R}_1(\tau))^2 = \mathcal{R}_0(t) = \mathcal{R}_0 = 1,$$

so

$$(\mathcal{R}_n)^i = \mathcal{R}_n \cdot (\mathcal{R}_n^2)^k = \mathcal{R}_n \cdot (\mathcal{R}_0)^k = \mathcal{R}_n \cdot \mathcal{R}_0 = \mathcal{R}_n,$$

and for $i = 2k$ (even for $k = 0, 1, 2, \dots$),

$$(\mathcal{R}_n)^i = (\mathcal{R}_n)^{2k} = (\mathcal{R}_n^2)^k = (\mathcal{R}_0)^k = \mathcal{R}_0 = 1.$$

Furthermore, when considering a set of Rademacher functions, \mathcal{R}_k , there are **exactly** $N = 2^k$ unique products as defined in (2.5), which correspond directly to the N Walsh functions that we seek to build. Table 2.3 shows the correspondence between the

Walsh function $w_i(t)$	Walsh index $\mathcal{Q}_i = \{q_{i1}, q_{i2}, \dots, q_{ik}\}$	Gray Code Index $G_i = \{g_{i1}, g_{i2}, \dots, g_{ik}\}$	Products $\mathcal{R}_m \mathcal{R}_n \dots$
$w_0(t)$	$\overbrace{(00 \dots 00)}^k$	$\overbrace{(00 \dots 00)}^k$	\mathcal{R}_0
$w_1(t)$	$(00 \dots 01)$	$(00 \dots 01)$	\mathcal{R}_1
$w_2(t)$	$(00 \dots 10)$	$(00 \dots 11)$	$\mathcal{R}_1 \mathcal{R}_2$
$w_3(t)$	$(00 \dots 11)$	$(00 \dots 10)$	\mathcal{R}_2
...
$w_{N-1}(t)$	$(11 \dots 11)$	$(10 \dots 00)$	\mathcal{R}_k

Table 2.3 Walsh Functions from Rademacher Functions.

Walsh functions of order N and the products of Rademacher functions. As shown above, other possible combinations of Rademacher functions that repeat elements are not unique (e.g., $\mathcal{R}_1\mathcal{R}_2\mathcal{R}_2 = \mathcal{R}_1$ since, $\mathcal{R}_2\mathcal{R}_2 = 1$.)

The last three sections have been concerned with defining, describing and motivating the Walsh functions and their component Rademacher functions. With this foundation, we can now address closure as a final step in proving the algebraic group properties. We will prove that the product of any two Walsh functions is not only contained in the set, but is a predictable member function as described by (2.1).

4. The Closure Property of Walsh Functions

The set of Walsh functions of order N forms an algebraic group under multiplication provided that the properties of closure, associativity, identity, and inverse, as defined in Section II.A.1, are satisfied. By defining the individual Walsh functions $w_j(t) \in W_N$ in terms of their component Rademacher functions by (2.5), we can prove that the set is closed. That is, for any $w_i(t), w_j(t) \in W_N$, $w_i(t) \cdot w_j(t) \in W_N$.

Clearly, if either of the Walsh functions $w_i(t)$ or $w_j(t)$ are the identity, $w_0(t)$, then closure holds. Accordingly, we let

$$w_i(t) = \prod_{\substack{m=1 \\ g_{i,m} \neq 0}}^k \mathcal{R}_{k+1-m}(t),$$

where $w_i(t) \neq w_0(t)$ has a corresponding Gray Code index of $G_i = (g_{i1}, g_{i2}, \dots, g_{ik})$, and

$$w_j(t) = \prod_{\substack{p=1 \\ g_{j,p} \neq 0}}^k \mathcal{R}_{k+1-p}(t),$$

where $w_j(t) \neq w_0(t)$ has a corresponding Gray Code index of $G_j = (g_{j1}, g_{j2}, \dots, g_{jk})$.

Then their product is

$$w_i(t) \cdot w_j(t) = \prod_{\substack{m=1 \\ g_{i,m} \neq 0}}^k \mathcal{R}_{k+1-m}(t) \cdot \prod_{\substack{p=1 \\ g_{j,p} \neq 0}}^k \mathcal{R}_{k+1-p}(t).$$

When we combine the factors, any Rademacher function, \mathcal{R}_{k+1-n} , that is in one but not both of the two products will survive: $(g_{i,n} = 1 \wedge g_{j,n} = 0) \vee (g_{i,n} = 0 \wedge g_{j,n} = 1)$ implies that \mathcal{R}_{k+1-n} survives the multiplication. If a Rademacher function is in both product terms, it will not be in the final product term since $\mathcal{R}_{k+1-n}^2 = \mathcal{R}_0 = 1$. Accordingly, $(g_{i,n} = 1 \wedge g_{j,n} = 1)$ implies that \mathcal{R}_{k+1-n} will not be in the final product. Clearly, if a Rademacher function is in neither product term, $(g_{i,n} = 0 \wedge g_{j,n} = 0)$, it will not be in the final product.

Accordingly, the combination of the two products can be rewritten as one product using a new Gray code index, call it $G_r = (g_{r1}, g_{r2}, \dots, g_{rk})$, where the $g_{r,n} = 1$ if \mathcal{R}_{k+1-n} survives the multiplication of products, and $g_{r,n} = 0$ if \mathcal{R}_{k+1-n} does not survive, or was never a part of the one of the products. From the description above, we know that $g_{r,n} = g_{i,n} \oplus g_{j,n}$ for $n=1, 2, \dots, k$. We continue with $w_i(t) \cdot w_j(t)$ as follows:

$$\begin{aligned} w_i(t) \cdot w_j(t) &= \prod_{\substack{m=1 \\ g_{i,m} \neq 0}}^k \mathcal{R}_{k+1-m}(t) \cdot \prod_{\substack{p=1 \\ g_{j,p} \neq 0}}^k \mathcal{R}_{k+1-p}(t) \\ &= \prod_{\substack{n=1 \\ g_{r,n} \neq 0}}^k \mathcal{R}_{k+1-n}(t), \end{aligned}$$

where $g_{r,n} = g_{i,n} \oplus g_{j,n}$. We recognize this final form to be that of the Walsh function $w_r(t)$, whose Gray Code index is determined by

$$G_r = (g_{r1}, g_{r2}, \dots, g_{rk}) = (g_{i1} \oplus g_{j1}, g_{i2} \oplus g_{j2}, \dots, g_{ik} \oplus g_{jk}) = G_i \oplus G_j.$$

Since $w_i(t) \cdot w_j(t) = w_r(t) \in W_N$, we know that the set of Walsh functions, W_N , is closed under multiplication. Furthermore, since Gray coding as defined by (2.4) is a one-to-one and onto mapping, we see that

$$G_r = G_i \oplus G_j \leftrightarrow Q_r = Q_i \oplus Q_j,$$

which proves (2.1).

B. WALSH ORTHOGONALITY EXTENDED

The most significant property of the Walsh functions as applied to the DS-CDMA cellular problem is that of orthogonality between two different Walsh functions. That is for any $w_j(t), w_k(t) \in W_N$,

$$\int_0^T w_j(t) w_k(t) dt = \begin{cases} 0 & \text{if } j \neq k \\ T & \text{if } j = k \end{cases}$$

In some applications, the integral of a product of three Walsh functions is of interest. Just

what is the value of the integral, $\int_0^T w_i(t) w_j(t) w_k(t) dt$? The answer depends on the

relationship between the three Walsh functions in the integral. For example, if

$w_i(t) w_j(t) = w_k(t)$, that is $Q_i \oplus Q_j = Q_k$, then we know that

$$\int_0^T w_i(t) w_j(t) w_k(t) dt = \int_0^T w_k(t) w_k(t) dt = T.$$

On the other hand, by closure we know that if $w_i(t) w_j(t) \neq w_k(t)$, it is equal to **some** Walsh function, call it $w_l(t)$, where $l \neq k$. Accordingly,

$$\int_0^T w_i(t) w_j(t) w_k(t) dt = \int_0^T w_l(t) w_k(t) dt = 0. \quad (2.7)$$

The fact that the integral value depends on the relationship of the Walsh functions is a troublesome result in the analysis of cellular BER performance because it requires a high degree of specificity, when the result needs to be applicable to the general case. Furthermore, when applying Walsh functions to eliminate intracell interference, the product of three Walsh functions integrated over the bit period needs to be (predictably) zero.

One way around this problem is to eliminate some of the Walsh functions from the complete set W_N , and force (2.7), which we use to define extended orthogonality, to be true for every Walsh function in the reduced set \tilde{W}_N . The downside to this solution is that by eliminating Walsh functions from our useable set, we reduce the number of mobile users that can be accommodated in the cell. This is because each user requires a unique Walsh function; when we have assigned all Walsh functions in the useable set, no new users may join. Accordingly, we need to ensure that (2.7) is enforced while eliminating the *minimum* number of Walsh functions and thereby maximizing the size of

our new set, \tilde{W}_N . Furthermore, once we determine the size of the maximum set, we will propose a method of generating the optimal reduced set, \tilde{W}_N .

1. Walsh Subgroups of Order Four

We went to great lengths in Section II.A to prove the closure property for the set of Walsh functions W_N . In order to extend the orthogonality of the Walsh functions as described by (2.7), we need the opposite of closure for our reduced set \tilde{W}_N . That is, for all the (non-identity) Walsh functions in our reduced set $w_i(t), w_j(t) \in \tilde{W}_N$, we need to ensure that their product is not in the reduced set,

$$w_i(t) \cdot w_j(t) \notin \tilde{W}_N, \quad (2.8)$$

for $i \neq j$ and $i, j \neq 0$.

To accomplish (2.8) we need only ensure that there are no Walsh subgroups of order four contained in the reduced set. A subgroup, S of a group G , is a subset of G which is a group itself (as defined in Section II.A.1). The subgroup is under the same operation as G , but restricted to the elements of S . Any Walsh subgroup, \mathcal{W}_{ijk} , of order four is of the form

$$\mathcal{W}_{ijk} = \{w_0(t), w_i(t), w_j(t), w_k(t)\}.$$

The subgroup is required to have the multiplicative identity element $w_0(t)$ and the elements of the subgroup must satisfy the inverse and closure properties. Since each element serves as its own inverse, it is the closure property that distinguishes subgroups

of order four from simple four-member subsets of W_N . In order to satisfy the closure property for subgroups, the three non-identity elements $w_i(t), w_j(t), w_k(t) \in \mathcal{W}_{ijk}^{\mathcal{P}}$ must satisfy the following:

$$w_i(t) \cdot w_j(t) = w_k(t), \quad (2.9)$$

which implies that $Q_i \oplus Q_j = Q_k$. Accordingly, we know that the product of any two of the non-identity elements results in the third non-identity element, since by modulo 2 addition, $Q_i \oplus Q_j = Q_k$ means $Q_i \oplus Q_k = Q_j$ and $Q_j \oplus Q_k = Q_i$, which imply $w_i(t)w_k(t) = w_j(t)$ and $w_j(t)w_k(t) = w_i(t)$, respectively. Furthermore, we know the product of any element, $w_s(t) \in \mathcal{W}_{ijk}^{\mathcal{P}}$ in the subgroup, with the identity is itself, namely $w_s(t)w_0(t) = w_s(t)$. Finally, the product of any $w_s(t) \in \mathcal{W}_{ijk}^{\mathcal{P}}$ with itself is the identity element, $w_s(t)w_s(t) = w_0(t)$. Therefore, (2.9) guarantees closure for a subgroup $\mathcal{W}_{ijk}^{\mathcal{P}} \subset W_N$ of order four.

Consequently, we see that any two non-identity Walsh functions uniquely determine the final non-identity member of the subgroup. For an example, let us look at a subgroup of order four from W_8 . For ease of notation, we will use Walsh sequences, $\mathbf{W}_8 = \{w_0, w_1, w_2, w_3, w_4, w_5, w_6, w_7\}$. We know that the identity is always a member of the subgroup. If we select w_1 , and w_6 as the first two non-identity members, the third is uniquely determined by $w_1 \oplus w_6$, or by $Q_1 \oplus Q_6 = Q_7$, as shown in Table 2.4.

	Q_j	w_j
w_1	(001)	(00001111)
w_6	(110)	(01011010)
w_7	(111)	(01010101)

Table 2.4 Building the subgroup $\{w_0, w_1, w_6, w_7\}$.

If we had started with any of the two non-identity elements in the above subgroup (e.g., w_1, w_7 or w_6, w_7), we would have produced the same subgroup, since any sum of the two non-identity elements results in the third. Continuing this process for all the pairs of non-identity elements results in a complete listing of all the subgroups of order four from W_8^* :

$$\begin{aligned} &\{w_0 w_1 w_2 w_3\}, \{w_0 w_1 w_4 w_5\}, \{w_0 w_1 w_6 w_7\}, \\ &\{w_0 w_2 w_4 w_6\}, \{w_0 w_2 w_5 w_7\}, \\ &\{w_0 w_3 w_4 w_7\}, \{w_0 w_3 w_5 w_6\} \end{aligned}$$

We will now consider the elimination of Walsh functions in order to break all subgroups of order four from the full set, W_N .

2. A Reduced Set of Walsh Functions

When forming our reduced set \tilde{W}_N of Walsh functions from the full set W_N , we want to break all subgroups of order four contained in W_N in order to satisfy (2.8). Our resulting set will no longer be an algebraic group but will extend the orthogonality property to satisfy (2.7). So exactly how many subgroups of order four are there in W_N ?

We can see from Section II.B.1 that for W_8 , there are seven subgroups of order four. We built those subgroups using all possible combinations of two non-identity elements, and eliminating redundant subgroups. The number of different combinations of size k from a set n is the binomial coefficient defined by

$$\binom{n}{k} \triangleq \frac{n!}{k!(n-k)!}.$$

Since there are $N-1$ non-identity elements for W_N , and we are generating combinations of two elements, the number of possible subgroups is based the binomial coefficient,

$$\binom{N-1}{2} = \frac{(N-1)(N-2)}{2}. \quad (2.10)$$

The binomial coefficient (2.10) determines how many different pairs of non-identity elements are contained in the set W_N , or \mathbf{W}_N^\bullet . For any single subgroup of order four, say $\mathcal{W}_{ijk} = \{w_0 w_i w_j w_k\}$, we know there are three pairs of non-identity elements, namely $w_i w_j$, $w_j w_k$, and $w_i w_k$. In effect, each subgroup is counted three times by (2.10). We scale (2.10) accordingly and determine that for any set of Walsh functions, W_N , order N , there are \mathcal{J}_N subgroups of order four, which is defined by

$$\mathcal{J}_N = \frac{1}{3} \binom{N-1}{2}. \quad (2.11)$$

Applying (2.11) to \mathbf{W}_8^\bullet , we calculate the number of subgroups of order four to be

$$\mathcal{J}_8 = \frac{7 \cdot 6}{3 \cdot 2} = 7, \text{ which is how many we found.}$$

Now that we know how many subgroups of order four are associated with W_N , namely \mathcal{S}_N , we can start eliminating Walsh functions from W_N to form the reduced set \tilde{W}_N . To demonstrate, we fall back to the subgroups of W_8 . In order to simplify the notation of the subgroups, we will use a tri-graph to represent each subgroup of order four. The tri-graph will reflect the Walsh index of the three non-identity members as shown for W_8 :

$$\begin{array}{ccc} \underbrace{\{w_0 w_1 w_2 w_3\}}_{1-2-3} & \underbrace{\{w_0 w_1 w_4 w_5\}}_{1-4-5} & \underbrace{\{w_0 w_1 w_6 w_7\}}_{1-6-7} \\ \\ \underbrace{\{w_0 w_2 w_4 w_6\}}_{2-4-6} & \underbrace{\{w_0 w_2 w_5 w_7\}}_{2-5-7} & \underbrace{\{w_0 w_3 w_4 w_7\}}_{3-4-7} & \underbrace{\{w_0 w_3 w_5 w_6\}}_{3-5-6} \end{array}$$

We will now begin to eliminate Walsh functions from W_8 , in order to form one possible reduced set \tilde{W}_8 . As we will see, the \tilde{W}_N are not unique. Further, the number of elements that must be eliminated to break all \mathcal{S}_N subgroups varies depending upon how the elements eliminated are chosen, and how that choice relates to past choices. For example, the elimination of w_1 from W_8 results in the following subgroups being broken :

$$1-2-3, 1-4-5, \text{ and } 1-6-7$$

and leaves unbroken:

$$2-4-6, 2-5-7, 3-4-7, \text{ and } 3-5-6$$

The elimination of w_2 results in the following additional subgroups being broken:

$$2-4-6 \text{ and } 2-5-7$$

and leaves unbroken:

3-4-7 and 3-5-6

The elimination of w_3 results in the final subgroups being broken:

3-4-7 and 3-5-6

By eliminating w_1 , w_2 , and w_3 from W_8^* , we effectively created a reduced set of Walsh functions $\tilde{W}_8 = \{w_0, w_4, w_5, w_6, w_7\}$, which has none of the subgroups of order four remaining from W_8^* , and accordingly satisfies (2.7). In this instance we only had to eliminate three elements to break all subgroups, leaving five useable Walsh functions with extended orthogonality. However, eliminating a different set of three elements may or may not break all the subgroups.

Let us begin again with W_8^* , and this time eliminate w_5 , w_6 , and w_7 . The elimination of w_5 results in the following subgroups being broken :

1-4-5, 2-5-7, and 3-5-6

and leaves unbroken:

1-2-3, 1-6-7, 2-4-6, and 3-4-7

The elimination of w_6 results in the following additional subgroups being broken:

1-6-7 and 2-4-6

and leaves unbroken:

1-2-3 and 3-4-7

The elimination of w_7 results in the subgroup 3-4-7 being broken, but leaves the subgroup 1-2-3 unbroken. In order to break all subgroups we must select one more element to eliminate from the yet-unbroken subgroup. If we choose to eliminate w_3 , we

end up with a different reduced set, $\tilde{W}_8 = \{w_0, w_1, w_2, w_4\}$ which satisfies (2.7), but has one fewer elements. It is clear that we need to determine the minimum number of eliminations necessary to break all subgroups, thereby generating a maximal set \tilde{W}_N , and develop a method to generate that maximal set consistently.

3. Maximizing the Reduced Set \tilde{W}_N

We saw that three channel eliminations, $(w_1 w_2 w_3)$, could produce the desired reduced set in the case of W_8^\bullet . On the other hand, **any** three channel eliminations, $((w_5 w_6 w_7)$, for example) did not produce the desired reduced set, since they did not break all the subgroups of order four in W_8^\bullet . The difference between these two scenarios is that the choices in the first case maximize the number of subgroups eliminated with each choice, while the second set of choices did not. Accordingly, we need to determine how many subgroups are broken with each elimination, if we assume we can maximize the number broken with each channel elimination.

If we consider the elements of W_N , we can see that each non-identity element $w_j(t) \in W_N$ is contained in exactly $N/2 - 1$ subgroups. This is because any single element $w_i(t)$ can combine with the remaining $N-2$ elements in only $N-2$ combinations $w_i(t)w_j(t)$ where $i \neq j$ and $i, j \neq 0$ as follows:

$$\left. \begin{array}{c} w_i(t)w_1(t) \\ w_i(t)w_2(t) \\ \vdots \\ w_i(t)w_j(t) \\ \vdots \\ w_i(t)w_k(t) \\ \vdots \\ w_i(t)w_{N-1}(t) \end{array} \right\} N-2.$$

Moreover, any one subgroup \mathcal{W}_{ijk} is counted twice as $w_i(t)w_j(t)$ and $w_i(t)w_k(t)$.

Accordingly, we see that $w_i(t)$ is contained in exactly $\frac{1}{2}(N-2) = N/2 - 1$ subgroups.

For at least the first channel elimination, $N/2 - 1$ subgroups are broken. For subsequent channel eliminations, the maximum number of subgroups broken depends on how many channel eliminations have already taken place. In order to better describe the channel elimination process, let

e_i = the Walsh channel removed on the i th elimination,

\mathcal{E}_i = the set of subgroups which contain the eliminated channel e_i ,

ℓ_i = the number additional subgroups broken by the i th channel elimination,

\mathcal{R}_i = the total number of unique subgroups broken by the first i channel eliminations, i.e., $\mathcal{R}_i = \sum_{j=1}^i \ell_j$,

\mathcal{Z}_i = the set of subgroups yet unbroken after the i th elimination, and

$||S||$ = the number of elements in the set S .

We know that when the number of broken subgroups equals the total number of subgroups, i.e., $\mathcal{R}_i = \mathcal{J}_N$, all subgroups have been broken, and we have a valid reduced set, \tilde{W}_N . Let us use \mathbf{W}_8 once again to illustrate the above notation, and demonstrate how to maximize the number of subgroups broken with each channel elimination.

Choosing $e_1 = w_5$ results in the following :

$$\begin{aligned}\mathcal{E}_1 &= \{1-4-5, 2-5-7, 3-5-6\} \text{ (all the subgroups containing } w_5), \\ \ell_1 &= 3, \\ \mathcal{B}_1 &= \ell_1 = 3, \text{ and} \\ \mathcal{U}_1 &= \{1-2-3, 1-6-7, 2-4-6, 3-4-7\}.\end{aligned}$$

For the first elimination we know that $\ell_1 = \llbracket \mathcal{E}_1 \rrbracket$, since all of the subgroups in \mathcal{E}_1 are newly broken. We can see that the set of unbroken subgroups, \mathcal{U}_1 , has four elements. We want to choose the next channel elimination such that the maximum number of subgroups are broken. We see that for **any** choice $e_2 = w_j \in \{w_1 w_2 w_3 w_4 w_6 w_7\}$ exactly two subgroups will be broken.

Choosing $e_2 = w_6$ results in

$$\begin{aligned}\mathcal{E}_2 &= \{1-6-7, 2-4-6, \cancel{3-5-6}\} \quad \cancel{3-5-6} \rightarrow \text{previously eliminated}, \\ \ell_2 &= 2, \\ \mathcal{B}_2 &= \ell_1 + \ell_2 = 5, \text{ and} \\ \mathcal{U}_2 &= \{1-2-3, 3-4-7\}.\end{aligned}$$

Since we already broke the subgroup 3-5-6, by eliminating w_5 , it is not counted in ℓ_2 , the number of subgroups broken by e_2 . Examination of \mathcal{U}_2 reveals that, in order to break the maximum number of remaining subgroups, we must next choose $e_3 = w_3$. This choice breaks the remaining two subgroups. Any other selection for e_3 breaks only one subgroup. Accordingly, choose $e_3 = w_3$, which results in

$$\begin{aligned}\mathcal{E}_3 &= \{1-2-3, 3-4-7, \cancel{3-5-6}\}, \\ \ell_3 &= \ell_2 = 2, \\ \mathcal{B}_3 &= \ell_1 + \ell_2 + \ell_3 = \ell_1 + 2\ell_2 = 7, \text{ and} \\ \mathcal{U}_3 &= \emptyset.\end{aligned}$$

We see that for the case of \mathbf{W}_8^* , eliminating a minimum of $N/2 - 1 = 3$ channels broke all $\mathcal{S}_8 = 7$ subgroups. If we had not optimized our choices, it could have taken more than $N/2 - 1$ eliminations, but we can find no way to eliminate all subgroups with less than $N/2 - 1$ eliminations. We have found that this result holds true in general for W_N , as we will sketch below.

For the general case, W_N , we assume that with each channel elimination we break the maximum possible number of subgroups as shown for \mathbf{W}_8^* . Furthermore, we observe the following properties:

$$\begin{aligned} \llbracket \mathcal{E}_i \rrbracket &= N/2 - 1 = \ell_i \text{ for all } i, \text{ and} \\ \llbracket \mathcal{E}_i \cap \mathcal{E}_j \rrbracket &= 1, \text{ since } e_i \text{ and } e_j \text{ are both contained in at most one subgroup.} \end{aligned}$$

For $i=1$, eliminate any e_1 . Since \mathcal{E}_1 contains $N/2 - 1$ elements which represent distinct subgroups, then we know that $\ell_1 = \llbracket \mathcal{E}_1 \rrbracket = N/2 - 1$ subgroups are broken by eliminating e_1 .

For $i=2$, eliminate any e_2 . The set \mathcal{E}_2 also contains $N/2 - 1$ elements. However, there is one element in \mathcal{E}_2 that was contained in \mathcal{E}_1 , since one of the subgroups must have both e_1 and e_2 . Accordingly, we know that $\ell_2 = \llbracket \mathcal{E}_2 \rrbracket - \llbracket \mathcal{E}_1 \cap \mathcal{E}_2 \rrbracket = (N/2 - 1) - 1 = N/2 - 2$ additional subgroups have been broken. A total of $\mathcal{B}_2 = \ell_1 + \ell_2$ subgroups have been broken after the second elimination.

For $i=3$, eliminate e_3 such that $\llbracket \mathcal{E}_1 \cap \mathcal{E}_2 \cap \mathcal{E}_3 \rrbracket = 1$ in order to maximize the number of broken subgroups. Accordingly, we know that

$$\ell_3 = [\mathcal{E}_3] - [\mathcal{E}_1 \cap \mathcal{E}_3] - [\mathcal{E}_2 \cap \mathcal{E}_3] + [\mathcal{E}_1 \cap \mathcal{E}_2 \cap \mathcal{E}_3] = \left(\frac{N}{2} - 1\right) - 2 + 1 = \frac{N}{2} - 2 = \ell_2,$$

and

$$\mathcal{B}_3 = \ell_1 + \ell_2 + \ell_3 = \ell_1 + 2\ell_2.$$

For $i=4$, eliminate e_4 such that $[\mathcal{E}_1 \cap \mathcal{E}_2 \cap \mathcal{E}_4] = [\mathcal{E}_1 \cap \mathcal{E}_3 \cap \mathcal{E}_4] = [\mathcal{E}_2 \cap \mathcal{E}_3 \cap \mathcal{E}_4] = 0$

in order to maximize the number of broken subgroups. Accordingly, we know that

$$\ell_4 = [\mathcal{E}_4] - [\mathcal{E}_1 \cap \mathcal{E}_4] - [\mathcal{E}_2 \cap \mathcal{E}_4] - [\mathcal{E}_3 \cap \mathcal{E}_4] = \left(\frac{N}{2} - 1\right) - 3 = \frac{N}{2} - 4,$$

and

$$\mathcal{B}_4 = \ell_1 + 2\ell_2 + \ell_4.$$

If we carry on in this manner, maximizing the number of broken subgroups with each channel elimination, we find that after $i = N/2 - 1$ channel eliminations, every subgroup in W_N is broken. The final \mathcal{B}_i , which we will call \mathcal{B}_f , at channel elimination $f = i = N/2 - 1$, is of the form

$$\mathcal{B}_f = \ell_1 + 2\ell_2 + 4\ell_4 + 8\ell_8 + 16\ell_{16} + \dots + \frac{N}{4}\ell_{\frac{N}{4}} \quad (2.12)$$

$$= \sum_j j \hat{\ell}_j, \quad j = 2^0, 2^1, 2^2, \dots, 2^{k-2} = \frac{N}{4},$$

where $\hat{\ell}_j = \frac{N}{2} - j$.

The pattern represented in (2.12) can be observed in Table 2.5 for W_{16} .

1-2-3	1-4-5	1-6-7	1-8-9	1-10-11	1-12-13	1-14-15
2-4-6	2-5-7	2-8-10	2-9-11	2-12-14	2-13-15	
3-4-7	3-5-6	3-8-11	3-9-10	3-12-15	3-13-14	
4-8-12	4-9-13	4-10-14	4-11-15			
5-8-13	5-9-12	5-10-15	5-11-14			
6-8-14	6-9-15	6-10-12	6-11-13			
7-8-15	7-9-14	7-10-13	7-11-12			

Table 2.5 The Set of Subgroups of Order Four for W_{16} .

In the table, we have organized the entire set of subgroups for W_{16} according to the smallest non-identity Walsh index in the subgroup. There are exactly $\mathcal{S}_{16} = \frac{1}{3}\binom{15}{2} = 35$ subgroups of order four in W_{16} . If we let $e_i = \omega_i$ for $i = 1, 2, \dots, N/2 - 1$, we successively eliminate each row in the Table 2.5, which means we have broken all the subgroups in the i th row with the i th elimination. The number of subgroups broken with the i th elimination, ℓ_i , is the number of elements in the i th row. For W_{16} ,

$$\begin{aligned}
\ell_1 &= 7 = N/2 - 1, \\
\ell_2 &= \ell_3 = 6 = N/2 - 2, \\
\ell_4 &= \ell_5 = \ell_6 = \ell_7 = 4 = N/2 - 4, \\
\mathcal{B}_1 \dots \mathcal{B}_7 &= \ell_1 + 2\ell_2 + 4\ell_4 = 35 = \mathcal{S}_{16}.
\end{aligned}$$

Accordingly, after $i = N/2 - 1 = 7$ channel eliminations, all $\mathcal{S}_{16} = 35$ subgroups are broken.

We now show that for a set of Walsh functions, W_N , of any order N , $i = N/2 - 1$ channel eliminations break all \mathcal{S}_N subgroups. Using (2.12), we know that

$$\mathcal{B}_f = \ell_1 + 2\ell_2 + 4\ell_4 + 8\ell_8 + 16\ell_{16} + \dots + \frac{N}{4}\ell_{\frac{N}{4}}$$

$$= \sum_j j\hat{\ell}_j, \quad j = 2^0, 2^1, 2^2, \dots, 2^{k-2} = \frac{N}{4},$$

where $\hat{\ell}_j = N/2 - j$. If we let

$$j = 2^n, \quad \text{and} \\ q_n = N/2 - 2^n,$$

then

$$\begin{aligned} \mathcal{B}_f &= \sum_j j\ell_j = \sum_{n=0}^{k-2} 2^n q_n = \sum_{n=0}^{k-2} 2^n \left(\frac{N}{2} - 2^n \right), \\ &= \frac{N}{2} \sum_{n=0}^{k-2} 2^n - \sum_{n=0}^{k-2} 2^{2n}, \quad (\text{geometric series}) \\ &= \frac{N}{2} \left(\frac{1-2^{k-1}}{1-2} \right) - \left(\frac{1-4^{k-1}}{1-4} \right) = \frac{N}{2} (2^{k-1} - 1) - \left(\frac{(2^{k-1})^2 - 1}{3} \right), \\ &= \frac{N^2 - 3N - 2}{6}, \\ &= \frac{1}{3} \left(\frac{(N-1)(N-2)}{2} \right) = \frac{1}{3} \binom{N-1}{2} = \mathcal{S}_N. \end{aligned}$$

We have found that $N/2 - 1$ channel eliminations is the minimum number required to break all subgroups of order four contained in W_N . Accordingly, we know that the remaining $N/2 + 1$ elements from W_N will make up the maximum set \tilde{W}_N . That is, any maximum set \tilde{W}_N will have exactly $N/2 + 1$ member functions. In the next section, we will propose a method for generating this maximum set \tilde{W}_N .

4. Generating a Maximum Set \tilde{W}_N

We saw in Section II.B.3 that, by eliminating the first $N/2 - 1$ channels from W_N , we can break all the subgroups of order four from W_N and generate a maximum set, \tilde{W}_N , which has extended orthogonality as defined by (2.7) for all elements in the set. By eliminating the first $N/2 - 1$ channels our reduced set looks like

$$\tilde{W}_N = \{w_0(t), w_{\frac{N}{2}}(t), w_{\frac{N}{2}+1}(t), \dots, w_{N-1}(t)\}.$$

For example,

$$\tilde{W}_{16} = \{w_0(t), w_8(t), w_9(t), w_{10}(t), w_{11}(t), w_{12}(t), w_{13}(t), w_{14}(t), w_{15}(t)\}.$$

While this method of generating \tilde{W}_N certainly works, it is rather rigid. We need a method that is more adaptable to various uses. For example, we may want to devise a valid reduced set \tilde{W}_N which includes specific Walsh functions that are already in use, or permanently assigned for various control functions. We may want to use the reduced set concept when assigning Walsh functions from the full set, as a best effort design. That is, to the maximum extent possible, the Walsh functions in use, or assigned, are from a valid reduced set, which can be adapted as channels (functions) are added or dropped, until user capacity exceeds that which can be supported by the reduced set.

There are many possible combinations of $N/2 + 1$ Walsh functions which form a valid reduced set \tilde{W}_N . We submit the following more flexible method of generating the set \tilde{W}_N :

- ❖ Start by selecting non-identity channels from the pool of channels from W_N to include in \tilde{W}_N . The identity, $w_0(t)$, will always a member of the maximum set, and therefore will not be considered during our selection process.
- ❖ Each new channel selected dictates the channels that must be discarded. At each step the newly selected channel is multiplied by each of the previously selected members of \tilde{W}_N to determine which elements from the pool of undesignated channels must be discarded.
- ❖ After exactly $N/2 - 1$ **distinct** channels have been discarded (eliminated), all undesignated channels from the pool are included in \tilde{W}_N .
- ❖ If the number of channels eliminated exceeds the target number $N/2 - 1$ during step i , go back and re-select another channel to keep for step i using the repeat final choice procedure detailed below.
- ❖ To repeat the final choice, select a channel that is the product of a previously kept channel with a previous discarded channel, $w_s(t) = w_k(t)w_d(t) \notin \tilde{W}_N$ which is not already a channel chosen to be kept.

For example, we will build a valid reduced set \tilde{W}_{16}^* from W_{16}^* as depicted in Table 2.6.

Step	Pool of undesignated channels	Keep in $\tilde{\mathbf{W}}_{16}$	Discard e_i	$\llbracket \{\cup e_i\} \rrbracket$
1	$\left\{ \begin{array}{l} w_1 w_2 w_3 w_4 w_5 w_6 w_7 w_8 \\ w_9 w_{10} w_{11} w_{12} w_{13} w_{14} w_{15} \end{array} \right\}$	w_1	none	0
2	$\left\{ \begin{array}{l} w_2 w_3 w_4 w_5 w_6 w_7 w_8 \\ w_9 w_{10} w_{11} w_{12} w_{13} w_{14} w_{15} \end{array} \right\}$	w_3	$w_1 \oplus w_3 = w_2$	1
3	$\left\{ \begin{array}{l} w_4 w_5 w_6 w_7 w_8 \\ w_9 w_{10} w_{11} w_{12} w_{13} w_{14} w_{15} \end{array} \right\}$	w_7	$w_1 \oplus w_7 = w_6$ $w_3 \oplus w_7 = w_4$	3
4	$\{w_5 w_8 w_9 w_{10} w_{11} w_{12} w_{13} w_{14} w_{15}\}$	w_{11}	$w_{10} w_8 w_{12}$	6
X	$\{w_5 w_9 w_{13} w_{14} w_{15}\}$	w_{14}	$w_{15} w_{13} w_9 w_5$	10
5	$\{w_5 w_9 w_{13} w_{14} w_{15}\}$	w_5	$w_4 w_6 w_2 w_{14}$	7
6	$\{w_9 w_{13} w_{15}\} \rightarrow$	$w_9 w_{13} w_{15}$	none	7

Table 2.6 Building a Valid Reduced Set $\tilde{\mathbf{W}}_{16}$.

For Step 1, all of \mathbf{W}_{16} is in the pool of undesignated channels from which we can choose. We select w_1 to keep in $\tilde{\mathbf{W}}_{16}$, and need not discard any channels. In Step 2, we take w_1 out of the pool of undesignated channels, and choose to keep w_3 . The choice of w_3 dictates that $w_2 = w_1 \oplus w_3$ must be discarded or eliminated. At this point the total number of channels eliminated, $\llbracket \{\cup e_i\} \rrbracket$, is 1. We continue in this manner until Step 5. In our first attempt at Step 5, we selected a channel to keep which resulted in too many

channel eliminations. We require $|\{\cup e_i\}| = N/2 - 1 = 7$ channel eliminations for \mathbf{W}_{16}^* in order to build a maximum set $\tilde{\mathbf{W}}_{16}^*$. Our choice in the initial Step 5 results in a total of 10 channel eliminations. Accordingly, we ignore that result and select $\mathbf{w}_5 = \mathbf{w}_1 \oplus \mathbf{w}_4$ using the repeat-final-choice procedure. This time we achieve the desired total number of channel eliminations, and accordingly build a maximum set $\tilde{\mathbf{W}}_{16}^* = \{\mathbf{w}_0 \mathbf{w}_1 \mathbf{w}_3 \mathbf{w}_5 \mathbf{w}_7 \mathbf{w}_9 \mathbf{w}_{11} \mathbf{w}_{13} \mathbf{w}_{15}\}$. It turns out that in Step 5 any other selection from \mathbf{w}_5 , \mathbf{w}_9 , \mathbf{w}_{13} , or \mathbf{w}_{15} , other than \mathbf{w}_{14} would have produced the desired result of one new channel elimination, namely \mathbf{w}_{14} . That is, any one of the following versions of Step 5 could be used.

5v3	$\{\mathbf{w}_5 \mathbf{w}_9 \mathbf{w}_{13} \mathbf{w}_{14} \mathbf{w}_{15}\}$	\mathbf{w}_9	$\mathbf{w}_8 \mathbf{w}_{10} \mathbf{w}_{14} \mathbf{w}_2$	7
5v4	$\{\mathbf{w}_5 \mathbf{w}_9 \mathbf{w}_{13} \mathbf{w}_{14} \mathbf{w}_{15}\}$	\mathbf{w}_{13}	$\mathbf{w}_{12} \mathbf{w}_{14} \mathbf{w}_{10} \mathbf{w}_6$	7
5v5	$\{\mathbf{w}_5 \mathbf{w}_9 \mathbf{w}_{13} \mathbf{w}_{14} \mathbf{w}_{15}\}$	\mathbf{w}_{15}	$\mathbf{w}_{14} \mathbf{w}_{12} \mathbf{w}_8 \mathbf{w}_4$	7

Let us consider the set-building process from the point of view of maximizing the subgroups broken with each elimination as we did in Section II.B.3. After Step 4 is complete, the only subgroups that had not yet been broken were, 1-14-15, 3-13-14, 5-11-14, 7-9-14. It is obvious that channel 14 needs to be eliminated, and choosing any other element to keep besides \mathbf{w}_{14} gives us the desired result.

To show that we have broken all 35 subgroups of order four from \mathbf{W}_{16}^* , we have reorganized the subgroups (from Table 2.5) around the channels eliminated, e_i , and in the order in which they were eliminated, as shown in Table 2.7.

$e_1 = w_2$	1-2-3	2-4-6	2-5-7	2-8-10	2-9-11	2-12-14	2-13-15
$e_2 = w_6$	1-6-7	3-5-6	6-8-14	6-9-15	6-10-12	6-11-13	
$e_3 = w_4$	1-4-5	3-4-7	4-8-12	4-9-13	4-10-14	4-11-15	
$e_4 = w_{10}$	1-10-11	3-9-10	5-10-15	7-10-13			
$e_5 = w_8$	1-8-9	3-8-11	5-8-13	7-8-15			
$e_6 = w_{12}$	1-12-13	3-12-15	5-9-12	7-11-12			
$e_7 = w_{14}$	1-14-15	3-13-14	5-11-14	7-9-14			

Table 2.7 The Set of Subgroups of Order Four for W_{16} .

The fact that we eliminated e_1 through e_7 proves that we have broken all subgroups in Table 2.5, one row at a time. Accordingly we have generated a valid maximum set, \tilde{W}_{16} , whose elements have extended orthogonality as defined by (2.7).

In Section II.B we have introduced the notion of extended orthogonality for Walsh functions. We have detailed the Walsh function subgroups of order four, as they play a key role in extending the orthogonality property. We have determined how many subgroups of order four exist, and how many channel eliminations are required to break those subgroups for a set of Walsh functions of order N to generate a reduced set of Walsh functions. Finally, we have proposed an adaptable method of generating a valid reduced set of Walsh functions that guarantees the maximum number of channels from the original set.

C. AUTOCORRELATION OF WALSH FUNCTIONS

The autocorrelation function of a deterministic signal, such as a signal built using Walsh functions, quantifies the degree of similarity between the signal and a time shifted version of itself. In contrast to a non-deterministic signal, the autocorrelation function of a deterministic signal can be evaluated precisely. In this section we will examine the autocorrelation functions for the Walsh functions, and consider the average autocorrelation for a set of Walsh functions.

1. Autocorrelation of Walsh Functions

In order to explore the autocorrelation function of Walsh functions, we will extend our definition and consider each Walsh function to be periodic with a period of T , which is consistent with their use in practice. On the forward channel, each mobile user is assigned a specific Walsh function. The data destined for that mobile user is encoded by successively applying the user's entire Walsh function to each data bit. Accordingly, the Walsh function is periodic, with period $T = \text{bit duration} = 1/\text{bit rate}$, and we will see that the corresponding autocorrelation functions are also periodic with period T .

We define the normalized autocorrelation function, $\alpha_i(u)$, for any periodic Walsh function $w_i(t) \in W_N$ by

$$\alpha_i(u) = \frac{1}{T} \int_0^T w_i(t) w_i(t-u) dt. \quad (2.13)$$

Although (2.13) does not shed much light on the Walsh autocorrelation functions, we can generate them numerically based on this definition. Let us look at the set of Walsh functions W_8 , depicted in Figure 2.6, and the corresponding autocorrelation functions, $\alpha_i(u)$, shown in Figure 2.7.

As shown in Figure 2.7, there are only $N/2+1=5$ unique autocorrelation functions, since $\alpha_1(u) = \alpha_2(u)$, $\alpha_3(u) = \alpha_4(u)$, $\alpha_5(u) = \alpha_6(u)$. In spread spectrum systems we define chip duration, T_c , to be the bit duration divided by the number of chips per bit, $T_c = T/N$. If we consider the Walsh functions of order eight, to be periodic with period T , and chip duration, $T_c = T/8$, we see in Figure 2.7 that, $w_2(t) = w_1(t - 2T_c)$ and $w_4(t) = w_3(t - T_c)$ and $w_5(t) = w_6(t - 2T_c)$. Since a time shift in a deterministic signal has no effect on its autocorrelation function, the Walsh functions that are time-shifted versions of each other have identical autocorrelation functions. We found that, for this reason, in any set W_N of Walsh functions there are exactly $N/2+1$ unique autocorrelation functions. They are

$$\alpha_0(u), \alpha_{N-1}(u) \text{ and } \alpha_{2i}(u) = \alpha_{2i-1}(u), \text{ for } i = 1, 2, \dots, N/2 - 1.$$

Furthermore, the autocorrelation functions of Walsh functions are piecewise continuous and linear within the intervals $t \in (nT_c, (n+1)T_c)$ for $n = 0, \pm 1, \pm 2, \dots$

While these observations regarding the autocorrelation functions for Walsh functions are interesting, they are not helpful in generating a representative autocorrelation function for a set of Walsh functions. Accordingly, we will develop an average autocorrelation function for a set of Walsh functions, W_N .

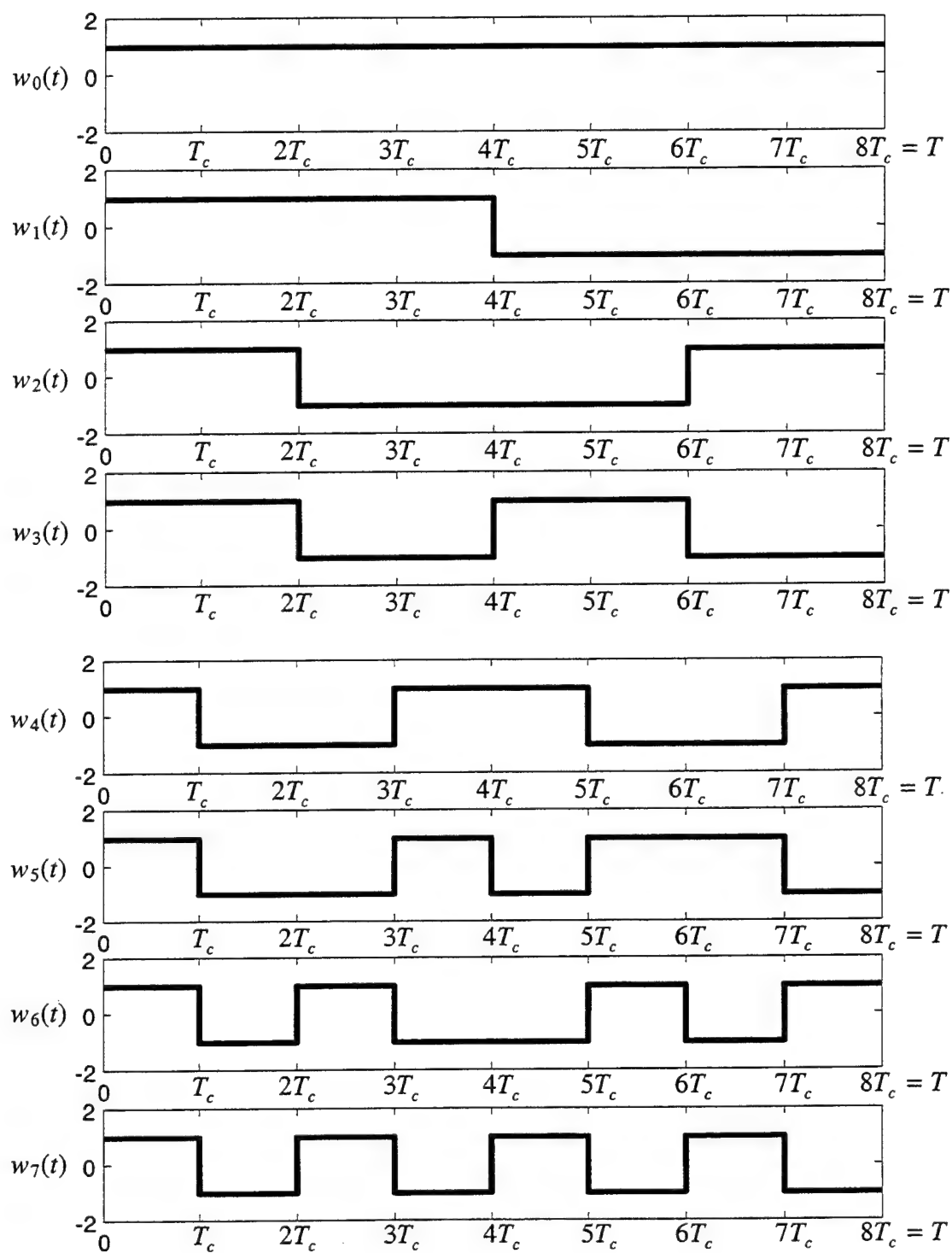


Figure 2.6 Set of Walsh Functions of Order Eight.

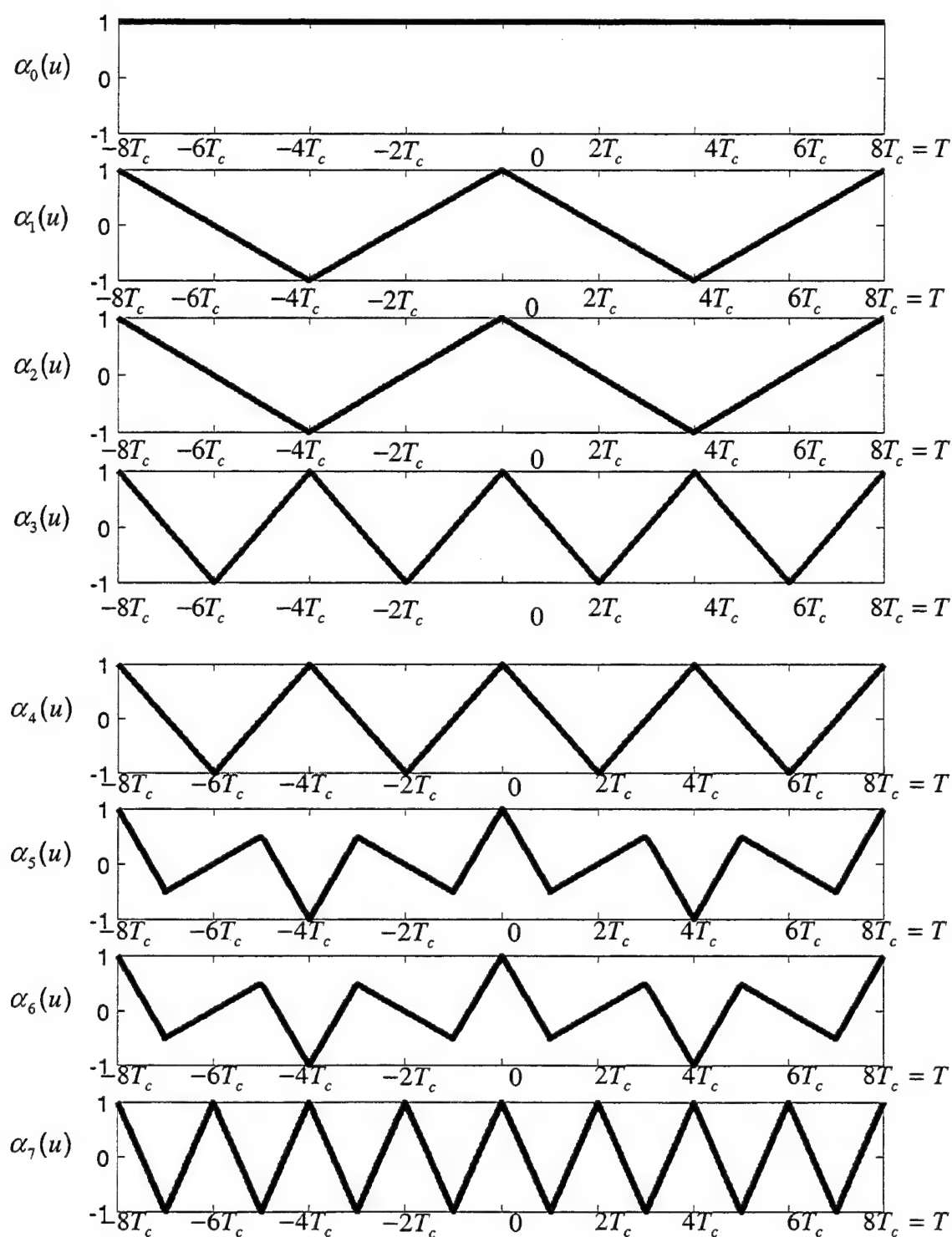


Figure 2.7 Set of Autocorrelation Functions for W_8 .

2. Average Autocorrelation of a Set of Walsh Functions W_N

We define the average autocorrelation function, $\mathcal{A}_N(u)$, for a set W_N of Walsh functions by

$$\mathcal{A}_N(u) = \frac{1}{N} \sum_{i=0}^{N-1} \alpha_i(u),$$

where $\alpha_i(u)$ is defined by (2.13). If we generate $\mathcal{A}_8(u)$ from the Walsh functions in the set W_8 , we get the average autocorrelation function depicted in Figure 2.8.

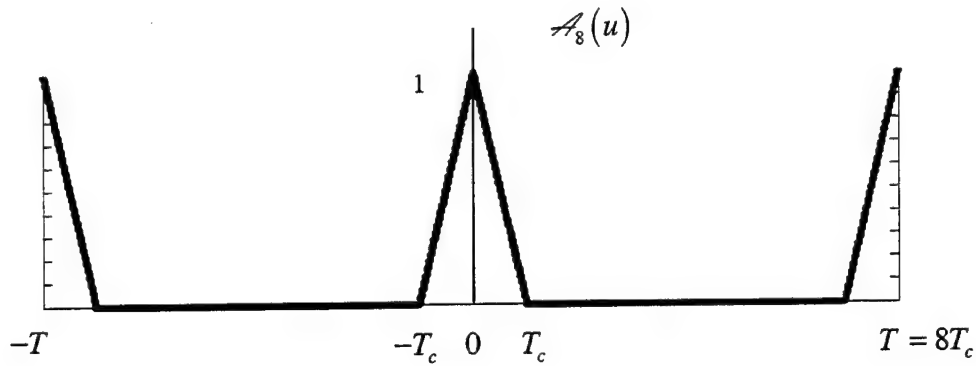


Figure 2.8 Average Autocorrelation Function, $\mathcal{A}_8(u)$ for the Set W_8 .

We find that the form of $\mathcal{A}_8(u)$ is similar to the form of the autocorrelation function for a random binary signal. A random binary signal is generated from an infinitely long binary random sequence in which the bits are independent and identically distributed random variables. The resulting normalized autocorrelation function for the random binary signal is defined after [15] by

$$\beta(u) = \begin{cases} 1 - \frac{|u|}{T_c}, & |u| \leq T_c \\ 0, & \text{otherwise} \end{cases} \quad (2.14)$$

This autocorrelation function is an aperiodic function, since it is generated from an aperiodic signal. On the other hand, we know that $\mathcal{A}_8(u)$ is periodic with period T .

Consequently, $\mathcal{A}_8(u)$ can be described analytically over the period $(-T/2, T/2)$ by

$$\mathcal{A}_8(u) = \begin{cases} 1 - \frac{|u|}{T_c}, & |u| \leq T_c \\ 0, & T_c < |u| \leq \frac{T}{2} = \frac{8T_c}{2} = 4T_c \end{cases}.$$

We found experimentally that this result can be generalized to a set of Walsh functions of any order N . That is, the average normalized autocorrelation function, $\mathcal{A}_N(u)$, can be written analytically over one period as follows:

$$\mathcal{A}_N(u) = \begin{cases} 1 - \frac{|u|}{T_c}, & |u| \leq T_c \\ 0, & T_c < |u| \leq \frac{T}{2} = \frac{NT_c}{2} \end{cases}, \quad (2.15)$$

where $\mathcal{A}_N(u)$ is periodic with period $T = NT_c$, as depicted in Figure 2.9.

Accordingly, we now have an analytical expression representing the average autocorrelation function, $\mathcal{A}_N(u)$, of a set W_N of Walsh functions. We will also consider another average autocorrelation function which excludes the identity Walsh function, $w_0(t)$, from the average. In a DS-CDMA system, the identity Walsh function is typically reserved for the pilot tone, and as such it cannot be assigned to a mobile user.

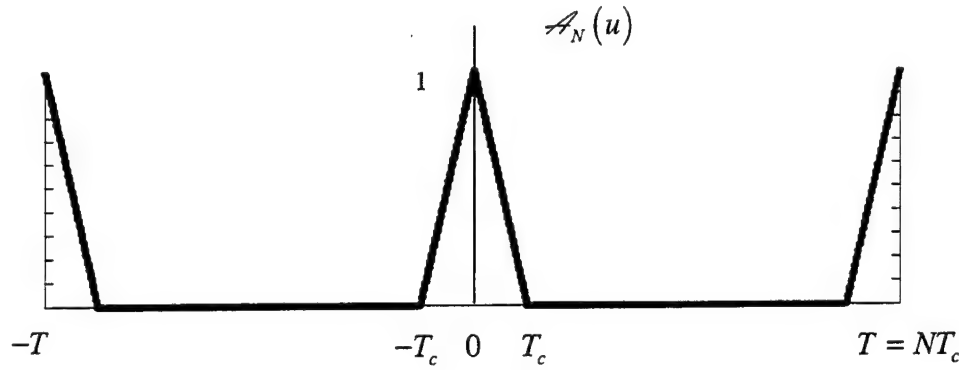


Figure 2.9 Average Autocorrelation Function, $\mathcal{A}_N(u)$ for the Set W_N .

Therefore, to determine the average autocorrelation function of Walsh functions that may be assigned to mobile users, we should exclude $w_0(t)$ and consequently $\alpha_0(u)$ from the set, and develop a different average autocorrelation function. Let us define the revised function, $\tilde{\mathcal{A}}_N(u)$, which represents the average autocorrelation of the non-identity Walsh functions, by

$$\tilde{\mathcal{A}}_N(u) = \frac{1}{N-1} \sum_{i=1}^{N-1} \alpha_i(u).$$

We return to W_8 for an example, and find the revised average autocorrelation function, $\tilde{\mathcal{A}}_8(u)$, to be as shown in Figure 2.10. The form of $\tilde{\mathcal{A}}_8(u)$ is similar to the autocorrelation function for pseudorandom or pseudo-noise (PN) signal. PN signals are generated by PN sequences, which are maximal length deterministic sequences. The PN signals are periodic with period $\hat{N}T_c$, where \hat{N} is the length of the PN sequence that generated the PN signal. When PN signals are used in conjunction with Walsh functions for DS-CDMA, $\hat{N} \gg N$. We will discuss PN sequences in more detail in Chapter 3.

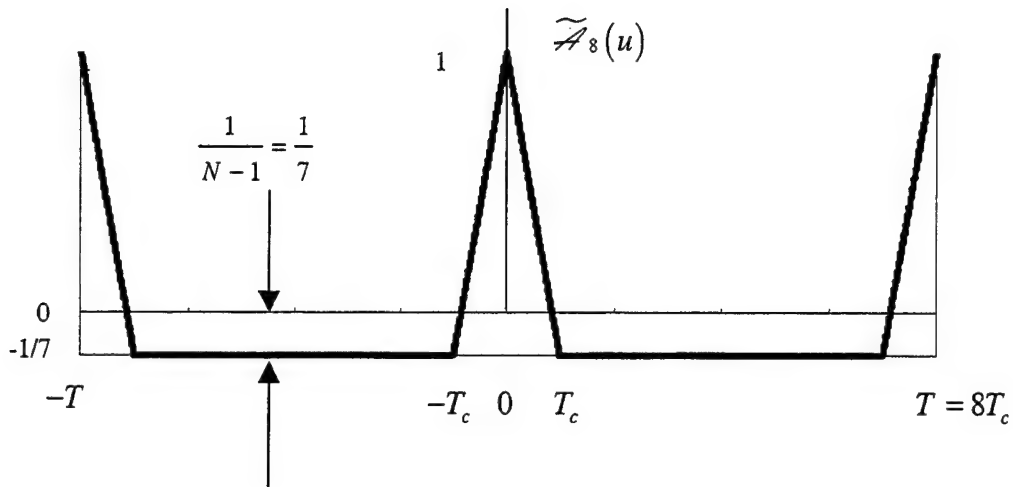


Figure 2.10 Revised Average Autocorrelation Function, $\widetilde{\mathcal{A}}_s(u)$ for the Set W_8 .

The autocorrelation function for a PN signal, $\mathcal{B}_{PN}(u)$, as adapted from [15], is defined by

$$\mathcal{B}_{PN}(u) = \begin{cases} 1 - \frac{|u|}{T_c} \left(1 + \frac{1}{\widehat{N}} \right), & 0 \leq |u| \leq T_c \\ -\frac{1}{\widehat{N}}, & T_c < |u| \leq \frac{\widehat{N}T_c}{2} \end{cases}, \quad (2.16)$$

which is periodic with period $\widehat{N}T_c$ as shown in Figure 2.11.

When the length of the generating PN sequence gets large, $\widehat{N} \rightarrow \infty$, the autocorrelation function of the PN signal approaches the autocorrelation function of a binary random signal, $\mathcal{B}_{PN}(u) \rightarrow \beta(u)$. Accordingly, for simplicity, the autocorrelation function of the PN signal, $\mathcal{B}_{PN}(u)$, is often modeled as the autocorrelation function of the random binary signal, $\beta(u)$, as in [18].

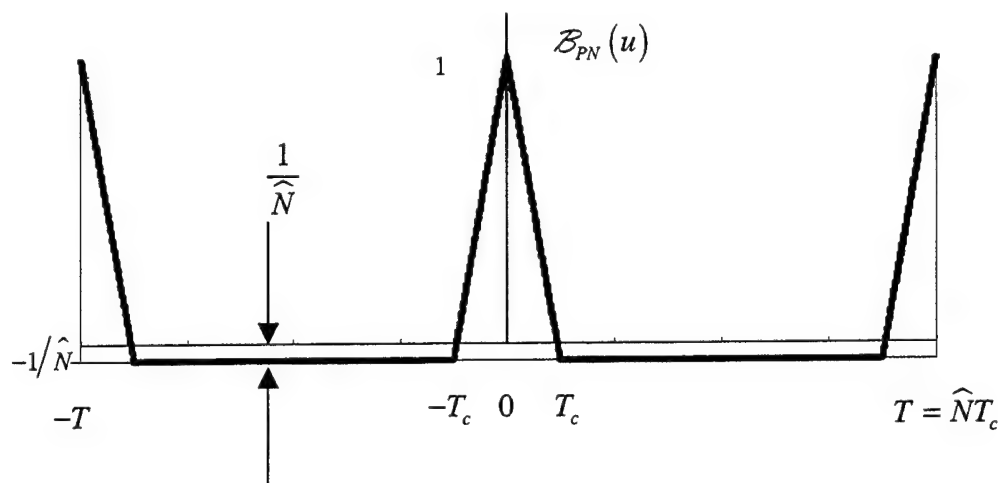


Figure 2.11 Autocorrelation Function of a PN Signal.

We found that for our revised average autocorrelation function, $\tilde{\mathcal{A}}_N(u)$, the form of $\tilde{\mathcal{A}}_s(u)$ held true for the general case as shown in Figure 2.12.

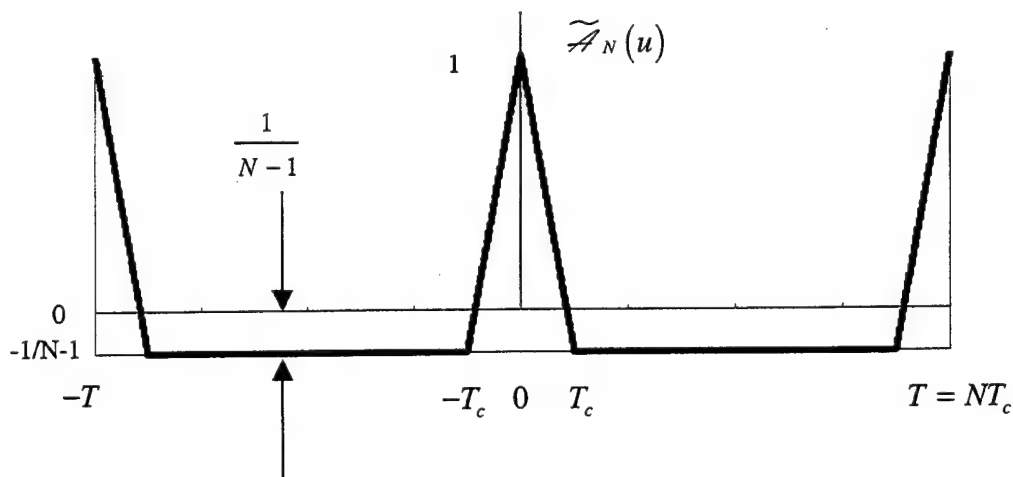


Figure 2.12 Revised Average Autocorrelation Function, $\tilde{\mathcal{A}}_N(u)$ for a Set W_N .

Accordingly, our revised average autocorrelation function for the set of non-identity Walsh functions can be described analytically by

$$\widetilde{\mathcal{A}}_N(u) = \begin{cases} 1 - \frac{|u|}{T_c} \left(1 + \frac{1}{N-1}\right), & 0 \leq |u| \leq T_c \\ \frac{-1}{N-1} & T_c < |u| \leq \frac{NT_c}{2} \end{cases} \quad (2.17)$$

We now have two possible analytical autocorrelation functions, $\mathcal{A}_N(u)$ and $\widetilde{\mathcal{A}}_N(u)$, which can represent the average autocorrelation functions of a set of Walsh functions, W_N .

D. SUMMARY

In Chapter 2, we investigated the definition and properties of Walsh functions as they apply to DS-CDMA systems. We explored the algebraic group properties of a set W_N of Walsh functions over multiplication, and we proved the closure property using Rademacher functions as building blocks for the Walsh functions. We introduced the notion of **extending** the orthogonality property for Walsh functions to ensure that the integral of any three non-identity Walsh functions over the bit interval is identically zero. We developed a method to generate a reduced set \widetilde{W}_N of Walsh functions, which extends orthogonality while maximizing the number of Walsh functions in the reduced set. We explored the autocorrelation functions for a set of Walsh functions, and developed two average autocorrelation functions, $\mathcal{A}_N(u)$ and $\widetilde{\mathcal{A}}_N(u)$, for the set of Walsh functions and the set of non-identity Walsh functions, respectively.

III. FORWARD CHANNEL MODEL

The forward channel in a DS-CDMA cellular system is the channel that carries traffic from the base station to mobile users, as depicted in Figure 3.1. As we transition from cellular systems that carry principally voice traffic to systems that must support data-type traffic at high data rates, the forward channel becomes more critical. For example, when mobile users attempt to **download** large amounts of data, it will be the forward channel that carries this data. In Chapter III, we will set up a channel model for a typical DS-CDMA cellular system, complete with channel fading and shadowing effects built into the model. We will ultimately characterize the input to a mobile user's receiver, which includes the traffic intended for the user, together with the noise and interference terms.

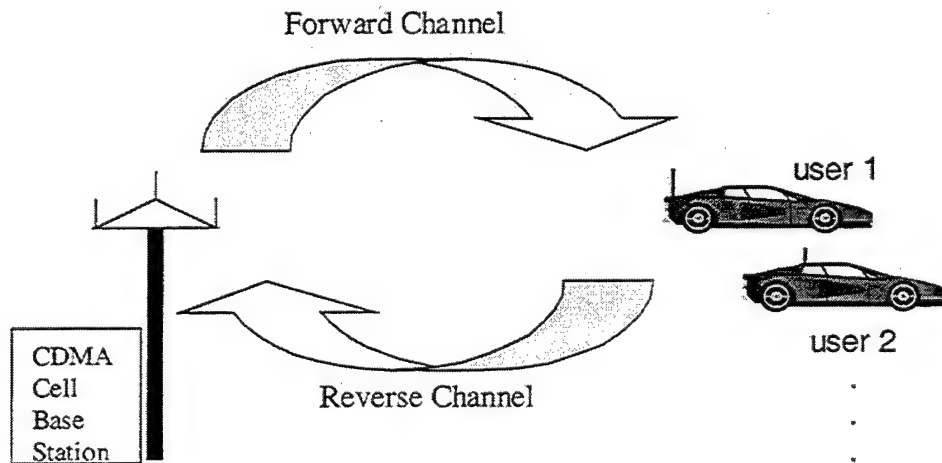


Figure 3.1 CDMA Forward and Reverse Channels.

Analysis of the forward channel is complicated by two facts; the channel is wireless and our users are **mobile**. These conditions give rise to reflection, diffraction, and scattering of the forward signal. The average signal power received by the mobile user on the forward channel varies as a function of distance from the base station and the terrain between them. Additionally, as the forward signal emanates (in many directions) from the base station, it reflects off buildings, trees, mountains, etc... It arrives at the receiver of the mobile user via many paths of different lengths, and at various signal strengths. The sum of the multipath signals changes as the user moves. This results in rapid fluctuations in the strength of the received signal.

Large-scale propagation models, which are used to determine the average signal power received, are discussed in Section III.B. Small-scale fading models, which characterize the rapid fluctuations of the received signal due to multipath effects, are also discussed in Section III.B. We combine these effects into our model in Section III.C.

A. BUILDING THE DS-CDMA FORWARD SIGNAL

We model the cells in our CDMA system as hexagons, using a basic seven-cell cluster as depicted in Figure 3.2. The hexagon in the center represents the cell of primary interest in our analysis. We assume that a base station is located in the center of each cell. We let K represent the total number of mobile users (or active channels) in the center cell, while K_i is the total number of mobile users (or active channels) in the adjacent cells $i = 1, 2, \dots, 6$.

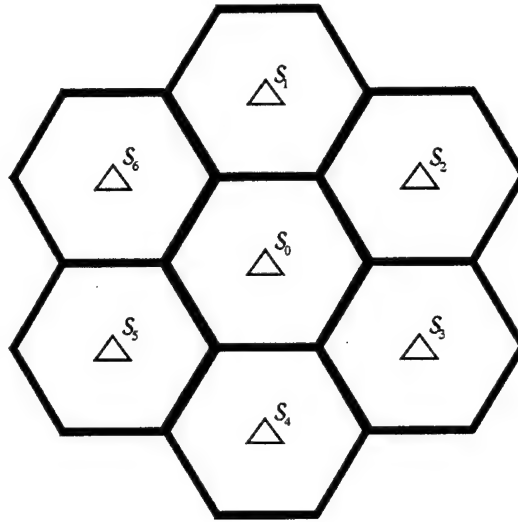


Figure 3.2 Seven-Cell Cluster.

In this section, we will describe the forward signal $S(t)$ that is transmitted by the base station in each cell. It includes the traffic for all active channels in the cell. The power spectrum of this traffic has been spread by a factor of N and then BPSK modulated. From the perspective of an individual mobile user in the center cell, the transmitted signal, $S_0(t)$, contains traffic intended for him plus intracell interference. Traffic that is received by a mobile user and that is intended for other users in his cell constitutes intracell interference. In addition, the signals $S_i(t)$ ($1 \leq i \leq 6$) transmitted by the base stations in the six adjacent cells constitute intercell interference to our mobile user. Intercell interference, or co-channel interference, is the traffic intended for mobile users in the adjacent cells.

1. Direct Sequence Spread Spectrum CDMA

Spectrum Spreading is a process in which the power spectrum of a base band signal is spread over a specified transmission bandwidth. Traditionally, spectrum spreading has been done for a variety of reasons, including anti-jam and low probability of intercept. In DS-CDMA cellular systems, we use spread spectrum as a multiple access technique. That is, given a finite bandwidth for many users in the cellular system, we optimize the use of the bandwidth by spreading all the user traffic across the band using PN spreading signals and Walsh functions for orthogonal cover. Each user despreads only that traffic which is destined for him, using the cell's PN signal and his unique Walsh function.

In Direct Sequence Spread Spectrum (DSSS) systems the spreading of the information signal is accomplished by multiplying the information signal by a spreading signal. We will represent the information signal intended for mobile user k as $b_k(t)$, which is a stream of binary data or bits, where $b_k(t) \in \{\pm 1\}$ within each bit interval of duration T . We spread each data bit by a factor of N using a spreading signal whose chip duration is $T_c = T/N$.

To illustrate spectrum spreading, we can spread a random binary signal, $x(t) \rightarrow x_s(t)$, by a factor of N . As shown in Figure 3.3, the main lobe of the power spectral density is spread by a factor of N , while the magnitude at $\mathcal{P}_{x_s}(0)$ is reduced by a factor of $1/N^2$. We used a spreading factor of $N=2$ to develop Figure 3.3, while our DS-CDMA system will use a spreading factor of 128.

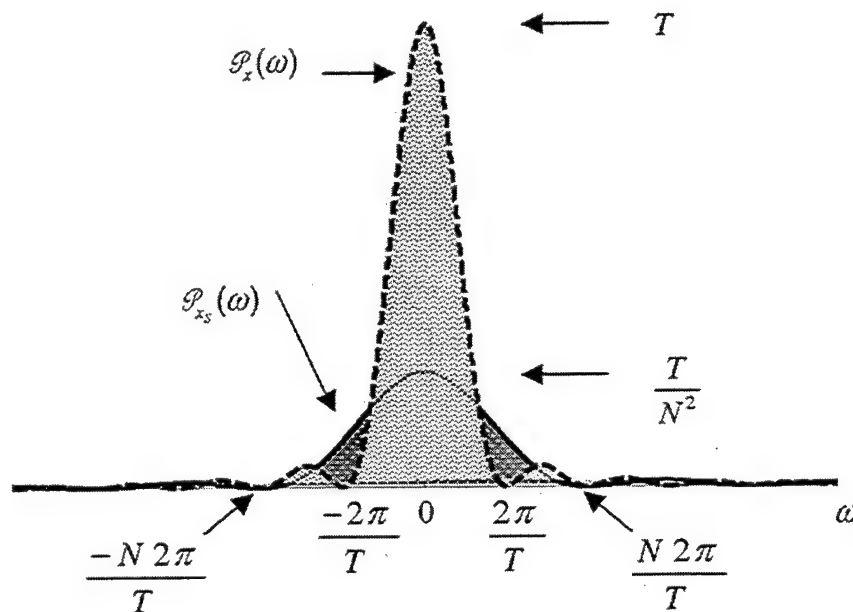


Figure 3.3 Spectrum Spreading by a factor of N .

As an example of DSSS, let us look at the first two bits of data intended for mobile user 3. We will use the two-bit binary sequence (01) whose waveform as shown in Figure 3.4 is defined by

$$b_3(t) = \begin{cases} 1, & t \in (0, T) \\ -1, & t \in (T, 2T) \end{cases}$$

To demonstrate direct sequence spectrum spreading we can use a Walsh function $w_3(t) \in W_4$, to spread $b_3(t)$ by a factor of $N=4$. By multiplying each bit in $b_3(t)$ by $w_3(t)$, we get a spread signal that represents the information in $b_3(t)$ as shown in Figure 3.4. The new signal has a power spectrum that is spread by a factor of four.

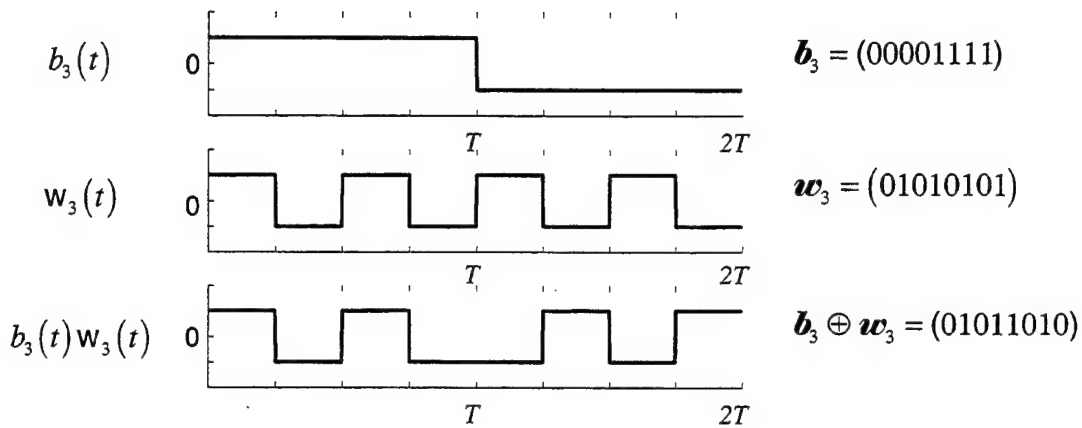


Figure 3.4 Direct Sequence Spreading of Two Data Bits Using $w_3(t)$.

We can also view the spreading process in terms of sequences, if we expand our information sequence so that each information bit is represented by $N=4$ elements in the information sequence. That is, $\mathbf{b}_3 = (00001111)$. The spreading process of the sequence \mathbf{b}_3 is a simple modulo two addition with the Walsh sequence, \mathbf{w}_3 , as depicted in Figure 3.5.

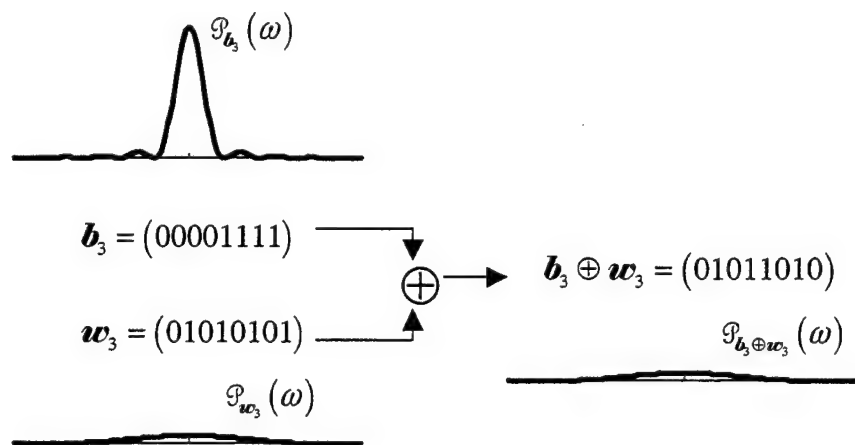


Figure 3.5 Spectrum Spreading of Two Data Bits Using Sequences.

In DS-CDMA systems, PN signals are used in conjunction with Walsh functions to spread the data signal. In the same manner that Walsh functions combat the intracell interference, the PN signals, to a lesser degree, combat the intercell interference. That is, each base station is assigned a unique PN signal. These PN signals can be made to be orthogonal to one another, but are not necessarily so. A truly random PN signal for each base station would be ideal but impractical, since it must be known to both the base station and all the potential users. Accordingly, we generate PN sequences deterministically from linear feedback shift registers (LFSR).

We represent the PN signal in the center cell as $c(t)$, and adjacent cell PN signals as $c_i(t)$ for $i = 1, 2, \dots, 6$. Since the mobile users in the center cell are not synchronized with base stations in adjacent cells, the use of even orthogonal PN signals does not completely eliminate the intercell interference in the same manner that Walsh functions eliminate intracell interference. However, the use of PN signals does ensure that the intercell traffic, which results in intercell interference, remains spread over the band and minimizes its effect on SNR.

Application of the PN signal also ensures that all of the user channels are spread the same chip duration, $T_c = T/N$. The application of the Walsh function $w_j(t) \in W_N$ alone does not guarantee a spreading factor of N . For example, if we had applied $w_1(t)$ vice $w_3(t)$ to spread data for mobile user 1, where $b_1(t) = b_3(t)$, the spreading would have only been by a factor of two rather than four, as shown in Figure 3.6.

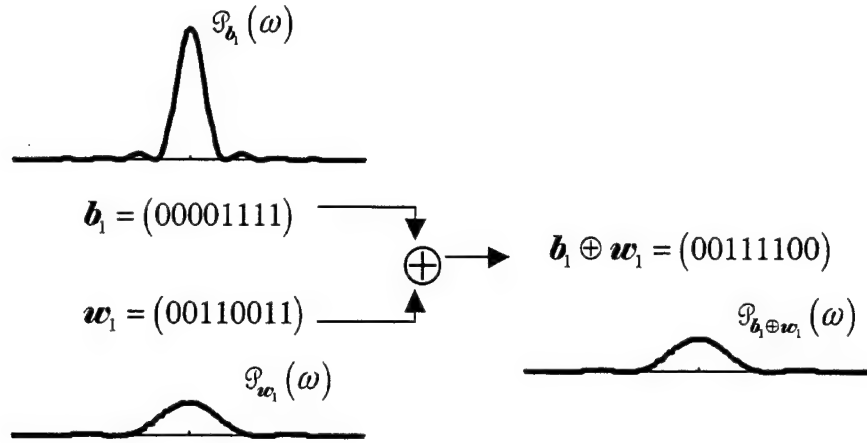


Figure 3.6 Spectrum Spreading of Two Data Bits Using $w_1(t)$.

Accordingly, the use of Walsh functions provides for orthogonal cover for intracell interference, while the PN signal accomplishes the true spreading and minimizes intercell interference.

The baseband spreading and despreading process for one data bit intended for user one in our DS-CDMA systems is depicted in Figure 3.7. We assume synchronization with the base station.

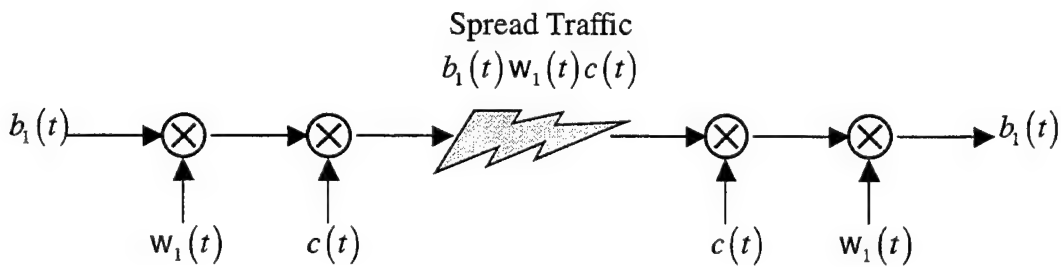


Figure 3.7 DS-CDMA Spreading and Despreading.

We can recover $b_1(t)$ from the spread traffic $b_1(t)w_1(t)c(t)$ because $w_1(t)w_1(t) = 1$ and $c(t)c(t) = 1$.

If we look at the process in terms of sequences, we can build a table which shows the spreading of one bit of information $b_1 = (0000)$, using both the Walsh function, $w_1 = (0011)$, and a PN sequence (for this particular bit interval), $c = (1011)$.

b_1	(0000)
w_1	(0011)
$b_1 \oplus w_1$	(0011)
c	(1011)
$b_1 \oplus w_1 \oplus c$	(1000)

Table 3.1 Spreading of One Information Bit using w_1 and c .

At the receiver, in order to despread the sequence and recover b_1 , we apply the PN and Walsh sequences again as shown in Table 3.2.

$b_1 \oplus w_1 \oplus c$	(1000)
c	(1011)
$b_1 \oplus w_1 \oplus c \oplus c = b_1 \oplus w_1$	(0011)
w_1	(0011)
$b_1 \oplus w_1 \oplus w_1 = b_1$	(0000)

Table 3.2 Despreading of One Information Bit using w_1 and c .

When another user with assigned Walsh function $w_2(t)$, for example, in the center cell, applies the center cell's PN signal and his Walsh function, $c(t)w_2(t)$, to the spread traffic, the output is still spread, as shown in Table 3.3.

$b_I \oplus w_1 \oplus c$	(1000)
c	(1011)
$b_I \oplus w_1 \oplus c \oplus c = b_I \oplus w_1$	(0011)
w_2	(0110)
$b_I \oplus w_1 \oplus w_2$	(0101)

Table 3.3 Application of w_2 to intracell traffic covered with w_1 .

Alternatively, if a user with assigned Walsh function $w_1(t)$ in an adjacent cell $i=6$, for example, received the spread traffic and applied his PN signal and Walsh function, $c_6(t+\tau)w_1(t+\tau)$, the output would also remain spread, $b_I(t)c(t)w_1(t)c_6(t+\tau)w_1(t+\tau)$. Here, τ represents a timing discrepancy due the lack of synchronization between the center cell and adjacent cell $i=6$. In fact, this output would likely be spread even further since the product of nonsynchronous PN signals and/or Walsh functions would contain some pulses with duration less than T_c as shown in Figure 3.8. Therefore the spreading factor would be greater than N , since the spread of the power spectrum is based upon the duration of the smallest pulse.

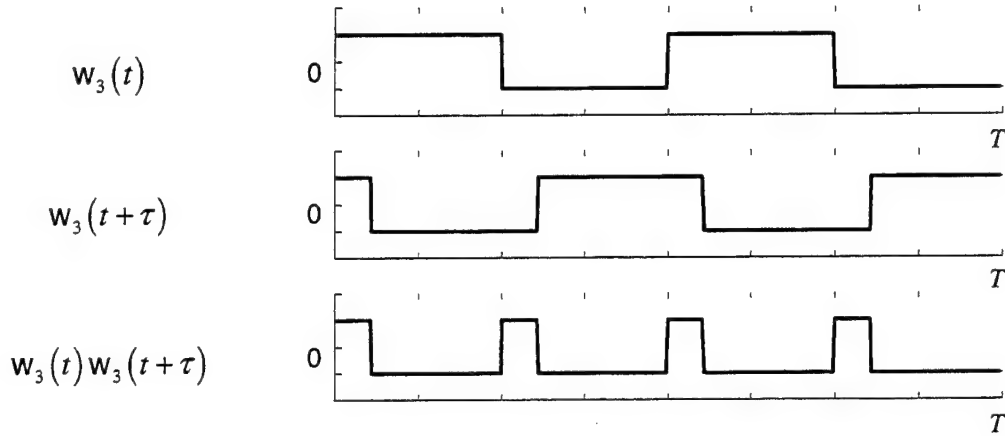


Figure 3.8 Product of Non-Synchronous Walsh Functions.

2. The Transmitted Signal $S(t)$

The base station in each cell must convert the information signal for user k into a DS-CDMA signal, amplify it to the desired power level, and BPSK modulate it for transmission, as shown for the center cell in Figure 3.9.

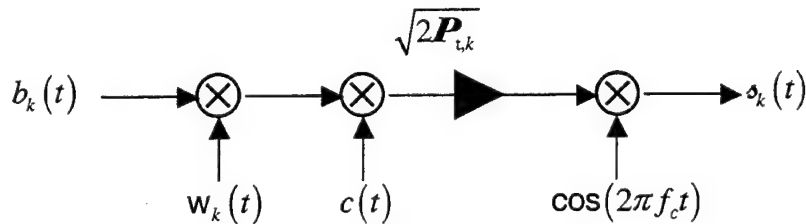


Figure 3.9 Spreading and Modulating the Information Signal.

Accordingly, the spread spectrum orthogonally-covered BPSK-modulated signal $s_k(t)$ that will be transmitted for user k is defined by

$$s_k(t) = \sqrt{2P_{t,k}} b_k(t) w_k(t) c(t) \cos(2\pi f_c t), \quad (3.1)$$

where

- k = the mobile user or channel k in the center cell,
- $\mathbf{P}_{t,k}$ = the average transmit power in the k th channel,
- $b_k(t)$ = the information signal consisting of binary data stream
for the k th user channel in center cell,
- $w_k(t)$ = the Walsh function for the k th user channel in center cell,
- $c(t)$ = PN spreading signal for the center cell, and
- f_c = the carrier frequency of the signal.

The base station in the center cell generates a signal, as defined in (3.1), for every user or active channel in the cell, to form a composite signal $S_0(t)$ that is transmitted into the channel as follows:

$$S_0(t) = \sum_{k=0}^{K-1} s_k(t) = \sum_{k=0}^{K-1} \sqrt{2\mathbf{P}_{t,k}} b_k(t) w_k(t) c(t) \cos(2\pi f_c t), \quad (3.2)$$

where K is the number of active channels in the center cell.

Once the signal $S_0(t)$ enters the channel, it is attenuated due to path loss and it is subject to fading and shadowing. In the next two sections we will discuss large-scale path loss and small-scale fading of the forward channel as they are used in our model.

B. PROPAGATION IN THE MOBILE RADIO CHANNEL

The signal transmitted from the base station to the mobile users loses a portion of its power along the way as a function of the distance it must travel and the terrain type across which it travels. This loss in signal power is called path loss, which we will

generally represent as L or \mathcal{L} in dB. We use large-scale propagation models to determine an average and/or median power received based on the separation distance between the transmitter and receiver and a general notion of the surrounding terrain/area, as discussed in Sections III.B.1 and III.B.2. These models, however, do not account for that fact that mobile users at a specific distance with the same general type of terrain may have local (dynamically changing) environments that are vastly different from one another. These differences result in variability of the path loss predicted by our large-scale propagation models. We model this variability as a lognormal random variable in Section III.B.3. Small-scale propagation models are used to model the effects of multipath propagation and are presented in Section III.B.4.

1. Large-Scale Path Loss

Large-scale propagation models are based on the type of environment through which the signal must travel. For example, in communications systems where there is a direct line-of-sight between transmitter and receiver we use the free-space propagation model as in [19]. We can predict the power received using the Friis free-space equation defined by

$$P_{fr} = \frac{P_t G_t G_r \lambda_c^2}{(4\pi)^2 d^2 L_s}, \quad (3.3)$$

where

- \mathbf{P}_{fr} = the free space power received,
- \mathbf{P}_{t} = the transmitted power,
- G_{t} = the transmitter antenna gain,
- G_{r} = the receiver antenna gain,
- λ_{c} = the wavelength of the carrier, $\lambda_{\text{c}} = \frac{c}{f_{\text{c}}}$,
- d = the separation distance between transmitter and receiver,
- L_{s} = the system (hardware) loss factor, and
- f_{c} = the carrier frequency.

Since our aim is to model the channel without regard to antenna gains and hardware losses, we will take $G_{\text{t}} = G_{\text{r}} = L_{\text{s}} = 1$. The free-space path loss \mathcal{L}_{fr} can be modeled as

$$\mathcal{L}_{\text{fr}}(d) = 10 \log \frac{\mathbf{P}_{\text{t}}}{\mathbf{P}_{\text{fr}}} = -20 \log \left(\frac{\lambda_{\text{c}}}{4\pi d} \right) \quad (\text{dB}). \quad (3.4)$$

The free-space power received \mathbf{P}_{fr} , as described by (3.3), and consequently the free-space path loss calculated by (3.4), are limited to distances d that are in the far field of the transmitting antenna. Accordingly, large-scale models use a power reference point calculated at a reference distance d_0 , which can then be related to the free-space power received by

$$\mathbf{P}_{\text{fr}}(d) = \mathbf{P}_{\text{fr}}(d_0) \left(\frac{d_0}{d} \right)^2 \quad d_0 \leq d.$$

The free-space reference power, $\mathbf{P}_{\text{fr}}(d_0)$, can either be based upon close-in measurements or calculated using (3.3).

The mobile communication channel cannot be accurately modeled using only the free-space propagation model. Typically a line-of-sight between the base station and the mobile user does not exist, due to buildings and other obstacles that lie in the path.

Propagations models for other than free space have been developed both analytically and empirically. Both approaches indicate that average received power decreases logarithmically as a function of distance [19]. The average path loss can be described as a function of a path-loss exponent n using

$$\overline{L}_n(d) \propto \left(\frac{d}{d_0} \right)^n. \quad (3.5)$$

The path-loss exponent, n , characterizes the rate of path loss and is dependent upon the propagation environment such as terrain, and obstructions to the path. Table 3.1 from [19] shows typical path-loss exponents for various conditions.

Environment	Path-loss exponent, n
Free Space	2
Urban area cellular radio	2.7 to 3.5
Shadowed urban cellular radio	3 to 5
In building line-of-sight	1.6 to 1.8
Obstructed in building	4 to 6
Obstructed in factories	2 to 3

Table 3.4 Path-loss exponents in Various Environments from [19].

By applying the appropriate path-loss exponent to our propagation model, we can determine an average path loss, \overline{L}_n , which represents the ensemble average of all

possible path losses for the given distance d . This average path loss, $\overline{L_n}$, or $\overline{\mathcal{L}_n}$ in dB, can be described by

$$\overline{\mathcal{L}_n}(d) = \overline{\mathcal{L}}(d_0) + 10n \log\left(\frac{d}{d_0}\right) \quad (\text{dB}), \quad (3.6)$$

where $\overline{\mathcal{L}}(d_0)$ is average loss at the power reference distance which can be specifically measured or, based on a free-space assumption, calculated using (3.4) as $\overline{\mathcal{L}}(d_0) = \mathcal{L}_{\text{fr}}(d_0)$. The key to using (3.6) in analysis is determining what path-loss exponent is appropriate for a given environment. While Table 3.4 is a good start, we can be more specific about our operating environment and consequently the loss associated with it. Accordingly, in the next section we will explore the Hata model, which allows for more specificity.

2. Hata Model

Propagation models are typically developed using both analytical and empirical methods. Empirical methods use measured data to produce a graphical or analytical expression, which well represents the actual data. As pointed out in [19], one of the simplest and most accurate empirical models for path loss in cluttered cellular systems is Okumura's model. Okumura's model is based entirely on measured data, which is represented graphically in [20] as a set of curves from which **median** path loss can be predicted.

The Hata model takes Okumura's graphical path loss data and represents it with a standard formula for an urban operating area which can be modified for other areas with

correction equations as presented in [21]. Hata's original model closely matches the predictions of the Okumura model for distances **greater** than 1 km. In [22], the Hata model was extended to cover distances on the order of 1 km and higher frequency ranges. We use the extended model since it better represents the size and frequency ranges of future cellular systems.

The extended Hata model, or COST-Hata model, uses the carrier frequency f_c , the heights of the base station and mobile antennae, h_{base} and h_{mobile} , the distance between the base station and mobile, d , and an operating area correction factor C_M to predict median path loss \mathcal{L}_H in dB as defined in [22] by

$$\begin{aligned} \mathcal{L}_H = & 46.3 + 33.9 \log \frac{f_c}{\text{MHz}} - 13.82 \log \frac{h_{\text{base}}}{\text{m}} - a(h_{\text{mobile}}) \\ & + \left(44.9 - 6.55 \log \frac{h_{\text{base}}}{\text{m}} \right) \log \frac{d}{\text{km}} + C_M, \end{aligned} \quad (3.7)$$

where

$$a(h_{\text{mobile}}) = \left(1.1 \log \frac{f_c}{\text{Mhz}} - 0.7 \right) \frac{h_{\text{mobile}}}{\text{m}} - \left(1.56 \log \frac{f_c}{\text{Mhz}} - 0.8 \right) \quad (\text{dB}),$$

and

$$C_M = \begin{cases} 0 \text{ dB, for medium sized city and suburban areas} \\ 3 \text{ dB, for metropolitan centers.} \end{cases}$$

As indicated in (3.7), frequency is measured in MHz, antennae heights are measured in meters (m), and separation distance is measured in kilometers (km). The extended Hata model is restricted to the following range of parameters:

f_c : 1500 Mhz to 2000 Mhz,
 h_{base} : 30 m to 200 m,
 h_{mobile} : 1 m to 10 m,
 d : 1 km to 20 km.

The Hata median loss, \mathcal{L}_H , predicted by (3.7) is comparable to the average loss, $\overline{\mathcal{L}_n}$, predicted by (3.6) as shown in Figure 3.10.

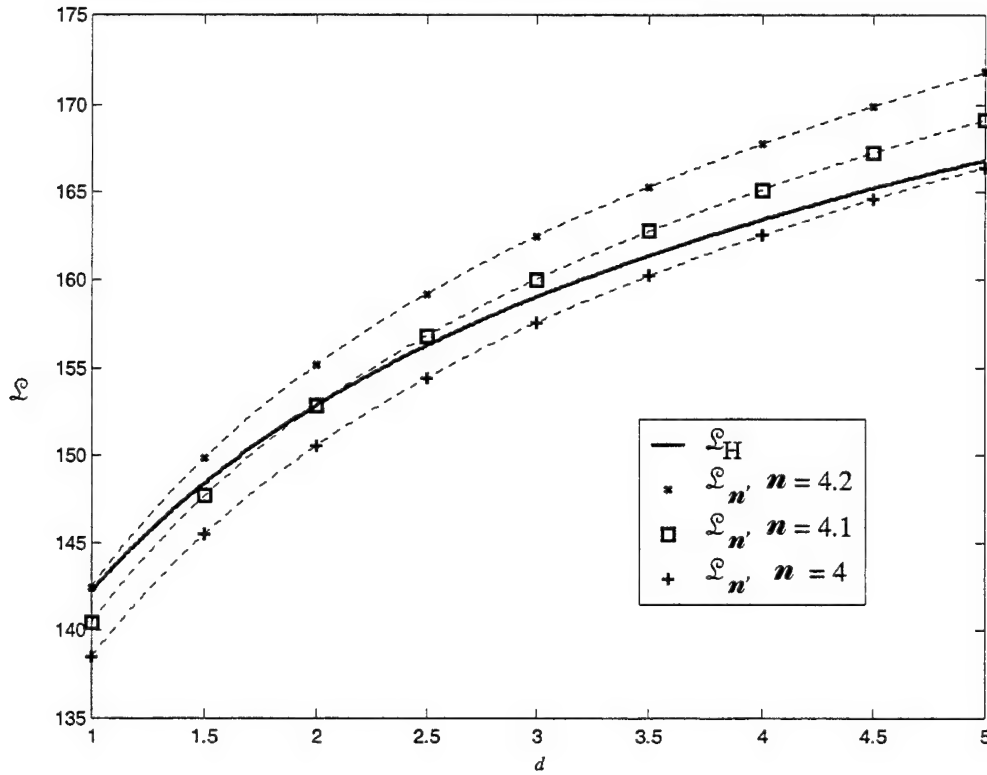


Figure 3.10 Comparison of Hata Loss and Average Loss.

We computed the losses depicted in Figure 3.10 for a range of distances, $1 \leq d \leq 5$ at a frequency, $f_c = 2000$ MHz. We computed the Hata loss, \mathcal{L}_H , for a large

city with the base station antenna height at 30m and the mobile antenna at 1m. For the average path loss $\overline{L_n}$, we used a range of path-loss exponents, which correspond to a shadowed large city environment from Table 3.4. We used a power reference distance, d_0 , of 10m.

It is clear that at any specific distance, there exists a reasonable path-loss exponent, n , such that $\mathcal{L}_H \approx \overline{\mathcal{L}_n}$. That is, from Figure 3.10 given any specific distance d , we could adjust n so that the curves representing \mathcal{L}_H and $\overline{\mathcal{L}_n}$ cross at d . Accordingly, we use the median path loss predicted by the Hata model in a similar way that the average path loss calculated using a path-loss exponent is used.

3. Lognormal Shadowing

The path loss predicted by the above methods represents an average or median value for a given distance. However, the actual path loss for mobile users in different locations but at the same distance from the base station can vary due to terrain differences, clutter, or foliage along their **specific** path. We call these variations in large-scale propagation shadow fading, or simply shadowing. Shadowing causes the actual path loss at a given distance to differ significantly from the predicted average or median path loss. These differences, measured in decibels, can be represented by a Gaussian random variable, since the measured path loss varies around a distance dependent average or median value. Our path loss with shadowing \mathcal{L}_x in terms of decibels is modeled by

$$\mathcal{L}_x(d) = \mathcal{L}(d) + \mathcal{X} \quad (\text{dB}), \quad (3.8)$$

where \mathcal{X} is a zero-mean Gaussian random variable $\mathcal{X} \sim \mathcal{N}(0, \sigma_{dB})$ with standard deviation σ_{dB} and where $\mathcal{L}(d)$ is a distance-dependent path loss. Since $\mathcal{L}(d)$ is a deterministic value and \mathcal{X} is a zero-mean Gaussian random variable, our shadowed path loss is a Gaussian random variable $\mathcal{L}_{\mathcal{X}} \sim \mathcal{N}(\mathcal{L}, \sigma_{dB})$ where \mathcal{L} is the mean and the median value of the random variable. The median value, or 50th percentile, of a random variable is that smallest value of the random variable where its cumulative distribution function (cdf) is 1/2. In terms of the probability distribution function (pdf), the median is the point at which the area under the pdf to the right of the point is equal to the area under the pdf to the left of the point. For the Gaussian random variable, the mean and median values are coincident. Accordingly, as model for $\mathcal{L}(d)$ in (3.8), we can use the predicted average path loss $\overline{\mathcal{L}_n}$ defined by (3.6) as in [19], or a predicted median path loss as in [15]. In our model, we will use the median path loss \mathcal{L}_H as predicted by the extended Hata model, which is defined by (3.7). Accordingly, we revise (3.8) to incorporate the Hata model as follows:

$$\mathcal{L}_{\mathcal{X}} = \mathcal{L}_H + \mathcal{X} \quad (\text{dB}). \quad (3.9)$$

Our shadowed path loss $\mathcal{L}_{\mathcal{X}}$ is a Gaussian distributed random variable $\mathcal{N}(\mathcal{L}_H, \sigma_{dB})$ with mean $\mu_{dB} = \mathcal{L}_H$ and standard deviation σ_{dB} , since it is the sum of a Gaussian random variable \mathcal{X} and a deterministic value \mathcal{L}_H . We can convert (3.9) from decibel to ratio format using

$$\begin{aligned} \mathcal{L}_{\mathcal{X}} &= 10 \log L_{\mathcal{X}}, \\ \mathcal{L}_H &= 10 \log L_H, \text{ and} \\ \mathcal{X} &= 10 \log X. \end{aligned}$$

The Gaussian random variable $\mathcal{X} \sim \mathcal{N}(0, \sigma_{dB})$ (in decibels) is converted to a lognormal random variable $X \sim \Lambda(0, \lambda \sigma_{dB})$, with parameters $\mu_X = \lambda \mu_{dB} = 0$ and $\sigma_X = \lambda \sigma_{dB}$, where $\lambda = \ln 10 / 10$ as derived and defined in Appendix III-A.1. Furthermore, our shadowed path loss in ratio form, L_X , has been converted to a lognormal random variable $L_X \sim \Lambda(\lambda \mathcal{L}_H, \lambda \sigma_{dB})$ as well, which yields the lognormal random variable L_X described by

$$L_X = L_H X. \quad (3.10)$$

The parameters μ_X and σ_X of the lognormal random variable $X \sim \Lambda(\mu_X, \sigma_X)$ are **not** the distribution's mean and standard deviation. We define the pdf and the moments for the lognormal random variable in Appendix III-A.2.

We have created a model for path loss that incorporates the Hata model and the effects of lognormal shadowing. In order to fold this path-loss model into our forward signal, we must look at the link analysis. In general, we know that the power received, \mathbf{P}_r , will be related to transmitted signal power, gains of the antennae, and the system and path losses as follows:

$$\mathbf{P}_r = \frac{\mathbf{P}_t G_t G_r}{LL_s} = \frac{\mathbf{P}_t}{L}, \quad (3.11)$$

where we have normalized the antennae gains and system loss to one. However, in our forward signal model, we need the flexibility to adjust the signal power allocated to individual channels. For example, we may want to increase the power in the pilot channel to enhance synchronization between the base station and the mobile users, and consequently aid the demodulation of the data signals. If we use \mathbf{P}_t as our baseline

signal power, meaning most channels will be transmitted with this signal power, then we can relate the signal power $\mathbf{P}_{t,k}$ in each channel k to this baseline using a power factor \mathcal{F}_k as follows:

$$\mathbf{P}_{t,k} = \mathcal{F}_k \mathbf{P}_t. \quad (3.12)$$

In general, our power factor will be $\mathcal{F}_k = 1$ for all channels, unless specifically stated otherwise. We can now modify (3.11) to be channel-specific using (3.12) as follows:

$$\mathbf{P}_{r,k} = \frac{\mathbf{P}_{t,k}}{L} = \frac{\mathcal{F}_k \mathbf{P}_t}{L}. \quad (3.13)$$

Finally, if we apply our Hata-lognormal model $L = L_H X$ for path loss, we transform the power received in the k -th channel into a random variable P_k as follows:

$$P_k = \frac{\mathcal{F}_k \mathbf{P}_t}{L_H (d) X}, \quad (3.14)$$

where

- \mathcal{F}_k = the power factor used to adjust
the power in the k -th channel,
- \mathbf{P}_t = the baseline signal power,
- L_H = the median path loss using the Hata model, and
- X = the Lognormal random variable $\Lambda(0, \lambda \sigma_{dB})$.

As shown in Appendix III-C, the inverse of a lognormal random variable is another lognormal random variable. Accordingly, the power received in the k th channel is a lognormal random variable $P_k \sim \Lambda(\mu_{P_k}, \lambda \sigma_{dB})$, where $\mu_{P_k} = \ln(\mathcal{F}_k \mathbf{P}_t / L_H)$.

In this section, we have developed a model for the power received by a mobile user that incorporates large-scale propagation losses and lognormal shadowing. In the next section we will model the effects of small-scale fading.

4. Small-Scale Fading Due to Multipath

Small-scale fading of a received signal is characterized by rapid fluctuations in the strength (or amplitude) of the signal. The fluctuations are a result of multiple copies of the transmitted signal bouncing off various obstacles and arriving at the receiver via different paths as depicted in Figure 3.11. The copies of the signal travel along paths of

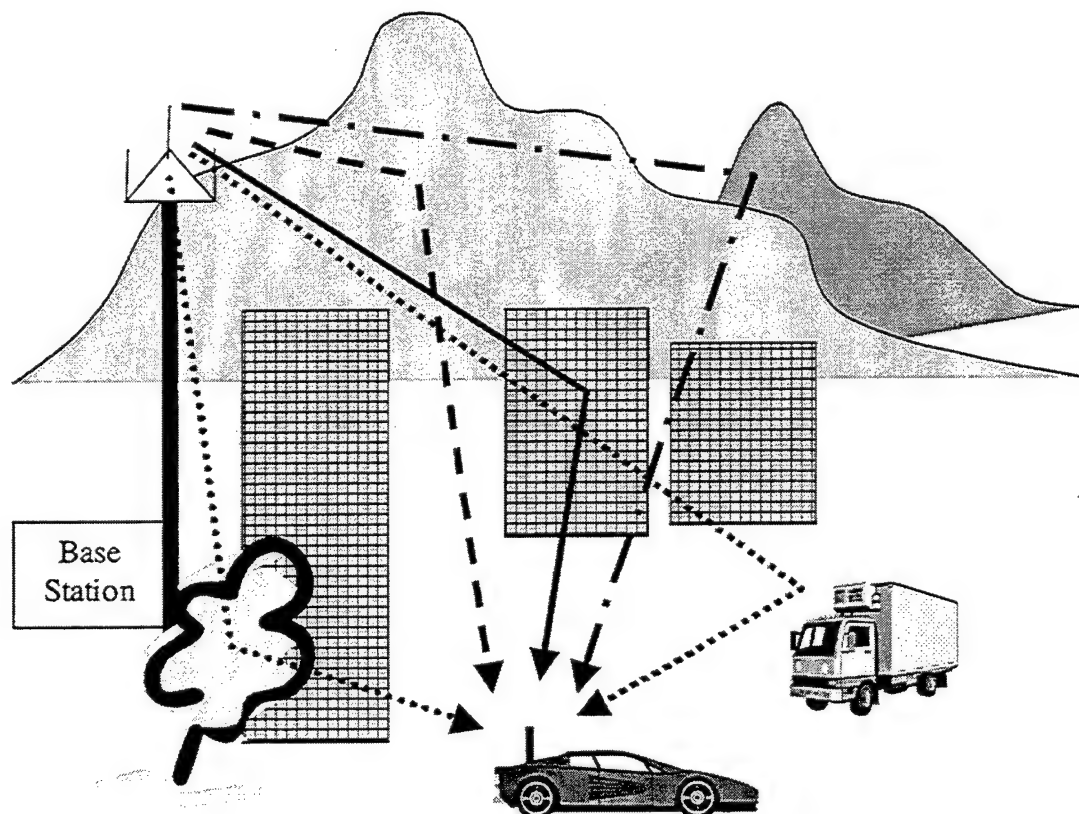


Figure 3.11 Multipath Propagation.

different lengths and therefore sustain losses of different amounts. When they arrive at the receiver, some copies are time-delayed as a result of the longer paths that they have traveled, and some of the copies have been reflected off moving objects, which induce a doppler-shift in the frequency of the signal. The receiver must process the sum of the multipath components in order to extract the information bit from the signal.

The success or failure of the receiver to correctly process each information bit (or symbol) depends upon the small-scale fading characteristics of the channel as compared with the signal characteristics such as bandwidth and bit (or symbol) period. Channel fading characteristics are classified according to two independent fading phenomena as described in [19]:

- ❖ Time Dispersion - fading due to the collective time delay of the multipath components of the received signal. (Flat/Frequency Selective)
- ❖ Frequency Dispersion - fading due to the collective doppler spread in the multipath components of the signal. (Fast/Slow)

The changes in signal amplitude due to doppler spread over one bit period can be characterized as fast or slow fading. Fast fading is caused by frequency dispersion in the signal, which results in distortion of the signal. If the frequency dispersion is great enough to dramatically affect the amplitude of the received multipath signal over the bit period, then it is called fast fading. In reality, fast fading environments have only been observed [19] when dealing with communication systems with very low data rates, (which result in very long bit periods as compared to the rate of change of the channel.)

In a slow-fading channel, the doppler spread of the multipath components of the signal does not significantly affect the amplitude of the received signal over the bit period. Accordingly, we consider the channel to be static (for the bit duration) with regard to frequency dispersion/distortion effects. Since our model is concerned with high data rates, our channel is modeled as slow-fading.

The effects on the received signal amplitude due to time delay or time dispersion of the multipath components of the signal result in either flat or frequency-selective fading. Frequency-selective fading occurs when the collective time delay of the multipath components exceeds the bit duration and consequently (negatively) affects the processing of the next information bit; this is called Inter-Symbol Interference (ISI). If we think of converting the multipath delay time of the channel into the frequency domain, we can describe the channel by a corresponding characteristic bandwidth. The channel bandwidths are inversely proportional to the time delay spread, which means long time delays correspond with narrow channel bandwidths. When the channel bandwidth is less than the bandwidth of the transmitted signal, we have frequency-selective fading and ISI in the channel.

On the other hand, in a flat-fading environment, the time dispersion of the multipath signal is less than the bit period, and the receiver is able to resolve the multipath signal. Flat-fading channels cause the amplitude of the received signal to vary with time over the bit due to the effects of the multipath propagation, but don't interfere with the adjacent information bits. The channel is time-varying because it changes as the receiver moves, and as reflectors or scatterers (of the multipath components) along the paths move or change. This characterizes multipath propagation. The most common

method for modeling the amplitude variations in a flat fading channel is by assuming that the amplitudes are distributed as a Rayleigh random variable R as defined in Appendix B.

Accordingly, we will use the Rayleigh flat-fading channel model to represent the small-scale fading effects due to multipath propagation in our channel model. In the next section we will combine the effects of large-scale path loss and small scale fading into a Rayleigh-lognormal channel model.

C. RAYLEIGH-LOGNORMAL CHANNEL MODEL

In Section III.B, we described the large-scale and small-scale propagation effects that are possible when a signal passes through a mobile channel. In Section III.C we will combine these effects to develop the Rayleigh-lognormal channel model. The Rayleigh-lognormal channel model can be described as a slow-flat-Rayleigh fading channel with lognormal shadowing and with path loss as predicted by the extended Hata model. We apply the Rayleigh-lognormal channel model to the signals in the DS-CDMA cellular system, and develop a received signal by a mobile user in center cell.

1. The Forward Signal $s_o(t)$

In order to develop the effects of our channel on the transmitted signal $S_o(t)$, as defined by (3.2), we will consider the signal in its complex envelope form as follows:

$$S_o(t) = \text{Re}\{\tilde{S}_o(t)e^{j2\pi f_c t}\}, \quad (3.15)$$

where $\tilde{S}_0(t)$ is the complex envelope of the transmitted signal defined by

$$\tilde{S}_0(t) = \sum_{k=0}^{K-1} \sqrt{2P_{t,k}} b_k(t) w_k(t) c(t). \quad (3.16)$$

As described in Section II.B, we know that the complex envelope $\tilde{S}_0(t)$ is affected by small-scale fading as modeled by the Rayleigh random variable as $R \cdot \tilde{S}_0(t)$. The large-scale path loss endured by the signal together with the lognormal shadowing is modeled by $\tilde{S}_0(t)/\sqrt{L_H X}$, using the path loss as predicted by the extended Hata model. Furthermore, there is a relative time delay τ_d introduced by the channel and a phase discrepancy θ_d between transmitting stations and the mobile user. Finally, the channel introduces additive noise $n(t)$ and interference $\varsigma(t)$ to the total received signal $r(t)$, which we investigate in later sections. The complete baseband channel model is graphically depicted in Figure 3.12.

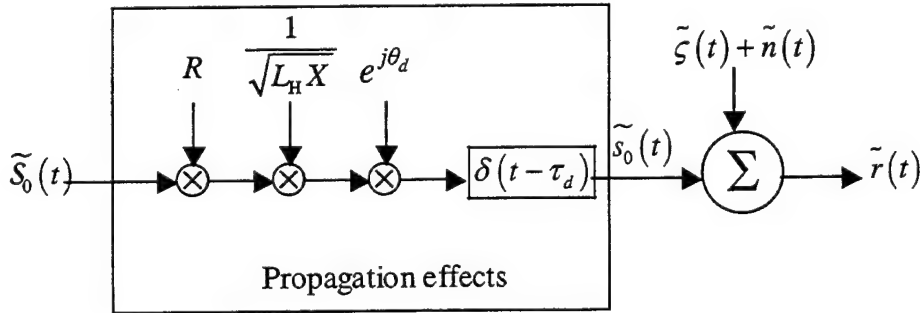


Figure 3.12 Baseband Rayleigh-Lognormal Channel Model.

We have used the symbols $\tilde{s}_0(t)$, $\tilde{\varsigma}(t)$, $\tilde{n}(t)$, and $\tilde{r}(t)$ to represent the lowpass equivalent signals for $s_0(t)$, $\varsigma(t)$, $n(t)$, and $r(t)$.

The forward signal $s_0(t)$ that will be received by a mobile user in the center cell as a result of the transmitted signal $S_0(t)$ passing through the Rayleigh-lognormal channel model has a complex envelope described by the following:

$$\begin{aligned}\tilde{s}_0(t) &= \tilde{S}_0(t - \tau_d) \frac{Re^{j\theta_d}}{\sqrt{L_H X}} \\ &= \sum_{k=0}^{K-1} R \sqrt{\frac{2\mathbf{P}_{\text{t},k}}{L_H X}} b_k(t - \tau_d) w_k(t - \tau_d) c(t - \tau_d) e^{j\theta_d} \\ &= \sum_{k=0}^{K-1} R \sqrt{2P_k} b_k(t - \tau_d) w_k(t - \tau_d) c(t - \tau_d) e^{j\theta_d} \\ &= \sum_{k=0}^{K-1} R \sqrt{2P_k} b_k(t) w_k(t) c(t),\end{aligned}\tag{3.17}$$

where P_k is defined by (3.14). Further, since the time and phase delays are relative amongst the base stations, we take $\tau_d = \theta_d = 0$ for the forward signal from the center cell's base station. We can describe the forward (bandpass) signal using its complex envelope as

$$\begin{aligned}s_0(t) &= \text{Re}\{\tilde{s}_0(t) e^{j2\pi f_c t}\} \\ &= \sum_{k=0}^{K-1} R \sqrt{2P_k} b_k(t) w_k(t) c(t) \cos(2\pi f_c t).\end{aligned}\tag{3.18}$$

A mobile user extracts his traffic from the composite signal $s_0(t)$ as described in Section III.A. However, as shown in Figure 3.12, the signal received by a mobile user includes Additive White Gaussian Noise (AWGN) $n(t)$ and co-channel (or intercell)

interference $\varsigma(t)$ from the adjacent cells in addition to the forward signal $s_0(t)$. We develop the co-channel interference term in the next section.

2. Co-Channel Interference $\varsigma(t)$

Just as the mobile user receives the composite signal $s_0(t)$ from the base station in his/her (the center) cell, he/she also receives a similar composite signal $s_i(t)$ from the base station in each adjacent cell. The sum of these constitutes co-channel interference. The base station in each adjacent cell generates a forward signal for users in their cell that passes through the channel and is received by a user in the center cell as defined by

$$s_i(t) = \sum_{j=0}^{K_i-1} R_i \sqrt{2P_{ij}} b_{ij}(t + \tau_i) w_{ij}(t + \tau_i) c_i(t + \tau_i) \cos(2\pi f_c t + \varphi_i), \quad (3.19)$$

with

- i = the adjacent cells $i = 1, 2, \dots, 6$,
- ij = mobile user or channel j in adjacent cell i ,
- K_i = the number of active channels in adjacent cell i ,
- R_i = Rayleigh fading random variable for signals from adjacent cell i ,
- P_{ij} = Lognormal Random Variable representing the average power received from the j th channel in adjacent cell i as defined below,
- $b_{ij}(t)$ = the information signal for the j th user channel in adjacent cell i ,
- $w_{ij}(t)$ = Walsh function for the j th user channel in adjacent cell i ,
- $c_i(t)$ = PN spreading signal for the adjacent cell i , and
- f_c = the carrier frequency of the signal.
- τ_i = the time delay from adjacent cell i , relative to the time delay from the center cell base station.
- φ_i = the phase delay from adjacent cell i , relative to the phase delay from the center cell base station.

We adapted P_{ij} from (3.14) to represent the average power received by a mobile user in the center cell from forward signal $s_i(t)$ in adjacent cell i channel j as follows:

$$P_{ij} = \frac{\mathcal{F}_{ij} P_t}{L_H(D_i) X_i}, \quad (3.20)$$

where

- \mathcal{F}_{ij} = the factor used to adjust the power in the j -th channel in adjacent cell i ,
- $L_H(D_i)$ = the median path loss using the Hata model at a separation distance D_i ,
- D_i = the distance separating the receiver from the base station in adjacent cell i , and
- X_i = Lognormal random variable $\Lambda(0, \sigma_{dB})$.

The co-channel interference $\zeta(t)$ is the sum of the composite signals from each of the adjacent cells as follows:

$$\zeta(t) = \sum_{i=1}^6 \sum_{j=0}^{K_i-1} R_i \sqrt{2P_{ij}} b_{ij}(t + \tau_i) w_{ij}(t + \tau_i) c_i(t + \tau_i) \cos(2\pi f_c t + \phi_i). \quad (3.21)$$

With the co-channel interference term defined, we will now proceed to define the complete signal received by a mobile user, $r(t)$.

3. The Received Signal $r(t)$

As described in Section III.C.1, the signal received by a mobile user in the center cell is comprised of the forward signal $s_0(t)$ sent from the user's base station,

interference $\zeta(t)$ from the six adjacent base stations, and Additive White Gaussian Noise

(AWGN) $n(t) \sim \mathcal{N}\left(0, \frac{N_0}{2}\right)$. Accordingly, our received signal $r(t)$ is defined by

$$\begin{aligned} r(t) &= s_0(t) + \zeta(t) + n(t) \\ &= \sum_{k=0}^{K-1} R \sqrt{2P_k} b_k(t) w_k(t) c(t) \cos(2\pi f_c t) \\ &\quad + \sum_{i=1}^6 \sum_{j=0}^{K_i-1} R_i \sqrt{2P_{ij}} b_{ij}(t + \tau_i) w_{ij}(t + \tau_i) c_i(t + \tau_i) \cos(2\pi f_c t + \varphi_i) + n(t). \end{aligned} \quad (3.22)$$

We will use the received signal to analyze the performance of the DS-CDMA system in a Rayleigh-fading channel with lognormal shadowing.

D. SUMMARY

In Chapter III, we have developed a mobile radio channel model, the Rayleigh-lognormal channel model, which combines both large-scale and small-scale propagation effects into a single model. The Rayleigh-lognormal channel model incorporates the large-scale median path loss as predicted by the extended Hata model and it includes the effects of lognormal shadowing. Small-scale propagation effects are built into our channel model using a slow-flat Rayleigh fading model. Combining large-scale and small-scale propagation models in this manner allows us to more accurately characterize the mobile radio channel in a single unified model. Accordingly, our model will allow for more complete analysis of the mobile radio channel than past models, which typically incorporated small- or large-scale propagation effects but not both.

We have also developed the forward channel of a typical DS-CDMA cellular system consisting of traffic from a cell's base station to mobile users in the cell. We

applied the Rayleigh-lognormal channel model to the signal transmitted from the base station in order to characterize the input signal to a mobile user's receiver. The received signal includes the traffic intended for the mobile user, traffic for other users in the cell (intracell interference,) traffic for users in adjacent cells (intercell interference,) and additive noise. We will use this received signal to develop a Signal-to-Noise plus Interference Ratio (SNIR) and for Bit Error Rate (BER) analysis in Chapter IV.

APPENDIX III-A LOGNORMAL RANDOM VARIABLE

1. Lognormal Random Variable Derived from a Gaussian Random Variable

Let \mathcal{X} be a Gaussian random variable with mean μ_{dB} and standard deviation σ_{dB} , denoted as $\mathcal{X} \sim \mathcal{N}(\mu_{dB}, \sigma_{dB})$. The pdf of the random variable \mathcal{X} is given by

$$p_{\mathcal{X}}(x) = \frac{1}{\sqrt{2\pi}\sigma_{dB}} e^{-\frac{(x-\mu_{dB})^2}{2\sigma_{dB}^2}}, \quad -\infty < x < \infty. \quad (3.23)$$

We can transform the random variable from units of decibels to ratio form using

$$\mathcal{X} = 10 \log X \quad \rightarrow \quad X = 10^{\frac{\mathcal{X}}{10}} = g(\mathcal{X}),$$

where $g(\mathcal{X})$ is the transformation function and its derivative is given by

$$g'(\mathcal{X}) = \frac{dg}{d\mathcal{X}} = \frac{\ln 10}{10} 10^{\frac{\mathcal{X}}{10}} = \frac{\ln 10}{10} X = \lambda X,$$

where

$$\lambda = \frac{\ln 10}{10}.$$

We know that since $g(\mathcal{X})$ is a monotonically increasing function, the pdf of the transformed variable can be developed as follows:

$$\begin{aligned}
p_x(x) &= \frac{1}{|g'(x)|} p_{\mathcal{X}}(x) \\
&= \frac{1}{|\lambda x|} p_{\mathcal{X}}(10 \log x) \\
&= \frac{1}{\lambda x \sqrt{2\pi} \sigma_{dB}} e^{-\frac{(10 \log x - \mu_{dB})^2}{2\sigma_{dB}^2}} \\
&= \frac{1}{x \sqrt{2\pi} \lambda \sigma_{dB}} e^{-\frac{\lambda^2 (10 \log x - \mu_{dB})^2}{2\lambda^2 \sigma_{dB}^2}} \\
&= \frac{1}{x \sqrt{2\pi} \lambda \sigma_{dB}} e^{-\frac{(\lambda 10 \log x - \lambda \mu_{dB})^2}{2(\lambda \sigma_{dB})^2}} \\
&= \frac{1}{x \sqrt{2\pi} \lambda \sigma_{dB}} e^{-\frac{((\ln 10) \log x - \lambda \mu_{dB})^2}{2(\lambda \sigma_{dB})^2}} \\
&= \frac{1}{x \sqrt{2\pi} \lambda \sigma_{dB}} e^{-\frac{(\ln x - \lambda \mu_{dB})^2}{2(\lambda \sigma_{dB})^2}} \\
&= \frac{1}{x \sqrt{2\pi} \lambda \sigma_{dB}} e^{-\frac{(\ln x - \mu_X)^2}{2\sigma_X^2}}, \quad x > 0,
\end{aligned} \tag{3.24}$$

where

$$\mu_X = \lambda \mu_{dB} \text{ and } \sigma_X = \lambda \sigma_{dB}. \tag{3.25}$$

We say that the random variable X has a lognormal distribution [23] with parameters μ_X and σ_X , and is represented as $X \sim \Lambda(\mu_X, \sigma_X)$ or, alternatively, in terms of the original parameters, $X \sim \Lambda(\lambda\mu_{dB}, \lambda\sigma_{dB})$.

The n th moment of X about the origin is given by

$$E\{X^n\} = e^{n\mu_X + \frac{n^2\sigma_X^2}{2}} = \exp\left(n\mu_X + \frac{n^2\sigma_X^2}{2}\right). \quad (3.26)$$

Accordingly, the mean of X is

$$E\{X\} = e^{\mu_X + \frac{\sigma_X^2}{2}}, \quad (3.27)$$

the second moment about the origin of X is

$$E\{X^2\} = e^{2\mu_X + 2\sigma_X^2}, \quad (3.28)$$

and the variance of X is

$$\text{Var}\{X\} = e^{2\mu_X + 2\sigma_X^2} (e^{\sigma_X^2} - 1). \quad (3.29)$$

Furthermore, the median of X is

$$\text{Med}(X) = e^{\mu_X}. \quad (3.30)$$

2. Transformation $Y = a/X$ of the Lognormal Random Variable

If $X \sim \Lambda(\mu_X, \sigma_X)$, we can define a transformation from X to a new random variable Y as follows:

$$Y = \frac{a}{X}, \quad a > 0.$$

We can find the distribution of Y as in Appendix IIIA.1, where our transform function is defined by

$$g(X) = \frac{a}{X},$$

$$\text{and } g'(X) = \frac{-a}{X^2}.$$

The pdf of Y is developed as

$$\begin{aligned} p_Y(y) &= \frac{1}{|g'(X)|} p_X(x) \\ &= \frac{1}{\left| \frac{-a}{x^2} \right|} p_X\left(\frac{a}{y}\right) \\ &= \frac{a}{y^2} p_X\left(\frac{a}{y}\right) \\ &= \frac{a}{y^2} \frac{1}{\left(\frac{a}{y}\right) \sqrt{2\pi}\sigma_X} e^{-\frac{\left(\ln\left(\frac{a}{y}\right) - \mu_X\right)^2}{2\sigma_X^2}} \\ &= \frac{1}{y\sqrt{2\pi}\sigma_X} e^{-\frac{(\ln a - \ln y - \mu_X)^2}{2\sigma_X^2}} \\ &= \frac{1}{y\sqrt{2\pi}\sigma_X} e^{-\frac{(\ln y - \ln a + \mu_X)^2}{2\sigma_X^2}} \\ &= \frac{1}{y\sqrt{2\pi}\sigma_Y} e^{-\frac{(\ln y - \mu_Y)^2}{2\sigma_Y^2}}, \end{aligned}$$

which is in the form of a lognormal random variable as defined by (3.24). Accordingly, our transformed random variable $Y \sim \Lambda(\mu_Y, \sigma_Y)$ is also lognormal with

$$\mu_Y = \ln a - \mu_X \quad \text{and} \quad \sigma_Y = \sigma_X. \quad (3.31)$$

Furthermore, if we want to represent the parameters in terms of decibels, we can convert as

$$\ln a = \ln 10 \log a = \lambda a,$$

with

$$a = 10 \log a.$$

Finally,

$$\mu_Y = \ln a - \mu_X = \lambda a - \lambda \mu_{dB} = \lambda (a - \mu_{dB}).$$

THIS PAGE INTENTIONALLY LEFT BLANK

IV. DS-CDMA PERFORMANCE ANALYSIS

In Chapter III, we developed a Rayleigh-lognormal channel model and described the signal received by a mobile user on the forward channel of a typical DS-CDMA cellular system, which has passed through the Rayleigh-lognormal channel model. In this chapter we assess the performance of such a system under various conditions, which can be adjusted in our model. We apply Forward Error Correction (FEC) Coding to the forward signal in the form of convolutional codes to obtain the coded probability of bit error. Due to the complexity of our channel model, we use statistical modeling of solutions and probability distributions in cases where no analytical solutions can be (reasonably) developed.

In order to assess the performance on the forward channel, we take mobile user one in the center cell as the receiving mobile user without any loss of generality in our final solution. We assume that mobile user one is located in the least optimum position within the cell, which is in any corner of the hexagon as shown in Figure 4.1.

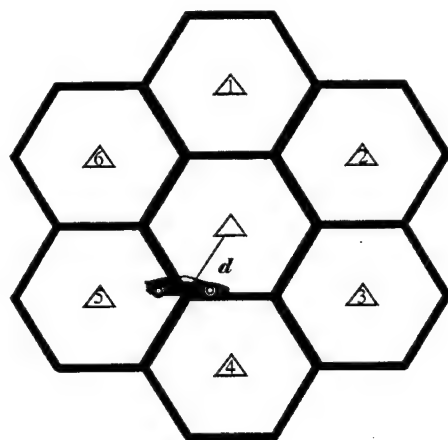


Figure 4.1 Mobile User One in the Seven Cell Cluster.

The distance from the base station in the center cell to mobile user one is d , while the distance from mobile user one to the base station in adjacent cell i is D_i . The length of each side of the hexagon is length d as well, which implies that the hexagon actually comprises six isosceles triangles. Using the geometry of the triangles, as shown in Figure 4.2, we can determine the distances from each base station as a function of d .

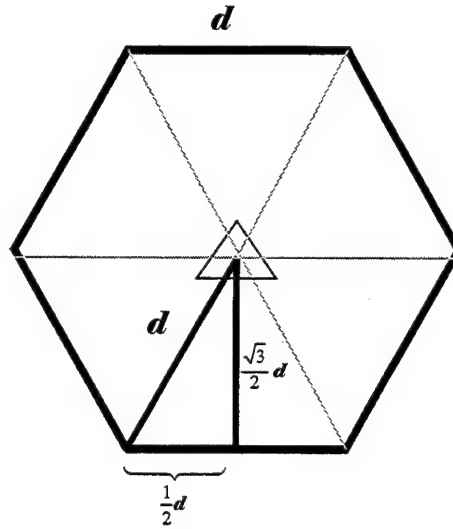


Figure 4.2 Geometry of the Cell Hexagon.

Accordingly, the distances from adjacent cell base stations, D_i , to mobile user one for the worst-case distance, d , from the base station in the center cell are as follows,

$$D_i = \begin{cases} d, & i = 4,5 \\ 2d, & i = 3,6 \\ \sqrt{7}d, & i = 1,2 \end{cases} \quad (4.1)$$

These distances, D_i , are used in computing the Hata median path loss for signals transmitted from the respective base stations, which contribute to the co-channel interference in the received signal. The median path loss of the information carrying signal from the center cell's base station is computed using the distance, d .

We are now prepared to proceed with the performance analysis of this system model. We develop the Signal-to-Noise plus Interference (SNIR) along with the corresponding uncoded probability of error $\tilde{\mathcal{P}}_e$ in Section IV.A. We apply convolution encoding to our system and derive a (coded) probability of error \mathcal{P}_e in Section IV.B. In Section IV.C, we develop a statistical model that allows us to analyze \mathcal{P}_e more completely, which we accomplish in Section IV.D.

A. PERFORMANCE OF THE BASIC SYSTEM

In order for mobile user one to extract the traffic intended for him from his base station, he must process the received signal $r(t)$ as defined in (3.22) one bit at a time. Mobile user one processes each bit of the signal as shown in Figure 4.3.

The upper branch in Figure 4.3 is the data branch, in which the data intended for mobile user one is despread, demodulated, and finally integrated over the bit to form a decision statistic, Y . The decision statistic Y is used to determine whether the processed bit was a logical 1 or 0. The lower branch in Figure 4.3 is the pilot recovery branch. In

the pilot recovery branch, the pilot tone, which is used to coherently demodulate the received signal, is extracted from the received signal. As shown in Figure 4.3, we use a

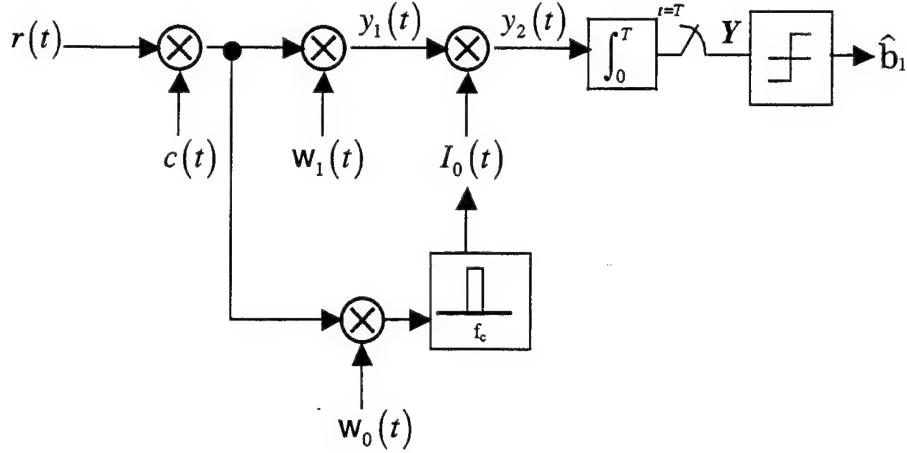


Figure 4.3 Processing the Received Signal $r(t)$.

very narrow filter around the carrier frequency to extract the pilot tone from the signals that remain spread over the band.

We examine the components of Figure 4.3 in detail in Sections IV.A.1-IV.A.2. In Section IV.A.3 and IV.A.4, we develop the SNIR and $\tilde{\mathcal{P}}_e$, respectively.

1. The Demodulated Signal $y_2(t)$

In this section, we develop the demodulated signal $y_2(t)$. Let us start with the data branch of Figure 4.3. We apply the cell's PN sequence, which is synchronized with the base station, followed by the Walsh sequence (in the form of time signals) in order to

despread and remove the orthogonal Walsh cover from the desired information bit as follows:

$$\begin{aligned}
 y_1(t) &= r(t)c(t)w_1(t) \\
 &= [s_0(t) + \varsigma(t) + n(t)]c(t)w_1(t) \\
 &= \underbrace{s_0(t)c(t)w_1(t)}_{I_1 + \gamma_1} + \underbrace{\varsigma(t)c(t)w_1(t)}_{\varsigma_1} + \underbrace{n(t)c(t)w_1(t)}_{n_1} \\
 &= I_1(t) + \gamma_1(t) + \varsigma_1(t) + n_1(t),
 \end{aligned} \tag{4.2}$$

where we have broken $y_1(t)$ into four components as defined below.

The first two components result from the processing of the forward signal from the base station in the center cell as follows:

$$\begin{aligned}
 I_1(t) + \gamma_1(t) &= s_0(t)c(t)w_1(t) \\
 &= \left(\sum_{k=0}^{K-1} R\sqrt{2P_k}b_k(t)w_k(t)c(t)\cos(2\pi f_c t) \right) c(t)w_1(t) \\
 &= \underbrace{\left(R\sqrt{2P_1}b_1(t)w_1(t)c(t)\cos(2\pi f_c t) \right)}_{k=1} c(t)w_1(t) \\
 &\quad + \left(\sum_{\substack{k=0 \\ k \neq 1}}^{K-1} R\sqrt{2P_k}b_k(t)w_k(t)c(t)\cos(2\pi f_c t) \right) c(t)w_1(t).
 \end{aligned}$$

The desired information bit, $b_1(t)$, is contained in the signal $I_1(t)$:

$$\begin{aligned}
 I_1(t) &= \left(R\sqrt{2P_1}b_1(t)w_1(t)c(t)\cos(2\pi f_c t) \right) c(t)w_1(t) \\
 &= R\sqrt{2P_1}b_1(t)\cos(2\pi f_c t).
 \end{aligned} \tag{4.3}$$

Intracell interference is contained in the term γ_1 :

$$\begin{aligned}
\gamma_1(t) &= \left(\sum_{\substack{k=0 \\ k \neq 1}}^{K-1} R\sqrt{2P_k} b_k(t) w_k(t) c(t) \cos(2\pi f_c t) \right) c(t) w_1(t) \\
&= \sum_{\substack{k=0 \\ k \neq 1}}^{K-1} R\sqrt{2P_k} b_k(t) w_k(t) w_1(t) \cos(2\pi f_c t).
\end{aligned} \tag{4.4}$$

The intercell interference is contained in the term $\varsigma_1(t)$:

$$\begin{aligned}
\varsigma_1(t) &= \left(\sum_{i=1}^6 \sum_{j=0}^{K_i-1} R_i \sqrt{2P_{ij}} b_{ij}(t + \tau_i) w_{ij}(t + \tau_i) c_i(t + \tau_i) \cos(2\pi f_c t + \varphi_i) \right) c(t) w_1(t) \\
&= \sum_{i=1}^6 \sum_{j=0}^{K_i-1} R_i \sqrt{2P_{ij}} b_{ij}(t + \tau_i) w_{ij}(t + \tau_i) w_1(t) c_i(t + \tau_i) c(t) \cos(2\pi f_c t + \varphi_i).
\end{aligned} \tag{4.5}$$

Finally, the thermal noise contribution is contained in the term $n_1(t)$ as follows:

$$n_1(t) = n(t) c(t) w_1(t). \tag{4.6}$$

The pilot tone for each base station is transmitted in Walsh channel zero, using $w_0(t)$. Accordingly, to recover the pilot tone and demodulate the information signal we despread the received signal and split off a copy to the pilot recovery branch, as shown in Figure 4.3. The unfiltered pilot signal, $p(t)$, can be described by

$$\begin{aligned}
p(t) &= r(t) c(t) w_0(t) \\
&= (s_0(t) + \varsigma(t) + n(t)) c(t) w_0(t) \\
&= \underbrace{s_0(t) c(t) w_0(t)}_{I_0 + \gamma_0} + \underbrace{\varsigma(t) c(t) w_0(t)}_{\varsigma_0} + \underbrace{n(t) c(t) w_0(t)}_{n_0} \\
&= I_0(t) + \gamma_0(t) + \varsigma_0(t) + n_0(t),
\end{aligned} \tag{4.7}$$

where we have (once again) broken the unfiltered pilot into four components.

The first two components are a result of the forward signal in the center cell and are defined by

$$\begin{aligned}
I_0(t) + \gamma_0(t) &= s_0(t) c(t) w_0(t) \\
&= \left(\sum_{k=0}^{K-1} R \sqrt{2P_k} b_k(t) w_k(t) c(t) \cos(2\pi f_c t) \right) c(t) w_0(t) \\
&= \underbrace{\left(R \sqrt{2P_0} b_0(t) w_0(t) c(t) \cos(2\pi f_c t) \right)}_{k=0} c(t) w_0(t) \\
&\quad + \left(\sum_{k=1}^{K-1} R \sqrt{2P_k} b_k(t) w_k(t) c(t) \cos(2\pi f_c t) \right) c(t) w_0(t),
\end{aligned}$$

where the desired pilot tone, $\cos(2\pi f_c t)$, is contained in the pilot recovery signal $I_0(t)$ as follows:

$$\begin{aligned}
I_0(t) &= \left(R \sqrt{2P_0} b_0(t) w_0(t) c(t) \cos(2\pi f_c t) \right) c(t) w_0(t) \\
&= R \sqrt{2P_0} \cos(2\pi f_c t),
\end{aligned} \tag{4.8}$$

since $b_0(t) = 1$ for all t .

The $\gamma_0(t)$ pilot recovery term contains intracell traffic and is defined by

$$\begin{aligned}
\gamma_0(t) &= \left(\sum_{k=1}^{K-1} R \sqrt{2P_k} b_k(t) w_k(t) c(t) \cos(2\pi f_c t) \right) c(t) w_0(t) \\
&= \sum_{k=1}^{K-1} R \sqrt{2P_k} b_k(t) w_k(t) \cos(2\pi f_c t).
\end{aligned} \tag{4.9}$$

The pilot recovery term $\varsigma_0(t)$ contains the intercell traffic given by

$$\begin{aligned}
\varsigma_0(t) &= \left(\sum_{i=1}^6 \sum_{j=0}^{K_i-1} R_i \sqrt{2P_{ij}} b_{ij}(t + \tau_i) w_{ij}(t + \tau_i) c_i(t + \tau_i) \cos(2\pi f_c t + \phi_i) \right) \\
&\quad c(t) w_0(t) \\
&= \sum_{i=1}^6 \sum_{j=0}^{K_i-1} R_i \sqrt{2P_{ij}} b_{ij}(t + \tau_i) w_{ij}(t + \tau_i) c_i(t + \tau_i) c(t) \cos(2\pi f_c t + \phi_i).
\end{aligned} \tag{4.10}$$

The pilot recover term $n_0(t)$ contains the noise as follows:

$$n_0(t) = n(t) c(t) w_0(t) = n(t) c(t). \tag{4.11}$$

We see that the terms $\gamma_0(t)$, $\varsigma_1(t)$, and $n_1(t)$ in $p(t)$ are still spread spectrum signals as compared to the narrowband component $I_0(t)$. Accordingly, when we filter $p(t)$ with a narrow bandpass filter centered at the carrier frequency f_c only the $I_0(t)$ term, which contains the desired pilot tone, will pass through.

We demodulate the received signal by applying the filtered pilot $I_0(t)$ to $y_1(t)$ which generates the demodulated signal $y_2(t)$ as follows:

$$\begin{aligned} y_2(t) &= y_1(t)I_0(t) = (I_1(t) + \gamma_1(t) + \varsigma_1(t) + n_1(t))I_0(t) \\ &= I_1I_0 + \gamma_1I_0 + \varsigma_1I_0 + n_1I_0. \end{aligned} \quad (4.12)$$

The desired information bit, $b_1(t)$ is now contained in the demodulated signal I_1I_0 defined by

$$\begin{aligned} I_1I_0 &= (R\sqrt{2P_1}b_1(t)\cos(2\pi f_c t))(R\sqrt{2P_0}\cos(2\pi f_c t)) \\ &= 2R^2\sqrt{P_0P_1}b_1(t)\cos^2(2\pi f_c t) \\ &= 2R^2\sqrt{P_0P_1}b_1(t)\left[\frac{1}{2}(1 + \cos(4\pi f_c t))\right] \\ &= R^2\sqrt{P_0P_1}b_1(t)(1 + \cos(4\pi f_c t)). \end{aligned} \quad (4.13)$$

The intracell interference is contained in the term γ_1I_0 :

$$\begin{aligned} \gamma_1I_0 &= \left(\sum_{\substack{k=0 \\ k \neq 1}}^{K-1} R\sqrt{2P_k}b_k(t)w_k(t)w_1(t)\cos(2\pi f_c t) \right) (R\sqrt{2P_0}\cos(2\pi f_c t)) \\ &= \sum_{\substack{k=0 \\ k \neq 1}}^{K-1} R^2 2\sqrt{P_0P_k}b_k(t)w_k(t)w_1(t)\cos^2(2\pi f_c t) \\ &= \sum_{\substack{k=0 \\ k \neq 1}}^{K-1} R^2\sqrt{P_0P_k}b_k(t)w_k(t)w_1(t)(1 + \cos(4\pi f_c t)). \end{aligned} \quad (4.14)$$

The intercell interference terms contained in the demodulated signal are contained in the term $\varsigma_1 I_0$:

$$\begin{aligned}
\varsigma_1 I_0 &= \left(\sum_{i=1}^6 \sum_{j=0}^{K_i-1} R_i \sqrt{2P_{ij}} b_{ij}(t+\tau_i) w_{ij}(t+\tau_i) w_1(t) c_i(t+\tau_i) c(t) \cos(2\pi f_c t + \varphi_i) \right) \\
&\quad R \sqrt{2P_0} (\cos(2\pi f_c t)) \\
&= R \sqrt{P_0} \sum_{i=1}^6 \sum_{j=0}^{K_i-1} 2R_i \sqrt{P_{ij}} b_{ij}(t+\tau_i) w_{ij}(t+\tau_i) w_1(t) c_i(t+\tau_i) c(t) \cdot \\
&\quad \cos(2\pi f_c t + \varphi_i) \cos(2\pi f_c t) \\
&= R \sqrt{P_0} \sum_{i=1}^6 \sum_{j=0}^{K_i-1} 2R_i \sqrt{P_{ij}} b_{ij}(t+\tau_i) w_{ij}(t+\tau_i) w_1(t) c_i(t+\tau_i) c(t) \cdot \\
&\quad \frac{1}{2} [\cos(\varphi_i) + \cos(4\pi f_c t + \varphi_i)] \\
&= R \sqrt{P_0} \sum_{i=1}^6 \sum_{j=0}^{K_i-1} R_i \sqrt{P_{ij}} b_{ij}(t+\tau_i) w_{ij}(t+\tau_i) w_1(t) c_i(t+\tau_i) c(t) \cdot \\
&\quad [\cos(\varphi_i) + \cos(4\pi f_c t + \varphi_i)].
\end{aligned} \tag{4.15}$$

The noise contained in the demodulated signal is found in the $n_1 I_0$:

$$\begin{aligned}
n_1 I_0 &= (n(t) c(t) w_1(t)) (R \sqrt{2P_0} \cos(2\pi f_c t)) \\
&= R \sqrt{2P_0} n(t) c(t) w_1(t) \cos(2\pi f_c t).
\end{aligned} \tag{4.16}$$

Accordingly, the demodulated signal $y_2(t)$ as defined by (4.12) through (4.16), is sent into the integrator to determine the decision statistic, Y .

2. The Decision Statistic Y

In this section we will develop the decision statistic Y , which will be used to determine whether the bit $b_1(t)$, for $t \in (0, T)$, is a logical zero or a logical one. We

calculate Y at time T by sending our demodulated signal $y_2(t)$ through an integrator as shown in Figure 4.3. This results in

$$\begin{aligned} Y &= \int_0^T y_2(t) dt \\ &= \int_0^T I_1 I_0 dt + \int_0^T \gamma_1 I_0 dt + \int_0^T \varsigma_1 I_0 dt + \int_0^T n_1 I_0 dt, \end{aligned} \quad (4.17)$$

where we integrate $y_2(t)$ term by term. Furthermore, we will fix the Rayleigh fading random variable at $R = r$ and the lognormal random variable representing the power received at $P_k = p_k$ in order to develop our decision statistic. This means that our decision statistic will be conditioned on $R = r$ and $P_k = p_k$, denoted by $Y|_{r,p_k}$. We will remove the conditioning from our solution later, by integrating out the dependence on the random variables. Accordingly, our decision statistic conditioned on the random variables R and P_k , is defined by

$$\begin{aligned} Y|_{r,p_k} &= \int_0^T y_2(t) dt \Big|_{r,p_k} \\ &= \underbrace{\int_0^T I_1 I_0 dt \Big|_{r,p_k}}_{\bar{Y}} + \underbrace{\int_0^T \gamma_1 I_0 dt \Big|_{r,p_k}}_0 + \underbrace{\int_0^T \varsigma_1 I_0 dt \Big|_{r,p_k}}_{\zeta} + \underbrace{\int_0^T n_1 I_0 dt \Big|_{r,p_k}}_{\eta}. \end{aligned} \quad (4.18)$$

We will develop each of these four components separately.

We begin with the first term, \bar{Y} , which is the output of the integrator containing our desired information bit. We define \bar{Y} by

$$\begin{aligned}
\bar{Y} &= \int_0^T I_1 I_0 dt \Big|_{r, p_k} \\
&= \int_0^T r^2 \sqrt{p_0 p_1} b_1(t) [1 + \cos(4\pi f_c t)] dt \\
&= r^2 \sqrt{p_0 p_1} b_1 \left[\int_0^T dt + \int_0^T \cos(4\pi f_c t) dt \right] \\
&= r^2 \sqrt{p_0 p_1} b_1 T,
\end{aligned} \tag{4.19}$$

where $b_k \in \{\pm 1\}$ corresponds with the time function $b_k(t)$, which is constant over the period $(0, T)$. We assume f_c is an integer multiple of $1/T$. Accordingly, b_1 is the desired information bit in the decision statistic $Y|_{r, p_k}$.

The intracell interference is completely eliminated from our decision statistic due to the orthogonality property of the Walsh functions as follows:

$$\begin{aligned}
\int_0^T \gamma_1 I_0 dt \Big|_{r, p_k} &= \int_0^T \sum_{\substack{k=0 \\ k \neq 1}}^{K-1} r^2 \sqrt{p_0 p_k} b_k(t) w_k(t) w_1(t) [1 + \cos(4\pi f_c t)] dt \\
&= r^2 \sum_{\substack{k=0 \\ k \neq 1}}^{K-1} \sqrt{p_0 p_k} b_k \left[\underbrace{\int_0^T w_k(t) w_1(t) dt}_0 + \underbrace{\int_0^T w_k(t) w_1(t) \cos(4\pi f_c t) dt}_0 \right] \\
&= 0,
\end{aligned} \tag{4.20}$$

where the first integral is zero due to the orthogonality of the Walsh functions, and the second integral is zero due to the fact we have further assumed that f_c is an integer multiple of $1/T_c$, or N/T . Since the product of Walsh functions is another Walsh function, we can break the interval $(0, T)$ into N pieces integrating over each chip interval.

The intercell interference contribution to the decision statistic is contained in the term ζ :

$$\begin{aligned}
\zeta &= \int_0^T \zeta_1 I_0 dt \Big|_{r, p_k} \\
&= \int_0^T r \sqrt{p_0} \sum_{i=1}^6 \sum_{j=0}^{K_i-1} R_i \sqrt{P_{ij}} b_{ij}(t + \tau_i) w_{ij}(t + \tau_i) w_1(t) c_i(t + \tau_i) c(t) \cdot \\
&\quad [\cos(\varphi_i) + \cos(4\pi f_c t + \varphi_i)] dt \\
&= r \sqrt{p_0} \int_0^T \sum_{i=1}^6 \sum_{j=0}^{K_i-1} R_i \sqrt{P_{ij}} b_{ij}(t + \tau_i) w_{ij}(t + \tau_i) w_1(t) c_i(t + \tau_i) c(t) \cos(\varphi_i) dt.
\end{aligned} \tag{4.21}$$

The additive noise contribution to the decision statistic is contained in the term η :

$$\begin{aligned}
\eta &= \int_0^T n_1 I_0 dt \Big|_{r, p_k} \\
&= \int_0^T r \sqrt{2p_0} n(t) c(t) w_1(t) \cos(2\pi f_c t) dt \\
&= r \sqrt{2p_0} \int_0^T n(t) c(t) w_1(t) \cos(2\pi f_c t) dt.
\end{aligned} \tag{4.22}$$

We can combine the noise and intercell interference terms in our decision statistic into a single term ξ :

$$\begin{aligned}
Y \Big|_{r, p_k} &= \bar{Y} + \zeta + \eta \\
&= \bar{Y} + \xi.
\end{aligned} \tag{4.23}$$

Accordingly, our decision statistic, conditioned on the random variables $R = r$ and $P_k = p_k$, is defined in (4.18) through (4.23). As defined, $Y \Big|_{r, p_k}$ is not particularly helpful in further developing the performance analysis for our system model. In order to move forward with our analysis, we will use the Gaussian Approximation from [25] and [26] to model our decision statistic. As the name implies, we model $Y \Big|_{r, p_k}$ as a Gaussian random variable \mathcal{Y} . The mean value is deterministic (for R and P_k fixed) and is given by

$$E\{\mathcal{Y}\} = \bar{Y}, \tag{4.24}$$

where \bar{Y} is defined by (4.19). The variance of our decision statistic is the sum of the variances of our co-channel interference term and noise term, which are assumed to be independent:

$$\mathcal{V}_{ar}\{\mathcal{Y}\} = \mathcal{V}_{ar}\{\zeta\} + \mathcal{V}_{ar}\{\eta\} = \mathcal{V}_{ar}\{\xi\} = \sigma_{\xi}^2. \quad (4.25)$$

Accordingly, we have modeled our decision statistic as a Gaussian random variable, $\mathcal{Y} \sim \mathcal{N}(\bar{Y}, \sigma_{\xi})$. This approximation of the decision statistic is based on the assumption that the co-channel interference term ζ and the additive noise term η can be modeled as independent zero-mean Gaussian random variables, as in [19]. We will use this approximation of our decision statistic to develop the SNIR and probability of error $\tilde{\mathcal{P}}_e$.

3. Signal-to-Noise Plus Interference Ratio

In this section we will develop a conditional SNIR for the DS-CDMA forward channel in the Rayleigh-lognormal fading channel. We will not remove the conditioning on the random variables $R = r$ and $P_k = p_k$ until we develop the probability of error $\tilde{\mathcal{P}}_e$ in Section IV.A.4. We define the SNIR at the output of the receiver as a ratio of the average power in the message component of the signal, to the average power of the noise and interference components, both taken at the output to the receiver after [27]. As developed in Section IV.A.2, our decision statistic \mathcal{Y} is made up of the message component of the signal \bar{Y} and the noise plus interference term ξ . Accordingly the conditional SNIR is defined by

$$\text{SNIR}|_{r,p_k} = \frac{\overline{Y}^2}{\sigma_\xi^2}, \quad (4.26)$$

where \overline{Y} is defined by (4.19), and σ_ξ^2 is yet to be developed from (4.25).

Since our co-channel interference contribution ζ is modeled as a zero-mean random variable, we define its variance by

$$\mathcal{V}_{\mathcal{A}\mathcal{R}}\{\zeta\} = \mathbb{E}\{\zeta^2\} = \frac{r^2 p_0 T^2}{3N} \sum_{i=1}^6 \sum_{j=0}^{K_i-1} \mathbb{E}\{R_i^2\} \mathbb{E}\{P_{ij}\}, \quad (4.27)$$

where the complete derivation of this term can be found in Appendix IV-A.

Similarly, the additive noise contribution to the decision statistic is zero-mean and its variance is developed as

$$\begin{aligned} \mathcal{V}_{\mathcal{A}\mathcal{R}}\{\eta\} &= \mathbb{E}\{\eta^2\} = \mathbb{E}\left\{\left(r\sqrt{2p_0}\int_0^T n(t)c(t)w_1(t)\cos(2\pi f_c t)dt\right)^2\right\} \\ &= \mathbb{E}\left\{\begin{aligned} &2r^2 p_0 \left(\int_0^T n(t)c(t)w_1(t)\cos(2\pi f_c t)dt\right) \cdot \\ &\left(\int_0^T n(\tilde{\lambda})c(\tilde{\lambda})w_1(\tilde{\lambda})\cos(2\pi f_c \tilde{\lambda})d\tilde{\lambda}\right) \end{aligned}\right\} \\ &= 2r^2 p_0 \mathbb{E}\left\{\int_0^T \int_0^T n(t)n(\tilde{\lambda})c(t)c(\tilde{\lambda})w_1(t)w_1(\tilde{\lambda})\cos(2\pi f_c t)\cos(2\pi f_c \tilde{\lambda})dtd\tilde{\lambda}\right\} \\ &= 2r^2 p_0 \int_0^T \int_0^T \mathbb{E}\{n(t)n(\tilde{\lambda})\}c(t)c(\tilde{\lambda})w_1(t)w_1(\tilde{\lambda})\cos(2\pi f_c t)\cos(2\pi f_c \tilde{\lambda})dtd\tilde{\lambda}, \end{aligned}$$

where we have taken the expectation operator into the integral. We assume $n(t)$ is a wide-sense stationary white noise process. Accordingly, the autocorrelation of the process is defined after [24] by

$$\mathbb{E}\{n(t)n(\tilde{\lambda})\} = \frac{N_0}{2} \delta(t - \tilde{\lambda}). \quad (4.28)$$

We substitute the autocorrelation function of the white noise process and continue developing the variance of η as

$$\begin{aligned}
\mathcal{V}_{\mathcal{A}}\{\eta\} &= 2r^2 p_0 \int_0^T \int_0^T \frac{N_0}{2} \delta(t - \lambda) c(t) c(\lambda) w_1(t) w_1(\lambda) \cdot \\
&\quad \cos(2\pi f_c t) \cos(2\pi f_c \lambda) dt d\lambda \\
&= 2r^2 p_0 \frac{N_0}{2} \int_0^T c^2(t) w_1^2(t) \cos^2(2\pi f_c t) dt \\
&= r^2 p_0 N_0 \int_0^T \frac{1}{2} [1 + \cos(4\pi f_c t)] dt \\
&= \frac{r^2 p_0 N_0}{2} \left[\int_0^T dt + \underbrace{\int_0^T \cos(4\pi f_c t) dt}_0 \right] \\
&= \frac{r^2 p_0 N_0 T}{2},
\end{aligned} \tag{4.29}$$

where $c^2(t) = 1$, and $w_1^2(t) = 1$.

Using (4.27) and (4.29), we can update the variance of the decision statistic defined by (4.25) as follows:

$$\begin{aligned}
\sigma_\xi^2 &= \mathcal{V}_{\mathcal{A}}\{\zeta\} + \mathcal{V}_{\mathcal{A}}\{\eta\} \\
&= \frac{r^2 p_0 T^2}{3N} \sum_{i=1}^6 \sum_{j=0}^{K_i-1} \mathbb{E}\{R_i^2\} \mathbb{E}\{P_{ij}\} + \frac{r^2 p_0 N_0 T}{2} \\
&= r^2 p_0 T \left[\frac{T}{3N} \sum_{i=1}^6 \sum_{j=0}^{K_i-1} \mathbb{E}\{R_i^2\} \mathbb{E}\{P_{ij}\} + \frac{N_0}{2} \right].
\end{aligned} \tag{4.30}$$

Accordingly, we define the conditional SNIR by

$$\begin{aligned}
\text{SNIR}|_{r, p_k} &= \frac{(\bar{Y})^2}{\sigma_\xi^2} = \frac{(r^2 \sqrt{p_0 p_1 T b_1})^2}{\sigma_\xi^2} \\
&= \frac{r^4 p_0 p_1 T^2}{r^2 p_0 T \left[\frac{T}{3N} \sum_{i=1}^6 \sum_{j=0}^{K_i-1} \mathbb{E}\{R_i^2\} \mathbb{E}\{P_{ij}\} + \frac{N_0}{2} \right]} \\
&= \frac{r^2 p_1}{\frac{1}{3N} \sum_{i=1}^6 \sum_{j=0}^{K_i-1} \mathbb{E}\{R_i^2\} \mathbb{E}\{P_{ij}\} + \frac{N_0}{2T}}.
\end{aligned} \tag{4.31}$$

By way of comparison, we can remove the fading and shadowing from our model by letting $p_1 = \mathbf{P}_{r,1}$ be the average received power in our information channel, and $P_{ij} = \mathbf{P}_{r,ij}$ be the average received power from the j th channel in adjacent cell i . The revised SNIR without fading, shadowing or the Hata-model incorporated would be

$$\begin{aligned}\widetilde{\text{SNIR}} &= \frac{\mathbf{P}_{r,1}}{\frac{1}{3N} \sum_{i=1}^6 \sum_{j=0}^{K_i-1} \mathbf{P}_{r,ij} + \frac{N_0}{2T}} \\ &= \frac{1}{\frac{1}{3N} \sum_{i=1}^6 \sum_{j=0}^{K_i-1} \frac{\mathbf{P}_{r,ij}}{\mathbf{P}_{r,1}} + \frac{N_0}{2T \mathbf{P}_{r,1}}}.\end{aligned}\tag{4.32}$$

This result corresponds with a similar analysis by Rappaport on the *reverse* channel of a CDMA Spread Spectrum system without fading or shadowing in [19].

4. Probability of Bit Error $\widetilde{\mathcal{P}}_e$

In order to develop the unconditional probability of bit error, we return to the decision statistic \mathcal{Y} , which by definition is conditioned upon random variables $R = r$ and $P_k = p_k$. When the decision statistic is a positive value the threshold detector will decide that the bit is positive (or a logical zero). Similarly, when the decision statistic is a negative value the threshold detector will choose the negative bit (or a logical one). Accordingly, we will have a decision error, or bit error, if the decision statistic $\mathcal{Y} < 0$, when $b_1 = +1$ was actually transmitted. We will also have a bit error if the decision statistic $\mathcal{Y} > 0$, when $b_1 = -1$ was the transmitted bit. Since the chances of a

logical zero or logical one being transmitted are equally likely, our probability of bit error can be described as

$$\widetilde{\mathcal{P}}_e \Big|_{r,p_k} = \frac{1}{2} \widetilde{\mathcal{P}}_e \Big|_{r,p_k,b_1=1} + \frac{1}{2} \widetilde{\mathcal{P}}_e \Big|_{r,p_k,b_1=-1} \quad (4.33)$$

Accordingly, we can determine the probability of error given that $b_1 = +1$ was the bit transmitted by

$$\begin{aligned} \widetilde{\mathcal{P}}_e \Big|_{r,p_k,b_1=1} &= \Pr \left[\mathcal{Y} \Big|_{b_1=1} < 0 \right] \\ &= \Pr \left[\bar{Y} \Big|_{b_1=1} + \xi < 0 \right] \\ &= \Pr \left[r^2 \sqrt{p_0 p_1} T + \xi < 0 \right]. \end{aligned}$$

Since our decision variable is modeled as a Gaussian random variable, $\mathcal{Y} \sim \mathcal{N}(\bar{Y}, \sigma_\xi)$,

the probability that $\mathcal{Y} \Big|_{b_1=1} < 0$ is the area under the left tail from $-\infty$ to 0 given by

$$\begin{aligned} \widetilde{\mathcal{P}}_e \Big|_{r,p_k,b_1=1} &= \int_{-\infty}^0 p_{\mathcal{Y}}(\mathcal{Y} \Big|_{b_1=1}) d\mathcal{Y} \\ &= \int_{-\infty}^0 \frac{1}{\sqrt{2\pi}\sigma_\xi} e^{-\frac{(\mathcal{Y} - \bar{Y} \Big|_{b_1=1})^2}{2\sigma_\xi^2}} d\mathcal{Y} \\ &= \frac{1}{\sqrt{2\pi}} \int_{-\infty}^{\frac{-\bar{Y} \Big|_{b_1=1}}{\sigma_\xi}} e^{-\frac{x^2}{2}} dx \\ &= \frac{1}{\sqrt{2\pi}} \int_{\frac{\bar{Y} \Big|_{b_1=1}}{\sigma_\xi}}^{\infty} e^{-\frac{x^2}{2}} dx \\ &= Q\left(\frac{\bar{Y} \Big|_{b_1=1}}{\sigma_\xi}\right) = Q\left(\sqrt{\frac{\bar{Y}^2}{\sigma_\xi^2}}\right) = Q\left(\sqrt{\text{SNIR} \Big|_{r,p_k}}\right), \end{aligned} \quad (4.34)$$

where $Q(x)$ is the Q-function defined by

$$Q(x) = \int_x^{\infty} \frac{1}{\sqrt{2\pi}} e^{-\frac{y^2}{2}} dy. \quad (4.35)$$

We find the conditional probability for $b_1 = -1$ and $\mathcal{Y}|_{b_1=-1} > 0$ in a similar manner. In this case the integral is evaluated from 0 to ∞ , and since $\bar{Y}|_{b_1=-1} = -\bar{Y}|_{b_1=1}$ the result for $\tilde{\mathcal{P}}_e|_{r,p_k,b_1=-1}$ is the same as (4.34). Accordingly, the total probability of bit error, calculated from (4.33), is

$$\begin{aligned}\tilde{\mathcal{P}}_e|_{r,p_1} &= Q\left(\sqrt{\text{SNIR}|_{r,p_1}}\right) \\ &= Q\left(\sqrt{\frac{r^2 p_1}{\frac{1}{3N} \sum_{i=1}^6 \sum_{j=0}^{K_i-1} \mathbb{E}\{R_i^2\} \mathbb{E}\{P_{ij}\} + \frac{N_0}{2T}}}\right).\end{aligned}\quad (4.36)$$

Since our SNIR is conditioned only on $R = r$ and $P_1 = p_1$, we revise our notation accordingly.

In order to remove the conditioning on the Rayleigh and lognormal random variables, $R = r$ and $P_1 = p_1$, we must integrate them over the range of their pdf's out of our solution. We remove the conditioning one random variable at a time in order to simplify the resulting expression representing the probability of error.

We remove the conditioning on $R = r$ from the probability of error as follows:

$$\begin{aligned}\tilde{\mathcal{P}}_e|_{p_1} &= \int_0^\infty \tilde{\mathcal{P}}_e|_{r,p_1} p_R(r) dr \\ &= \int_0^\infty Q\left(\sqrt{\text{SNIR}|_{r,p_1}}\right) p_R(r) dr \\ &= \int_0^\infty Q\left(\sqrt{\frac{r^2 p_1}{\frac{1}{3N} \sum_{i=1}^6 \sum_{j=0}^{K_i-1} \mathbb{E}\{R_i^2\} \mathbb{E}\{P_{ij}\} + \frac{N_0}{2T}}}\right) p_R(r) dr.\end{aligned}\quad (4.37)$$

We see that the probability of bit error, conditioned only on $P_1 = p_1$, is a function of $R^2 = r^2$, which is a chi-square random variable with two degrees of freedom. Accordingly, we transform the conditional SNIR after [24], by letting

$$\begin{aligned}\psi_2 &= \frac{R^2 p_1}{\frac{1}{3N} \sum_{i=1}^6 \sum_{j=0}^{K_i-1} \mathbb{E}\{R_i^2\} \mathbb{E}\{P_{ij}\} + \frac{N_0}{2T}} \\ &= \alpha|_{p_1} R^2,\end{aligned}\tag{4.38}$$

where

$$\alpha|_{p_1} = \frac{p_1}{\frac{1}{3N} \sum_{i=1}^6 \sum_{j=0}^{K_i-1} \mathbb{E}\{R_i^2\} \mathbb{E}\{P_{ij}\} + \frac{N_0}{2T}}.\tag{4.39}$$

Accordingly, our SNIR ψ_2 (conditioned on $P_1 = p_1$) is a chi-square random variable with two degrees of freedom, whose mean can be described by

$$\overline{\psi_2} = \mathbb{E}\{\psi_2\} = \mathbb{E}\{\alpha|_{p_1} R^2\} = \alpha|_{p_1} \mathbb{E}\{R^2\} = \alpha|_{p_1},\tag{4.40}$$

where we have normalized the underlying Rayleigh random variable, such that $\mathbb{E}\{R^2\} = 1$. We revise (4.37) using the transform variable, ψ_2 , and corresponding chi-square pdf from [24] as follows:

$$\begin{aligned}\widetilde{\mathcal{P}}_e|_{p_1} &= \int_0^\infty Q(\sqrt{\psi_2}) p_{\psi_2}(\psi_2) d\psi_2 \\ &= \frac{1}{2} \left(1 - \sqrt{\frac{\psi_2}{2 + \psi_2}} \right).\end{aligned}\tag{4.41}$$

The details of the integration in (4.41) can be found in Appendix IV-B.1. Thus, we have removed the conditioning on one of our random variables, initially conditioned as $R = r$, from our probability of bit error.

To remove the dependency of $\widetilde{\mathcal{P}}_e$ on the lognormal random variable $P_1 = p_1$, we must integrate the solution over the range of the pdf of p_1 as follows:

$$\begin{aligned}\widetilde{\mathcal{P}}_e &= \int_{-\infty}^{\infty} \widetilde{\mathcal{P}}_e \Big|_{p_1} p_{P_1}(p_1) dp_1 \\ &= \frac{1}{2} - \frac{1}{2\sqrt{2\pi}\lambda\sigma_{dB}} \int_0^{\infty} \frac{1}{x\sqrt{\mathcal{V}x+1}} e^{\frac{-(\ln x)^2}{2(\lambda\sigma_{dB})^2}} dx,\end{aligned}\tag{4.42}$$

where

$$\begin{aligned}\mathcal{V} &= \frac{2}{3N} \sum_{i=1}^6 \sum_{j=0}^{K_i-1} \frac{\mathcal{F}_{ij}}{\mathcal{F}_1} \frac{L_H(\mathbf{d})}{L_H(\mathbf{D}_i)} \mathbb{E}\left\{\frac{1}{X_i}\right\} + \frac{N_0}{E_b} \\ &= \frac{2\exp\left(\frac{\lambda^2\sigma_{dB}^2}{2}\right)}{3N} \sum_{i=1}^6 \sum_{j=0}^{K_i-1} \frac{\mathcal{F}_{ij}}{\mathcal{F}_1} \frac{L_H(\mathbf{d})}{L_H(\mathbf{D}_i)} + \frac{N_0}{E_b},\end{aligned}\tag{4.43}$$

and where we have normalized $\mathbb{E}\{R_i^2\} = \mathbb{E}\{R^2\} = 1$. We also have taken

$\mathbb{E}\{1/X_i\} = \mathbb{E}\{X_i\} = \exp\left(\frac{\lambda^2\sigma_{dB}^2}{2}\right)$ as developed in Appendix III-A where $\mu_x = \lambda\mu_{dB} = 0$.

Furthermore, we have introduced a new variable $E_b = \mathcal{F}_1 \mathbf{P}_t T / L_H(\mathbf{d})$, which represents a **baseline** received bit energy without the effects of fading or shadowing. The details of the conversion of (4.42) and (4.43) into the original model terms can be found in Appendix IV-B.2.

We have developed the probability of bit error for the uncoded system given in (4.42) and (4.43). The performance of the uncoded cellular system under normal operating conditions is quite poor ($\widetilde{\mathcal{P}}_e \approx 1/2$). Accordingly, for our performance analysis to be meaningful, we must add forward error correction (FEC) coding to the system, which we will accomplish in the next section.

B. CONVOLUTIONAL ENCODING OF DS-CDMA

In order to improve the performance of the DS-CDMA cellular system operating in the Rayleigh-lognormal channel, we institute forward error correction in the form of convolutional codes. We use an (n, k) encoder, which implies that for every k information bits, n coded bits are produced by the encoder and that the code rate R_{cc} is given by $R_{cc} = k/n$. The coded bits are spread, orthogonally covered, BPSK modulated, and transmitted by the base stations, in the same manner as the uncoded bits. In order to preserve the bit rate of the system, the bit duration for the coded system is reduced as $T_{cc} = TR_{cc} = T k/n$.

The convolutional encoder has a constraint length of ν , which means that a single information bit can affect the output of the encoder for a maximum of ν shifts, as defined in [27]. Accordingly, at least one of the k shift registers that make up the encoder has a length of $\nu - 1$.

1. Viterbi Branch and Path Metrics

To decode the information bit stream, we use the Viterbi Algorithm with soft-decision decoding. The output of our demodulator, Y from Figure 4.3, will be the input to the decoder. The decoder examines sequences of coded-demodulated bits, which we denote y_{jm} , to determine the most likely information bit stream for mobile user 1. The decoding decisions are based upon metrics developed from the input sequences. We will

analyze the performance of the coded system in a manner similar to that of Proakis [24], in which the Viterbi algorithm was applied to an additive white Gaussian noise channel with soft-decision decoding.

In order to simplify the performance analysis, we can assume that the all zero sequence (or $b_1(t) = 1$ for all t) was transmitted [24]. Accordingly, we will redefine our demodulator output from (4.23) to accommodate the analysis of coded sequences as follows:

$$y_{jm} \Big|_{r_{jm}, p_{k,jm}} = \bar{Y}_{jm}^c + \xi_{jm}^c, \quad (4.44)$$

where the subscript j specifies the branch (or information bit) in the trellis of the decoder, while the m specifies the position of the coded bit within the j th branch such that $m = 1, 2, \dots, n$, and where

$$\bar{Y}_{jm}^c = r_{jm}^2 \sqrt{p_{0,jm} p_{1,jm}} T_{cc}, \quad (4.45)$$

and

$$\begin{aligned} \xi_{jm}^c &= \zeta_{jm}^c + \eta_{jm}^c, \\ &= r_{jm}^2 \sqrt{p_{0,jm}} \int_{j(m-1)T_{cc}}^{jmT_{cc}} \sum_{i=1}^6 \sum_{j=0}^{K_i-1} R_i \sqrt{P_{ij}} b_{ij}(t + \tau_i) w_{ij}(t + \tau_i) w_1(t) c_i(t + \tau_i) c(t) \cos(\phi_i) dt + \\ &\quad + r_{jm}^2 \sqrt{2p_{0,jm}} \int_{j(m-1)T_{cc}}^{jmT_{cc}} n(t) c(t) w_1(t) \cos(2\pi f_c t) dt, \end{aligned} \quad (4.46)$$

with

$$j(m-1) \doteq \begin{cases} j(m-1), & m \neq 1 \\ (j-1)n, & m = 1 \text{ and } j \neq 1. \\ 0, & m = 1 \text{ and } j = 1 \end{cases}$$

Statistically, the decoder output \mathcal{Y}_{jm} , which is conditioned upon $R_{jm} = r_{jm}$ and $P_k = p_{k,jm}$, is approximated by a Gaussian random variable, just like $Y|_{r,p_k}$ in the uncoded system. Its moments are adapted from the uncoded case and are defined by

$$\mathbb{E}\{\mathcal{Y}_{jm}\} = \bar{Y}_{jm}^c, \quad (4.47)$$

and

$$\begin{aligned} \mathcal{V}\text{ar}\{\mathcal{Y}_{jm}\} &= \mathcal{V}\text{ar}\{\xi_{jm}^c\} \\ &= \frac{r_{jm}^2 p_{0,jm} T_{cc}^2}{3N} \sum_{i=1}^6 \sum_{j=0}^{K_i-1} \mathbb{E}\{R_i^2\} \mathbb{E}\{P_{ij}\} + \frac{r_{jm}^2 p_{0,jm} N_0 T_{cc}}{2} \\ &= r_{jm}^2 p_{0,jm} T_{cc} \left[\frac{T_{cc}}{3N} \sum_{i=1}^6 \sum_{j=0}^{K_i-1} \mathbb{E}\{R_i^2\} \mathbb{E}\{P_{ij}\} + \frac{N_0}{2} \right] \\ &= \sigma_{\xi_{jm}^c}^2. \end{aligned} \quad (4.48)$$

The Viterbi soft-decision decoder branch and path metrics are developed using \mathcal{B} branches per path through the trellis, and n coded bits per branch. For simplicity, we view each coded bit, as estimated by the i th path through the trellis, as a logically coded bit, denoted $c_{jm}^{(i)} \in \{0,1\}$, rather than a voltage, $b_{jm}^{c(i)} \in \{\pm 1\}$, such that, $b_{jm}^{c(i)} = 1 - 2c_{jm}^{(i)}$.

The Viterbi algorithm branch metrics in each path i for branch j are calculated after [24] as

$$\mu_j^{(i)} = \sum_{m=1}^n \mathcal{Y}_{jm} (1 - 2c_{jm}^{(i)}). \quad (4.49)$$

These are summed over \mathcal{B} branches to form path metrics

$$\begin{aligned}
CM^{(\epsilon)} &= \sum_{j=1}^B \mu_j^{(\epsilon)} \\
&= \sum_{j=1}^B \sum_{m=1}^n y_{jm} (1 - 2c_{jm}^{(\epsilon)}).
\end{aligned} \tag{4.50}$$

For example, if we let the all-zero path through the trellis (which is the correct path) be denoted as $\epsilon = 0$, then $c_{jm}^{(0)} = 0$, for all jm , and

$$\begin{aligned}
CM^{(0)} &= \sum_{j=1}^B \mu_j^{(0)} \\
&= \sum_{j=1}^B \sum_{m=1}^n y_{jm} (1 - 2c_{jm}^{(0)}) \\
&= \sum_{j=1}^B \sum_{m=1}^n y_{jm}.
\end{aligned} \tag{4.51}$$

Furthermore, if we let any competing path through the trellis, which decodes as a combination of zeros and ones, be denoted as $\epsilon = 1$, then its path metric can be described by

$$\begin{aligned}
CM^{(1)} &= \sum_{j=1}^B \mu_j^{(1)} \\
&= \sum_{j=1}^B \sum_{m=1}^n y_{jm} (1 - 2c_{jm}^{(1)}).
\end{aligned} \tag{4.52}$$

For any incorrect path $\epsilon = 1$, we know that $c_{jm}^{(1)} = 1$ in a finite number of coded bits, which we will denote as d bits. Accordingly, when we compare the coded bits in the correct path with the coded bits in the incorrect path, they are different in only the d positions in which $c_{jm}^{(1)} = 1$. We can use this fact to develop the probability of error for any path through the trellis that is a distance d from the all-zero path.

2. First-Event Error Probability

The first-event error probability is defined as the probability that at a node \mathcal{B} in the trellis, one of the competing paths merges with the correct path for the first time **and** the competing path has a path metric that exceeds the all-zero path metric [24]. When this happens, the decoder discards the correct path in favor of the incorrect path, which results in decoding error, and consequently bit errors. Using the path metrics defined by (4.51) and (4.52), we can compute a first-event error probability for a path $\ell = 1$ that is a distance d from the correct path as follows:

$$\begin{aligned}
 \mathcal{P}_2(d) \Big|_{r_{jm}, p_{k,jm}} &= \Pr\{CM^{(1)} \geq CM^{(0)}\} \\
 &= \Pr\{CM^{(1)} - CM^{(0)} \geq 0\} \\
 &= \Pr\left\{-2 \sum_{j=1}^{\mathcal{B}} \sum_{m=1}^n y_{jm} c_{jm}^{(1)} \geq 0\right\} \\
 &= \Pr\left\{\sum_{\ell=1}^d y'_{\ell} \leq 0\right\},
 \end{aligned} \tag{4.53}$$

where the new index ℓ runs over the set of d bits in which the two paths differ, or $y'_{\ell} = y_{jm}$, for $c_{jm}^{(1)} = 1$. Accordingly, the set $\{y'_{\ell}\}$ are independent and identically distributed Gaussian random variables, whose sum

$$y_{\ell} = \sum_{\ell=1}^d y'_{\ell}, \tag{4.54}$$

is also a Gaussian random variable with a mean

$$\begin{aligned}
\mathbb{E}\{\mathcal{Y}_\ell\} &= \sum_{\ell=1}^d \mathbb{E}\{\mathcal{Y}'_\ell\} = \sum_{\ell=1}^d r_\ell^2 \sqrt{p_{0,\ell} p_{1,\ell}} T_{cc} \\
&= \sum_{\ell=1}^d r_\ell^2 \sqrt{\left(\frac{\mathcal{F}_0 \mathbf{P}_t}{L_H(\mathbf{d}) x_\ell} \right) \left(\frac{\mathcal{F}_1 \mathbf{P}_t}{L_H(\mathbf{d}) x_\ell} \right)} T_{cc} \\
&= \frac{\sqrt{\mathcal{F}_0 \mathcal{F}_1} \mathbf{P}_t T_{cc}}{L_H(\mathbf{d})} \sum_{\ell=1}^d r_\ell^2 \frac{1}{x_\ell} \\
&= \frac{\sqrt{\mathcal{F}_0 \mathcal{F}_1} \mathbf{P}_t T_{cc}}{L_H(\mathbf{d})} \sum_{\ell=1}^d r_\ell^2 \tilde{x}_\ell \\
&= \overline{\mathcal{Y}_\ell}.
\end{aligned} \tag{4.55}$$

We converted the (fixed) terms $p_{0,\ell}$ and $p_{1,\ell}$, back to the original random variables, using (3.14) adapted as follows:

$$p_{k,\ell} = \frac{\mathcal{F}_k \mathbf{P}_t}{L_H(\mathbf{d}) x_\ell}, \tag{4.56}$$

where $X_\ell = x_\ell$ is our lognormal random variable, $X_\ell \sim \Lambda(0, \lambda \sigma_{dB})$. As shown in Appendix III-A.2, the transformation of $\widetilde{X}_\ell = 1/X_\ell$ results in another lognormal random variable, where $\widetilde{X}_\ell \sim \Lambda(0, \lambda \sigma_{dB})$.

The variance of the Gaussian random variable \mathcal{Y}_ℓ is defined by

$$\begin{aligned}
\mathcal{V}_{ar}\{\mathcal{Y}_\ell\} &= \sum_{\ell=1}^d \mathcal{V}_{ar}\{\mathcal{Y}'_\ell\} = \sum_{\ell=1}^d \sigma_{\xi_\ell}^2 \\
&= \sum_{\ell=1}^d r_\ell^2 p_{0,\ell} T_{cc} \left[\frac{T_{cc}}{3N} \sum_{i=1}^6 \sum_{j=0}^{K_i-1} \mathbb{E}\{R_i^2\} \mathbb{E}\{P_{ij}\} + \frac{N_0}{2} \right] \\
&= \sum_{\ell=1}^d r_\ell^2 \tilde{x}_\ell \left(\frac{\mathcal{F}_0 \mathbf{P}_t T_{cc}}{L_H(\mathbf{d})} \left[\frac{T_{cc}}{3N} \sum_{i=1}^6 \sum_{j=0}^{K_i-1} \mathbb{E}\{R_i^2\} \mathbb{E}\{P_{ij}\} + \frac{N_0}{2} \right] \right) \\
&= \sigma_{\mathcal{Y}_\ell}^2.
\end{aligned} \tag{4.57}$$

Accordingly, we can modify (4.53) using (4.54) through (4.57) as follows,

$$\begin{aligned}
\mathcal{P}_2(\mathbf{d}) \Big|_{r_\ell, p_{k,\ell}} &= \Pr\{\mathcal{Y} \leq 0\} \\
&= Q\left(\frac{\overline{\mathcal{Y}}}{\sigma_{\mathcal{Y}}}\right) = Q\left(\sqrt{\frac{\overline{\mathcal{Y}}^2}{\sigma_{\mathcal{Y}}^2}}\right) \\
&= Q\left(\sqrt{\frac{\frac{\mathcal{F}_0 \mathcal{F}_1 \mathbf{P}_t^2 T_{cc}^2 \left(\sum_{\ell=1}^d r_\ell^2 \tilde{x}_\ell\right)^2}{L_H^2(\mathbf{d})}}{\left(\frac{\mathcal{F}_0 \mathbf{P}_t T_{cc}}{L_H(\mathbf{d})} \left[\frac{T_{cc}}{3N} \sum_{i=1}^6 \sum_{j=0}^{K_i-1} \mathbb{E}\{R_i^2\} \mathbb{E}\{P_{ij}\} + \frac{N_0}{2} \right] \right) \sum_{\ell=1}^d r_\ell^2 \tilde{x}_\ell}}}\right) \\
&= Q\left(\sqrt{\frac{\sum_{\ell=1}^d r_\ell^2 \tilde{x}_\ell}{\frac{L_H(\mathbf{d})}{\mathcal{F}_1 \mathbf{P}_t T_{cc}} \left[\frac{T_{cc}}{3N} \sum_{i=1}^6 \sum_{j=0}^{K_i-1} \mathbb{E}\{R_i^2\} \mathbb{E}\{P_{ij}\} + \frac{N_0}{2} \right]}}}\right) \\
&= Q\left(\sqrt{\frac{\sum_{\ell=1}^d r_\ell^2 \tilde{x}_\ell}{\alpha}}\right) \\
&= Q\left(\sqrt{\frac{\mathcal{Z}_d}{\alpha}}\right) = \mathcal{P}_2(\mathbf{d}) \Big|_{z_d},
\end{aligned} \tag{4.58}$$

where we have introduced a new random variable $\mathcal{Z}_d = z_d$, which is the sum of d multiplicative chi-square(with 2 degrees of freedom)-lognormal random variables given by

$$\mathcal{Z}_d = \sum_{\ell=1}^d R_\ell^2 \widetilde{X}_\ell, \tag{4.59}$$

and where

$$\begin{aligned}
\alpha &= \frac{L_H(\mathbf{d})}{\mathcal{F}_1 \mathbf{P}_t T_{cc}} \left[\frac{T_{cc}}{3N} \sum_{i=1}^6 \sum_{j=0}^{K_i-1} \mathbb{E}\{R_i^2\} \mathbb{E}\{P_{ij}\} + \frac{N_0}{2} \right] \\
&= \frac{L_H(\mathbf{d})}{\mathcal{F}_1 \mathbf{P}_t T_{cc}} \left[\frac{T_{cc}}{3N} \sum_{i=1}^6 \sum_{j=0}^{K_i-1} \mathbb{E}\{R_i^2\} \frac{\mathcal{F}_{ij} \mathbf{P}_t}{L_H(\mathbf{D}_i)} \mathbb{E}\left\{\frac{1}{X_i}\right\} + \frac{N_0}{2} \right] \\
&= \frac{1}{3N} \sum_{i=1}^6 \sum_{j=0}^{K_i-1} \mathbb{E}\{R_i^2\} \frac{\mathcal{F}_{ij} L_H(\mathbf{d})}{\mathcal{F}_1 L_H(\mathbf{D}_i)} \mathbb{E}\left\{\frac{1}{X_i}\right\} + \frac{L_H(\mathbf{d}) N_0}{2 \mathcal{F}_1 \mathbf{P}_t T_{cc}} \\
&= \frac{\exp\left(\frac{\lambda^2 \sigma_{dB}^2}{2}\right)}{3N} \sum_{i=1}^6 \sum_{j=0}^{K_i-1} \frac{\mathcal{F}_{ij} L_H(\mathbf{d})}{\mathcal{F}_1 L_H(\mathbf{D}_i)} + \frac{N_0}{2E_c}.
\end{aligned} \tag{4.60}$$

Here we have reverted to the original lognormal random variable using (4.48), and taken

$$\mathbb{E}\{R_i^2\} = 1, \text{ and } \mathbb{E}\left\{\frac{1}{X_i}\right\} = \exp\left(\frac{\lambda^2 \sigma_{dB}^2}{2}\right); \quad E_c = (\ell/n) E_b \text{ is the coded bit energy.}$$

If we assume that we can find the pdf $p_{z_d}(z_d)$ for the new random variable, then we can remove the conditioning of the first-event error probability by integrating across its pdf to obtain

$$\begin{aligned}
\mathcal{P}_2(\mathbf{d}) &= \int_{-\infty}^{\infty} \mathcal{P}_2(\mathbf{d})|_{z_d} p_{z_d}(z_d) dz_d \\
&= \int_{-\infty}^{\infty} Q\left(\sqrt{\frac{z_d}{\alpha}}\right) p_{z_d}(z_d) dz_d,
\end{aligned} \tag{4.61}$$

where $\mathcal{P}_2(\mathbf{d})$ is the probability of first-event error for a path that is distance \mathbf{d} from the all-zero path and that merges with the all-zero path at node \mathcal{B} . For a given convolutional code, there are many such paths of differing distances that could merge with the all-zero path at node \mathcal{B} . Accordingly, we can calculate an upper bound on our first-event error probability, \mathcal{P}_2 , by summing all the possible paths as follows [24],

$$\mathcal{P}_2 \leq \sum_{\mathbf{d}=\mathbf{d}_{\text{free}}}^{\infty} A_{\mathbf{d}} \mathcal{P}_2(\mathbf{d}), \tag{4.62}$$

where A_d is the total number of paths that is a distance d from the all-zero path and that mergers with the all zero path for the first time at node \mathcal{B} . We can also calculate an upper bound on the probability of bit error \mathcal{P}_e using the total number of information bit errors β_d that is associated with selecting a path of distance d from the all zero path:

$$\mathcal{P}_e \leq \frac{1}{K} \sum_{d=d_{\min}}^{\infty} \beta_d \mathcal{P}_2(d). \quad (4.63)$$

For any particular convolutional code, the values of A_d and β_d can be calculated. Accordingly, we have developed a probability of error, \mathcal{P}_e , for the coded DS-CDMA cellular system in the Rayleigh-lognormal channel, contingent upon finding the distribution for our random variable \mathcal{Z}_d , which is a non-trivial undertaking. We address the difficulties and propose a solution to this problem in the next section.

C. APPROXIMATING THE SUM OF MULTIPLICATIVE CHI-SQUARE2-LOGNORMAL RANDOM VARIABLES

In Section IV.B, we developed an upper bound on the probability of bit error \mathcal{P}_e for the coded system. This bound depends upon all possible path errors $\mathcal{P}_2(d)$, as defined by (4.61), that are at distance d from the correct path. In order to calculate $\mathcal{P}_2(d)$ for a specific distance d , we must first find the probability density function for the sum of d chi-square2-lognormal random variables as defined by (4.59), where the chi-square2-lognormal notation represents a multiplicative chi-square (with 2 degrees of freedom)-lognormal random variable. In Section IV.A, we developed the probability of

bit error, $\tilde{\mathcal{P}}_e$, for the uncoded case by integrating out its dependency on the chi-square and the lognormal random variables separately. The fact that $\mathcal{P}_2(d)$ is dependent on the sum of d chi-square2-lognormal complicates the situation for the coded system. If we let $\mathcal{M} = R^2 X$ represent our single chi-square2-lognormal random variable, then we can reasonably find the pdf for \mathcal{M} , which we represent as $p_{\mathcal{M}}(m)$. The random variable \mathcal{Z}_d , which is a sum of d chi-square2-lognormal random variables, has a probability distribution function that can only be determined by convolving $p_{\mathcal{M}}(m)$ with itself d times as follows:

$$p_{\mathcal{Z}_d}(z_d) = \underbrace{p_{\mathcal{M}_1}(m_1) * p_{\mathcal{M}_2}(m_2) * \dots * p_{\mathcal{M}_d}(m_d)}_d.$$

Furthermore, for any particular convolutional encoder we require a series of $\mathcal{P}_2(d)$ for $d = d_{free}, d_{free} + 1, d_{free} + 2, \dots$ in order to calculate the upper bound on the probability of bit error, \mathcal{P}_e as defined in (4.63). If we truncate the series by using only the first five terms, e.g.,

$$\mathcal{P}_e \leq \frac{1}{K} \sum_{d=d_{free}}^{d_{free}+4} \beta_d \mathcal{P}_2(d),$$

we will need to perform $5d_{free} + 10$ convolutions, or integrations, to determine \mathcal{P}_e for a particular operating scenario. In our analysis, we will consider convolutional encoders with a code rate of $1/2$ and constraint lengths ranging from 7 to 9. Typically, d_{free} for such encoders ranges from 10 to 12. Accordingly, for each operating scenario that we wish to consider, we would need to perform between 60 and 70 convolutions in order to

calculate the upper bound on the probability of bit error, \mathcal{P}_e for that *set of data*. The computational cost in performing these integrations is too high a price to pay, which explains why analysis of coded DS-CDMA systems that include both fading and shadowing models has not previously been accomplished.

Our situation would be greatly improved if our channel model only considered the case of Rayleigh fading. For example, we can modify (4.58) to eliminate the lognormal shadowing, which results in

$$\begin{aligned}
 \widehat{\mathcal{P}}_2(\mathbf{d}) \Big|_{r_\ell} &= Q \left(\sqrt{\frac{\sum_{\ell=1}^d r_\ell^2}{\frac{1}{3N} \sum_{i=1}^6 \sum_{j=0}^{K_i-1} \mathbb{E}\{R_i^2\} \frac{\mathcal{F}_{ij}}{\mathcal{F}_1} \frac{L_H(\mathbf{d})}{L_H(\mathbf{D}_i)} + \frac{N_0}{2E_c}}} \right) \\
 &= Q \left(\sqrt{\sum_{\ell=1}^d \widehat{\psi}_\ell} \right) \\
 &= Q \left(\sqrt{\widehat{\psi}_{2d}} \right) = \widehat{\mathcal{P}}_2(\mathbf{d}) \Big|_{\widehat{\psi}_{2d}},
 \end{aligned} \tag{4.64}$$

where $\widehat{\psi}_{2d}$ is the sum of d chi-square random variables, $\widehat{\psi}_\ell$, with two degrees of freedom. The distribution of $\widehat{\psi}_{2d}$ is chi-square with $2d$ degrees of freedom [24]. Accordingly, we remove the dependence on the random variable $\widehat{\psi}_{2d}$ by integrating across its pdf, obtaining

$$\begin{aligned}
 \widehat{\mathcal{P}}_2(\mathbf{d}) &= \int_{-\infty}^{\infty} \widehat{\mathcal{P}}_2(\mathbf{d}) \Big|_{\widehat{\psi}_{2d}} p_{\widehat{\psi}_{2d}}(\widehat{\psi}_{2d}) d\widehat{\psi}_{2d} \\
 &= \int_{-\infty}^{\infty} Q \left(\sqrt{\widehat{\psi}_{2d}} \right) p_{\widehat{\psi}_{2d}}(\widehat{\psi}_{2d}) d\widehat{\psi}_{2d},
 \end{aligned}$$

which has a closed form solution as defined in [24] for L-fold diversity and adapted for $L = d$ by

$$\widehat{\mathcal{P}}_2(d) = \mu^d \sum_{k=0}^{d-1} \binom{d-1+k}{k} (1-\mu)^k, \quad (4.65)$$

where

$$\mu = \frac{1}{2} \left(1 - \sqrt{\frac{\mathbb{E}\{\widehat{\psi}_\ell\}}{2 + \mathbb{E}\{\widehat{\psi}_\ell\}}} \right),$$

and where $\mathbb{E}\{\widehat{\psi}_\ell\}$ is defined by

$$\begin{aligned} \mathbb{E}\{\widehat{\psi}_\ell\} &= \mathbb{E} \left\{ \frac{R_\ell^2}{\frac{1}{3N} \sum_{i=1}^6 \sum_{j=0}^{K_i-1} \mathbb{E}\{R_i^2\} \frac{\mathcal{F}_{ij}}{\mathcal{F}_1} \frac{L_H(\mathbf{d})}{L_H(\mathbf{D}_i)} + \frac{N_0}{2E_c}} \right\} \\ &= \frac{\mathbb{E}\{R_\ell^2\}}{\frac{1}{3N} \sum_{i=1}^6 \sum_{j=0}^{K_i-1} \mathbb{E}\{R_i^2\} \frac{\mathcal{F}_{ij}}{\mathcal{F}_1} \frac{L_H(\mathbf{d})}{L_H(\mathbf{D}_i)} + \frac{N_0}{2E_c}}. \end{aligned}$$

For example, Figure 4.4 depicts the upper bound on the probability of bit error for a DS-CDMA in a Rayleigh fading channel using (4.65) and (4.63) using a rate $\frac{1}{2}$ convolutional encoder with constraint length $v=8$ as compared with the uncoded system. The extended Hata model for a large city is incorporated with parameters $d=1$ km; $f_c=2$ GHz; $h_{\text{base}}=30$ m; $h_{\text{mobile}}=1$ m. By way of comparison, Figure 4.4 also includes the probability of bit error for the coded and uncoded system in an AWGN channel with an average received Signal-to-Noise Ratio (SNR) per bit of $\overline{\gamma}_b = E_b/N_0$.

The average received SNR per bit for the Rayleigh fading channel is developed as follows:

$$\overline{\gamma_b} = \mathbb{E} \left\{ \frac{R^2 \mathcal{P}_T}{N_0 L_H(\mathbf{d})} \right\} = \mathbb{E} \{ R^2 \} \frac{E_b}{N_0} = \frac{E_b}{N_0},$$

since we have normalized $\mathbb{E} \{ R^2 \} = 1$.

As shown in Figure 4.4, the DS-CDMA system can achieve a probability of bit error in the Rayleigh fading channel of 10^{-6} using FEC ($R_{cc} = 1/2; \nu=8$) with an average SNR of approximately 9 dB with 10 users per cell. In the uncoded case, we see the

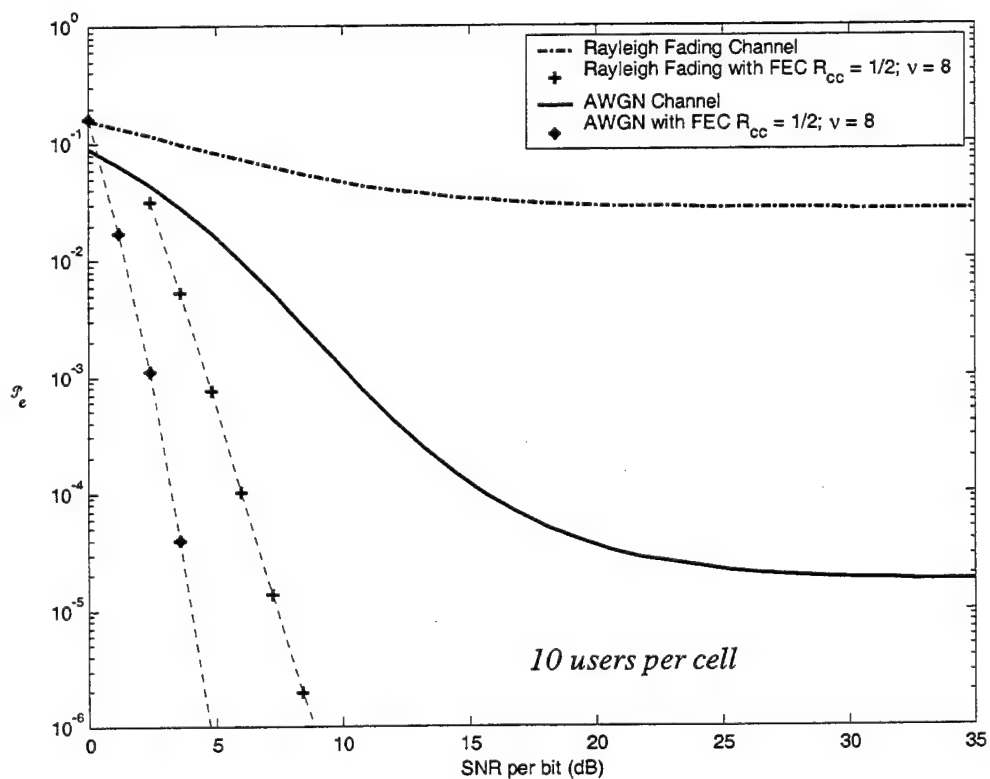


Figure 4.4 Performance of a DS-CDMA System in a Rayleigh Fading Channel.

interference floor for the Rayleigh fading channel and the AWGN channel developing at an average SNR per bit of 20 dB. Accordingly, in the case of Rayleigh fading only, we can calculate the upper bound on the probability of bit error defined by (4.63) using the closed form solution in (4.65) for $\mathcal{P}_2(d)$ without performing any convolutions.

If we consider the case of lognormal shadowing only (no Rayleigh fading), we modify (4.61) as follows:

$$\begin{aligned}\widehat{\mathcal{P}}_2(d)\Big|_{x_\ell} &= Q\left(\sqrt{\frac{\sum_{\ell=1}^d x_\ell}{\alpha}}\right) \\ &= Q\left(\sqrt{\frac{x_d}{\alpha}}\right) = \widehat{\mathcal{P}}_2(d)\Big|_{x_d},\end{aligned}\tag{4.66}$$

where α is defined by (4.60). We have also introduced a new random variable

$\mathcal{X}_d = x_d = \sum_{\ell=1}^d x_\ell$, which is a sum of lognormal random variables $X_\ell \sim \Lambda(0, \lambda\sigma_{dB})$ fixed

at $X_\ell = x_\ell$. In order to remove the conditioning on x_d , we must determine its probability distribution function.

Since the sum of lognormal random variables appears in many important communications, radar, and antennae problems, considerable effort has been given in finding its distribution function [30]-[33]. While no closed form solution for the distribution function has been found, there is agreement that the sum of lognormal random variables can be approximated as another lognormal random variable. Accordingly, in order to model the sum of independent lognormal random variables as another lognormal random variable, we must determine suitable parameters for the

model. There have been many different approaches to finding the lognormal model parameters, such as moment matching or cumulant matching [33]. For example, the cumulant matching approach seeks model parameters, for which the Cumulative Distribution Function (CDF) of the model lognormal random variable matches the CDF of the sum of lognormal random variables (as simulated using Monte Carlo methods.) Once the lognormal model parameters are determined using one of the methods outlined in [33], the approximated distribution is completely specified. Accordingly, for the case of strictly lognormal shadowing, we can remove the conditioning of $\widehat{\widehat{\mathcal{P}}}_2(\mathbf{d})$ on $\mathcal{X}_d = x_d$ by approximating it as another lognormal random variable. Consequently, we can solve for the upper bound on the probability of bit error using (4.63) for lognormal shadowing only.

In summary, the distribution of the sum of d chi-square random variables with 2 degrees of freedom is chi-square with $2d$ degrees of freedom. Furthermore, the distribution of the sum of lognormal random variables can be approximated as lognormal. In light of these two facts, we will approximate our sum of d chi-square2-lognormal random variables, \mathcal{Z}_d , as a multiplicative chi-square(with $2d$ degrees of freedom)-lognormal random variable.

1. Defining the Model $\widetilde{\mathcal{Z}}_d$

In order to approximate \mathcal{Z}_d as a chi-square $2d$ -lognormal random variable, we first represent our model $\widetilde{\mathcal{Z}}_d$ in terms of its two factors defined by

$$\widetilde{\mathcal{Z}}_d = \mathcal{Y}_{2d} \mathcal{X}_z, \quad (4.67)$$

where \mathcal{Y}_{2d} is a chi-square random variable with $2d$ degrees of freedom, whose distribution is completely specified based on the underlying Rayleigh random variable, i.e., $\mathcal{Y}_{2d} = \sum_d R^2$. Accordingly, the moments of \mathcal{Y}_{2d} are defined by

$$\begin{aligned} \mathbb{E}\{\mathcal{Y}_{2d}\} &= d\mathbb{E}\{R^2\} = d, \\ \mathbb{E}\{\mathcal{Y}_{2d}^2\} &= d + d^2, \\ \text{and } \mathcal{V}\{\mathcal{Y}_{2d}\} &= d, \end{aligned} \quad (4.68)$$

where we have normalized $\mathbb{E}\{R^2\} = 1$. Furthermore, $\mathcal{X}_z \sim \Lambda(\mu_z, \sigma_z)$ is the lognormal component of $\widetilde{\mathcal{Z}}_d$, where the model parameters μ_z and σ_z are yet to be developed. The moments of \mathcal{X}_z are given in Appendix III-A by (3.27) through (3.29).

We develop the moments for our model by assuming that \mathcal{Y}_{2d} and \mathcal{X}_z , from which we obtain

$$\begin{aligned} \mathbb{E}\{\widetilde{\mathcal{Z}}_d\} &= \mathbb{E}\{\mathcal{Y}_{2d} \mathcal{X}_z\} = \mathbb{E}\{\mathcal{Y}_{2d}\} \mathbb{E}\{\mathcal{X}_z\} \\ &= d \exp\left(\mu_z + \frac{\sigma_z^2}{2}\right). \end{aligned} \quad (4.69)$$

The second moment of $\widetilde{\mathcal{Z}}_d$ can be developed from the second moments of \mathcal{Y}_{2d} and \mathcal{X}_z as follows:

$$\begin{aligned} \mathbb{E}\{\widetilde{\mathcal{Z}}_d^2\} &= \mathbb{E}\{\mathcal{Y}_{2d}^2 \mathcal{X}_z^2\} = \mathbb{E}\{\mathcal{Y}_{2d}^2\} \mathbb{E}\{\mathcal{X}_z^2\} \\ &= (d + d^2) \exp(2\mu_z + 2\sigma_z^2). \end{aligned} \quad (4.70)$$

Finally, the variance of $\widetilde{\mathcal{Z}}_d$ can be developed from its first and second moments defined by

$$\mathcal{V}_{ar}\{\widetilde{\mathcal{Z}}_d\} = d e^{2\mu_z + \sigma_z^2} \left[(1+d) e^{\sigma_z^2} - d \right]. \quad (4.71)$$

The remaining step in approximating \mathcal{Z}_d as chi-square $2d$ -lognormal is in determining the model parameters μ_z and σ_z^2 for \mathcal{X}_z . We develop these two parameters by relating the mean (4.69) and variance (4.71) of our model $\widetilde{\mathcal{Z}}_d$ with a **scaled** version of mean and variance of the original chi-square2-lognormal random variable, R^2X .

To establish a value for μ_z , which is related to the original chi-square2-lognormal channel conditions, we observe in simulations that the mean of \mathcal{Z}_d is proportional to d times the mean of the original chi-square2-lognormal. Accordingly, we equate the mean of our model with d times the mean of R^2X scaled by a factor of \mathcal{G}_1 as follows:

$$\mathbb{E}\{\widetilde{\mathcal{Z}}_d\} = \mathcal{G}_1 d \mathbb{E}\{R^2X\} = \mathcal{G}_1 d \exp\left(\frac{\sigma_x^2}{2}\right),$$

where $\sigma_x^2 = \lambda^2 \sigma_{dB}^2$ is the parameter from our original lognormal shadowing random variable, $X \sim \Lambda(0, \sigma_x)$. By applying (4.69), we solve for

$$\mu_z = \frac{(\sigma_x^2 - \sigma_z^2)}{2} + \ln(\mathcal{G}_1). \quad (4.72)$$

In order to define the parameter σ_z^2 , we observe that the variance of \mathcal{Z}_d is proportional to d times the variance of the original chi-square2-lognormal. Accordingly, we equate the variance of our model with d times the variance of R^2X scaled by a factor of \mathcal{G}_2 as follows:

$$\mathcal{V}\text{ar}\{\widetilde{\mathcal{Z}}_d\} = g_2 d \mathcal{V}\text{ar}\{R^2 X\} = g_2 d e^{\sigma_x^2} [2e^{\sigma_x^2} - 1].$$

By applying (4.71), we solve for

$$\sigma_z^2 = \ln \left[\frac{g_2}{g_1^2} (2e^{\sigma_x^2} - 1) + d \right] - \ln(1 + d). \quad (4.73)$$

The scaling factors g_1 and g_2 of the mean and variance, respectively, vary with σ_{dB} and are chosen such that the CDF of our model $\widetilde{\mathcal{Z}}_d$ best matches the CDF of \mathcal{Z}_d for $d = 8, 9, \dots, 16$. Table 4.1 depicts the values of g_1 and g_2 for each σ_{dB} as determined by simulation.

σ_{dB}	g_1	g_2
2	1	.9875
3	1	.9625
4	1	.9125
5	1	.8125
6	.9375	.4875
7	.9125	.3375
8	.8625	.2
9	.8	.1

Table 4.1 Values of g_1 and g_2 for $\widetilde{\mathcal{Z}}_d$.

With the model parameters completely specified, we can now develop the pdf of $\widetilde{\mathcal{Z}}_d$ using the marginal densities of its components; namely \mathcal{Y}_{2d} and \mathcal{X}_z . We return to

the transformation defined by (4.67) and fix $X_z = x$, which implies that $\widetilde{Z}_d|_x = xY_{2d}$.

The conditional pdf of $\widetilde{Z}_d|_x$ is given by

$$\begin{aligned} p_{\widetilde{Z}_d|_x}(z|x) &= \frac{1}{|x|} p_{Y_{2d}}\left(\frac{z}{x}\right) \\ &= \frac{1}{x\Gamma(d)} \frac{z^{d-1}}{x^{d-1}} \exp\left(\frac{-z}{x}\right) \\ &= \frac{1}{x^d\Gamma(d)} z^{d-1} \exp\left(\frac{-z}{x}\right), \quad \frac{z}{x} \geq 0. \end{aligned}$$

We remove the conditioning of \widetilde{Z}_d on $X_z = x$ as follows:

$$\begin{aligned} p_{\widetilde{Z}_d}(z) &= \int_{-\infty}^{\infty} p_{\widetilde{Z}_d|_x}(z|x) p_{X_z}(x) dx \\ &= \int_0^{\infty} \frac{1}{x^d\Gamma(d)} z^{d-1} \exp\left(\frac{-z}{x}\right) \frac{1}{x\sqrt{2\pi}\sigma_z} \exp\left(\frac{-(\ln x - \mu_z)^2}{2\sigma_z^2}\right) dx \\ &= \frac{z^{d-1}}{\sqrt{2\pi}\sigma_z\Gamma(d)} \int_0^{\infty} \frac{1}{x^{d+1}} \exp\left(\frac{-z}{x} - \frac{(\ln x - \mu_z)^2}{2\sigma_z^2}\right) dx, \quad z \geq 0, \end{aligned} \tag{4.74}$$

where μ_z and σ_z^2 are defined by (4.72) and (4.73), respectively.

We have developed a distribution for the chi-square $2d$ -lognormal random variable \widetilde{Z}_d , which approximates the distribution of a sum of d chi-square2-lognormal random variables. In the next section we will look at specific examples of the model and compare performance results using our model with the results as predicted by Monte Carlo simulations.

2. Testing the Model $\widetilde{\mathcal{Z}}_d$

In this section we will explore the usefulness of our model as it applies to bit error analysis of DS-CDMA with FEC. As an example, we will consider the case of $\sigma_{dB} = 7$ with rate $\frac{1}{2}$ convolution encoding with $\nu = 8$ and approximate the probability of bit error using the first five terms of the union bound from (4.63). Accordingly, we will examine our model's ability to approximate $\mathcal{P}_2(d)$ for $d = 10$ through 14, since these are the key parameters when employing rate $\frac{1}{2}$ convolutional encoding with constraint lengths 7 and 8.

Figures 4.5 through 4.9 show histograms for \mathcal{Z}_d with $\sigma_{dB} = 7$ and $\mathbb{E}\{R^2\} = 1$, which were formed by generating d sets of chi-square2-lognormal distributed data consisting of 400,000 independent samples per set and summing over the d sets. We have over-plotted the histogram with the pdf of our model, $\widetilde{\mathcal{Z}}_d$.

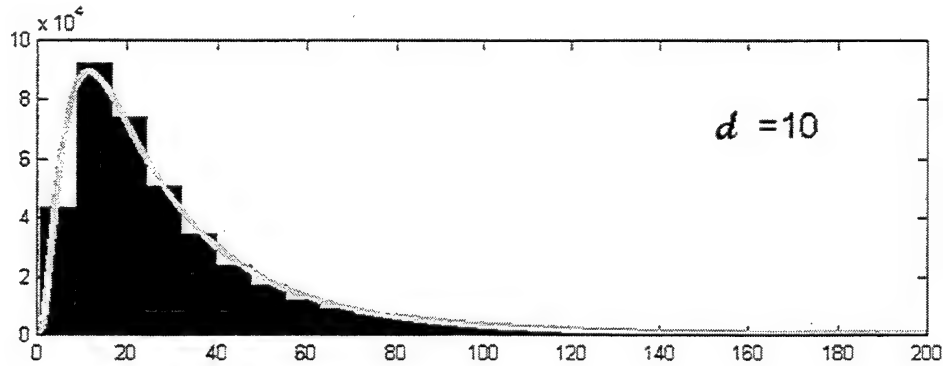


Figure 4.5 Histogram of \mathcal{Z}_{10} and the PDF for $\widetilde{\mathcal{Z}}_{10}$ for $\sigma_{dB} = 7$.

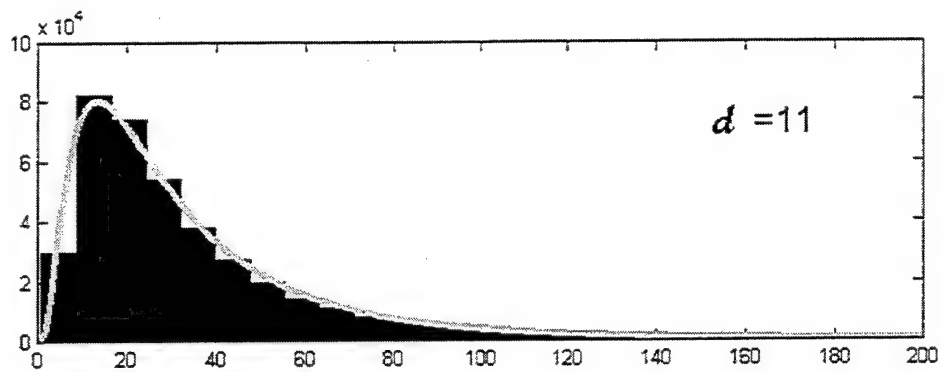


Figure 4.6 Histogram of Z_{11} and the PDF for \widetilde{Z}_{11} for $\sigma_{dB} = 7$.

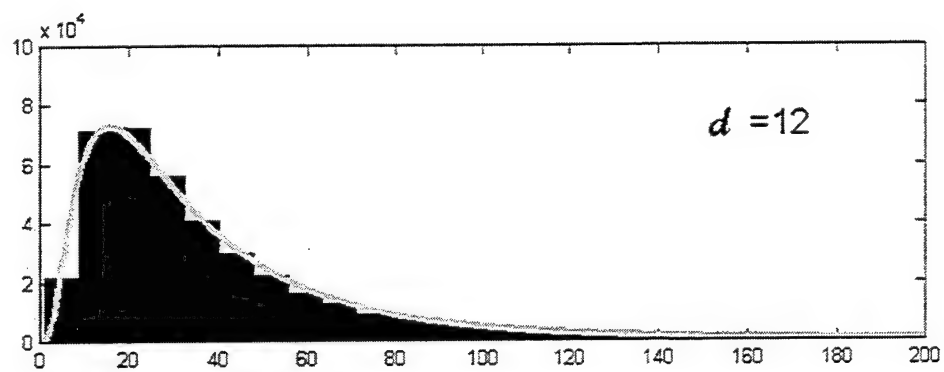


Figure 4.7 Histogram of Z_{12} and the PDF for \widetilde{Z}_{12} for $\sigma_{dB} = 7$.

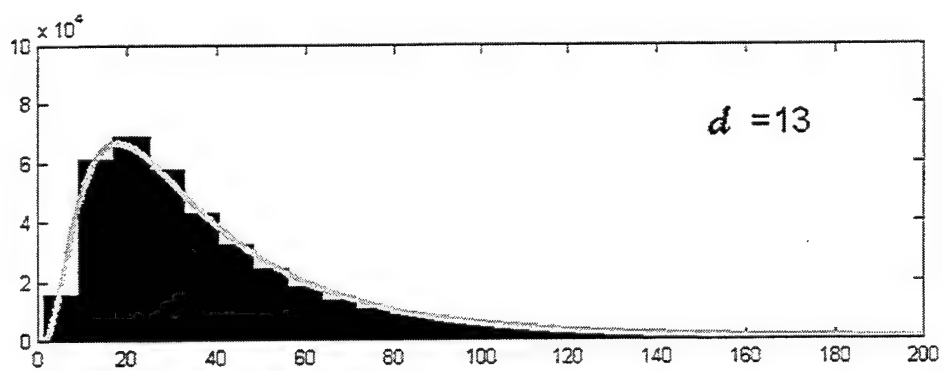


Figure 4.8 Histogram of Z_{13} and the PDF for \widetilde{Z}_{13} for $\sigma_{dB} = 7$.

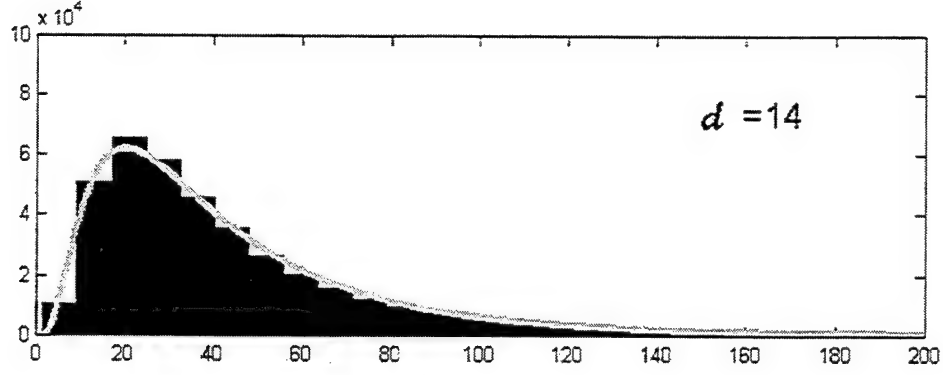


Figure 4.9 Histogram of Z_{14} and the PDF for \widetilde{Z}_{14} for $\sigma_{dB} = 7$.

We know that the distribution of Z_d is *not* chi-square $2d$ -lognormal as approximated by \widetilde{Z}_d . The real question is whether \widetilde{Z}_d can well approximate Z_d in calculating the first-event error probability as defined (4.61). In order to determine this answer, we evaluate the integral in (4.58) by simulation and compare with the result predicted by our model. We simulate the integral by generating d independent samples from the chi-square2-lognormal distribution and summing them to form one realization for z_d and consequently one realization, ρ_1 , for $\mathcal{P}_2(d)$. We repeat this process 100,000 times and form our point estimate, $\overline{\rho}$, for $\mathcal{P}_2(d)$ as follows:

$$\overline{\rho} = \frac{1}{10^5} \sum_{i=1}^{10^5} \rho_i. \quad (4.75)$$

Figures 4.10 through 4.14 show the point estimates for the simulated $\mathcal{P}_2(d)$ as compared with its approximation using our model for the case of $\sigma_{dB} = 7$ with 10 users per adjacent cell and $d = 10$ through 14. In this case, our model well approximates the simulated result for $\mathcal{P}_2(d)$.

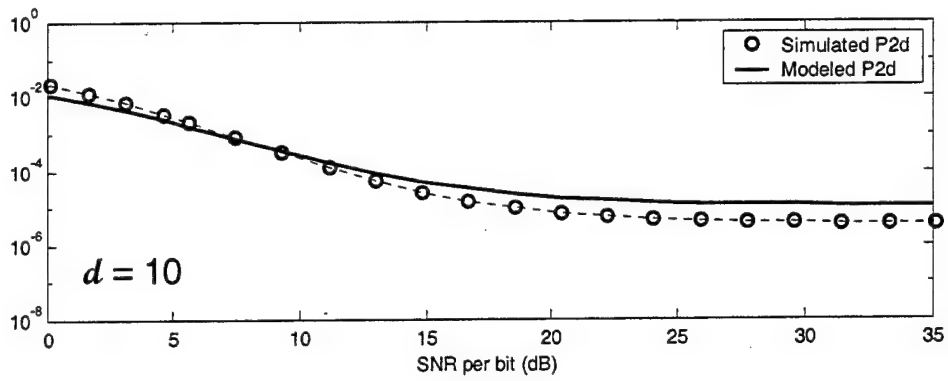


Figure 4.10 First Event Error Probability $\mathcal{P}_2(10)$ for $\sigma_{dB} = 7$ with 10 users per cell.

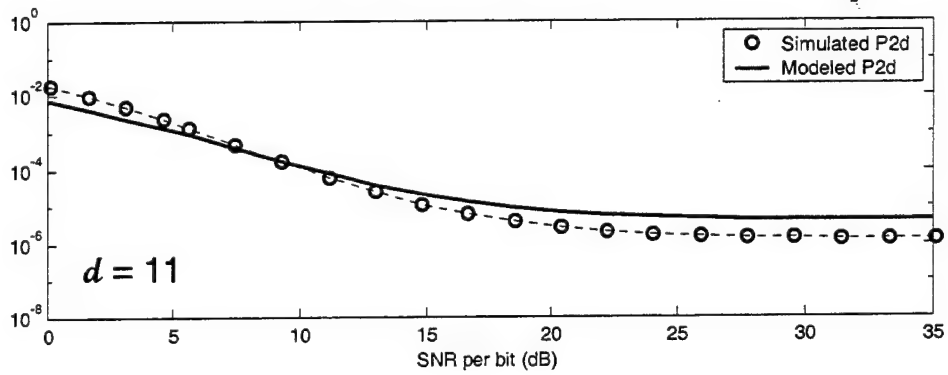


Figure 4.11 First Event Error Probability $\mathcal{P}_2(11)$ for $\sigma_{dB} = 7$ with 10 users per cell.

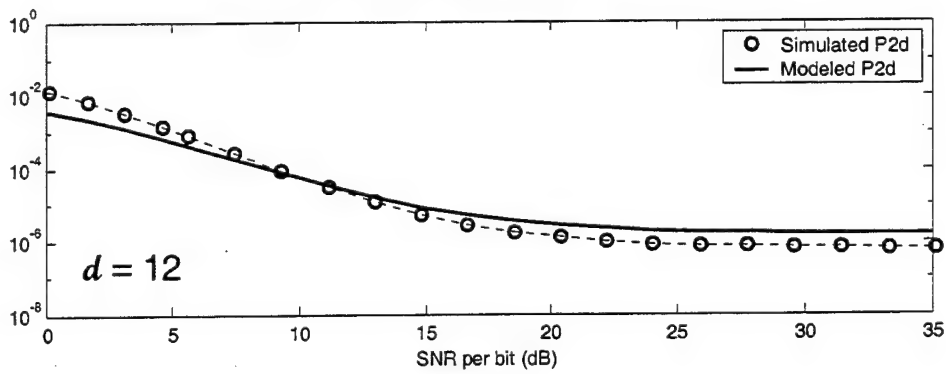


Figure 4.12 First Event Error Probability $\mathcal{P}_2(12)$ for $\sigma_{dB} = 7$ with 10 users per cell.

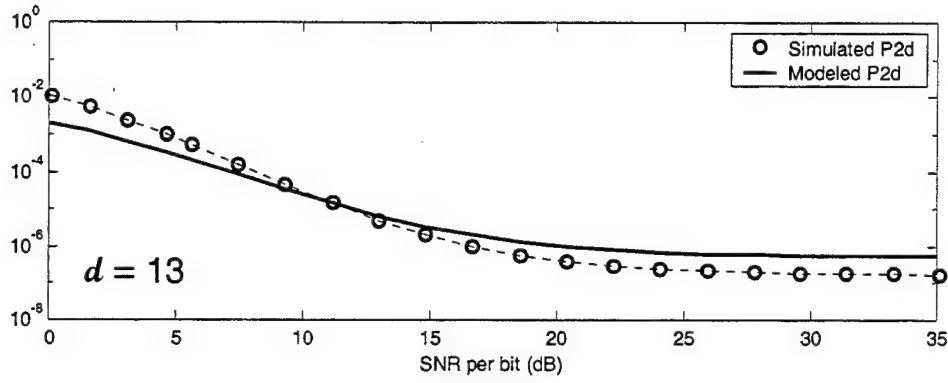


Figure 4.13 First Event Error Probability $\mathcal{P}_2(13)$ for $\sigma_{dB} = 7$ with 10 users per cell.

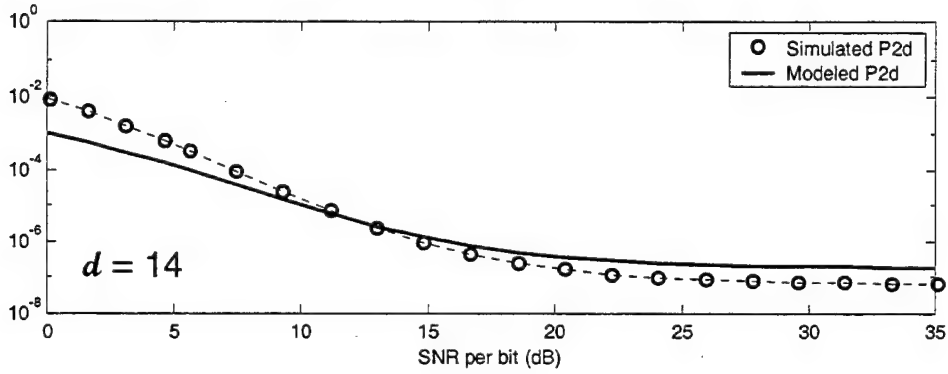


Figure 4.14 First Event Error Probability $\mathcal{P}_2(14)$ for $\sigma_{dB} = 7$ with 10 users per cell.

We incorporate these results into (4.63) to determine the probability of bit error using the first five terms in the union bound. For a rate $\frac{1}{2}$ convolutional encoder with constraint length of $\nu = 8$, we obtain a modeled and simulated probability of bit error as shown in Figure 4.15. The average received SNR per bit for the Rayleigh-lognormal channel in Figure 4.15 is

$$\overline{\gamma_b} = \mathbb{E} \left\{ \frac{R^2 \mathcal{F}_1 \mathbf{P}_t^T}{N_0 L_H(\mathbf{d}) X} \right\} = \mathbb{E} \{ R^2 \} \mathbb{E} \{ 1/X \} \frac{E_b}{N_0} = \mathbb{E} \{ X \} \frac{E_b}{N_0}. \quad (4.76)$$

By selecting a constraint length of $v=8$ as an example, we incorporate the modeled and simulated results of $\mathcal{P}_2(d)$ for $d=10$ through 14 since $d_{\text{free}}=10$ and $\beta_{10}=2$, $\beta_{11}=22$, $\beta_{12}=60$, $\beta_{13}=148$, $\beta_{14}=340$. In the case of 10 users per cell, small differences between the modeled and simulated $\mathcal{P}_2(d)$, as shown in Figures 4.10 through 4.15, grow larger when their weighted sums are applied in the union bound (4.63), although the differences are still quite small (on the order of 10^{-4}). Nevertheless, these differences do not outweigh the usefulness of our model in analyzing the performance of

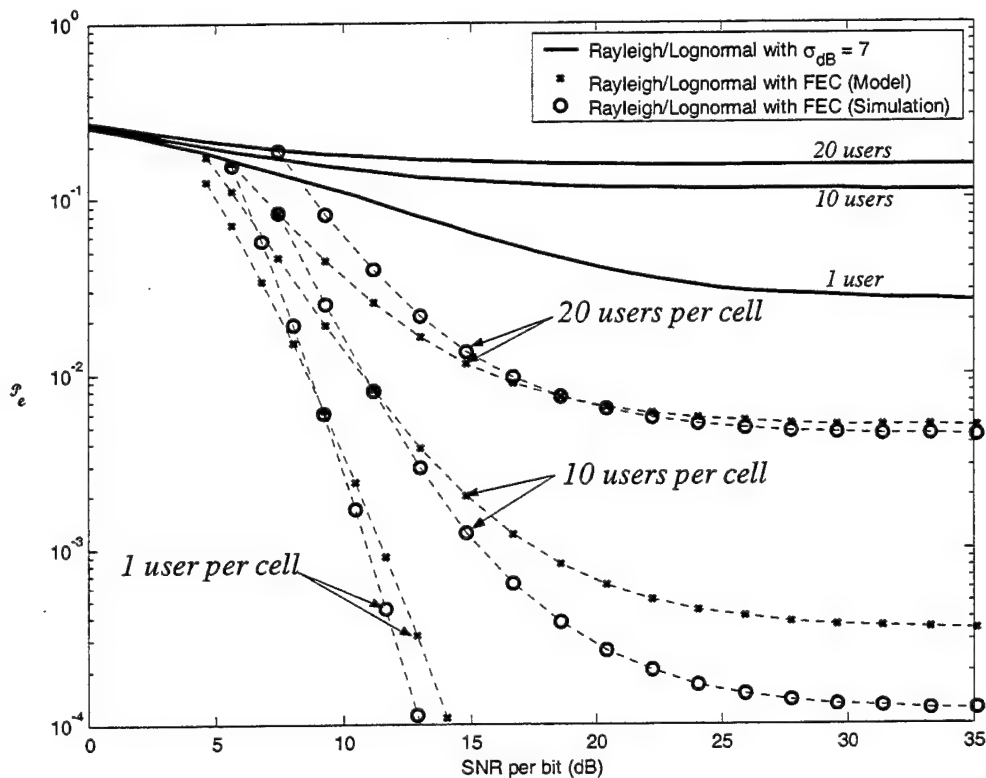


Figure 4.15 Probability of Bit Error for DS-CDMA with Rayleigh Fading and Lognormal Shadowing ($\sigma_{dB} = 7$) using a Rate $\frac{1}{2}$ Convolution Encoder with $v = 8$.

DS-CDMA cellular systems. In particular, the model closely matches the simulated result in the range from 10 to 15 dB, which is a practical range in which DS-CDMA cellular systems operate. Furthermore, the differences in the modeled and simulated results are most noteworthy when the interference floor is in a range between 10^{-3} and 10^{-7} , where even the slightest differences are magnified due to the logarithmic presentation of results.

We should note that both the modeled and simulated results predict that the coded system has inferior performance to the uncoded system for low SNR per bit (less than 5 dB). This misleading prediction is a result of using the union bound to upper bound the probability of bit error.

Appendix IV-C provides graphical results similar to Figure 4.15 for $\sigma_{dB} = 2, 3, \dots, 9$. In the next section we will use these results to explore the performance analysis of a DS-CDMA cellular system with FEC operating in a Rayleigh fading and lognormal shadowing environment.

D. BIT ERROR ANALYSIS OF DS-CDMA WITH FEC

In Section IV.C, we developed a model which approximates the distribution for a sum of multiplicative chi-square(with 2 degrees of freedom)–lognormal random variables. In this section we use that approximation to analyze the performance of DS-CDMA with FEC. For example, using the same parameters from the previous section, we can compare the probability of bit error for AWGN, Rayleigh fading, and Rayleigh-

lognormal channels. Figure 4.16 shows these results for 10 users per adjacent cell, in which we vary the lognormal shadowing parameter σ_{dB} from 2 to 9.

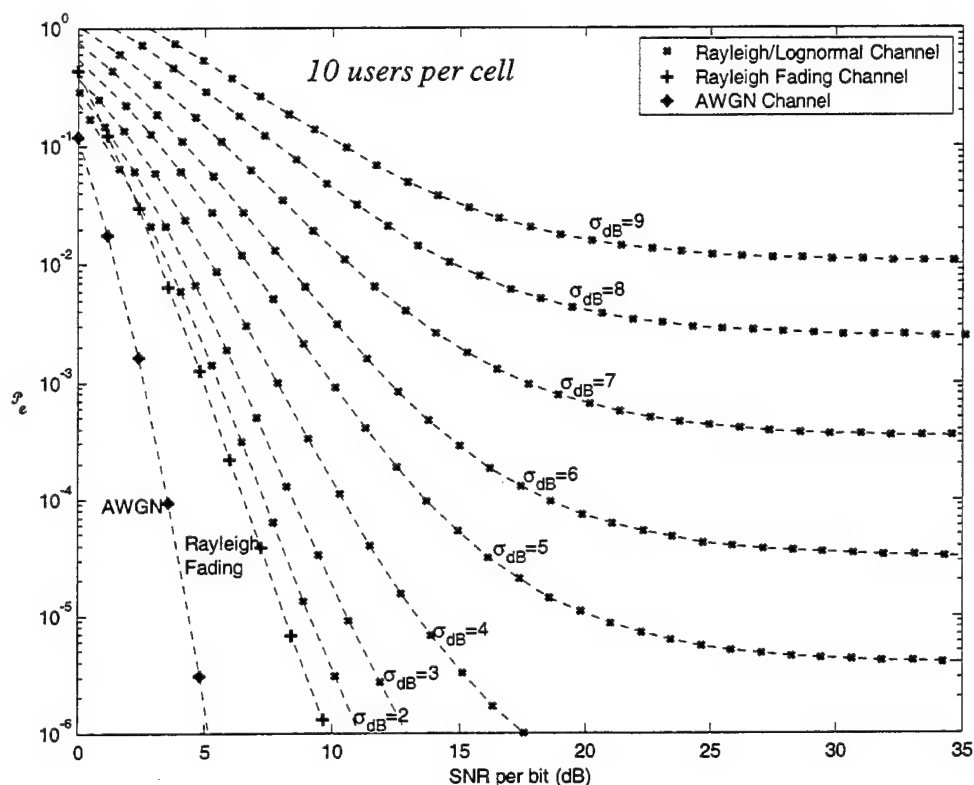


Figure 4.16 Probability of Bit Error for DS-CDMA with FEC in Various Channel Conditions with 10 users per cell ($R_{cc} = 1/2$ and $v = 8$).

As depicted in Figure 4.16, when lognormal shadowing is added to a pure Rayleigh fading Channel, the probability of bit error drifts away from that of the pure Rayleigh channel as we increase the lognormal shadowing parameter from 2 to 9.

We can also consider performance of the DS-CDMA system with FEC in terms of the number of users per cell that can be supported at a given SNR per bit. If we fix the

average SNR per bit at 15 dB, we can predict the probability of bit error for a range of users and for $\sigma_{dB} = 2, 3, \dots, 9$ as shown in Figure 4.17. The number of users per cell

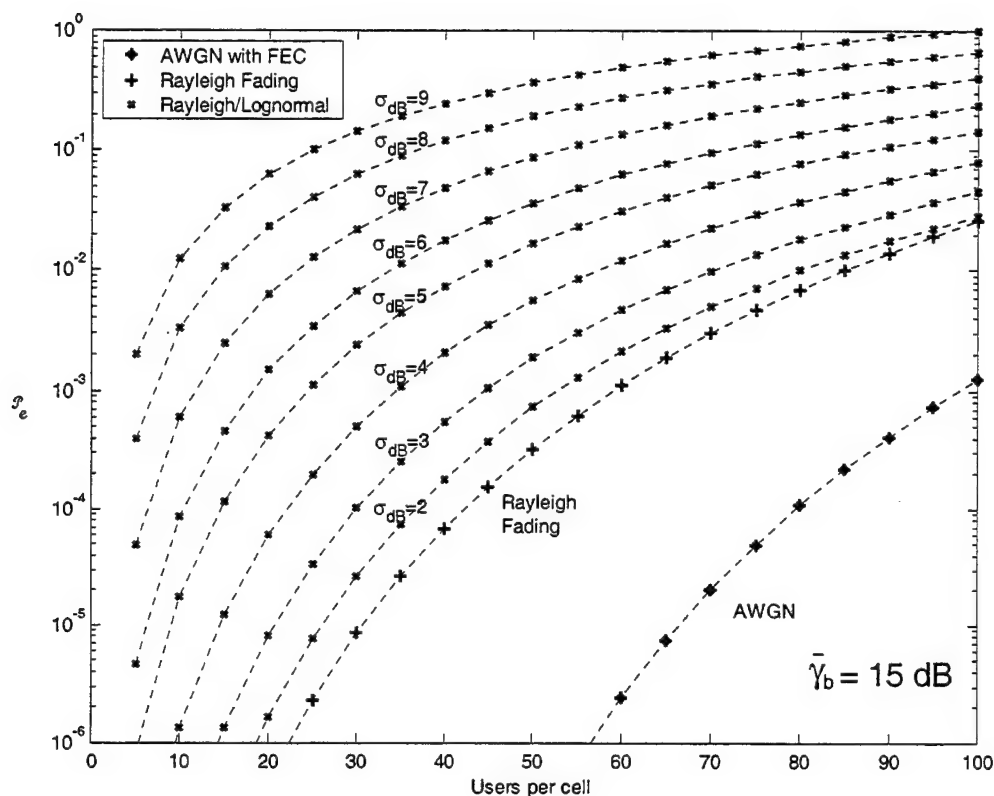


Figure 4.17 Probability of Bit Error for DS-CDMA with FEC in Various Channel Conditions with the Average SNR = 15 dB ($R_{cc} = 1/2$ and $v = 8$).

determines the amount of intercell interference received by a mobile user. As the intercell interference increases, so does the probability of bit error. In order to achieve a desired probability of bit error, system designers could limit the number of users based on the channel conditions as indicated in Figure 4.17. For example, a DS-CDMA system with FEC operating in a channel with Rayleigh fading and lognormal shadowing with a

fading parameter of $\sigma_{dB} = 7$ would be limited to 11 users (active channels) in order to maintain a probability of bit error of 10^{-3} or less.

We can further limit the amount of intercell interference by sectoring the cells into 3 or 6 sectors of 120° or 60° sectors, respectively. This is accomplished by replacing the omni-directional antenna at the base station with several directional antennas, which radiate within a desired sector. Accordingly, if we assume that the users are evenly distributed in the adjacent cells, the amount of intercell interference is reduced to $1/3$ or

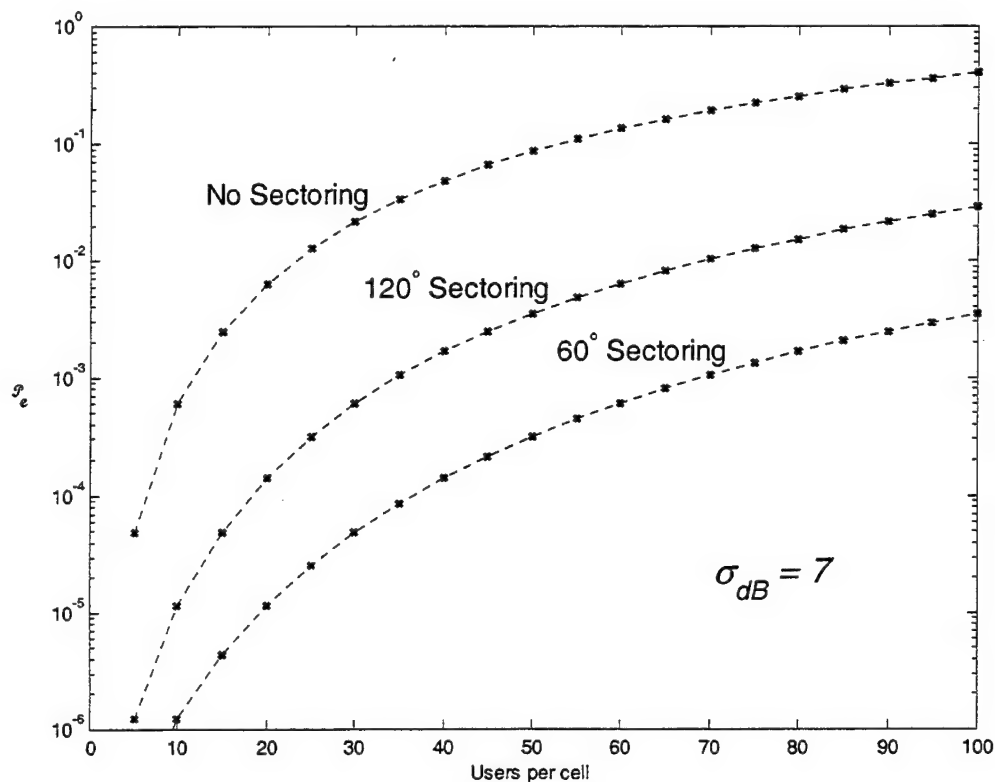


Figure 4.18 Probability of Bit Error for DS-CDMA using Sectoring for $\sigma_{dB} = 7$ with an SNR per Bit of 15 dB ($R_{cc} = 1/2$ and $v = 8$).

1/6 of its original value. By reducing the intercell interference with sectoring, the performance of our DS-CDMA cellular system operating in a channel with Rayleigh fading and lognormal shadowing is greatly improved. Figure 4.18 shows the dramatic increase in performance for the case of $\sigma_{dB} = 7$.

E. SUMMARY

In this chapter we developed a signal-to-noise plus interference ratio and the probability of bit error for a DS-CDMA cellular system operating in a Rayleigh fading channel with lognormal shadowing which incorporates the extended Hata model. We added convolutional encoding for forward error correction and developed an expression for the upper bound on the probability of bit error, which depends on the sum of multiplicative chi-square(with two degrees of freedom)-lognormal random variables. In order to evaluate the expression for specific operating conditions, we approximated the sum of d chi-square-lognormal random variables as a multiplicative chi-square(with $2d$ degrees of freedom)-lognormal random variable. This approximation allowed us to analyze the performance of the DS-CDMA cellular system operating in a Rayleigh-lognormal channel under a range of operating conditions.

In analyzing the performance of our DS-CDMA system in this chapter, we placed our intended mobile user in the worst-case position: at the edge of the cell. Under this scenario, two of the interfering base stations are as close to the mobile as is his/her own base station. Each active channel from those two interfering base stations is received as

interference at roughly the same power level as that of intended traffic. Accordingly, our results are very pessimistic. In the next Chapter, we provide more realistic results by assuming that the mobile user's position is randomly distributed in the cell.

APPENDIX IV-A VARIANCE OF THE COCHANNEL INTERFERENCE

In developing the variance for the cochannel interference term, ζ , we separate the term according to the individual channel contributions as follows:

$$\begin{aligned}
 \zeta &= r\sqrt{p_0} \int_0^T \sum_{i=1}^6 \sum_{j=0}^{K_i-1} R_i \sqrt{P_{ij}} b_{ij}(t+\tau_i) w_{ij}(t+\tau_i) w_1(t) c_i(t+\tau_i) c(t) \cos(\varphi_i) dt \\
 &= r\sqrt{p_0} \sum_{i=1}^6 \sum_{j=0}^{K_i-1} \underbrace{\int_0^T R_i \sqrt{P_{ij}} b_{ij}(t+\tau_i) w_{ij}(t+\tau_i) w_1(t) c_i(t+\tau_i) c(t) \cos(\varphi_i) dt}_{I_{ij}} \quad (4.77) \\
 &= r\sqrt{p_0} \sum_{i=1}^6 \sum_{j=0}^{K_i-1} I_{ij},
 \end{aligned}$$

where I_{ij} is the contribution to the co-channel interference term from the individual co-channel, j in the adjacent cell, i . We can manipulate I_{ij} into a simpler form as follows:

$$\begin{aligned}
 I_{ij} &= \int_0^T R_i \sqrt{P_{ij}} b_{ij}(t+\tau_i) w_{ij}(t+\tau_i) w_1(t) c_i(t+\tau_i) c(t) \cos(\varphi_i) dt \\
 &= R_i \sqrt{P_{ij}} \cos(\varphi_i) \int_0^T \underbrace{b_{ij}(t+\tau_i) w_{ij}(t+\tau_i) c_i(t+\tau_i)}_{a_{ij}(t+\tau_i)} \underbrace{w_1(t) c(t)}_{d_1(t)} dt \quad (4.78) \\
 &= R_i \sqrt{P_{ij}} \cos(\varphi_i) \int_0^T a_{ij}(t+\tau_i) d_1(t) dt,
 \end{aligned}$$

where $a_{ij}(t) = b_{ij}(t) w_{ij}(t) c_i(t)$ and $d_1(t) = w_1(t) c(t)$ are simply *other* PN signals, whose precise form is of little significance in our analysis.

We develop the interference power contribution from an individual intercell channel from the second moment since the co-channel interference is modeled as zero-mean. Accordingly,

$$\begin{aligned}
\mathbb{E}\{I_{ij}^2\} &= \mathbb{E}\left\{\left(R_i \sqrt{P_{ij}} \cos(\varphi_i) \int_0^T a_{ij}(t + \tau_i) d_1(t) dt\right)^2\right\} \\
&= \mathbb{E}\left\{R_i^2 P_{ij} \cos^2(\varphi_i) \left(\int_0^T a_{ij}(t + \tau_i) d_1(t) dt\right) \left(\int_0^T a_{ij}(\tilde{\lambda} + \tau_i) d_1(\tilde{\lambda}) d\tilde{\lambda}\right)\right\} \\
&= \frac{\mathbb{E}\{R_i^2\} \mathbb{E}\{P_{ij}\}}{2} \mathbb{E}\left\{\int_0^T \int_0^T a_{ij}(t + \tau_i) a_{ij}(\tilde{\lambda} + \tau_i) d_1(t) d_1(\tilde{\lambda}) dt d\tilde{\lambda}\right\} \\
&= \frac{\mathbb{E}\{R_i^2\} \mathbb{E}\{P_{ij}\}}{2} \int_0^T \int_0^T \underbrace{\mathbb{E}\{a_{ij}(t + \tau_i) a_{ij}(\tilde{\lambda} + \tau_i)\}}_{\beta(t - \tilde{\lambda})} \underbrace{\mathbb{E}\{d_1(t) d_1(\tilde{\lambda})\}}_{\beta(t - \tilde{\lambda})} dt d\tilde{\lambda} \\
&= \frac{\mathbb{E}\{R_i^2\} \mathbb{E}\{P_{ij}\}}{2} \int_0^T \int_0^T \beta^2(t - \tilde{\lambda}) dt d\tilde{\lambda},
\end{aligned}$$

where $\beta(u)$ is defined by (2.14) to be the autocorrelation function for a random binary signal and used here to represent the autocorrelation function of a PN signal. Additionally, we determined $\mathbb{E}\{\cos \varphi_i\} = 1/2$, by assuming the phase discrepancy φ_i to be uniformly distributed between $(0, 2\pi)$. In order to continue our analysis, we perform a change of variables, from $(t, \tilde{\lambda})$ to (u, v) , defined by

$$\begin{aligned}
u &= t - \tilde{\lambda}, & \text{and} & & u + v &= 2t, \\
v &= t + \tilde{\lambda}, & & & u - v &= -2\tilde{\lambda},
\end{aligned}$$

thus,

$$t = \frac{1}{2}(u + v), \quad \text{and} \quad \tilde{\lambda} = \frac{1}{2}(v - u).$$

We calculate the Jacobian determinant of the transformation as follows,

$$J_{t\tilde{\lambda}} = \det \begin{pmatrix} \frac{\partial t}{\partial u} & \frac{\partial \tilde{\lambda}}{\partial u} \\ \frac{\partial t}{\partial v} & \frac{\partial \tilde{\lambda}}{\partial v} \end{pmatrix} = \det \begin{pmatrix} \frac{1}{2} & -\frac{1}{2} \\ \frac{1}{2} & \frac{1}{2} \end{pmatrix} = \frac{1}{2}.$$

The new limits of integration are determined to be

$$-T < u < T \text{ and } |u| < v < 2T - |u|,$$

as shown in Figure 4.19.

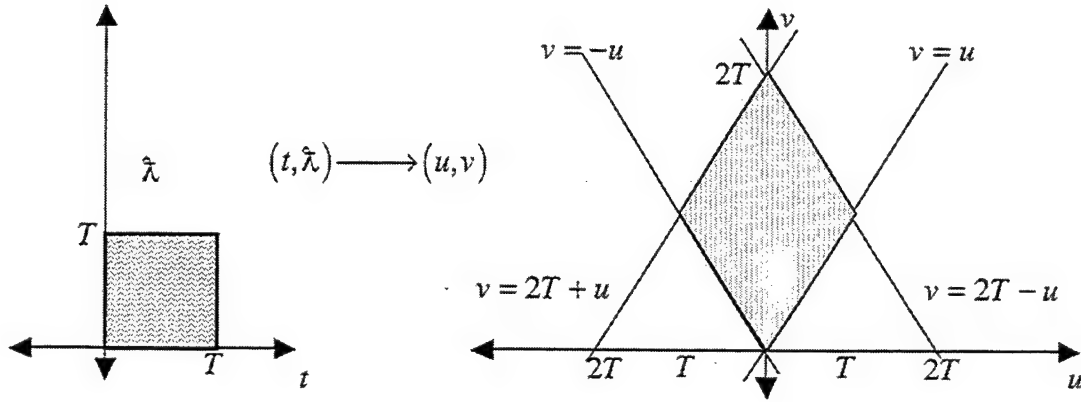


Figure 4.19 Transformation of the limits of integration, $(t, \lambda) \rightarrow (u, v)$.

Applying the change of variables, from (t, λ) to (u, v) , we find that

$$\begin{aligned} \mathbb{E}\{I_{ij}^2\} &= \frac{\mathbb{E}\{R_i^2\} \mathbb{E}\{P_{ij}\}}{2} \int_{-T}^T \int_{|u|}^{2T-|u|} \beta^2(u) J_{i\lambda} dv du \\ &= \frac{\mathbb{E}\{R_i^2\} \mathbb{E}\{P_{ij}\}}{2} \int_{-T}^T \int_{|u|}^{2T-|u|} \beta^2(u) \frac{1}{2} dv du \\ &= \frac{\mathbb{E}\{R_i^2\} \mathbb{E}\{P_{ij}\}}{2} \int_0^T \int_u^{2T-u} \beta^2(u) dv du \\ &= \frac{\mathbb{E}\{R_i^2\} \mathbb{E}\{P_{ij}\}}{2} \int_0^T \int_u^{2T-u} \beta^2(u) dv du \\ &= \frac{\mathbb{E}\{R_i^2\} \mathbb{E}\{P_{ij}\}}{2} \int_0^T \beta^2(u) (2T - 2u) du, \end{aligned}$$

where we took advantage of the fact that the region of integration is symmetric about the v axis as shown in Figure 4.19.

We finish the development of $\mathbb{E}\{I_{ij}^2\}$ by substituting for $\beta(u)$ as defined by (2.14) as follows:

$$\begin{aligned}
 \mathbb{E}\{I_{ij}^2\} &= \frac{\mathbb{E}\{R_i^2\}\mathbb{E}\{P_{ij}\}}{2} \int_0^{\frac{T}{N}} \left(1 - \frac{Nu}{T}\right)^2 (2T - 2u) du \\
 &= \frac{\mathbb{E}\{R_i^2\}\mathbb{E}\{P_{ij}\}}{2} \int_0^{\frac{T}{N}} \left(1 - \frac{2Nu}{T} + \frac{N^2u^2}{T^2}\right) (2T - 2u) du \\
 &= \frac{\mathbb{E}\{R_i^2\}\mathbb{E}\{P_{ij}\}}{2} 2 \left(Tu - Nu^2 + \frac{N^2u^3}{3T} - \frac{u^2}{2} + \frac{2Nu^3}{3T} - \frac{N^2u^4}{4T^2} \right) \Bigg|_0^{\frac{T}{N}} \quad (4.79) \\
 &= \frac{\mathbb{E}\{R_i^2\}\mathbb{E}\{P_{ij}\}}{2} \left(\frac{2T^2}{3N} - \frac{T^2}{6N^2} \right) \\
 &\approx \mathbb{E}\{R_i^2\}\mathbb{E}\{P_{ij}\} \frac{T^2}{3N} \quad \text{for } N \gg 1.
 \end{aligned}$$

Accordingly, we can define and develop the cochannel interference term using the contributions of the individual channels, assuming those contributions are independent of one another:

$$\begin{aligned}
 \mathcal{O}_{\mathcal{A}r}\{\zeta\} &= \mathbb{E}\{\zeta^2\} = \mathbb{E}\left\{ \left[r\sqrt{p_0} \sum_{i=1}^6 \sum_{j=0}^{K_i-1} I_{ij} \right]^2 \right\} \\
 &= r^2 p_0 \sum_{i=1}^6 \sum_{j=0}^{K_i-1} \mathbb{E}\{I_{ij}^2\} \quad (4.80) \\
 &= \frac{r^2 p_0 T^2}{3N} \sum_{i=1}^6 \sum_{j=0}^{K_i-1} \mathbb{E}\{R_i^2\} \mathbb{E}\{P_{ij}\}.
 \end{aligned}$$

APPENDIX IV-B DEVELOPING THE UNCODED PROBABILITY OF BIT ERROR

1. Removing Dependency on the Chi-square R.V.

In order to remove the dependency of $\tilde{\mathcal{P}}_e$ on the chi-square random variable, ψ_2 , we convert the Q-function to the error function and integrate across the chi-square pdf, obtaining

$$\begin{aligned}\tilde{\mathcal{P}}_e\big|_{p_1} &= \int_0^\infty Q(\sqrt{\psi_2}) p_{\psi_2}(\psi_2) d\psi_2 \\ &= \int_0^\infty \frac{1}{2} \left[1 - \operatorname{erf}\left(\sqrt{\frac{\psi_2}{2}}\right) \right] p_{\psi_2}(\psi_2) d\psi_2 \\ &= \frac{1}{2} \int_0^\infty p_{\psi_2}(\psi_2) d\psi_2 - \frac{1}{2} \int_0^\infty \operatorname{erf}\left(\sqrt{\frac{\psi_2}{2}}\right) p_{\psi_2}(\psi_2) d\psi_2 \\ &= \frac{1}{2} - \frac{1}{2} \int_0^\infty \operatorname{erf}\left(\sqrt{\frac{\psi_2}{2}}\right) p_{\psi_2}(\psi_2) d\psi_2,\end{aligned}$$

where

$$Q(z) = \frac{1}{2} \left[1 - \operatorname{erf}\left(\sqrt{\frac{z}{2}}\right) \right].$$

Since ψ_2 is a chi-square random variable with mean value of $\overline{\psi_2}$ as defined in (4.40), we replace its pdf :

$$\begin{aligned}\tilde{\mathcal{P}}_e\big|_{p_1} &= \frac{1}{2} - \frac{1}{2} \int_0^\infty \operatorname{erf}\left(\sqrt{\frac{\psi_2}{2}}\right) \frac{1}{\overline{\psi_2}} e^{\frac{-\psi_2}{\overline{\psi_2}}} d\psi_2 \\ &= \frac{1}{2} - \frac{1}{2\overline{\psi_2}} \int_0^\infty \operatorname{erf}\left(\sqrt{\frac{\psi_2}{2}}\right) e^{\frac{-\psi_2}{\overline{\psi_2}}} d\psi_2.\end{aligned}$$

We have a change of variables, from ψ_2 to x , where

$$x = \sqrt{\frac{\psi_2}{2}}, \quad (4.81)$$

which results in

$$\begin{aligned} \widetilde{\mathcal{P}}_e \Big|_{p_1} &= \frac{1}{2} - \frac{1}{2\gamma_b} \int_0^\infty \operatorname{erf}(x) e^{\frac{-2x^2}{\gamma_b}} 4x dx \\ &= \frac{1}{2} - \frac{2}{\gamma_b} \underbrace{\int_0^\infty \operatorname{erf}(x) e^{\frac{-2x^2}{\gamma_b}} x dx}_{I(x)}, \end{aligned} \quad (4.82)$$

where the integral, $I(x)$, has an analytical solution as defined in a general form in [28]

by equation 4.3.8 as

$$\int_0^\infty \operatorname{erf}(ax) e^{-\mathcal{C}^2 x^2} x^p dx = \frac{a}{\sqrt{\pi}} \mathcal{C}^{p-2} \Gamma\left(\frac{p}{2} + 1\right) {}_2F_1\left(\frac{1}{2}, \frac{p}{2} + 1; \frac{3}{2}; \frac{-a}{\mathcal{C}^2}\right), \quad (4.83)$$

provided that $\operatorname{Re}\{\mathcal{C}^2\} > 0$, and $\operatorname{Re}\{p\} > -2$, and where ${}_2F_1(a_1, a_2; b_1; z)$ is a hypergeometric series, also called the Gaussian hypergeometric function.

The hypergeometric series is defined after [29] equation 9.100 as

$$\begin{aligned} {}_2F_1(a_1, a_2; b_1; z) &= 1 + \frac{a_1 a_2}{b_1 \cdot 1} z + \frac{a_1(a_1+1)a_2(a_2+1)}{b_1(b_1+1) \cdot 1 \cdot 2} z^2 + \\ &\quad + \frac{a_1(a_1+1)(a_1+2)a_2(a_2+1)(a_2+2)}{b_1(b_1+1)(b_1+2) \cdot 1 \cdot 2 \cdot 3} z^3 + \dots, \end{aligned} \quad (4.84)$$

which converges inside the unit circle, $|z| < 1$, provided $a_1, a_2, b_1 > 0$.

In our case, $a = 1$, $\mathcal{C} = \sqrt{\frac{2}{\psi_2}}$, and $p = 1$. Accordingly, our integral, $I(x)$

becomes

$$\begin{aligned}
I(x) &= \frac{1}{\sqrt{\pi}} \left(\sqrt{\frac{2}{\psi_2}} \right)^{-3} \Gamma\left(\frac{3}{2}\right) {}_2F_1\left(\frac{1}{2}, \frac{3}{2}; \frac{3}{2}; \frac{-\overline{\psi_2}}{2}\right) \\
&= \frac{1}{\sqrt{\pi}} \left(\frac{\overline{\psi_2}}{2} \right)^{\frac{3}{2}} \frac{\sqrt{\pi}}{2} {}_2F_1\left(\frac{1}{2}, \frac{3}{2}; \frac{3}{2}; \frac{-\overline{\psi_2}}{2}\right) \\
&= \frac{1}{2} \left(\frac{\overline{\psi_2}}{2} \right)^{\frac{3}{2}} {}_2F_1\left(\frac{1}{2}, \frac{3}{2}; \frac{3}{2}; \frac{-\overline{\psi_2}}{2}\right),
\end{aligned} \tag{4.85}$$

where the hypergeometric series converges, since we know our that our SNIR is much less than 1, and consequently, $\left| \frac{-\overline{\psi_2}}{2} \right| < 1$. Furthermore, the form of the hypergeometric series in (4.85), constitutes a special form of the series, which can be represented as an elementary function as defined by equation 9.121.1 in [29] as

$${}_2F_1(-n, \beta; \beta; -z) = (1+z)^n, \tag{4.86}$$

where in our case, $z = \frac{\overline{\psi_2}}{2}$, $n = -\frac{1}{2}$. Applying (4.86), to our result in (4.85), we find that

$$\begin{aligned}
I(x) &= \frac{1}{2} \left(\frac{\overline{\psi_2}}{2} \right)^{\frac{3}{2}} \left(1 + \frac{\overline{\psi_2}}{2} \right)^{\frac{1}{2}} \\
&= \frac{\overline{\psi_2}}{4} \sqrt{\frac{\overline{\psi_2}}{2 + \overline{\psi_2}}}.
\end{aligned} \tag{4.87}$$

Substituting into (4.82), with $I(x)$ found in (4.87), we obtain a probability of bit error

$$\begin{aligned}
\tilde{\mathcal{P}}_e|_{p_1} &= \frac{1}{2} - \frac{2}{\psi_2} I(x) \\
&= \frac{1}{2} - \frac{2}{\psi_2} \left(\frac{\overline{\psi_2}}{4} \sqrt{\frac{\overline{\psi_2}}{2 + \overline{\psi_2}}} \right) \\
&= \frac{1}{2} \left(1 - \sqrt{\frac{\overline{\psi_2}}{2 + \overline{\psi_2}}} \right).
\end{aligned} \tag{4.88}$$

2. Removing Dependency on the Lognormal R.V.

In order to remove the dependency of $\tilde{\mathcal{P}}_e$ on the lognormal random variable, we revert $\alpha = \alpha(p_1)$ into its original form, defined by (4.39), as follows:

$$\begin{aligned}
\tilde{\mathcal{P}}_e &= \int_{-\infty}^{\infty} \tilde{\mathcal{P}}_e|_{p_1} p_{R_1}(p_1) dp_1 = \int_{-\infty}^{\infty} \frac{1}{2} \left(1 - \sqrt{\frac{\gamma_b}{2 + \gamma_b}} \right) dp_1 \\
&= \int_0^{\infty} \frac{1}{2} \left(1 - \sqrt{\frac{\alpha|_{p_1}}{2 + \alpha|_{p_1}}} \right) p_{R_1}(p_1) dp_1 \\
&= \frac{1}{2} \left[\int_0^{\infty} p_{R_1}(p_1) dp_1 - \int_0^{\infty} \sqrt{\frac{\alpha|_{p_1}}{2 + \alpha|_{p_1}}} p_{R_1}(p_1) dp_1 \right] \\
&= \frac{1}{2} \left[1 - \int_0^{\infty} \sqrt{\frac{p_1}{\frac{2}{3N} \sum_{i=1}^6 \sum_{j=0}^{K_i-1} \mathbb{E}\{R_i^2\} \mathbb{E}\{P_{ij}\} + \frac{N_0}{T} + p_1}} p_{R_1}(p_1) dp_1 \right] \\
&= \frac{1}{2} \left[1 - \int_0^{\infty} \sqrt{\frac{1}{\frac{2}{3N} \sum_{i=1}^6 \sum_{j=0}^{K_i-1} \frac{\mathbb{E}\{P_{ij}\}}{p_1} + \frac{N_0}{p_1 T} + 1}} p_{R_1}(p_1) dp_1 \right].
\end{aligned}$$

The lognormal random variables p_1 and P_{ij} revert back to their original form using (3.14) and (3.20) respectively, as follows:

$$\begin{aligned}
\tilde{\mathcal{P}}_e &= \frac{1}{2} - \frac{1}{2} \int_0^\infty \sqrt{\frac{1}{\frac{2}{3N} \sum_{i=1}^6 \sum_{j=0}^{K_i-1} \frac{\mathbb{E} \left\{ \frac{\mathcal{F}_{ij} \mathbf{P}_t}{L_H(\mathbf{D}_i) X_i} \right\}}{\left(\frac{\mathcal{F}_1 \mathbf{P}_t}{L_H(\mathbf{d}) x} \right)} + \frac{N_0}{T \left(\frac{\mathcal{F}_1 \mathbf{P}_t}{L_H(\mathbf{d}) x} \right)} + 1}} p_{P_1}(p_1) dp_1 \\
&= \frac{1}{2} - \frac{1}{2} \int_0^\infty \sqrt{\frac{1}{\frac{2}{3N} \sum_{i=1}^6 \sum_{j=0}^{K_i-1} \frac{\mathcal{F}_{ij}}{\mathcal{F}_1} \frac{L_H(\mathbf{d})}{L_H(\mathbf{D}_i)} x \mathbb{E} \left\{ \frac{1}{X_i} \right\} + \frac{x L_H(\mathbf{d}) N_0}{\mathcal{F}_1 \mathbf{P}_t T} + 1}} p_X(x) dx \\
&= \frac{1}{2} - \frac{1}{2} \int_0^\infty \sqrt{\frac{1}{\underbrace{\left(\frac{2}{3N} \sum_{i=1}^6 \sum_{j=0}^{K_i-1} \frac{\mathcal{F}_{ij}}{\mathcal{F}_1} \frac{L_H(\mathbf{d})}{L_H(\mathbf{D}_i)} \mathbb{E} \left\{ \frac{1}{X_i} \right\} + \frac{N_0}{E_b} \right)}_{\mathcal{Q}} x + 1}} p_X(x) dx \\
&= \frac{1}{2} - \frac{1}{2} \int_0^\infty \sqrt{\frac{1}{\mathcal{Q} x + 1}} p_X(x) dx,
\end{aligned}$$

where $X \sim \Lambda(0, \lambda \sigma_{dB})$ and $E_b = \mathcal{F}_1 \mathbf{P}_t T / L_H(\mathbf{d})$. Accordingly, the unconditional probability of bit error is defined by

$$\begin{aligned}
\tilde{\mathcal{P}}_e &= \frac{1}{2} - \frac{1}{2} \int_0^\infty \sqrt{\frac{1}{\mathcal{Q} x + 1}} \frac{1}{x \sqrt{2\pi \lambda \sigma_{dB}}} e^{\frac{-(\ln x)^2}{2(\lambda \sigma_{dB})^2}} dx \\
&= \frac{1}{2} - \frac{1}{2\sqrt{2\pi \lambda \sigma_{dB}}} \int_0^\infty \frac{1}{x \sqrt{\mathcal{Q} x + 1}} e^{\frac{-(\ln x)^2}{2(\lambda \sigma_{dB})^2}} dx.
\end{aligned}$$

APPENDIX IV-C **MODELED AND SIMULATED PROBABILITY OF BIT
ERROR FOR THE RAYLEIGH-LOGNORMAL CHANNEL
USING 120° ANTENNA SECTORING**

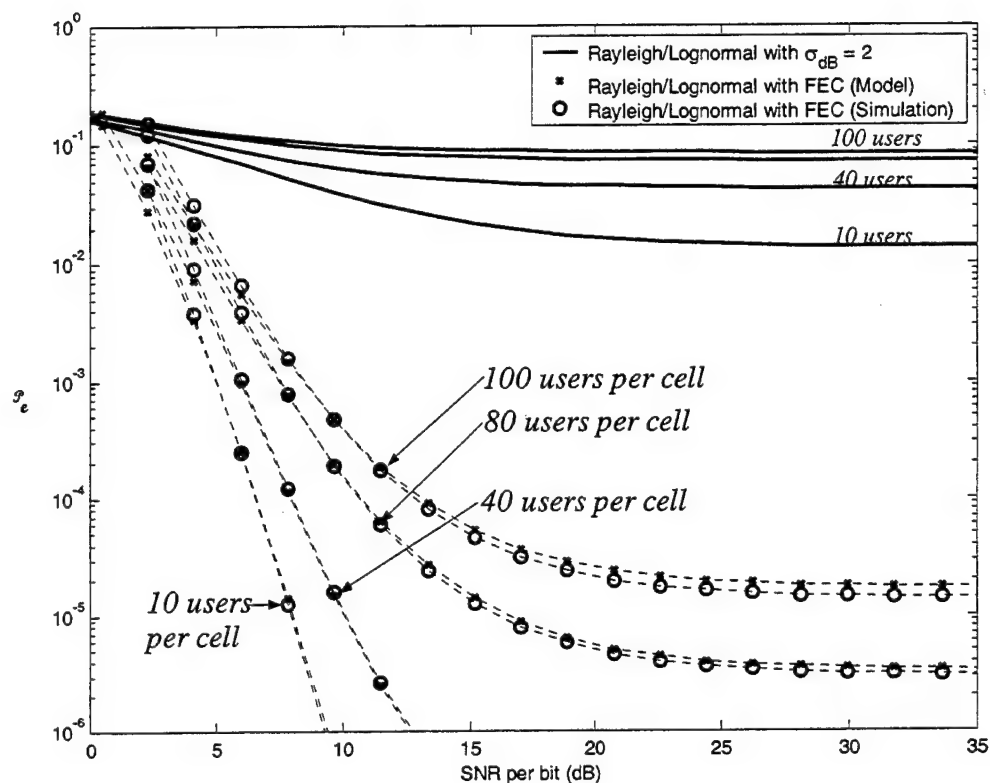


Figure 4.20 Probability of Bit Error for DS-CDMA with Rayleigh Fading and Lognormal Shadowing ($\sigma_{dB} = 2$) using 120° Sectoring ($R_{cc} = 1/2$ and $v=8$).

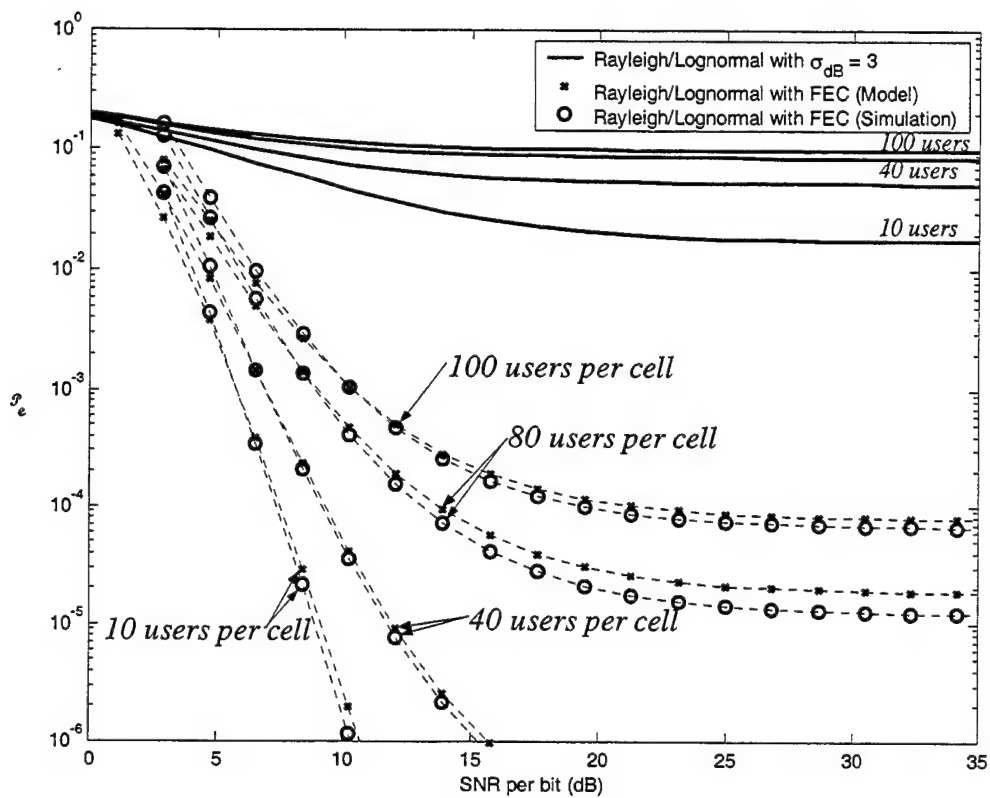


Figure 4.21 Probability of Bit Error for DS-CDMA with Rayleigh Fading and Lognormal Shadowing ($\sigma_{dB} = 3$) using 120° Sectoring ($R_{cc} = 1/2$ and $v=8$).

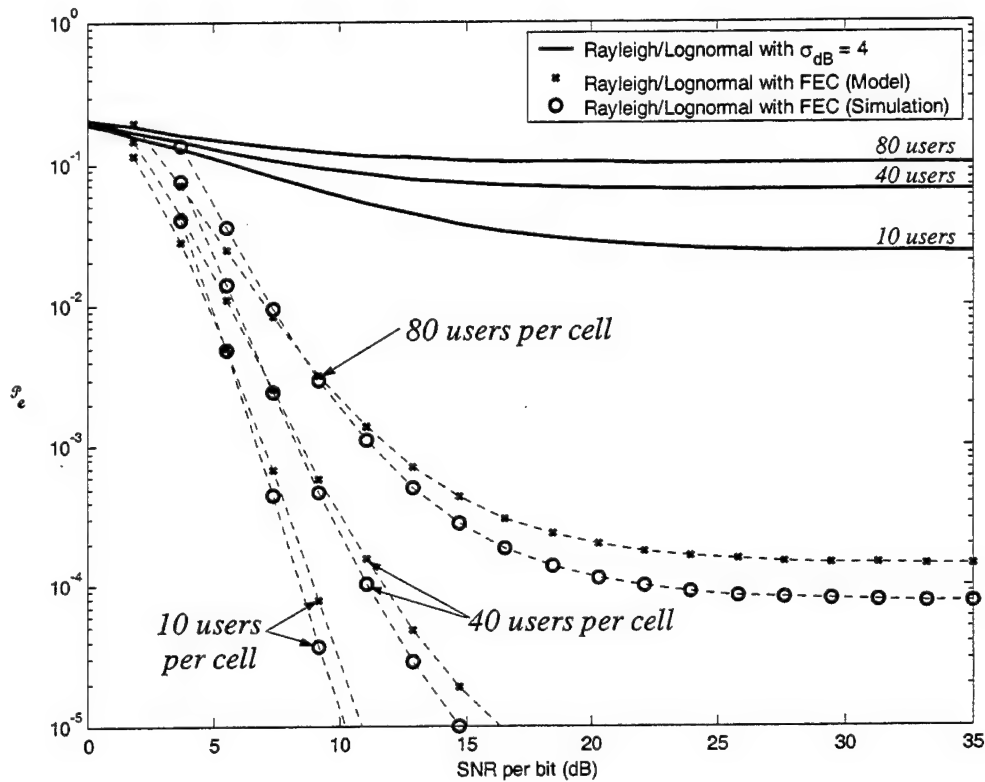


Figure 4.22 Probability of Bit Error for DS-CDMA with Rayleigh Fading and Lognormal Shadowing ($\sigma_{dB} = 4$) using 120° Sectoring ($R_{cc} = 1/2$ and $v=8$).

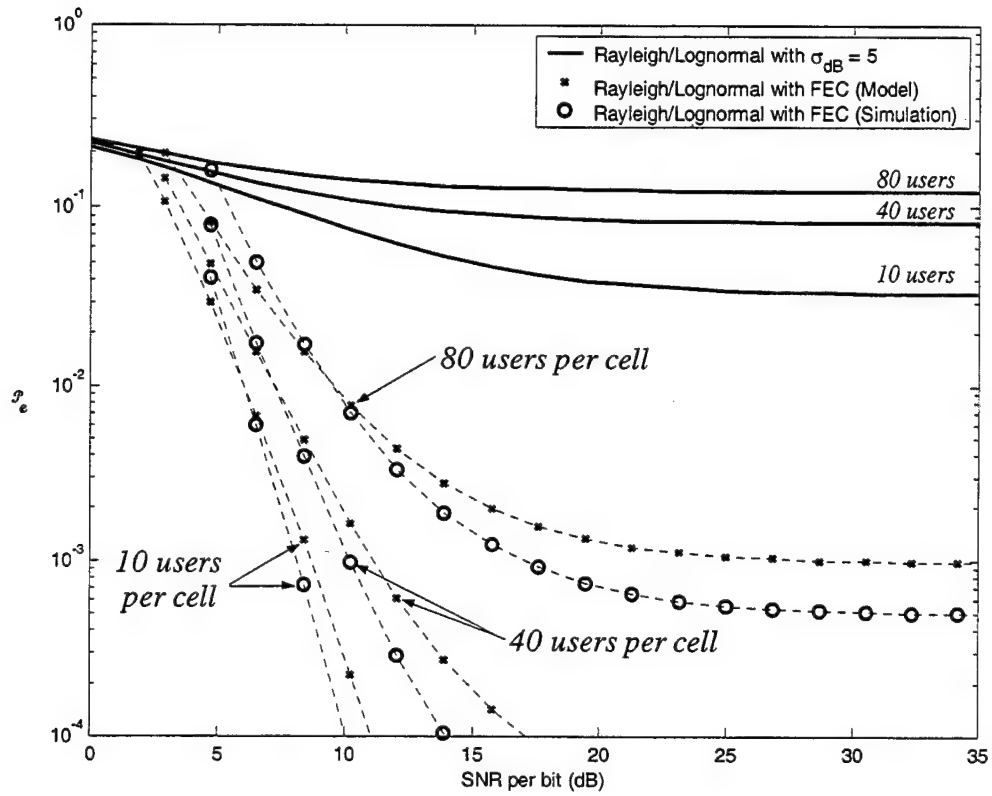


Figure 4.23 Probability of Bit Error for DS-CDMA with Rayleigh Fading and Lognormal Shadowing ($\sigma_{dB} = 5$) using 120° Sectoring ($R_{cc} = 1/2$ and $v=8$).

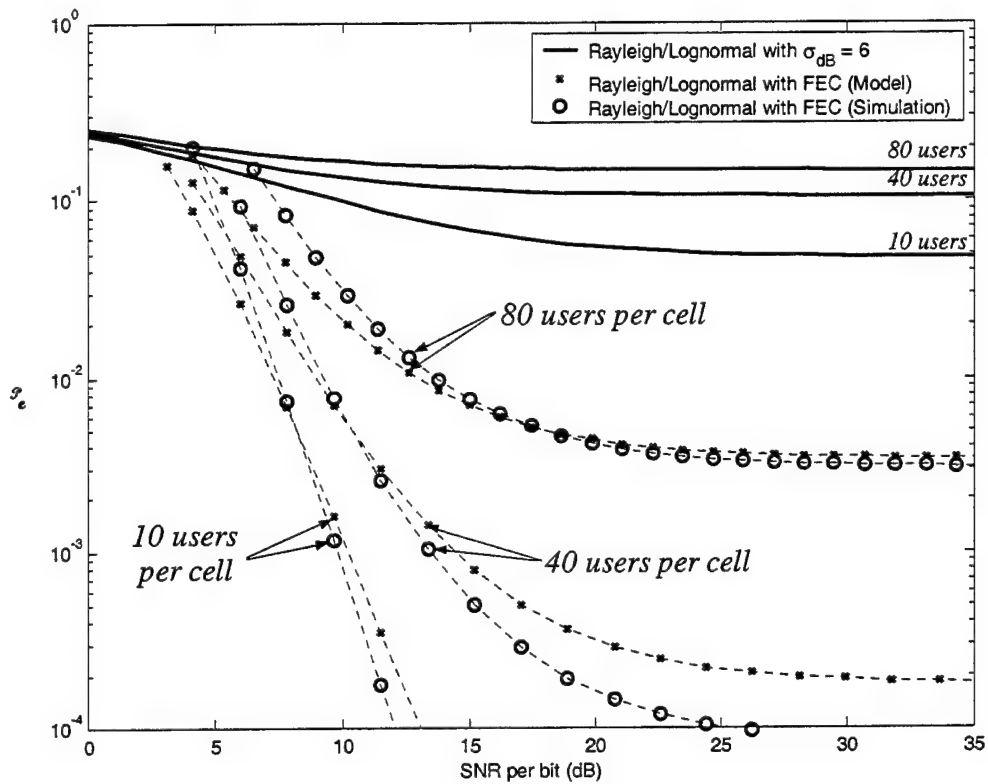


Figure 4.24 Probability of Bit Error for DS-CDMA with Rayleigh Fading and Lognormal Shadowing ($\sigma_{dB} = 6$) using 120° Sectoring ($R_{cc} = 1/2$ and $v=8$).

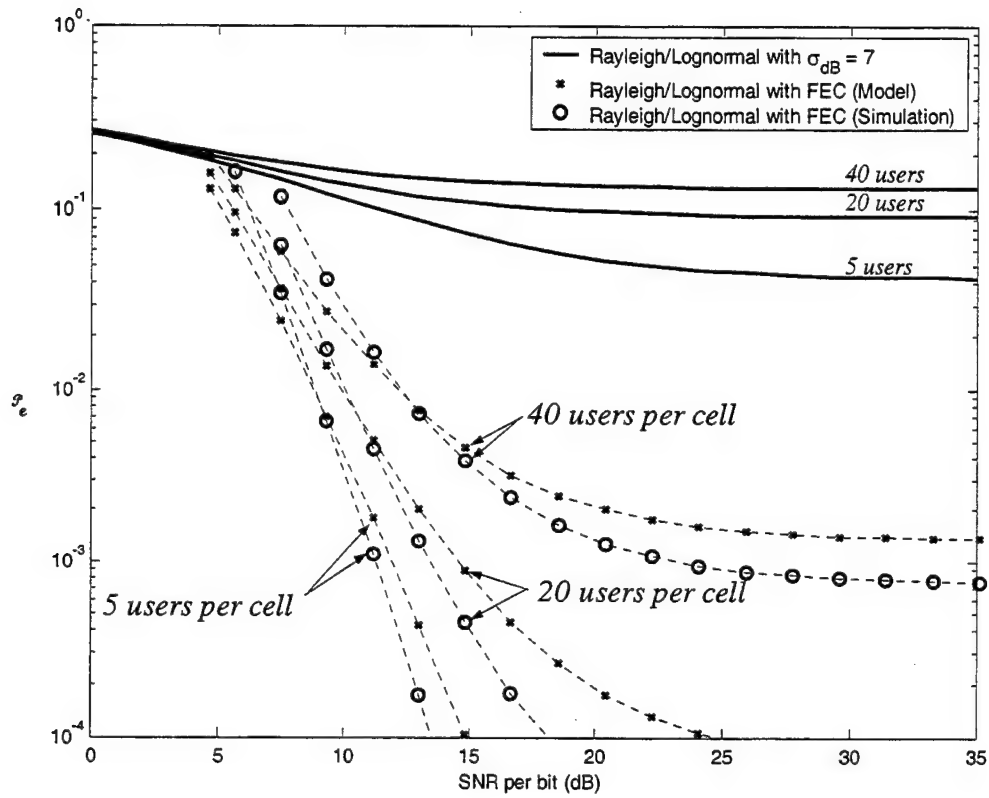


Figure 4.25 Probability of Bit Error for DS-CDMA with Rayleigh Fading and Lognormal Shadowing ($\sigma_{dB} = 7$) using 120° Sectoring ($R_{cc} = 1/2$ and $v=8$).

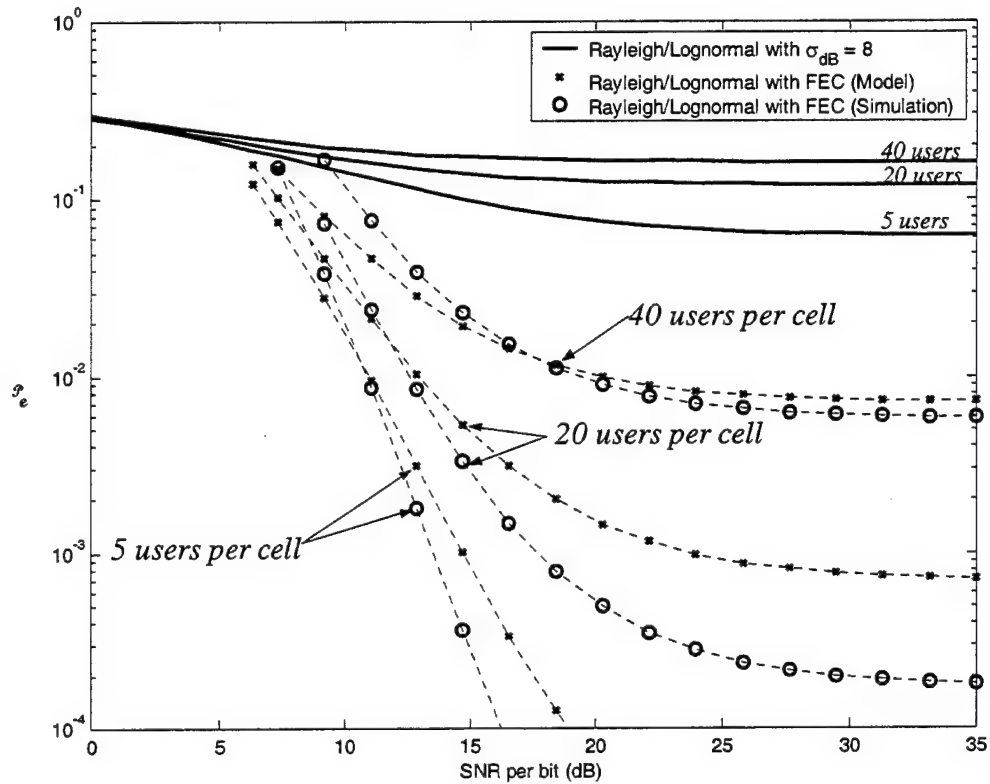


Figure 4.26 Probability of Bit Error for DS-CDMA with Rayleigh Fading and Lognormal Shadowing ($\sigma_{dB} = 8$) using 120° Sectoring ($R_{cc} = 1/2$ and $v=8$).

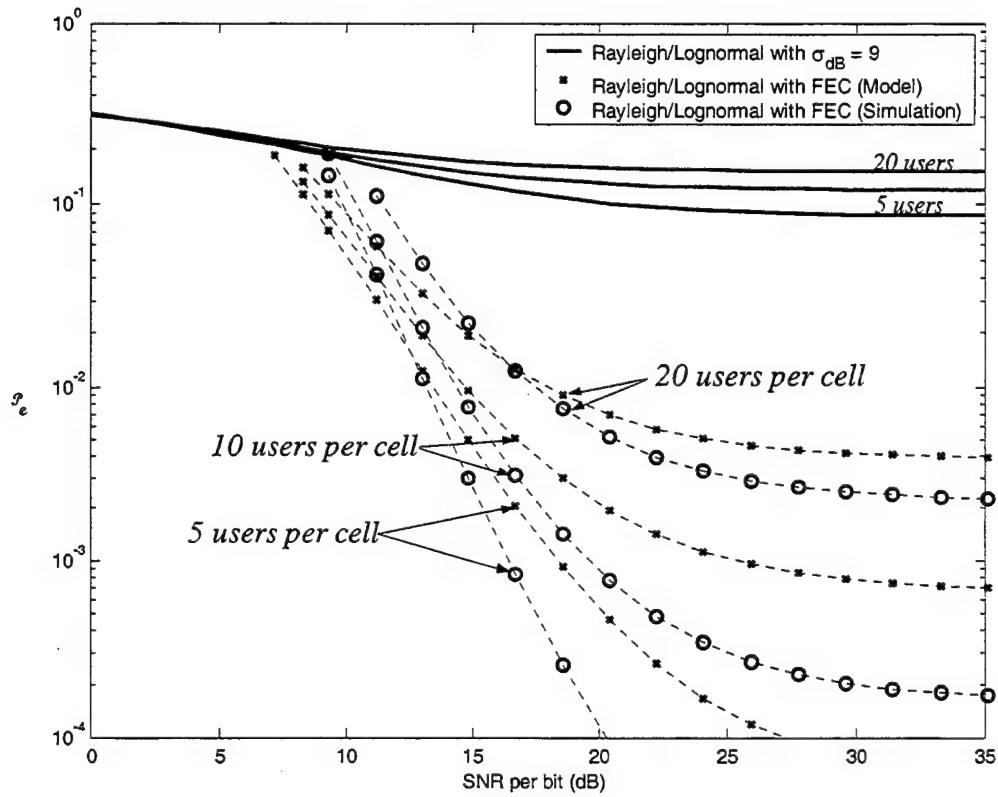


Figure 4.27 Probability of Bit Error for DS-CDMA with Rayleigh Fading and Lognormal Shadowing ($\sigma_{dB} = 9$) using 120° Sectoring ($R_{cc} = 1/2$ and $v=8$).

V. INCORPORATING USER DISTRIBUTION AND POWER CONTROL INTO THE FORWARD CHANNEL MODEL

In Chapter IV, we analyzed the performance of the forward channel in a DS-CDMA cellular system by assuming that our intended mobile user was situated in the outer corner of the hexagonal cell. We can obtain a more realistic view of typical performance of the forward channel by assuming that the users are randomly distributed within the cell according to a specified probability distribution. The position of the intended mobile in the cell is represented by a random variable from the specified distribution, which we incorporate into a revised probability of bit error in Section V.A.

In Section V.B we build on the user distribution analysis to incorporate power control into the forward channel model. That is, instead of transmitting at a constant rate of power in each user channel as in Section V.A, the base station adjusts the transmit power in each channel to ensure the power received by all mobile users is equal and adequate. By reducing the power in the user channels to only that which is required, we aim to reduce co-channel interference and enhance overall system performance.

To simplify our analysis, we will replace our hexagonal cells with overlapping circular cells as depicted in Figure 5.1. The overlap accounts for soft-handoff of mobile users between cells. We take the center base station to be the origin of a polar coordinate system. Accordingly, the position of our intended mobile user in the center cell is represented by (r, θ) , where $0 < r \leq 1$ and $-\pi < \theta \leq \pi$. Based on the underlying hexagonal geometry depicted in Figure 4.2, we know that the distance from the base

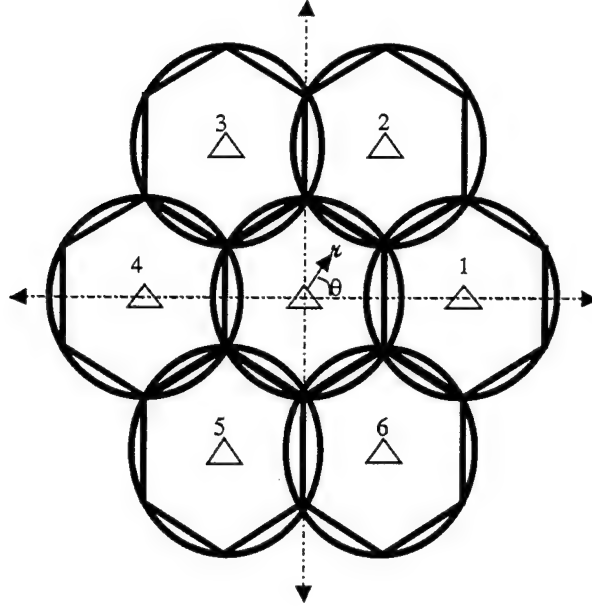


Figure 5.1 Circular Seven-Cell Cluster.

station in the center cell, to each of the adjacent base stations is $\sqrt{3}$, since we normalized $d = 1$. The adjacent base stations are separated by an angle of $\pi/3$ with respect to the origin. Using the geometry of the cell cluster, we determine the distance, \mathcal{D}_i , from each adjacent base station to the mobile user in the center cell as a function of u and θ , as follows:

$$\mathcal{D}_i = \begin{cases} \sqrt{u^2 - 2\sqrt{3}u \cos \theta + 3}, & i = 1 \\ \sqrt{u^2 - \sqrt{3}u \cos \theta - 3u \sin \theta + 3}, & i = 2 \\ \sqrt{u^2 + \sqrt{3}u \cos \theta - 3u \sin \theta + 3}, & i = 3 \\ \sqrt{u^2 + 2\sqrt{3}u \cos \theta + 3}, & i = 4 \\ \sqrt{u^2 + \sqrt{3}u \cos \theta + 3u \sin \theta + 3}, & i = 5 \\ \sqrt{u^2 - \sqrt{3}u \cos \theta + 3u \sin \theta + 3}, & i = 6 \end{cases} \quad (5.1)$$

The development of \mathcal{D}_i can be found in detail in Appendix V-A.

Since we aim to randomize the intended mobile user's position within the cell, we are also randomizing the distances \mathcal{D}_i . These distances are used in calculating the path loss for the intended information signal and the co-channel interference. The randomization of the distances complicates the use of the Hata model in predicting path loss. Accordingly, the performance analysis in this chapter will use the average path loss $\overline{L_n}(d)$ as predicted by (3.5), with a path loss exponent of $n = 4$.

We modify the analysis from Chapter IV to reflect this change. Specifically, if we assume that the fixed position of the intended mobile user is known precisely (\mathbf{r}_t, θ_t) , we revise (4.60) as follows:

$$\begin{aligned}\tilde{\alpha} &= \frac{\exp\left(\frac{\lambda^2 \sigma_{dB}^2}{2}\right)}{3N} \sum_{i=1}^6 \sum_{j=0}^{K_i-1} \frac{\mathcal{F}_{ij} \overline{L_n}(\mathbf{r}_t)}{\mathcal{F}_1 \overline{L_n}(\mathcal{D}_i)} + \frac{N_0}{2E_c} \\ &= \frac{\exp\left(\frac{\lambda^2 \sigma_{dB}^2}{2}\right)}{3N} \sum_{i=1}^6 \sum_{j=0}^{K_i-1} \frac{\mathcal{F}_{ij} \mathbf{r}_t^n}{\mathcal{F}_1 \mathcal{D}_i^n} + \frac{N_0}{2E_c},\end{aligned}\tag{5.2}$$

where \mathcal{D}_i is defined by (5.1) and where E_c is given by

$$E_c = \frac{\mathcal{F}_1 \mathbf{P}_t T_{cc}}{\overline{L_n}(\mathbf{r}_t)} = \frac{\mathcal{F}_1 \mathbf{P}_t T_{cc}}{\mathbf{r}_t^n}.\tag{5.3}$$

Using $\tilde{\alpha}$ we can determine the first-event error probability and the upper bound on the probability of bit error using (4.61) and (4.63), respectively. Figure 5.2 shows the probability of bit error using a path loss exponent of $n = 4$, as it compares with the

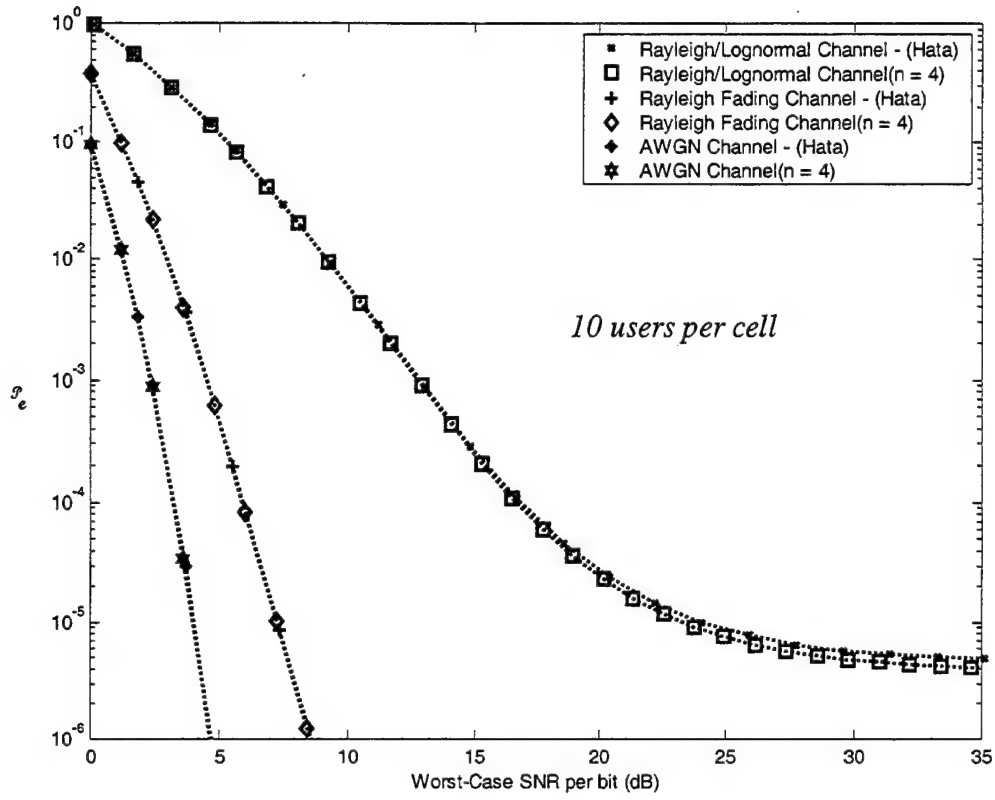


Figure 5.2 Comparison of Probability of Bit Error for DS-CDMA in a Rayleigh-Lognormal ($\sigma_{dB} = 7$) Channel using 120° Sectoring ($R_{cc} = 1/2$ and $v=8$).

probability of bit error using the extended Hata model as from Chapter IV where

$r_f = d = 1$ km and where the worst-case SNR is given by

$$\overline{\gamma_b} = \mathbb{E} \left\{ \frac{R^2 \mathcal{P}_T}{N_0 L_n(r_f) X} \right\} = \mathbb{E} \{ R^2 \} \mathbb{E} \{ 1/X \} \frac{E_b}{N_0} = \mathbb{E} \{ X \} \frac{E_b}{N_0}. \quad (5.4)$$

A. USER DENSITY IN THE CELL

In this section we assume that our users are physically distributed in the cell according to a given distribution, rather than placing our intended user in the worst-case position in the cell. This allows us to assess the typical performance of the forward channel in our DS-CDMA cellular system. In order to incorporate user distribution into our performance analysis of the forward channel, we require a joint probability density function in terms of r and θ that represents a user's position within the cell.

We define a user density, $G(r)$, as the *normalized* number of users per unit of area at a distance r from the base station [34]. Since the user density is a function of (only) distance, r , from the base station and not a function of θ , we have assumed that the user density is circularly symmetric about the origin. Accordingly, the number of normalized users in a differential ring of width dr at a radius r is given by

$$G(r)2\pi r dr.$$

The total *normalized* number of users within a distance r from the base station can then be viewed as the cumulative distribution function for an individual user's distance, r , from the base station given by

$$F_r(r) = \int_0^r G(s)2\pi s ds, \quad r > 0.$$

Accordingly, the probability density function $p_r(r)$ for a user's distance from the base station is given by

$$p_r(r) = \frac{dF_r(r)}{dr} = 2\pi r G(r), \quad r > 0. \quad (5.5)$$

Since we assume circular symmetry, the probability density function $p_\theta(\theta)$ for the angular position of a user is uniformly distributed as follows:

$$p_\theta(\theta) = \frac{1}{2\pi}, \quad -\pi < \theta \leq \pi. \quad (5.6)$$

By assuming independence of r , and θ , we develop a joint pdf for a user's position within the cell:

$$p_{r,\theta}(r, \theta) = p_r(r) p_\theta(\theta) = r G(r). \quad (5.7)$$

Consequently, for any valid pdf $p_r(r)$, we can determine the user density function $G(r)$ using (5.5) and the joint pdf for a user's position within the cell using (5.7). For example, if we assume the user density in the cell is uniform as defined by

$$G(r) = \frac{1}{\pi}, \quad 0 < r \leq 1, \quad (5.8)$$

we can determine the distribution for the user's distance from the base station using (5.5). In this case, the distribution is linear:

$$p_r(r) = 2r, \quad 0 < r \leq 1. \quad (5.9)$$

The joint pdf for a user's position in the cell is obtained by applying (5.7) as follows:

$$p_{r,\theta}(r, \theta) = \frac{r}{\pi}, \quad 0 < r \leq 1, \quad -\pi < \theta \leq \pi \quad (5.10)$$

To incorporate this result into our performance analysis, we modify our expression for the first-event error probability defined by (4.61) and (5.2) (conditioned on $\mathbf{R} = \mathbf{r}$ and $\Theta = \theta$) as follows:

$$\begin{aligned}\widetilde{\mathcal{P}}_2(\mathbf{d}) &= \int_{-\pi}^{\pi} \int_0^1 \left(\mathcal{P}_2(\mathbf{d}) \Big|_{\mathbf{r}, \theta} \right) p_{\mathbf{r}, \theta}(\mathbf{r}, \theta) d\mathbf{r} d\theta \\ &= \int_{-\pi}^{\pi} \int_0^1 \int_{-\infty}^{\infty} Q \left(\sqrt{\frac{z_d}{\hat{\alpha}}} \right) p_{z_d}(z_d) p_{\mathbf{r}, \theta}(\mathbf{r}, \theta) dz_d d\mathbf{r} d\theta,\end{aligned}\quad (5.11)$$

where

$$\hat{\alpha} = \frac{\exp\left(\frac{\lambda^2 \sigma_{dB}^2}{2}\right)}{3N} \sum_{i=1}^6 \sum_{j=0}^{K_i-1} \frac{\mathcal{F}_{ij}}{\mathcal{D}_i^n} \frac{\mathbf{r}^n}{\mathcal{D}_i^n} + \frac{N_0}{2\hat{E}_c}.\quad (5.12)$$

In view of the fact that the baseline bit energy received energy, \hat{E}_c , is a function of \mathbf{r} , it is also random variable defined by

$$\hat{E}_c = \frac{\mathcal{F}_1^{\mathbf{P}T_{cc}}}{L_n(\mathbf{r})} = \frac{\mathcal{F}_1^{\mathbf{P}T_{cc}}}{\mathbf{r}^n} = \frac{E_c \mathbf{r}^n}{\mathbf{r}^n},\quad (5.13)$$

where E_c is the baseline bit energy for the fixed worst-case position given by (5.3).

In the case of linear user distribution, the first-event error probability is developed using equations (5.10) through (5.13) as follows:

$$\begin{aligned}\widetilde{\mathcal{P}}_2(\mathbf{d}) &= \int_{-\pi}^{\pi} \int_0^1 \int_{-\infty}^{\infty} Q \left(\sqrt{\frac{z_d}{\hat{\alpha}}} \right) p_{z_d}(z_d) p_{\mathbf{r}, \theta}(\mathbf{r}, \theta) dz_d d\mathbf{r} d\theta \\ &= \int_{-\pi}^{\pi} \int_0^1 \int_{-\infty}^{\infty} \frac{\mathbf{r}}{\pi} Q \left(\sqrt{\frac{z_d}{\frac{\exp\left(\frac{\lambda^2 \sigma_{dB}^2}{2}\right)}{3N} \sum_{i=1}^6 \sum_{j=0}^{K_i-1} \frac{\mathcal{F}_{ij}}{\mathcal{D}_i^n} \frac{\mathbf{r}^n}{\mathcal{D}_i^n} + \frac{N_0 \mathbf{r}^n}{2E_c \mathbf{r}^n}}} \right) p_{z_d}(z_d) dz_d d\mathbf{r} d\theta.\end{aligned}\quad (5.14)$$

The upper bound on the probability of bit error is given by (4.63) using the first-event error probability defined in (5.14). Furthermore, we can implement antenna sectoring as in Chapter IV, which simply reduces the number of sectorized users in cell i to K_i/S , where S is the number of sectors.

We simulated the integral in (5.14) for the sectorized system using 100,000 Monte Carlo trials. Figure 5.3 depicts performance results using the linear user distribution and 120° antenna sectoring as it compares with our worst-case user position results from

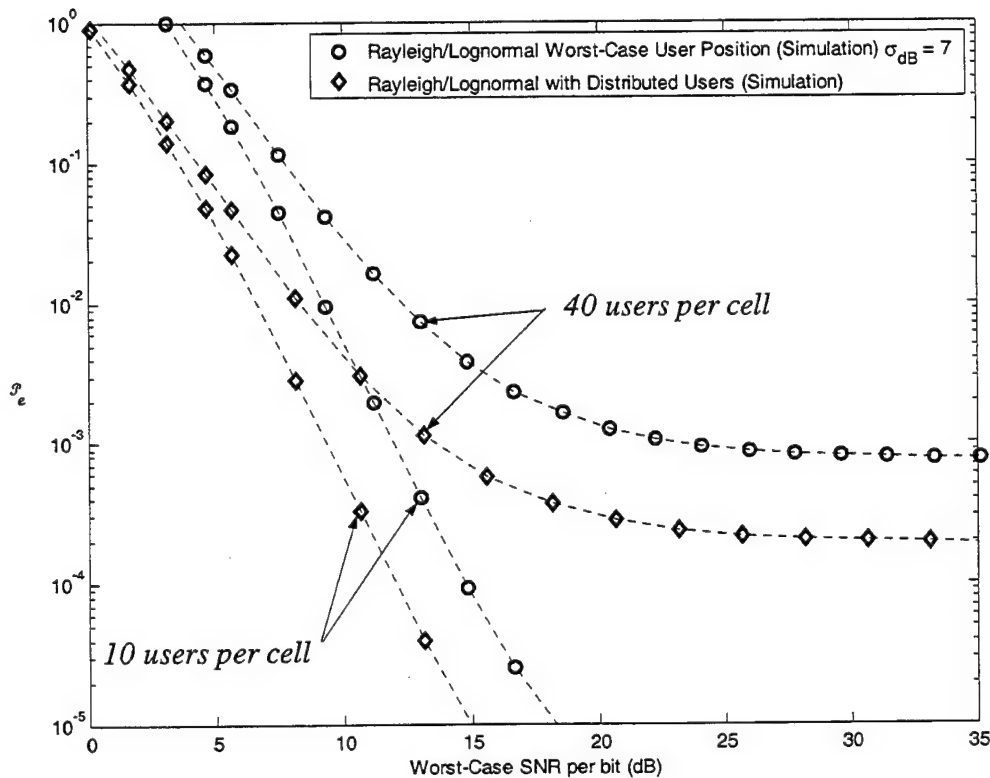


Figure 5.3 Probability of Bit Error for DS-CDMA with Rayleigh Fading and Lognormal Shadowing ($\sigma_{dB} = 7$) using a Linear User Distribution with 120° Sectoring and FEC ($R_{cc} = 1/2$ and $v=8$).

Chapter IV using the SNR per bit as defined by (5.4). As shown in the figure, accommodating the linear user distribution into the analysis indicates better performance (~ 3 to 4 dB) than that predicted by our worst-case scenario. The linear distribution, however, still presumes that the user's position is more likely to be toward the edge of the cell, since $E\{\mathbf{r}\} = 2/3$, and the edge of the cell is at $\mathbf{r} = 1$. Accordingly, using the linear user distribution in the performance analysis of the forward channel is more realistic than the worst-case scenario, however, it is not an overly optimistic view.

B. RANDOMIZING TRANSMIT POWER ON THE FORWARD TRAFFIC CHANNELS

In the previous section, we added user distribution to our analysis in order to better assess the performance of the forward channel. In this section, we will take advantage of the user distribution to adjust the transmit power in each user channel in a way that ensures the power received by each user is equal. By reducing the transmit power in the user channels to only that which is necessary, we intend to reduce the co-channel interference experienced by users in other cells.

The goal in our power-controlled system is to ensure that the power received by all mobile users is at the target power level \mathbf{P} by adjusting the transmit power in each channel, k , with the power control factor α_k . We can relate the target power received to the **baseline** transmit power, \mathbf{P}_t , by an attenuation factor as follows

$$\mathbf{P} = \frac{\mathbf{P}_t}{\alpha}, \quad (5.15)$$

where \mathbf{P} , \mathbf{P}_t , and \mathbf{a} are constant for all users in all cells. When the mobile user receives the information signal, the actual power received is measured and reported back to the base station for adjustment. At the point the mobile user measures his received power and reports it to the base station, it is no longer a random variable as described by (3.14), rather it is a realization of the random variable, which is known precisely and represented in our analysis as follows:

$$\mathbf{P}_k = \frac{\mathbf{P}_{t,k}}{L_n(d_k)x_k} = \frac{\mathcal{F}_k \mathbf{P}_t}{L_n(d_k)x_k} = \frac{\mathcal{F}_k \mathbf{a} \mathbf{P}}{d_k^n x_k}, \quad (5.16)$$

where d_k is the user's actual distance to the base station, and x_k is the shadowing experienced by the user. Accordingly, in order for the power received by all users to be at the target level \mathbf{P} , the base station must adjust the power factor such that

$$\mathcal{F}_k = \frac{d_k^n x_k}{\mathbf{a}}, \quad (5.17)$$

With perfect power control, the power received by intended mobile is simply

$$\mathbf{P}_k = \frac{\mathcal{F}_k \mathbf{P}_t}{d_k^n x_k} = \mathbf{P}. \quad (5.18)$$

By adjusting the power factor to achieve the target power received by all users, we have defeated the lognormal shadowing effect on the information signal.

We develop the power received by our mobile user from the forward signal in adjacent cell i channel j from (3.20) as follows:

$$P_{ij} = \frac{\mathcal{F}_{ij} \mathbf{P}_t}{L_n(\mathcal{D}_i) X_i} = \frac{\mathcal{F}_{ij}^n \hat{X}_{ij} \mathbf{P}}{L_n(\mathcal{D}_i) X_i}, \quad (5.19)$$

where

- X_i = Lognormal random variable $\Lambda(0, \lambda \sigma_{dB})$ representing shadowing on the forward signal from base station i , as received by the mobile in the center cell.
- \mathcal{U}_j = Random variable representing the distance between mobile user j in adjacent cell i and the base station in cell i . The probability distribution function is also $p_R(\mathcal{U})$.
- \widehat{X}_{ij} = Lognormal random variable $\Lambda(0, \lambda \sigma_{dB})$ representing shadowing on the forward signal from base station i , as received by mobile user j in cell i .

Accordingly, the power received from the adjacent cells is a random variable based upon user distribution and lognormal shadowing. When we incorporate (5.18) and (5.19) into our performance analysis we find that the first-event error probability is defined by

$$\begin{aligned}
 \widetilde{\mathcal{P}}_2(d) \Big|_{r_e, \mathcal{U}, \theta} &= Q \left(\sqrt{\frac{\mathcal{U}^2}{\sigma_{\mathcal{U}}^2}} \right) \\
 &= Q \left(\sqrt{\frac{\mathbf{P}^2 T_{cc}^2 \left(\sum_{\ell=1}^d r_{\ell}^2 \right)^2}{\left(\frac{T_{cc}}{3N} \sum_{i=1}^6 \sum_{j=0}^{K_i-1} \mathbb{E}\{R_i^2\} \mathbb{E}\{P_{ij}\} + \frac{N_0}{2} \right) \mathbf{P} T_{cc} \sum_{\ell=1}^d r_{\ell}^2}} \right) \\
 &= Q \left(\sqrt{\frac{\sum_{\ell=1}^d r_{\ell}^2}{\mathbf{P} T_{cc} \left[\frac{T_{cc}}{3N} \sum_{i=1}^6 \sum_{j=0}^{K_i-1} \mathbb{E}\{R_i^2\} \mathbb{E}\{P_{ij}\} + \frac{N_0}{2} \right]}} \right)
 \end{aligned}$$

$$\begin{aligned}
&= Q \left(\sqrt{\frac{\sum_{\ell=1}^d r_{\ell}^2}{\frac{1}{3N} \sum_{i=1}^6 \sum_{j=0}^{K_i-1} \mathbb{E}\{R_i^2\} \frac{1}{\mathbf{P}} \mathbb{E}\left\{\frac{\boldsymbol{\nu}_j^n \widehat{X}_{ij} \mathbf{P}}{\mathcal{D}_i^n X_i}\right\} + \frac{N_0}{2E_c}}}} \right) \\
&= Q \left(\sqrt{\frac{\sum_{\ell=1}^d r_{\ell}^2}{\frac{1}{3N} \sum_{i=1}^6 \sum_{j=0}^{K_i-1} \mathbb{E}\{R_i^2\} \frac{\mathbb{E}\{\boldsymbol{\nu}_j^n\} \mathbb{E}\{\widehat{X}_{ij}\} \mathbb{E}\{1/X_i\}}{\mathcal{D}_i^n} + \frac{N_0}{2E_c}}} \right) \quad (5.20) \\
&= Q \left(\sqrt{\frac{\sum_{\ell=1}^d r_{\ell}^2}{\frac{\exp\{\lambda^2 \sigma_{dB}^2\}}{3N} \sum_{i=1}^6 \sum_{j=0}^{K_i-1} \frac{\mathbb{E}\{\boldsymbol{\nu}_j^n\}}{\mathcal{D}_i^n} + \frac{N_0}{2E_c}}} \right),
\end{aligned}$$

where $\mathbb{E}\{\widehat{X}_{ij}\} = \mathbb{E}\{X_i\} = \mathbb{E}\{1/X_i\} = \exp\{\lambda^2 \sigma_{dB}^2/2\}$ and where we fix $\mathbf{P}T_{cc} = E_c$ as defined by (5.3) for comparative purposes. Accordingly, we remove the dependency on r_{ℓ} as in (4.65) as follows:

$$\widetilde{\mathcal{P}}_2(d) \Big|_{\kappa, \theta} = \mu^d \sum_{k=0}^{d-1} \binom{d-1+k}{k} (1-\mu)^k, \quad (5.21)$$

where

$$\begin{aligned}
\mu &= \frac{1}{2} \left(1 - \sqrt{\frac{\mathbb{E}\{\widehat{\psi}_{\ell}\}}{2 + \mathbb{E}\{\widehat{\psi}_{\ell}\}}} \right) \\
&= \frac{1}{2} \left(1 - \sqrt{\frac{1}{\frac{2 \exp\{\lambda^2 \sigma_{dB}^2\}}{3N} \sum_{i=1}^6 \sum_{j=0}^{K_i-1} \frac{\mathbb{E}\{\boldsymbol{\nu}_j^n\}}{\mathcal{D}_i^n} + \frac{N_0}{E_c} + 1}}}} \right),
\end{aligned}$$

since $\mathcal{E}\{\widehat{\psi}_\ell\}$ is defined by

$$\begin{aligned}\mathcal{E}\{\widehat{\psi}_\ell\} &= \mathcal{E}\left\{\frac{R_\ell^2}{\frac{\exp\{\lambda^2 \sigma_{dB}^2\}}{3N} \sum_{i=1}^6 \sum_{j=0}^{K_i-1} \mathcal{E}\{R_i^2\} \frac{\mathcal{E}\{\mathbf{r}_j^n\}}{\mathcal{D}_i^n} + \frac{N_0}{2E_c}}\right\} \\ &= \frac{\mathcal{E}\{R_\ell^2\}}{\frac{\exp\{\lambda^2 \sigma_{dB}^2\}}{3N} \sum_{i=1}^6 \sum_{j=0}^{K_i-1} \mathcal{E}\{R_i^2\} \frac{\mathcal{E}\{\mathbf{r}_j^n\}}{\mathcal{D}_i^n} + \frac{N_0}{2E_c}} \\ &= \frac{1}{\frac{\exp\{\lambda^2 \sigma_{dB}^2\}}{3N} \sum_{i=1}^6 \sum_{j=0}^{K_i-1} \frac{\mathcal{E}\{\mathbf{r}_j^n\}}{\mathcal{D}_i^n} + \frac{N_0}{2E_c}}.\end{aligned}$$

Finally, we remove the dependency on the random variables \mathbf{r} and θ , which are contained in the terms \mathcal{D}_i , as follows:

$$\begin{aligned}\widetilde{\mathcal{P}}_2(\mathbf{d}) &= \int_{-\pi}^{\pi} \int_0^1 \left(\widetilde{\mathcal{P}}_2(\mathbf{d}) \Big|_{\mathbf{r}, \theta} \right) p_{\mathbf{r}, \theta}(\mathbf{r}, \theta) d\mathbf{r} d\theta \\ &= \int_{-\pi}^{\pi} \int_0^1 \mu^{\mathbf{d}} \sum_{k=0}^{\mathbf{d}-1} \binom{\mathbf{d}-1+k}{k} (1-\mu)^k p_{\mathbf{r}, \theta}(\mathbf{r}, \theta) d\mathbf{r} d\theta.\end{aligned}\tag{5.22}$$

Using the linear user distribution from Section V.A, we define the first-event error probability by

$$\widetilde{\mathcal{P}}_2(\mathbf{d}) = \frac{1}{\pi} \int_{-\pi}^{\pi} \int_0^1 \mu^{\mathbf{d}} \sum_{k=0}^{\mathbf{d}-1} \binom{\mathbf{d}-1+k}{k} (1-\mu)^k d\mathbf{r} d\theta.\tag{5.23}$$

We can calculate an upper bound on the probability of bit error using (4.63) and (5.23). Furthermore, we implement antenna sectoring as in Chapter IV. Figure 5.4 compares the probability of bit error for a cellular system using forward power control

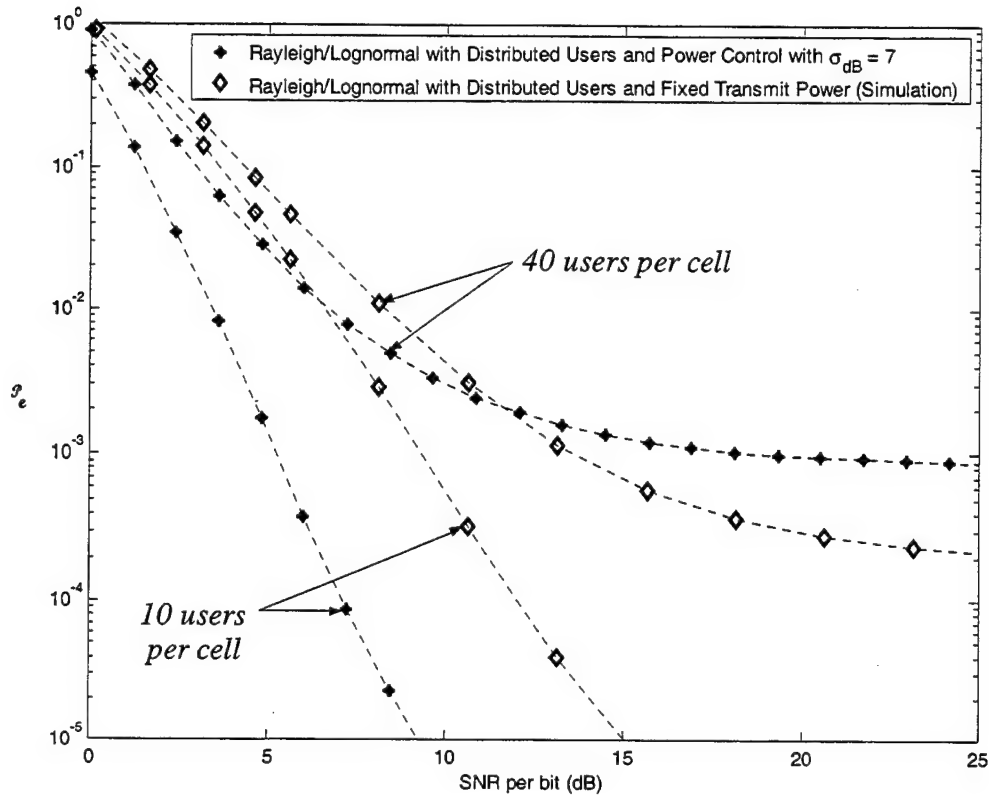


Figure 5.4 Probability of Bit Error for DS-CDMA with Rayleigh Fading and Lognormal Shadowing ($\sigma_{dB} = 7$) using Forward Power Control and Linear User Distribution with 120° Sectoring and FEC ($R_{cc} = 1/2$ and $v=8$).

with the fixed-power results from Section V.A. The average received SNR per bit for the Rayleigh-lognormal channel with perfect power control is developed as follows:

$$\overline{\gamma_b} = \mathbb{E} \left\{ \frac{R^2 \mathcal{P}_t}{N_0 d_k^n x_k} \right\} = \mathbb{E} \{ R^2 \} \frac{\mathcal{P}_t}{N_0} = \frac{E_b}{N_0}.$$

In the case of 10 users per cell, the power-controlled system clearly outperforms the system with fixed power (~ 5 dB). For 40 users per cell, however, the power-controlled system outperforms the fixed-power system for $\overline{\gamma_b} < 12$ dB, at which point the

interference floor begins to develop. We see that the interference floor for the power-controlled system is actually higher than the interference floor for the fixed-power system. In order to explain this, let us examine the isolated co-channel interference contribution from (5.20) as it compares with its equivalent expression in (5.14) for the fixed-power system. In order to ensure that the received power for all users is equal in the power-controlled system, we adjusted the power in the forward channel to overcome lognormal shadowing effects. By doing so, we have in effect *increased* the expected value of the co-channel interference by a factor of $E\{X\} = \exp(\lambda^2 \sigma_{dB}^2 / 2)$ over the fixed-power system. This extra factor of $E\{X\}$ is a result of randomizing the transmit power in the forward channel.

In spite of the increased co-channel interference, the performance of the power-controlled system is far superior to that of the fixed-power system for lognormal shadowing environments of $\sigma_{dB} < 6$ with 120° antenna sectoring. Under these circumstances, the benefits eliminating the lognormal shadowing from the intended signal outweigh the increased co-channel interference. Consequently, we can achieve a probability of bit error of less than 10^{-3} without entering the interference-limited region of operation. As shown in Appendix V-B, the power-controlled system can accommodate as many as 100 users per cell using 120° sectoring for $\sigma_{dB} < 6$. For $\sigma_{dB} = 6$, the power-controlled system can accommodate up to 80 users using 120° sectoring and still achieve the desired probability of bit error of 10^{-3} .

In designing a system with power control that operates in more intense lognormal shadowing environments ($\sigma_{dB} > 6$), we must ensure that our system is not working in the interference-limited region. For example, if we expect our system to work in the $\overline{\gamma_b} = 15$ dB range, the system could accommodate up to roughly 30 users per

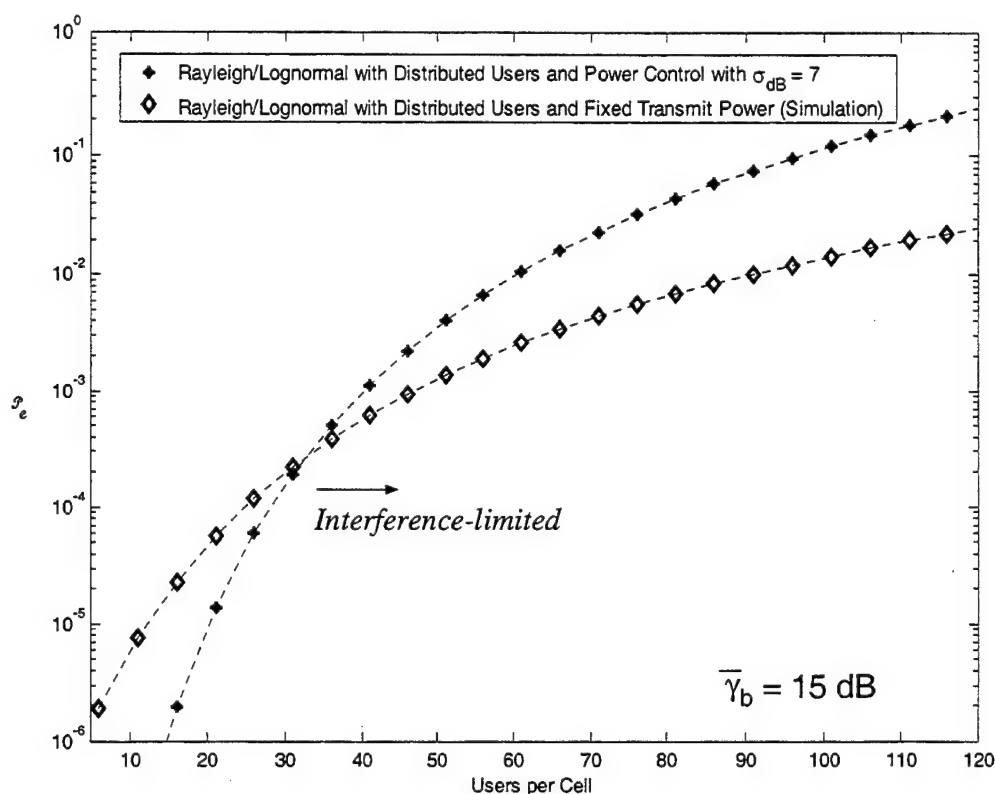


Figure 5.5 Probability of Bit Error for DS-CDMA with Rayleigh Fading and Lognormal Shadowing ($\sigma_{dB} = 7$) vs. Users per Cell using Linear User Distribution with 120° Sectoring and FEC ($R_{cc} = 1/2$ and $v=8$).

cell in a $\sigma_{dB} = 7$ shadowing environment using 120° sectoring. Adding more users would degrade performance due to operating in the interference-limited region as indicated in Figure 5.5.

If a greater user capacity is required, we could increase the number of sectors per cell to six. The power-controlled system operating in a $\sigma_{dB} = 7$ shadowing environment could support up to 70 users per cell using 60° antenna sectoring without operating in the interference-limited region as shown in Figure 5.6.

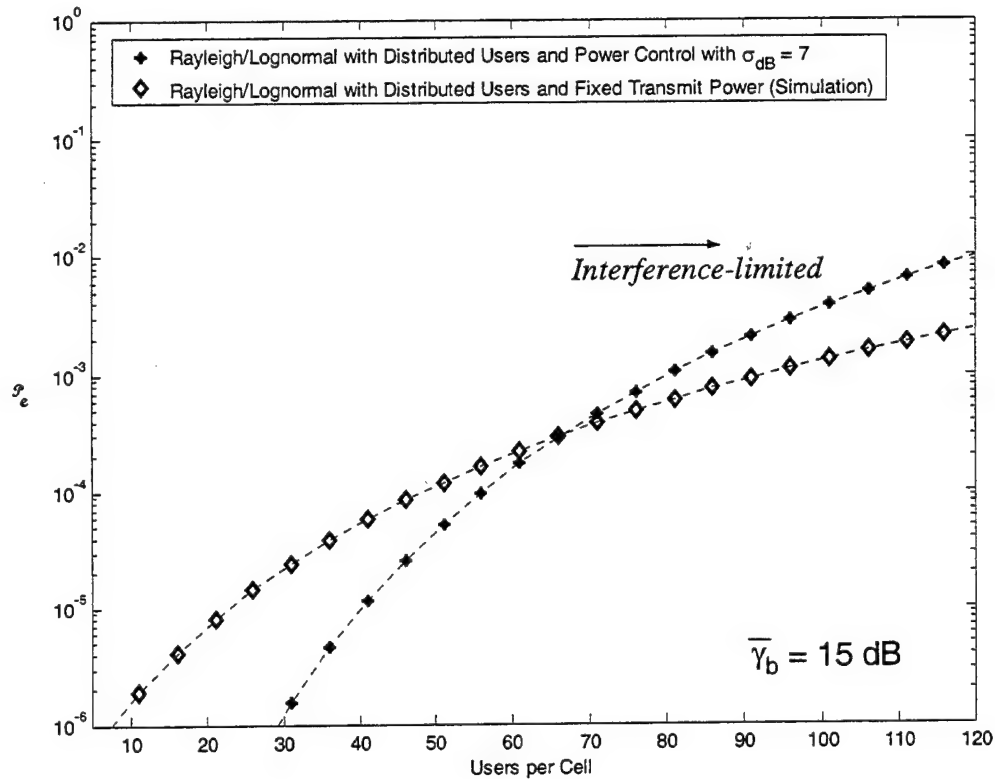


Figure 5.6 Probability of Bit Error for DS-CDMA with Rayleigh Fading and Lognormal Shadowing ($\sigma_{dB} = 7$) vs. Users per Cell using Linear User Distribution with 60° Sectoring with and FEC ($R_{cc} = 1/2$ and $v=8$).

The use of sectoring to alleviate the co-channel interference in support of power control only works up to a point. For a shadowing environment of $\sigma_{dB} = 8$, for example, the 6-sector system can accommodate up to roughly 27 users prior to becoming

interference-limited at an SNR per bit of $\overline{\gamma_b} = 15$ dB, which could be an acceptable user capacity. In an environment where $\sigma_{dB} = 9$, however, even with 60° sectoring we are interference limited with as few as 12 operators working at $\overline{\gamma_b} = 15$. Accordingly, implementing power control in such environments demands some additional method of interference mitigation for the system to be viable. Appendix V-B contains complete performance results for the power-controlled system operating in a lognormal environment of $\sigma_{dB} > 6$ using 60° sectoring.

Accordingly, we have shown that by *carefully* adding power control to the forward traffic channel, we can greatly improve the performance of our DS-CDMA cellular system operating in a Rayleigh-lognormal channel.

C. SUMMARY

In this chapter, we improved upon the performance analysis of Chapter IV for a DS-CDMA cellular system operating in a Rayleigh fading and lognormal shadowing environment, by randomizing user positions in the cell, rather than assuming the worst-case scenario. We presented a revised upper bound for the probability of bit error, which incorporated the user distribution within the cell. We analyzed the performance of the system using a linear user distribution based upon the *density* of users being uniform throughout the cell. We found that the performance of the system improved by 3 to 4 dB for our test case of $\sigma_{dB} = 7$.

In Section V.B, we implemented a power-control technique that ensures the power received by all users is equal. In doing so, we randomized the transmit power in each user channel to overcome the effects of lognormal-shadowing and distance dependent path loss. We found that, with proper implementation, the power-controlled system can greatly increase performance and user capacity of the forward channel. A system designer must, however, steer clear of the interference-limited region in heavily shadowed environments.

APPENDIX V-A GEOMETRY OF PATH LOSS DISTANCES

In this appendix we develop the path loss distances from the mobile user to each of the adjacent base stations in terms of r and θ . In all cases, we use the geometry of the triangle depicted in Figure 5.7 in order to determine \mathcal{D}_i .

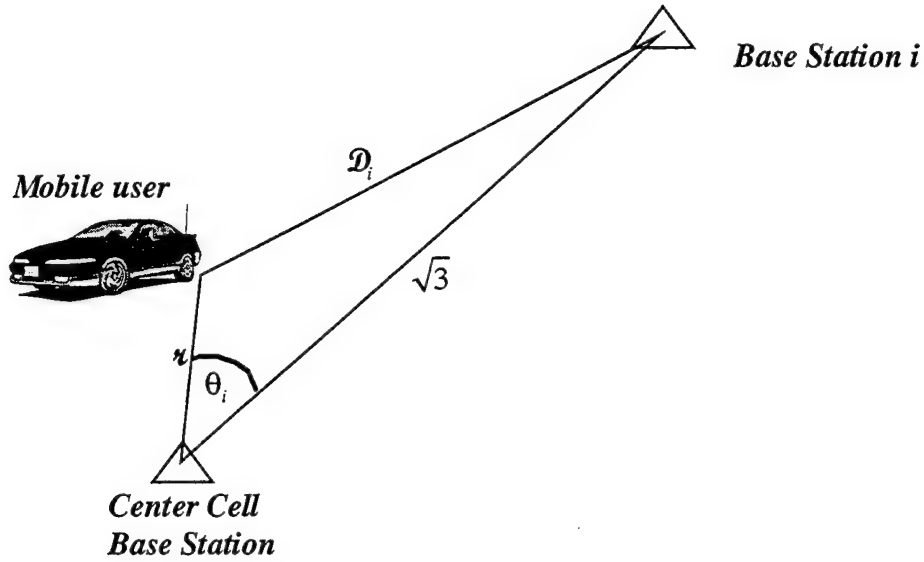


Figure 5.7 Key Triangle of Relationships.

We define θ_i as the angle between the mobile user and base station i . Using side-angle relations in plane triangles, we determine that

$$\mathcal{D}_i^2 = r^2 + 3 - 2\sqrt{3}r \cos \theta_i. \quad (5.24)$$

Accordingly, we seek to determine θ_i as a function of θ , which ensures that each \mathcal{D}_i is only a function of r and θ .

1. The Development of \mathcal{D}_1

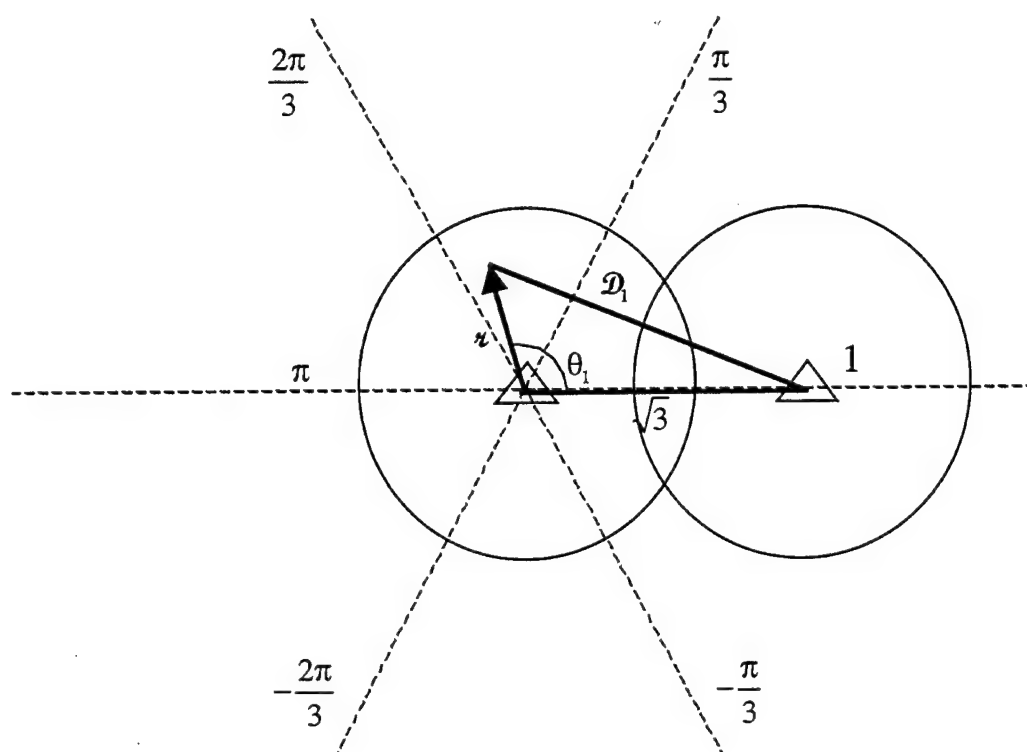


Figure 5.8 Geometry for \mathcal{D}_1 .

In determining θ_1 , we must consider two cases:

Case I: $0 < \theta \leq \pi$ (Figure 5.8), $\theta_1 = \theta$.

Case II: $-\pi < \theta \leq 0$ $\theta_1 = -\theta$.

Since $\cos \theta = \cos(-\theta)$, we take $\theta_1 = \theta$ to determine \mathcal{D}_1 from (5.24) as follows:

$$\begin{aligned} \mathcal{D}_1 &= \sqrt{r^2 - 2\sqrt{3}r \cos \theta_1 + 3} \\ &= \sqrt{r^2 - 2\sqrt{3}r \cos \theta + 3}. \end{aligned} \tag{5.25}$$

2. The Development of \mathcal{D}_2

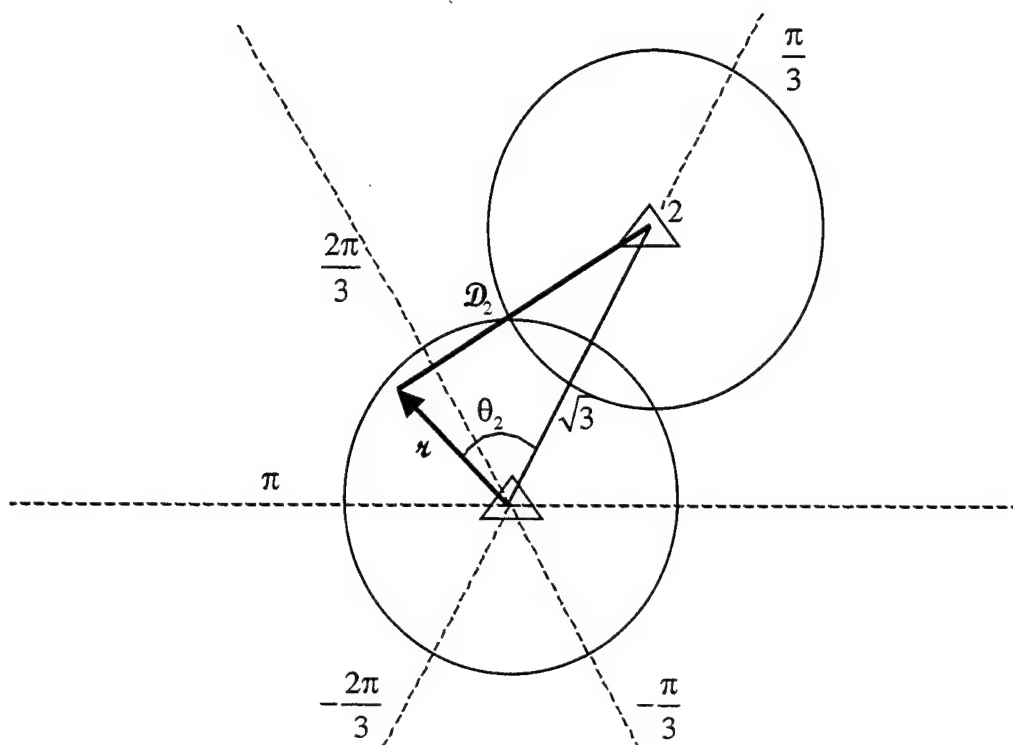


Figure 5.9 Geometry for \mathcal{D}_2 .

In determining θ_2 , we must consider four cases:

$$\text{Case I:} \quad 0 < \theta \leq \frac{\pi}{3} \quad \theta_2 = \frac{\pi}{3} - \theta = -\left(\theta - \frac{\pi}{3}\right).$$

$$\text{Case II:} \quad \frac{\pi}{3} < \theta \leq \pi \quad (\text{Figure 5.9}) \quad \theta_2 = \theta - \frac{\pi}{3}.$$

$$\text{Case III:} \quad -\frac{2\pi}{3} < \theta \leq 0 \quad \theta_2 = \frac{\pi}{3} - \theta = -\left(\theta - \frac{\pi}{3}\right).$$

$$\text{Case IV:} \quad -\pi < \theta \leq -\frac{2\pi}{3} \quad \theta_2 = \theta - \frac{\pi}{3}.$$

Since $\cos\left(\theta - \frac{\pi}{3}\right) = \cos\left(-\left(\theta - \frac{\pi}{3}\right)\right)$, we can take $\theta_2 = \theta - \frac{\pi}{3}$ to determine \mathcal{D}_2

from (5.24) as follows:

$$\begin{aligned}
 \mathcal{D}_2 &= \sqrt{\kappa^2 - 2\sqrt{3}\kappa \cos \theta_2 + 3} \\
 &= \sqrt{\kappa^2 - 2\sqrt{3}\kappa \cos\left(\theta - \frac{\pi}{3}\right) + 3} \\
 &= \sqrt{\kappa^2 - 2\sqrt{3}\kappa \left(\cos \theta \cos \frac{\pi}{3} + \sin \theta \sin \frac{\pi}{3}\right) + 3} \\
 &= \sqrt{\kappa^2 - \sqrt{3}\kappa \cos \theta - 3\kappa \sin \theta + 3}.
 \end{aligned} \tag{5.26}$$

3. The Development of \mathcal{D}_3

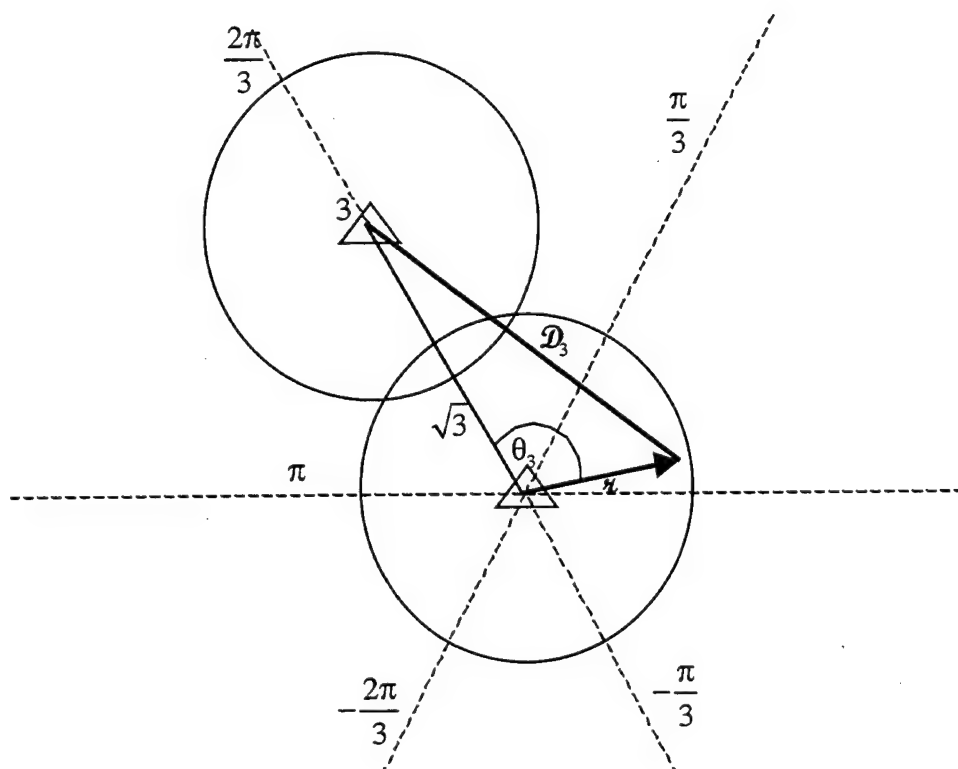


Figure 5.10 Geometry for \mathcal{D}_3 .

In determining θ_3 , we must consider four cases:

$$\text{Case I:} \quad 0 < \theta \leq \frac{2\pi}{3} \quad (\text{Figure 5.10}) \quad \theta_3 = \frac{2\pi}{3} - \theta = -\left(\theta - \frac{2\pi}{3}\right).$$

$$\text{Case II:} \quad \frac{2\pi}{3} < \theta \leq \pi \quad \theta_3 = \theta - \frac{2\pi}{3}.$$

$$\text{Case III:} \quad -\frac{\pi}{3} < \theta \leq 0 \quad \theta_3 = \frac{2\pi}{3} - \theta = -\left(\theta - \frac{2\pi}{3}\right).$$

$$\text{Case IV:} \quad -\pi < \theta \leq -\frac{\pi}{3} \quad \theta_3 = \theta - \frac{2\pi}{3}.$$

Since $\cos\left(\theta - \frac{2\pi}{3}\right) = \cos\left(-\left(\theta - \frac{2\pi}{3}\right)\right)$, we can take $\theta_3 = \theta - \frac{2\pi}{3}$ to determine

\mathcal{D}_3 from (5.24) as follows:

$$\begin{aligned} \mathcal{D}_3 &= \sqrt{\kappa^2 - 2\sqrt{3}\kappa \cos\theta_3 + 3} \\ &= \sqrt{\kappa^2 - 2\sqrt{3}\kappa \cos\left(\theta - \frac{2\pi}{3}\right) + 3} \\ &= \sqrt{\kappa^2 - 2\sqrt{3}\kappa \left(\cos\theta \cos\frac{2\pi}{3} + \sin\theta \sin\frac{2\pi}{3}\right) + 3} \\ &= \sqrt{\kappa^2 + \sqrt{3}\kappa \cos\theta - 3\kappa \sin\theta + 3}. \end{aligned} \tag{5.27}$$

4. The Development of \mathcal{D}_4

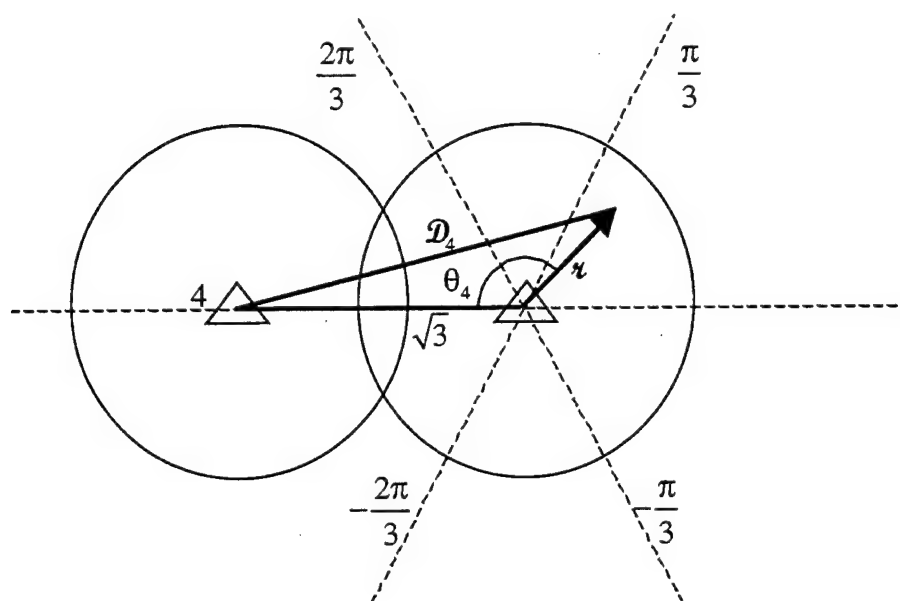


Figure 5.11 Geometry for \mathcal{D}_4 .

In determining θ_4 , we must consider two cases:

Case I: $0 < \theta \leq \pi$ (Figure 5.11) $\theta_4 = \pi - \theta$.

Case II: $-\pi < \theta \leq 0$ $\theta_4 = \pi + \theta$.

Since $\cos(\pi + \theta) = \cos(\pi - \theta) = -\cos \theta$, we take $\cos \theta_4 = -\cos \theta$ to determine

\mathcal{D}_4 from (5.24) as follows:

$$\begin{aligned} \mathcal{D}_4 &= \sqrt{r^2 - 2\sqrt{3}r \cos \theta_4 + 3} \\ &= \sqrt{r^2 + 2\sqrt{3}r \cos \theta + 3}. \end{aligned} \tag{5.28}$$

5. The Development of \mathcal{D}_5

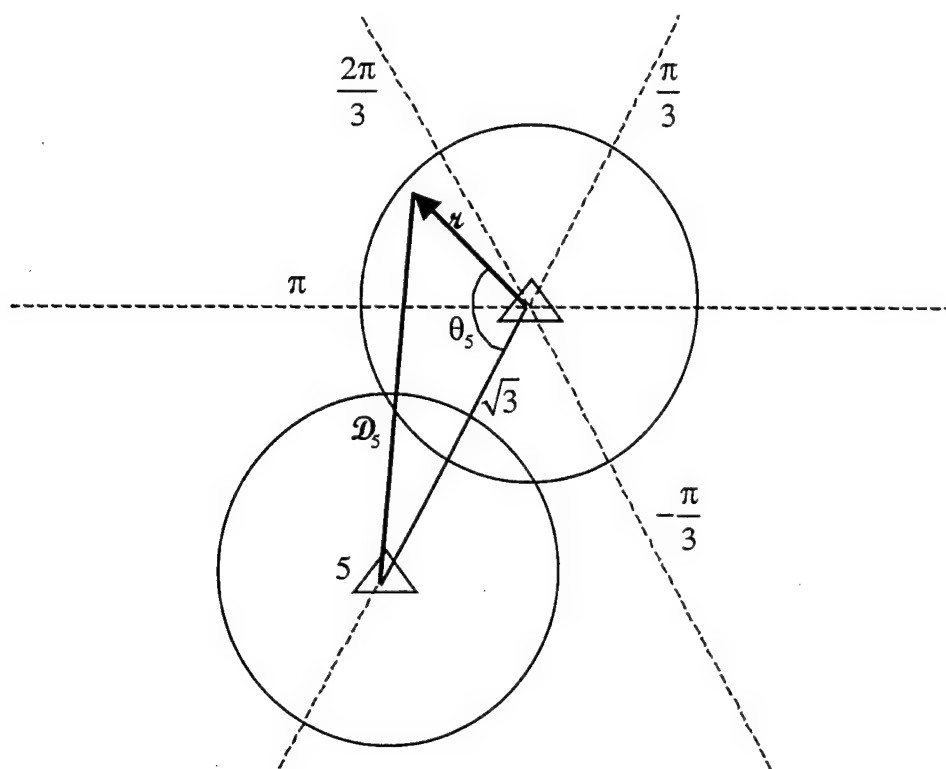


Figure 5.12 Geometry for \mathcal{D}_5 .

In determining θ_5 , we must consider four cases:

$$\text{Case I:} \quad 0 < \theta \leq \frac{\pi}{3} \quad \theta_5 = \theta + \frac{2\pi}{3}.$$

$$\text{Case II:} \quad \frac{\pi}{3} < \theta \leq \pi \quad (\text{Figure 5.12}) \quad \theta_5 = -\left(\theta + \frac{2\pi}{3}\right).$$

$$\text{Case III:} \quad -\frac{2\pi}{3} < \theta \leq 0 \quad \theta_5 = \theta + \frac{2\pi}{3}.$$

$$\text{Case IV:} \quad -\pi < \theta \leq -\frac{2\pi}{3} \quad \theta_5 = -\left(\theta + \frac{2\pi}{3}\right).$$

Since $\cos\left(\theta + \frac{2\pi}{3}\right) = \cos\left(-\left(\theta + \frac{2\pi}{3}\right)\right)$, we can take $\theta_5 = \theta + \frac{2\pi}{3}$ to determine

\mathcal{D}_5 from (5.24) as follows:

$$\begin{aligned}\mathcal{D}_5 &= \sqrt{\kappa^2 - 2\sqrt{3}\kappa \cos \theta_5 + 3} \\ &= \sqrt{\kappa^2 - 2\sqrt{3}\kappa \cos\left(\theta + \frac{2\pi}{3}\right) + 3} \\ &= \sqrt{\kappa^2 - 2\sqrt{3}\kappa \left(\cos \theta \cos \frac{2\pi}{3} - \sin \theta \sin \frac{2\pi}{3}\right) + 3} \\ &= \sqrt{\kappa^2 + \sqrt{3}\kappa \cos \theta + 3\kappa \sin \theta + 3}.\end{aligned}$$

6. The Development of \mathcal{D}_6

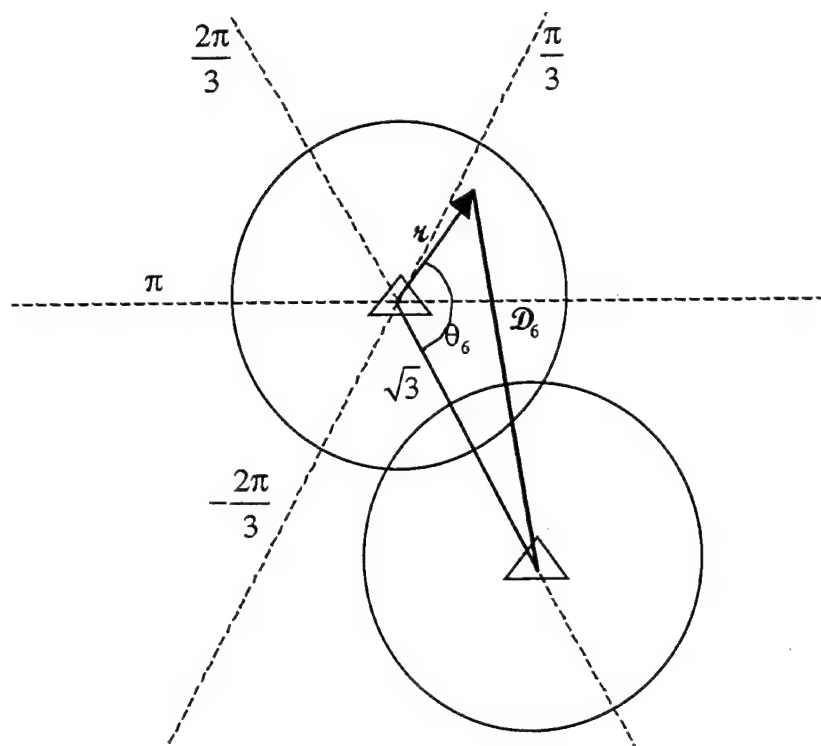


Figure 5.13 Geometry for \mathcal{D}_6 .

In determining θ_6 , we must consider four cases:

$$\text{Case I:} \quad 0 < \theta \leq \frac{2\pi}{3} \quad (\text{Figure 5.13}) \quad \theta_6 = \theta + \frac{\pi}{3}.$$

$$\text{Case II:} \quad \frac{2\pi}{3} < \theta \leq \pi \quad \theta_6 = -\left(\theta + \frac{\pi}{3}\right).$$

$$\text{Case III:} \quad -\frac{\pi}{3} < \theta \leq 0 \quad \theta_6 = \theta + \frac{\pi}{3}.$$

$$\text{Case IV:} \quad -\pi < \theta \leq -\frac{2\pi}{3} \quad \theta_6 = -\left(\theta + \frac{\pi}{3}\right).$$

Since $\cos\left(\theta + \frac{\pi}{3}\right) = \cos\left(-\left(\theta + \frac{\pi}{3}\right)\right)$, we take $\theta_6 = \theta + \frac{\pi}{3}$ to determine \mathcal{D}_6 from

(5.24) as follows:

$$\begin{aligned} \mathcal{D}_6 &= \sqrt{\kappa^2 - 2\sqrt{3}\kappa \cos \theta_6 + 3} \\ &= \sqrt{\kappa^2 - 2\sqrt{3}\kappa \cos\left(\theta + \frac{\pi}{3}\right) + 3} \\ &= \sqrt{\kappa^2 - 2\sqrt{3}\kappa \left(\cos \theta \cos \frac{\pi}{3} - \sin \theta \sin \frac{\pi}{3}\right) + 3} \\ &= \sqrt{\kappa^2 - \sqrt{3}\kappa \cos \theta + 3\kappa \sin \theta + 3}. \end{aligned} \tag{5.29}$$

APPENDIX V-B PROBABILITY OF BIT ERROR FOR THE RAYLEIGH-LOGNORMAL CHANNEL USING FORWARD CHANNEL POWER CONTROL

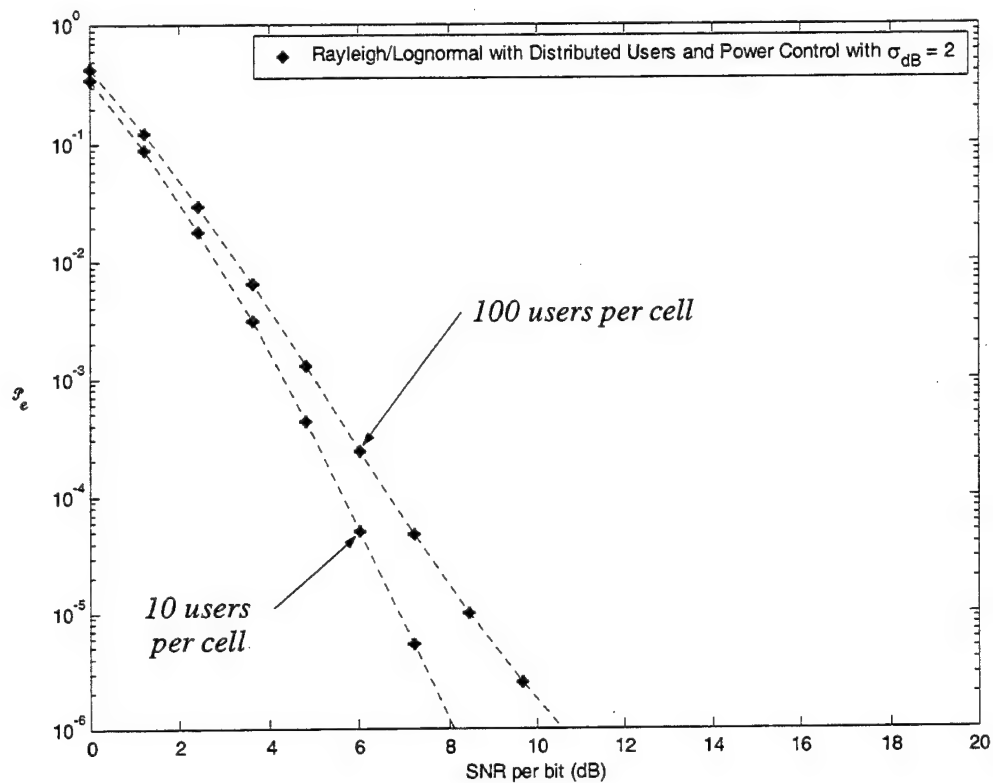


Figure 5.14 Probability of Bit Error for DS-CDMA with Rayleigh Fading and Lognormal Shadowing ($\sigma_{dB} = 2$) using Power Control and 120° Sectoring ($R_{cc} = 1/2$ and $v=8$).

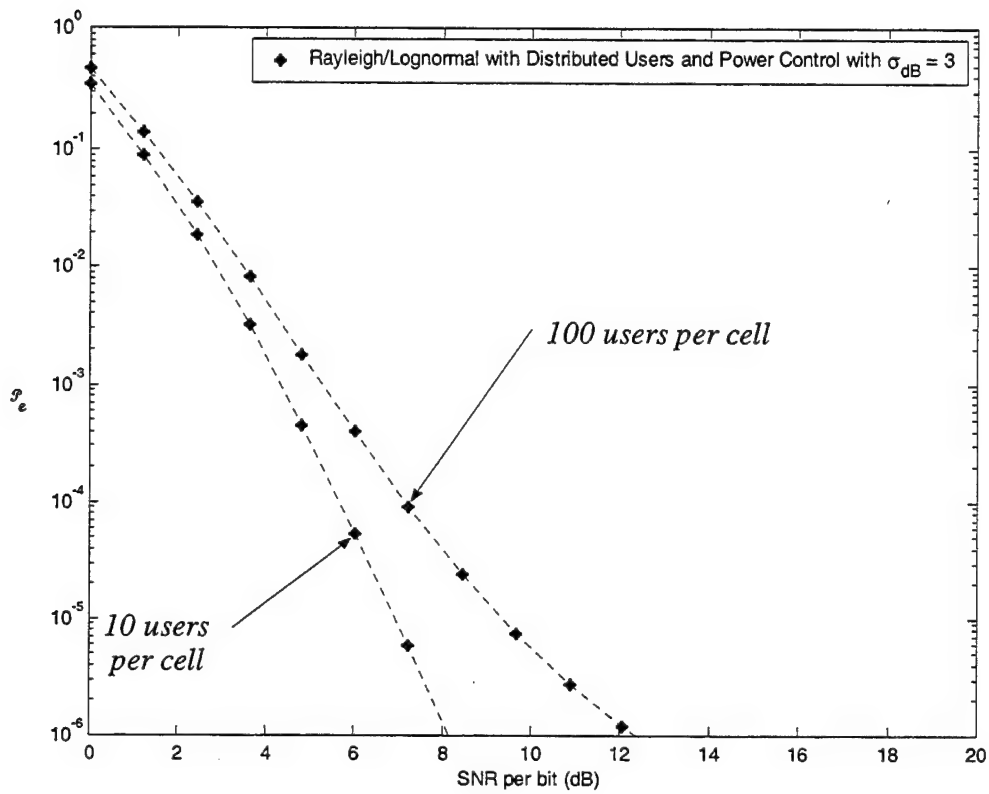


Figure 5.15 Probability of Bit Error for DS-CDMA with Rayleigh Fading and Lognormal Shadowing ($\sigma_{dB} = 3$) using Power Control and 120° Sectoring ($R_{cc} = 1/2$ and $v=8$).

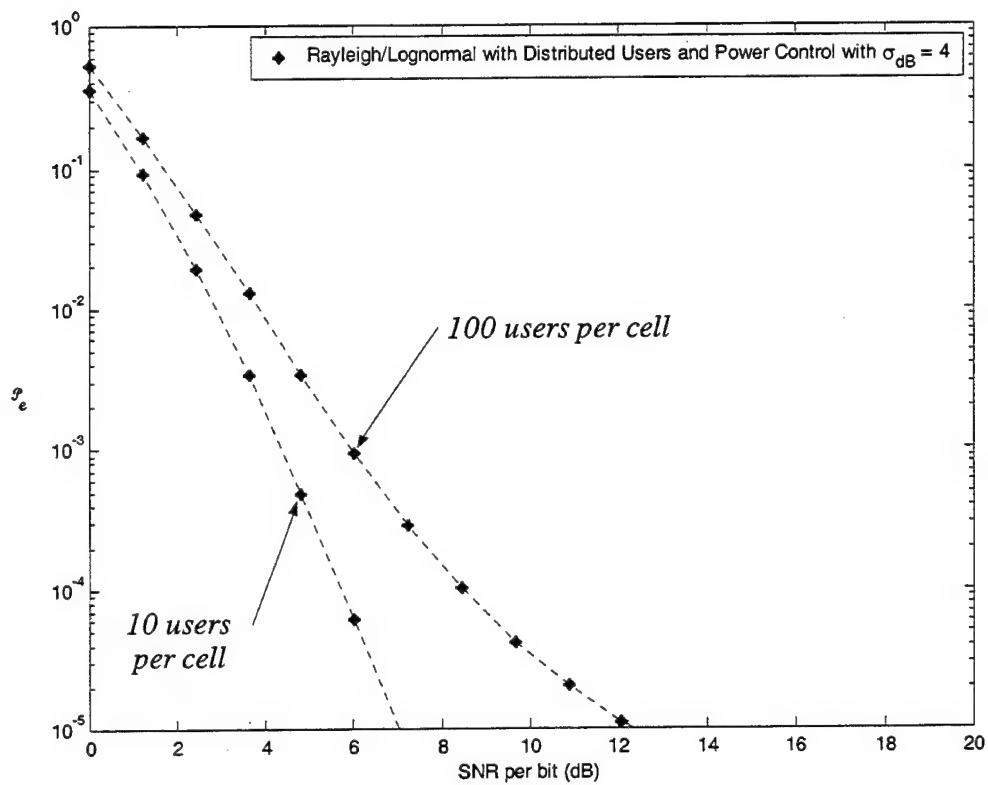


Figure 5.16 Probability of Bit Error for DS-CDMA with Rayleigh Fading and Lognormal Shadowing ($\sigma_{dB} = 4$) using Power Control and 120° Sectoring ($R_{cc} = 1/2$ and $v=8$).

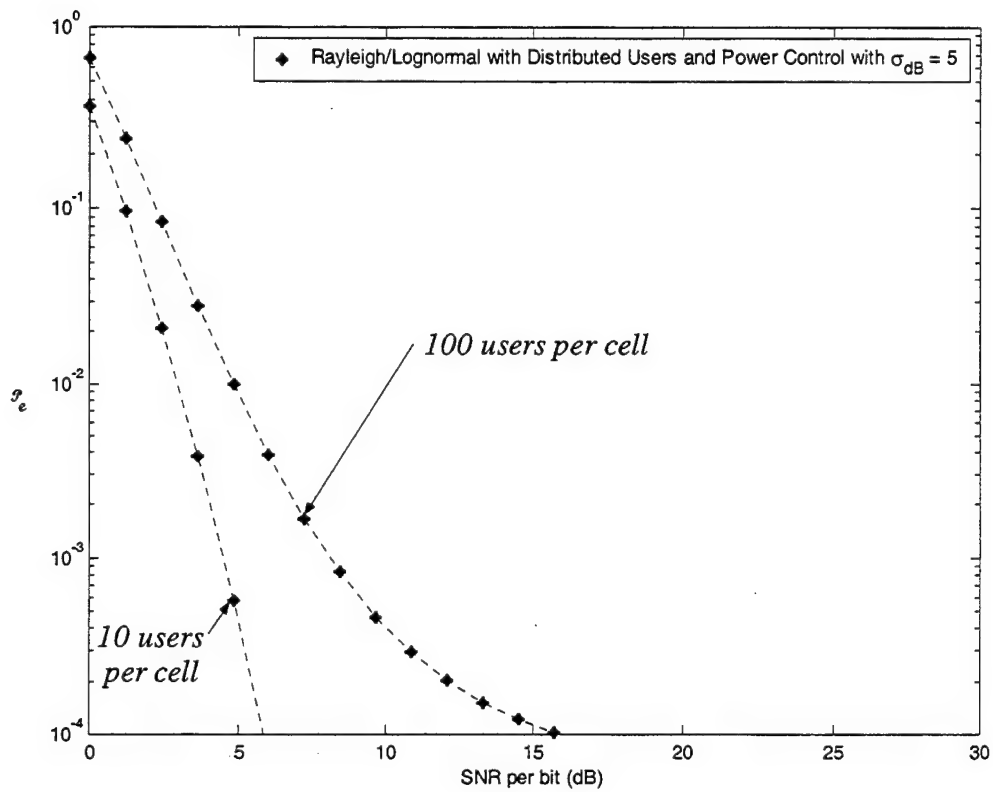


Figure 5.17 Probability of Bit Error for DS-CDMA with Rayleigh Fading and Lognormal Shadowing ($\sigma_{dB} = 5$) using Power Control and 120° Sectoring ($R_{cc} = 1/2$ and $v=8$).

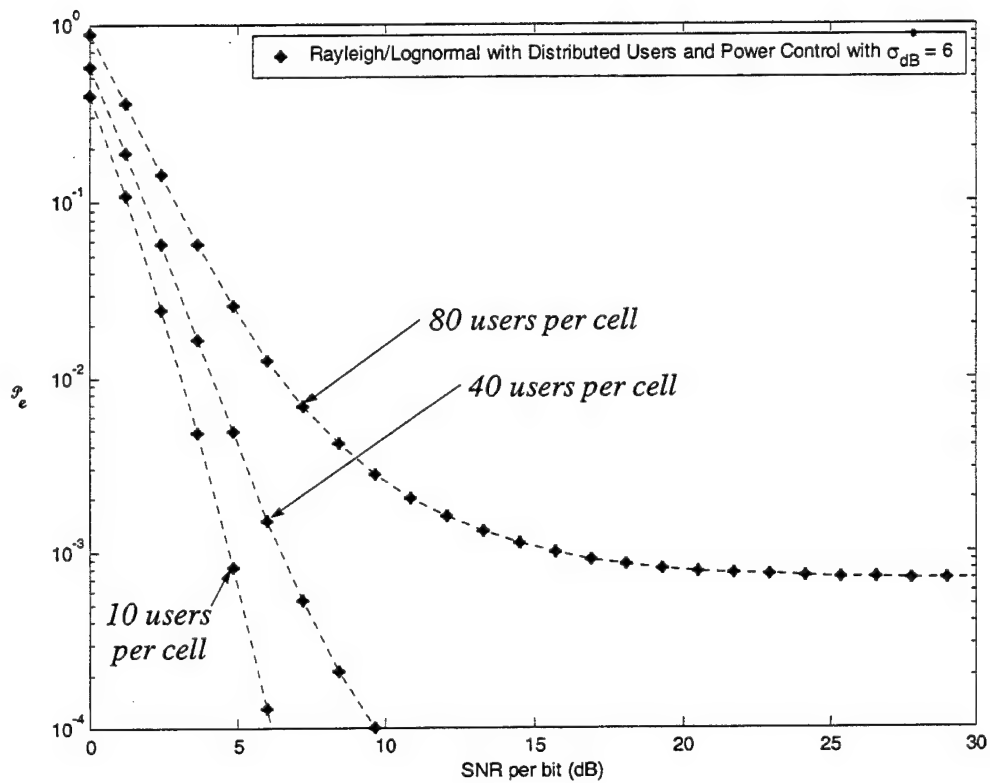


Figure 5.18 Probability of Bit Error for DS-CDMA with Rayleigh Fading and Lognormal Shadowing ($\sigma_{dB} = 6$) using Power Control and 120° Sectoring ($R_{cc} = 1/2$ and $v=8$).

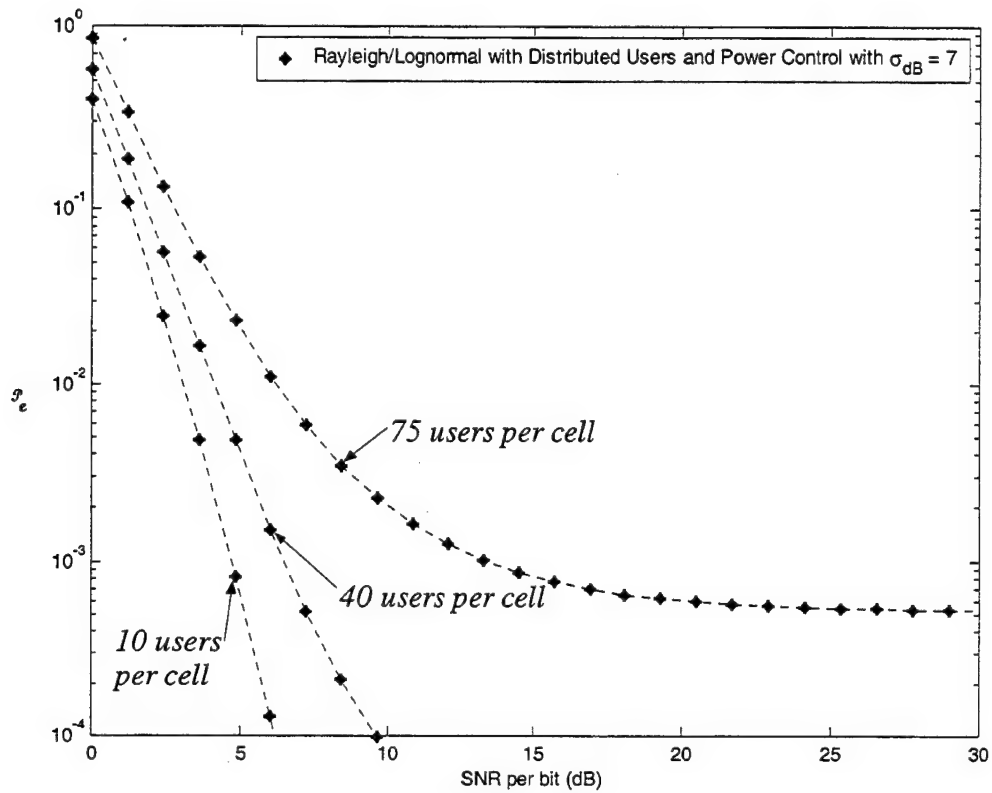


Figure 5.19 Probability of Bit Error for DS-CDMA with Rayleigh Fading and Lognormal Shadowing ($\sigma_{dB} = 7$) using Power Control and 60° Sectoring ($R_{cc} = 1/2$ and $v=8$).

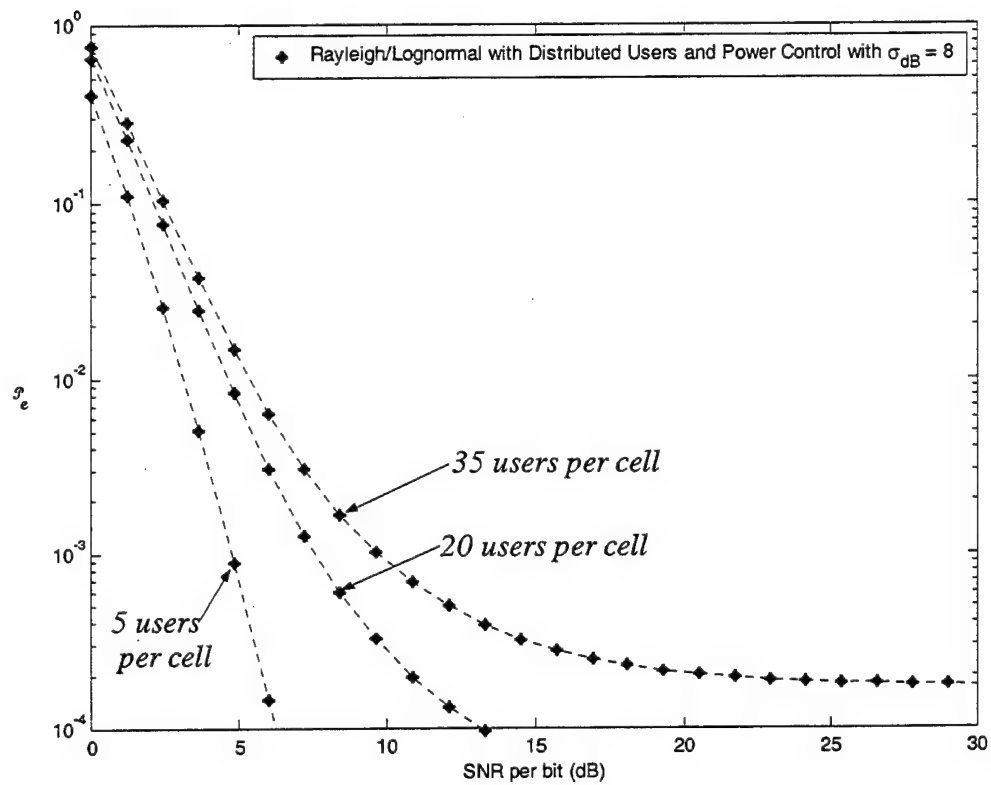


Figure 5.20 Probability of Bit Error for DS-CDMA with Rayleigh Fading and Lognormal Shadowing ($\sigma_{dB} = 8$) using Power Control and 60° Sectoring ($R_{cc} = 1/2$ and $v=8$).

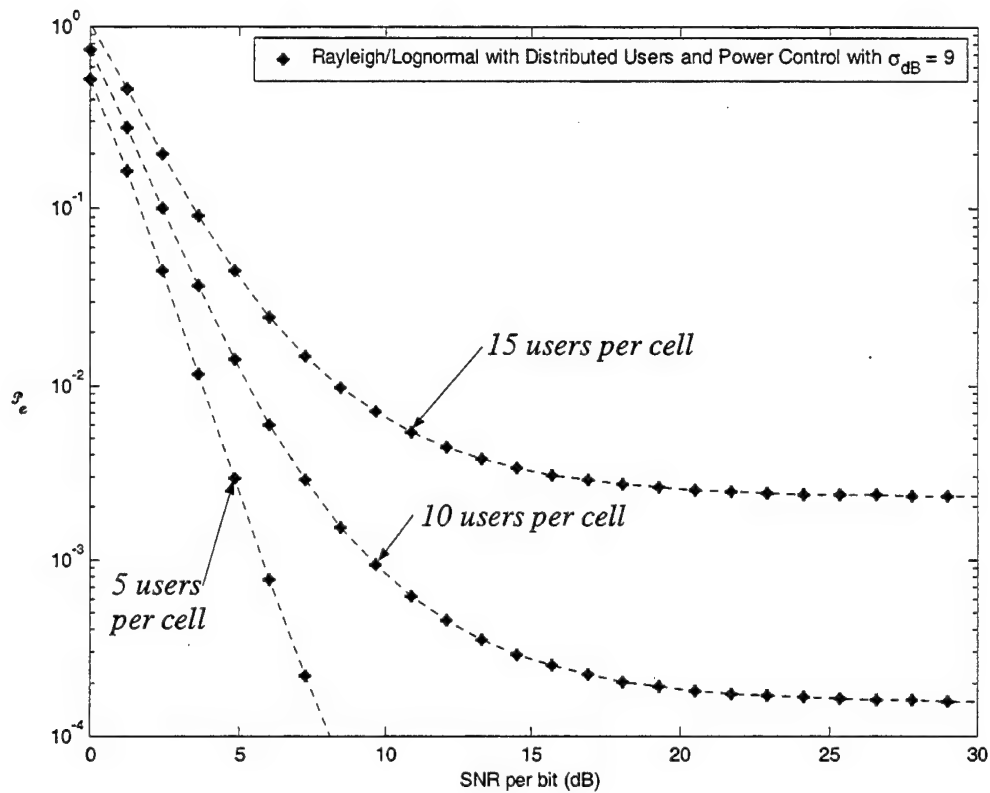


Figure 5.21 Probability of Bit Error for DS-CDMA with Rayleigh Fading and Lognormal Shadowing ($\sigma_{dB} = 9$) using Power Control and 60° Sectoring ($R_{cc} = 1/2$ and $v=8$).

VI. CONCLUSIONS AND FUTURE WORK

In this thesis, we have explored and developed many tools for analyzing the performance of the forward channel of a sectored DS-CDMA cellular system with FEC operating in a Rayleigh fading and lognormal shadowing environment. We will now summarize the work and conclusions and outline areas of future work.

A. CONCLUSIONS

In Chapter II, we examined the algebraic properties and generation of a set of Walsh functions, and proved the closure property for a set of Walsh functions. We developed the notion of extending the orthogonality property for a reduced set Walsh functions so that product of any *three* Walsh functions from the reduced set is identically zero when integrated over the bit period. We proposed a method to generate this reduced set and determined the maximum number of Walsh functions in the reduced set that ensures extended orthogonality. We concluded the chapter by developing the autocorrelation functions for a set of Walsh functions and by describing the average autocorrelation function for the entire set.

In Chapter III, we developed a forward channel model for the DS-CDMA cellular system that combined the effects of large-scale and small-scale propagation into a single unified model. We used the extended Hata model to predict large-scale path loss and incorporated lognormal shadowing. We also included small-scale propagation effects into the model using slow-flat Rayleigh fading. We developed the composite signal

received by a mobile user in the worst-case position consisting of the signals from the center and adjacent base stations, which have traveled through the Rayleigh-lognormal channel.

In Chapter IV, we developed a Signal-to-Noise plus Interference Ratio (SNIR) and the bit-error probability for the DS-CDMA cellular system in a Rayleigh-lognormal channel by using Gaussian approximation. We incorporated Forward Error Correction (FEC) in the form of convolutional encoding with soft-decision decoding into our forward channel model and develop a revised upper bound on the probability of bit error. We approximated a sum of d multiplicative chi-square(two degrees of freedom)-lognormal random variables as a multiplicative chi-square(with $2d$ degrees of freedom)-lognormal random variable, in order to evaluate the probability of bit error for the DS-CDMA system with FEC operating in the Rayleigh-lognormal channel. Our modeled performance results compared favorably with the Monte Carlo simulated results. Specifically, we found that the model was quite accurate in the SNR per bit range of $\overline{\gamma}_b = 10$ to 15 dB. In predicting the interference floor, the model effectively upper bounded the Monte Carlo simulated results. Using our model to approximate the sum of d multiplicative chi-square(two degrees of freedom)-lognormal random variables in the performance analysis of DS-CDMA cellular systems operating in a Rayleigh-lognormal channel is a fast, effective and, accordingly, a very valuable tool for system designers.

We concluded Chapter IV by incorporating antenna sectoring into our forward channel model. Lastly, we analyzed the performance of our forward channel model

operating in the Rayleigh-lognormal channel under a wide range of shadowing conditions and for various numbers of users per cell.

In Chapter V, we modified the performance analysis developed in Chapter IV to incorporate user distribution within the cell by assuming that the user's position is random according to a specified distribution. We revised the upper bound on the probability of bit error for the DS-CDMA cellular system with FEC in a Rayleigh-lognormal channel to accommodate distributed users. Accordingly, we developed a more realistic view of typical performance for our forward channel model. We analyzed the performance of the system using a linear user distribution and found that system performance was 3 to 4 dB better than predicted by our worst-case analysis.

We concluded Chapter V by introducing forward channel power control as a means of enhancing the overall performance of the system. We analyzed the performance of the system with power control under a wide range of shadowing conditions and for various numbers of users per cell. We found that in light to medium shadowing environments ($\sigma_{dB} < 6$) power control can greatly enhance the performance of the forward channel and accordingly increase user capacity. In heavily shadowed environments, performance is enhanced *provided* that the system is not operating in the interference-limited region, which is a function of required user capacity and the shadowing parameter σ_{dB} .

B. FUTURE WORK

There is much opportunity for further research in the area of DS-CDMA cellular systems operating in a Rayleigh fading and lognormal shadowing channels. For example, implementation of FEC using Serially Concatenated Convolutional Codes (SCCC) would enhance our analysis. The use of concatenated codes with interleavers can improve the performance of the cellular system by overcoming any burst errors that may arise due to multipath propagation effects.

Our analysis in Chapter V incorporated a user distribution based on uniform user density within the cell. There are many other user densities and distributions that could be explored and that may better reflect user distribution in practice.

In implementing fast power control in Chapter V, we assumed that the base station was not limited in the total amount of power transmitted. That is, in order to achieve the target receive power level for every user and overcome shadowing regardless of severity, the base station was free to boost power to whatever level was required. Of course in practice, the base station would be limited in total transmit power. Accordingly, an analysis that caps the base station's total transmit power and considers power allocation to the service channels would be insightful.

Finally, the analysis of the forward channel developed in this thesis should be extended to the reverse channel of a DS-CDMA cellular system in a Rayleigh fading and lognormal shadowing environment.

LIST OF REFERENCES

- [1] E. Dahlman, B. Gudmundson, M. Nilsson, J. Skold, "UMTS/IMT-2000 Based on Wideband CDMA," *IEEE Communications Magazine*, pp. 70-80, Sep. 1998.
- [2] F. Adachi, M. Sawahashi, H. Suda, "Wideband DS-CDMA for Next-Generation Mobile Communications Systems," *IEEE Communications Magazine*, pp. 56-69, Sep. 1998.
- [3] T. Ojanpera and R. Prasad, "An Overview of Air Interface Multiple Access for IMT-2000/UMTS," *IEEE Communications Magazine*, pp. 82-95, Sep. 1998.
- [4] W. Ye and A. M. Haimovich, "Performance of Cellular CDMA with Cell Site Antenna Arrays, Rayleigh Fading, and Power Control Error," *IEEE Transactions on Communications*, vol. 48, no. 7, pp. 1151-1159, July 2000.
- [5] T. T. Tjhung and C. C. Chai, "Distribution of SIR and Performance of DS-CDMA Systems in Lognormally Shadowed Rician Channels," *IEEE Transactions on Vehicular Technology*, vol. 49, no. 4, pp. 1110-1125, July 2000.
- [6] B. Hashem and E. S. Sousa, "On the Capacity of Cellular DS/CDMA Systems Under Slow Rician/Rayleigh-Fading Channels," *IEEE Transactions on Vehicular Technology*, vol. 49, no. 5, pp. 1752-1759, Sep. 2000.
- [7] A. J. Viterbi, A. M. Viterbi, E. Zehavi, "Performance of Power-Controlled Wideband Terrestrial Digital Communication," *IEEE Transactions on Communications*, vol. 41, no. 4, pp. 559-569, Apr. 1993.
- [8] R. D. Cideciyan, E. Eleftheriou, M. Rupf, "Concatenated Reed-Solomon/Convolutional Coding for Data Transmission in CDMA-Based Cellular Systems," *IEEE Transactions on Communications*, vol. 45, no. 10, pp. 1291-1303, Oct. 1997.
- [9] A. M. Earnshaw and S. D. Blostein, "A Combined Soft-Decision Deinterleaver/Decoder for the IS95 Reverse Link," *IEEE Transactions on Vehicular Technology*, vol. 49, no. 2, pp. 448-456, Mar. 2000.
- [10] P. Frenger, P. Orten, T. Ottosson, "Code-Spread CDMA Using Maximum Free Distance Low-Rate Convolutional Codes," *IEEE Transactions on Communications*, vol. 48, no. 1, pp. 135-144, Jan. 2000.
- [11] O. K. Tonguz, M. M. Wang, "Cellular CDMA Networks Impaired by Rayleigh Fading: System Performance with Power Control," *IEEE Transactions on Vehicular Technology*, vol. 43, no. 3, pp. 515-527, Aug. 1994.

- [12] L. B. Milstein, T. S. Rappaport, R. Barghouti, "Performance Evaluation for Cellular CDMA," *IEEE Journal on Selected Areas in Communications*, vol. 10, no. 4, pp. 680-689, May 1992.
- [13] S. W. Oh, K. L. Cheah, K. H. Li, "Forward-Link BER Analysis of Asynchronous Cellular DS-CDMA over Nakagami-Faded Channels Using Combined PDF Approach," *IEEE Transactions on Vehicular Technology*, vol. 49, no. 1, pp. 173-180, Jan. 2000.
- [14] J. L. Walsh, "A Closed Set of Normal Orthogonal Functions," *American Journal of Mathematics*, vol. 45, pp. 5-24, 1923.
- [15] J. S. Lee and L. E. Miller, *CDMA Systems Engineering Handbook*, Artech House, 1998.
- [16] N. J. Bloch, *Abstract Algebra with Applications*, Englewood Cliffs, NJ: Prentice-Hall, 1987.
- [17] B. Golubov, A. Efimov, V. Skvortsov, *Walsh Series and Transforms*, Kluwer Academic Publishers, 1991.
- [18] G. L. Turin, "Introduction to Spread-Spectrum Antimultipath Techniques and Their Application to Urban Digital Radio," *IEEE Proceedings*, vol. 68, no. 3, pp. 328-353, March 1980.
- [19] T. S. Rappaport, *Wireless Communications: Principles & Practice*, Upper Saddle River, New Jersey: Prentice Hall PTR, 1996.
- [20] Y. Okumura, et al., "Field Strength and Its Variability in VHF and UHF Land-Mobile Radio Service," *Reviews of the Electrical Communications Laboratory (Japan)*, vol. 16, no. 9-10, pp. 825-873, September-October 1968.
- [21] M. Hata, "Empirical Formula for Propagation Loss in Land Mobile Radio Services," *IEEE Transactions on Vehicular Technology*, vol. VT-29, no. 3, pp. 317-325, Aug. 1980.
- [22] COST 231, "Urban Transmission Loss Models for Mobile Radio in the 900 and 1,800 MHz bands (Revision 2)," COST 231 TD(90)119 Rev. 2, The Hague, The Netherlands, Sep. 1991.
- [23] E. L. Crow and K. Shimizu, *Lognormal Distributions: Theory and Applications*, New York: Marcel Dekker, Inc., 1988.
- [24] J. G. Proakis, *Digital Communications*, Boston, Massachusetts. WCB/McGraw-Hill, 1993.

- [25] M. B. Pursley, D. V. Sawate, W. E. Stark, "Performance Evaluation for Phase-Coded Spread-Spectrum Multiple-Access Communication - Part II: Code Sequence Analysis," *IEEE Transactions on Communications*, vol. COM-25, no. 8, Aug. 1987.
- [26] R. K. Morrow, Jr., and J. S. Lehnert, "Bit-to-Bit Error Dependence in Slotted DS/SSMA Packet Systems with Random Signature Sequences," *IEEE Transactions on Communications*, vol. 37, no. 10, Oct. 1989.
- [27] S. S. Haykin, *An Introduction to Analog and Digital Communications*, New York, John Wiley and Sons, 1989.
- [28] E. W. Ng and M. Geller, "A Table of Integrals of the Error Functions," *Journal of Research of the National Bureau of Standards - B. Mathematical Sciences*, vol. 73B, no. 1, January-March 1969.
- [29] I. S. Gradshteyn and I. M. Ryzhik, *Table of Integrals, Series, and Products*, San Diego, CA, Academic Press, 1994.
- [30] S. C. Schwartz and Y. S. Yeh, "On the Distribution Function and Moments of Power Sums with Log-Normal Components," *Bell System Technical Journal*, vol. 61, no. 7, pp. 1441-1462, Sep. 1982.
- [31] D. Schleher, "Generalized Gram-Charlier Series with Application to the Sum of Lognormal Variates," *IEEE Transactions on Information Theory*, pp. 275-280, Mar. 1977.
- [32] N. C. Beaulieu, A. A. Abu-Dayya, and P. J. McLane, "Estimating the Distribution of a Sum of Independent Lognormal Variables," Queen's University Tech. Report #9401, Jan. 1994.
- [33] A. A. Abu-Dayya, N. C. Beaulieu, "Comparison of Methods of Computing Lognormal Sum Distributions and Outages for Digital Wireless Applications," in *Conf. Rec. SUPERCOMM '94*, vol. 3, pp. 1270-1275, May 1994.
- [34] N. Abramson, "The Throughput of Packet Broadcasting Channels," *IEEE Transactions on Communications*, vol. COM-25, pp. 117-128, Jan. 1977.

THIS PAGE INTENTIONALLY LEFT BLANK

BIBLIOGRAPHY

- A. Abdi, H. Hasemi, S. Nader-Esfahani, "On the PDF of the Sum of Random Vectors," *IEEE Transactions on Communications*, vol. 48, no. 1, pp. 7-12, Jan. 2000.
- M. S. Alouini and A. Goldsmith, "Capacity of Nakagami Multipath Fading Channels," in *Proceedings 1997 IEEE 47th Annual International Vehicular Technology Conference (VTC '97)*, pp. 358-362 Phoenix, AZ, May, 1997.
- J. C. Arnbak and W. Blitterswijk, "Capacity of Slotted ALOHA in Rayleigh-Fading Channels," *Journal on Selected Areas of Communications*, vol. SAC-5, pp. 261-269, Feb. 1987.
- N. Bambos, "Toward Power-Sensitive Network Architectures in Wireless Communications: Concepts, Issues, and Design Aspects," *IEEE Personal Communications*, pp. 50-59, June 1998.
- R. Buz, "Information Theoretic Limits on Communications over Multipath Fading Channels," Ph.D. Dissertation, Dept. Electrical and Computer Eng., Queen's Univ. 1994.
- E. Biglieri, J. Proakis, S. Shamai, "Fading Channels: Information-Theoretic and Communications Aspects," *IEEE Transactions on Information Theory*, vol. 44, no. 6, pp. 2619-2692, Oct. 1998.
- E. Biglieri, G. Caire, G. Taricco, "Coding and Modulation Under Power Constraints," *IEEE Personal Communications*, pp. 32-39, June 1998.
- E. Biglieri, G. Caire, G. Taricco, J. Ventura-Traveset, "Co-channel interference in cellular mobile radio systems with coded PSK and diversity," *Wireless Personal Communications*, vol. 6, no. 1-2, pp. 39-68, Jan. 1998.
- E. H. Dinan and B. Jabbari, "Spreading Codes for Direct Sequence CDMA and Wideband CDMA Cellular Networks," *IEEE Communications Magazine*, pp. 48-54, Sep. 1998.
- G. P. Efthymoglou, V. A. Aalo, H. Helmken, "Performance Analysis of Coherent DS-CDMA Systems in a Nakagami Fading Channel with Arbitrary Parameters," *IEEE Transactions on Vehicular Technology*, vol. 46, no. 2, May 1997.
- K. Gilhousen *et al.* "On the Capacity of a Cellular CDMA System," *IEEE Transactions on Vehicular Technology*, vol. 40, no. 2, pp. 303-312, May 1991.

A. Goldsmith, "Design and Performance of High-Speed Communication Systems over Time-Varying Radio Channels," Ph.D. Dissertation, Dept. of Electrical Eng. and Computer Science, Univ. of California at Berkeley, 1994.

A. Goldsmith and P. Varaiya, "Capacity of Fading Channels with Channel Side Information," *IEEE Transaction on Information Theory*, vol. 43, no. 6, pp. 1986-1992, Nov. 1997.

M. S. Ismail and T. A. Rahman, "Forward-Link Performance of CDMA Cellular System," *IEEE Transactions on Vehicular Technology*, vol. 49, no. 5, pp. 1692-1696, Sep. 2000.

W. C. Y. Lee, "Overview of Cellular CDMA," *IEEE Transactions on Vehicular Technology*, vol. 40, no. 2, pp. 291-302, May 1991.

T. M. Lok and J. S. Lehnert, "Error Probabilities for Generalized Quadriphase DS/SSMA Communication Systems with Random Signature Sequences," *IEEE Transactions on Communications*, vol. 44, no. 7, pp. 876-885, July 1996.

M. P. Lotter and P. Rooyen, "Modeling Spatial Aspects of Cellular CDMA/SDMA Systems," *IEEE Communications Letters*, vol. 3, no. 5, pp. 128-131, May 1999.

M. P. Lotter and P. Rooyen, "Cellular Channel Modeling and the Performance of DS-CDMA Systems with Antenna Arrays," *IEEE Journal on Selected Areas in Communications*, vol. 17, no. 12, pp. 2181-2196, Dec. 1999.

L. B. Milstein, "Wideband Code Division Multiple Access," *IEEE Journal on Selected Areas in Communications*, vol. 18, no. 8, pp. 1344-1354, Aug 2000.

A. Papoulis, *Probability, Random Variables, and Stochastic Processes*, Boston MA: WCB McGraw-Hill, 1991.

R. L. Pickholtz, L. B. Milstein, D. L. Schilling, "Spread Spectrum for Mobile Communications," *IEEE Transactions on Vehicular Technology*, vol. 40, no. 2, pp. 313-322, May 1991.

H. Suzuki, "A Statistical Model for Urban Radio Propagation," *IEEE Transactions on Communications*, vol. COM-25, no. 7, pp. 673-680, July 1977.

W. M. Tam and F.C. M. Lau, "Analysis of Power Control and Its Imperfections in CDMA Cellular Systems," *IEEE Transactions on Vehicular Technology*, vol. 48, no. 5, pp. 1706-1717, Sep. 1999.

Y. S. Yeh, J. Wilson, S. C. Schwartz, "Outage Probability in Mobile Telephony with Directive Antennas and Macrodiversity," *IEEE Journal on Selected Areas in Communications*, vol. SAC-2, no. 4, July 1984.

THIS PAGE INTENTIONALLY LEFT BLANK

INITIAL DISTRIBUTION LIST

1. Defense Technical Information Center 2
8725 John J. Kingman Road, Suite 0944
Ft. Belvoir, VA 22060-6218

2. Dudley Knox Library 2
Naval Postgraduate School
411 Dyer Road
Monterey, CA 93943-5101

3. Commander Naval Security Group 1
Code N6
9800 Savage Road, Suite 6585
Fort Meade, MD 20755-6585

4. Commanding Officer, Naval Information Warfare Activity..... 1
9800 Savage Road, Suite 6585
Fort Meade, MD 20755-6000

5. Chairman, Code EC..... 1
Department of Electrical and Computer Engineering
Naval Postgraduate School
Monterey, CA 93943-5000

6. Chairman, Code MA 1
Department of Mathematics
Naval Postgraduate School
Monterey, CA 93943-5000

7. Professor Tri T. Ha(EC/Ha) 5
Department of Electrical and Computer Engineering
Naval Postgraduate School
Monterey, CA 93943-5000

8. Professor Charles Therrien (EC/Ti) 1
Department of Electrical and Computer Engineering
Naval Postgraduate School
Monterey, CA 93943-5000

9. Professor R. Clark Robertson (EC/Rc) 1
Department of Electrical and Computer Engineering
Naval Postgraduate School
Monterey, CA 93943-5000

10. Professor Jovan Lebaric (EC/Lb) 1
 Department of Electrical and Computer Engineering
 Naval Postgraduate School
 Monterey, CA 93943-5000

11. Professor Craig Rasmussen (MA/Ra) 1
 Department of Mathematics
 Naval Postgraduate School
 Monterey, CA 93943-5000

12. Professor Chris Frenzen (MA/Fr) 1
 Department of Mathematics
 Naval Postgraduate School
 Monterey, CA 93943-5000

13. Professor Rama Janaswamy (EC/Js) 1
 Department of Electrical and Computer Engineering
 Naval Postgraduate School
 Monterey, CA 93943-5000

14. Cryptologic Research Laboratory 1
 Department of Electrical and Computer Engineering
 Naval Postgraduate School
 Monterey, CA 93943-5000

15. CDR Jan Tighe 1
 Naval Information Warfare Activity
 9800 Savage Road, Suite 6585
 Fort Meade, MD 20755-6000

16. Professor James A. Chinn 1
 Department of Mathematics
 Broward Community College
 3501 Southwest Davie Rd
 Davie, FL 33314

17. Dr. Beverly James 1
 McArthur High School
 6501 Hollywood Blvd.
 Hollywood, FL 33024